Physics of flow, sediment transport, hydraulic geometry, and channel geomorphic adjustment during flash floods in an ephemeral river, the Paria River, Utah and Arizona

by

David Joseph Topping

A dissertation submitted in partial fulfillment
of the requirements for the degree of

Doctor of Philosophy

University of Washington

1997

Approved by _____
Chairperson of Supervisory Committee

Program Authorized
to Offer Degree Department of Geological Sciences

Date May 30, 1997

VOLUME 1

© Copyright 1997

David Joseph Topping

Doctoral Dissertation

In presenting this dissertation in partial fulfillment of the requirements for the Doctoral degree at the University of Washington, I agree that the Library shall make its copies freely available for inspection. I further agree that extensive copying of this dissertation as allowable only for scholarly purposes, consistent with "fair use" as prescribed in the U.S. Copyright Law. Requests for copying or reproduction of this dissertation may be referred to University Microfilms, 1490 Eisenhower Place, P.O. Box 975, Ann Arbor, MI 48106, to whom the author has granted " the right to reproduce and sell (a) copies of the manuscript in microfilm and/or (b) printed copies of the manuscript made from microfilm."

Signature David G. Tonjum

Date May 30, 1997

University of Washington

Abstract

Physics of flow, sediment transport, hydraulic geometry, and channel geomorphic adjustment during flash floods in an ephemeral river, the Paria River, Utah and Arizona

by David Joseph Topping

Chairperson of the Supervisory Committee
Professor J. Dungan Smith
Department of Geological Sciences

In-channel flow and sediment transport processes are physically coupled to the geomorphic adjustment of alluvial river channels through mass conservation of each sediment size class between the bed and the flow. This dissertation examines, in a rigorous, physically based context, the hydrology, sediment transport, channel geometry, hydraulic geometry, and channel geomorphic adjustment during floods of an ephemeral river, the Paria River. This study relies on equal amounts of historically, field-, and theoretically based research. All hydrologic, sediment-transport, and channel-geometric data collected in the Paria River system from 1872 to 1996 are analyzed. These analyses indicate that the hydrology has been effectively stationary since 1923, and that equilibrium cross-section geometries of channels with similar longitudinal slopes have been stable since 1872. All data are placed in the context of two models, a hydraulic geometry model and a geomorphically coupled, flow and sediment-transport model. The first of these models allows evaluation of channel changes to be made in the context of equivalent hydraulic geometries; equivalent hydraulic geometries are channel geometries that transport the same amount of water and sediment. Placement of all hydrologic and channel-geometric data into the context of this model indicates that channel changes that have occurred over the last 120 years have been between equivalent hydraulic geometries and are not driven by changes in hydrology and sediment transport, i.e., changes in climate. The second of these models physically couples the reach-averaged geomorphic adjustment of a channel during a flood to the in-channel flow and sediment-transport processes through mass conservation of each sediment size class between the bed and the flow. Modeling suggests that, from 1923 to 1996, sand loads have remained constant, while silt and clay loads may have decreased. Sediment transport in the Paria is "duration limited"; over the period of record, most of the sand, silt, and clay has moved at the mean instantaneous discharge, while most of the gravel has moved at the highest discharges.

TABLE OF CONTENTS

List of figures viii

List of tables xiii

List of symbols used in the text xiv

Note on numerical format xx

Chapter 1: Introduction 1

Chapter 2: Historical analysis of hydrology and channel geometry: The case for minimal change in the Paria River from 1872 to 1996 6

Section 2.1: Introduction 6

Section 2.2: Brief description of the river system 6

Section 2.3: Previous work 13

Section 2.4: Paria River hydrology 15

2.4a: Introduction 15

2.4b: History of stream gaging on the Paria River by the U.S. Geological Survey 15

2.4b-1: Lees Ferry, AZ - Station 09382000 15

1923-1996 discharge measurements 16

Discharge measurements during floods 18

The three different indirect methods used by the USGS to estimate peak flood discharges 19

Suspended-sediment and bed-sediment measurements 21

2.4b-2: Near Cannonville, UT - Station 09381500 21

2.4b-3: Near Kanab, UT - Station 09381800 22

2.4c: Methodology for discharge recomputation 22

2.4c-1: Lees Ferry, AZ 22

The three initial stage-discharge rating curves 24

Grand Canyon backcalculation method 24

Step-backwater method 31

Superelevation method 34

The three final stage-discharge rating curves and shifts 35

2.4c-2: Near Cannonville, UT 35

2.4c-3: Near Kanab, UT 37

2.4d: The Paria River instantaneous discharge time series at Lees Ferry, AZ .. 38
Evaluation of error in published discharge records 43
Comparison of recomputed mean daily discharges to published mean daily discharges 44
2.4e: Hydrologic-trend analyses at Lees Ferry, AZ 44
Annual flow volume 45
Instantaneous discharge, peak flood discharge, flood volume, and flood duration 49
Discharge of overbank peaks and duration of overbank flows 53
2.4f: Flood-frequency analyses at Lees Ferry, AZ 53
2.4g: Flow-duration analysis at Lees Ferry, AZ 58
2.4h: Comparison of peak flood discharge and flood-frequency analyses at the three gages 60
2.4i: Hydrologic summary with climatic implications 64
Section 2.5: Modern and historically based research in the Paria River system ... 66
2.5a: The Paria River at Lees Ferry, AZ in 1993 68
The 1993 field program 68
Detailed description of the Lees Ferry study area in 1993 69
2.5a-1: The 1993 Lees Ferry 3-reach composite and reach-averaged cross-section 79
Method for constructing a reach-averaged cross-section 81
The 1993 reach-averaged cross-section 81
2.5b: The Paria River at Lees Ferry, AZ from 1872 to 1994 85
2.5b-1: Source and evaluation of information comprising the 1872-1994 channel geometry data set 86
USGS slope-area surveys 87
NPS and USBR topographic surveys 87
USGS discharge measurement field notes 87
Aerial photographs 88
General Land Office cadastral surveys 88
Written descriptions of the channel 89
Ground-based photographs 89
2.5b-2: Changes in the lateral position of the channel 97
2.5b-3: Changes in the vertical position of the channel; the base-level control of the Colorado River on the Paria River 100

1872-1993 longitudinal profiles of the Paria River in the Lees Ferry study area 101

Local nature of Paria River channel bed aggradation and degradation over time 103

Post-1963 channel entrenchment and the pre-1963 seasonal interplay of the Paria and Colorado rivers at the confluence 104

Pre-1963 seasonally fluctuating base level of the Paria River 117

Causes of other changes in minimum bed elevation at the post-1925 gage site 119

2.5b-4: Reach-averaged cross-sectional channel geometry from 1872 to 1994 119

2.5b-4a: Comparative analysis of reach-averaged Paria River cross-section geometry 122

Data from reaches with longitudinal bed slopes approximately equal to the equilibrium bed slope of 0.0035 (Category 1 data) 123

Data from reaches with longitudinal bed slopes greater than 0.004 or less than 0.002 (Category 2 data) 125

Stability of the reach-averaged Paria River cross-sectional geometry during extreme events 125

Detailed descriptions of the data used in the comparative analysis of reach-averaged Paria River cross-section geometry 127

2.5b-4b: Statistical analysis of Paria River cross-section geometry 133

Methodology 133

Application of the method to the analysis of Paria River cross-section geometry 135

Comparison of topwidths of flow in the discharge measurement cross-sections with widths from the 1993 survey 138

2.5b-4c: Discussion of analyses of cross-section channel geometry and problems associated with stratigraphic analyses 140

2.5b-5: Has sediment been stored in the Lees Ferry reach since 1939? ... 143

2.5b-6: Bed sediment 145

2.5c: The Paria River below Cannonville, UT from 1951 to 1994 148

The 1994 field program 148

Detailed description of the Cannonville study area in 1994 150

Constraints on the rate of headcut retreat and the possible age of the incised reach 157

Summary of the Cannonville study area 164

2.5d: The Paria River in the vicinity of Paria, Rock House, and Adairville, UT from 1877 to 1996 164

The 1994 and 1996 field programs and description of the river in 1994-1996 165

Reconstruction of changes in channel length, sinuosity, and slope from 1877 to 1976 170

Bankfull width of the channel and existence of floodplains near Paria in 1918 176

2.5e: The Paria River below the near Kanab, Utah gage from 1970 to 1995 ..177

2.5f: Summary of Paria River channel properties 177

Modern 177

Past changes 180

Section 2.6: Hydraulic geometry of the Paria River 181

2.6a: Introduction and working hypothesis 181

A physically based formulation of hydraulic geometry 182

2.6b: Reach-averaged maximum bankfull depth 187

2.6c: Application of the hydraulic geometry model to the modern Paria River system 190

Model-based speculation on changes in hydraulic geometry with climate 196

2.6d: Application of the hydraulic geometry model to historical channel geometric changes in the Lees Ferry, AZ and Paria-Adairville, UT reaches with hydrologic and sediment-transport implications 199

Lees Ferry, AZ reach 199

Paria-Adairville, UT reach 201

2.6e: Hydraulic geometry summary with implications for the prediction of long-term sediment transport rates in the Paria River basin 204

Chapter 3: Development and testing of a geomorphically coupled flow and sediment-transport model 206

Section 3.1: Introduction 206

Section 3.2: Suspended sediment in the Paria River 207

3.2a: Introduction and presentation of the data 207

3.2b: Methods of USGS sample collection and laboratory analysis 210

Sample collection in the field 210

Grain-size analysis 212

3.2c: Statistical analysis of the Paria River grain-size analyzed suspended-sediment data 214

Discussion 217

Section 3.3: Physical framework for a geomorphically coupled flow and sediment-transport model 225

Conservation of momentum and application of reach averaging 225

Physical justification of modeling the unsteady Paria River with a steady flow model 227

Overview of the geomorphically coupled flow and sediment-transport model 230

Section 3.4: Quantitative description of the bed for mass conservation 234

Section 3.5: The flow component of the model 240

Stress partitioning 240

Structure of the eddy viscosity 241

Spatially averaged gravel form drag 242

Spatially averaged dune form drag 243

The flow-model equation 245

Skin-friction roughness for cases of no sediment transport and bedload transport 247

Nature of roughness and drag in suspended-sediment-transporting flows over either antidunes or upper-plane bed 247

Section 3.6: The suspended-sediment component of the model 253

Density stratification due to high suspended-sediment concentration gradients 255

Sediment velocity and the nonzero velocity of water in the presence of suspended sediment 257

Concentration profiles for the *m* components of suspended sediment ... 257

Settling velocity of suspended sediment and the "hindered settling" effect 258

The lower boundary condition 259

Is lateral diffusion of suspended sediment important? 260

Section 3.7: Calculation of fluid and sediment discharge through the model-predicted cross-section 262

Section 3.8: Sensitivity of model predictions to varying the thickness of the sand, silt, and clay layer 263

Section 3.9: Tests of the flow and sediment-transport model against laboratory data 269

Section 3.10: Test of the flow and sediment-transport model against data from the Rio Puerco 286

Chapter 4: Application of the geomorphically coupled flow and sediment-transport model to the Paria River with tests of the model predictions against data 290

Section 4.1: Introduction 290

Section 4.2: Model inputs 290

Section 4.3: The seven tests of the model 291

4.3a: TEST 1: Magnitude of cross-section enlargement during a flood 291

4.3b: TEST 2: Magnitude of cross-section widening during a flood 298

4.3c: TEST 3: Comparison of model-predicted and measured maximum depth, area, and mean velocity as a function of fluid discharge 302

4.3d: TEST 4: Occurrence of dunes and antidunes in the channel 308

4.3e: TEST 5: Comparison of model-predicted and measured depth-integrated suspended-sediment concentrations in each size class 313

Differences between measurable and predictable suspended-sediment concentrations 313

Modeling depth-integrated suspended-sediment samplers 316

Comparison of model-predicted and measured depth-integrated concentrations of suspended sand 317

Comparison of model-predicted and measured sorting of suspended sand 330

Comparison of model-predicted and measured concentration of suspended silt and clay 330

4.3f: TEST 6: Comparison of model-predicted and quasi-daily measured depth-integrated suspended-sediment concentrations 336

4.3g: TEST 7: Comparison of model-predicted and measured cross-stream differences in depth-integrated sediment concentration 339

Section 4.4: Hyperconcentrated flows 340

Section 4.5: Model-predicted sediment fluxes through the model-predicted cross-section 344

Application of the model to the period of gage record 344

Comparison of the model predictions with previously published estimates of sediment loads 349

The effective discharge of the Paria River at Lees Ferry, AZ with implications for the stability of the equilibrium bankfull channel geometry since 1872 358

Section 4.6: Summary and conclusions 361

Chapter 5: Conclusions 363

References 367

Appendix 1: Statistical analysis of Paria River cross-section geometry 378

Appendix 2: Statistical analysis of the grain-size analyzed Paria River suspended-sediment data 379

Appendix 3: Velocity profiles over upper-plane beds and antidunes 398

Pocket material: Plate 1

LIST OF FIGURES

1.1: Mouth of the Paria River 3

2.1: Map of the Paria River drainage basin 7

2.2: Longitudinal profile of the Paria River 9

2.3: Bedrock narrows, bedrock control, and landslides in the Lower Paria River Gorge 10

2.4: Map of the Lees Ferry, AZ study area 17

2.5: Map of the eastern Grand Canyon region 27

2.6: Example of the Grand Canyon backcalculation method 28

2.7: Error in the published peak discharges of the Paria River 33

2.8: Stage-discharge ratings A, B, and C of the Paria River at Lees Ferry, AZ 36

2.9: Instantaneous discharge time series of the Paria River at Lees Ferry, AZ 39

2.10: Annual flow volume of the Paria River at Lees Ferry, AZ 48

2.11: Trends in peak flood discharge, flood volume, flood duration, discharge of overbank peaks, and duration of overbank flows 50

2.12: Flood-frequency curves for the Paria River at Lees Ferry, AZ 55

2.13: Flow-duration curves for the Paria River at Lees Ferry, AZ 59

2.14: Streamwise behavior of the peak discharge of floods 61

2.15: Comparison of the flood-frequency distribution at the three gaging stations 62

2.16: Regional composite of tree-ring width data 67

2.17: Comparison of cross-section shapes from equilibrium and incised reaches 70

2.18: Typical portion of the Paria River bed 73

2.19: The four gravel grain-size distributions in the Lees Ferry study area 74

2.20: Locations of the four sediment environments in the 1993 reach-averaged cross-section 76

2.21: Surface waves over antidunes at a flow depth of 40 cm, planar water surface at near-bankfull stage 78

2.22: The reach at Cableway 2 in 1964-1968 and Reach 2 in 1993 80

2.23: Reach-averaged cross-sections for Reaches 1, 2, and 3 of the 1993 3-reach composite 82

2.24: The 1993 Lees Ferry reach-averaged cross-section 83

2.25: Comparison of repeat ground-based photography and surveyed cross-sections . 91

2.26: Lateral positions of the Paria River channel in the Lees Ferry study area from 1872 to 1993 98

2.27: Surveyed cross-sections at 21 locations ..... Plate 1

2.28: Longitudinal profiles of the lower Paria River in 1872-1873, 1921-1929, 1939-1940, 1957-1963, and 1993 102

2.29: Temporal changes in minimum bed elevation at 23 locations ..... Plate 1

2.30: The lower Paria River in 1939, 1960, and 1995 106

2.31: Natural (1935-1940) and artificial (1993-1995) geometries of the confluence .. 108

2.32: Natural (1915-1921) and artificial (1995) geometries of the confluence 110

2.33: Elevation of Colorado River backwater in lowermost Paria River 116

2.34: Causes of other changes in minimum bed elevation 120

2.35: Category 1 cross-section geometry data in the Lees Ferry study area 124

2.36: Category 2 cross-section geometry data in the Lees Ferry study area 126

2.37: The lower Paria River channel in 1873, 1911, and 1915 128

2.38: Flow topwidth as a function of measured maximum depth 137

2.39: Comparsion of channel widths from the 1923-1972 discharge measurements with channel widths from the 1993 Lees Ferry survey 139

2.40: Comparison of Hereford's Lees Ferry stratigraphic section to surveyed topography in 1939, 1963, and 1993 141

2.41: Sediment storage in the Lees Ferry study area from 1925 to 1993 144

2.42: Grain-size distributions of Paria River sand, silt, and clay in the Lees Ferry study area in 1958-1971 and 1993 146

2.43: Map of the Cannonville study area in 1963 and 1994 149

2.44: Equilibrium reach of the Cannonville study area in 1994 151

2.45: Longitudinal profiles in the Cannonville study area from 1951, 1952, 1963, and 1994 154

2.46: Reach at the near Cannonville, UT gage in 1951 and 1994 155

2.47: Incised reach below near Cannonville, UT gage in 1994 158

2.48: Equilibrium reach of the Paria River below the Cannonville study area in 1994-1997 161

2.49: Portions of the 1877 cadastral survey map of Bailey and Burrill (1877) 166

2.50: Map of Paria River thalweg in 1877, 1917, and 1976 in the Paria-Adairville, UT reach 168

2.51: Cross-section P-1 at the site of the 1877 irrigation dam above Paria, UT 171

2.52: Cross-section RH-3 near Rock House, UT 172

2.53: Channel and floodplain above Paria, UT in 1918 175

2.54: Near Kanab, UT annual-crest gage in 1995 178

2.55: Cross-section *LG-4* in 1995 179

2.56: Hydraulic geometry model definition sketch 184

2.57: Model-predicted and measured bankfull depth 189

2.58: Gravel grain-size distributions in the Cannonville study area in 1958 & 1994, the Lower Gorge in 1995, and the Lees Ferry study area in 1993 192

2.59: Model-predicted and measured maximum bankfull depth in the Paria River 193

2.60: Model-predicted and measured cross-section geometries at Lees Ferry and Cannonville 194

2.61: Model-predicted and measured 1872-1993 Lees Ferry cross-section geometries 200

3.1: Concentration and cross-stream difference in concentration of suspended sediment as functions of the instantaneous fluid discharge 208

3.2: Concentration of suspended sand and suspended silt and clay as functions of instantaneous fluid discharge 209

3.3: Sediment samplers used to collect the data 211

3.4: Cumulative grain-distribution of flocculated and deflocculated silt and clay 213

3.5: Differences in the grain-size analyzed suspended-sediment data 218

3.6: Paria River flood bore 228

3.7: Velocity measurements at 0.8*h* as a function of the square root of *h* 231

3.8: Simplified model flow chart 232

3.9: Comparison of the unweighted, normalized number of particles with area-weighted concentration 236

3.10: Area of the bed covered by and unit volume of sand, silt, and clay as a function of the thickness of the sand, silt, and clay layer 239

3.11: Conceptual initial and converged model-predicted configuration of the bed 244

3.12: Dependence of dune wavelength and height on the fraction of the bed grain-size distribution that is suspended 246

3.13: Dependence of $(z_0)_{sf}$ on the near-bed concentration of suspended sediment 249

3.14: Form drag and roughness in the upper-plane bed and antidune experiments of Guy and others 252

3.15: Vertical profiles of model-predicted quantities for various thicknesses of the sand, silt, and clay layer 264

3.16: Model predictions as a function of the measurements of Kennedy (1961) and Guy and others 271

3.17: Measurements and model predictions as functions of the total boundary shear stress in each experiment of Kennedy (1961) and Guy and others (1966) 277

3.18: Model-predicted and measured suspended-sediment concentration and velocity profiles in the Rio Puerco 288

4.1: Water temperature of the Paria River at Lees Ferry, AZ 292

4.2: Model predictions of channel enlargement 294

4.3: Comparison of the model-predicted measured cross-section at Q=38.2 m^3/s 295

4.4: Cross-section area as a function of maximum depth 297

4.5: Upstream views of the reach above the gage on September 18, 1963 and in February 1951 showing locations of sand 299

4.6: Model-predicted and measured width of the flow at seven different elevations above the deepest point in the cross-section 300

4.7: Measured and model-predicted cross-section maximum depth, area, and mean velocity as a function of instantaneous fluid discharge 303

4.8: Velocity profile measured in the center of the channel on December 14, 1962 ..307

4.9: Model predictions at two test verticals in the channel 309

4.10: Model-predicted suspended-sediment concentration profiles for the eleven different size classes of sediment and the lower limits of the sampling range for the depth-integrated suspended-sediment samplers 315

4.11: Model-predicted and measured concentrations of suspended total sand and suspended sand in each size class 318

4.12: Model-predicted and measured D_{16}, D_{50}, and D_{84} of the suspended sand 331

4.13: Model-predicted and measured concentrations of suspended silt and clay 334

4.14: Ratio of 10-1-47 through 9-30-75 model-predicted to measured suspended-sediment concentration as a function of the instantaneous fluid discharge 337

4.15: Model-predicted "sampled" and measured range in depth-integrated suspended-sediment concentration 341

4.16: Measured and model-predicted "sampled" depth-integrated concentration of suspended sand as a function of the depth-integrated concentration of suspended sediment 343

4.17: Model-predicted fluxes of total load, suspended load, and bedload as function of fluid discharge 345

4.18: Cumulative volume of fluid (water + suspended sediment) and model-cumulative volumes of sediment, silt & clay, sand, and sand in each size class passing the Paria River gage at Lees Ferry, AZ 350

4.19: Model-predicted normalized annual loads of silt & clay, sand, 0.0625 mm sand and 1.41 mm sand 354

4.20: Cumulative volume of sand, silt & clay, and gravel as a function of the instantaneous fluid discharge 359

LIST OF TABLES

2.1: Flood rankings with past and present methodologies of peak-discharge determination for the ten largest Paria River floods of the 20th century 25

2.2: Summary of hydrologic-trend analyses 46

2.3: Grain-size distributions of the four sand, silt, and clay sediment types 77

2.4: Descriptions of Colorado River backwatering events on the Paria River in 1948, 1949, and 1952 114

2.5: Summary of the statistical analysis of channel cross-section geometry 136

2.6: Changes in channel length, sinuosity, and slope from 1877 to 1976 in the Paria-Adairville, UT reach 174

2.7: Predicted and measured hydraulic geometry properties for the Paria River in 1993-1996 195

2.8: Modeled 1990's initial magnitudes and model-predicted changes in dependent hydraulic geometry variables 197

2.9: Predicted reach-scale channel-geometric changes near Paria, UT from 1877 to 1976 keeping reach-averaged hydraulic geometry constant 202

3.1: Results of the statistical analysis of the grain-size analyzed suspended-sediment data 216

3.2: Total shear velocity and skin-friction roughness parameter comparisons for the Guy and others (1966) upper-plane bed and antidune flume experiments 251

4.1: Comparison of model-predicted "sampled" depth-integrated suspended-sediment concentrations to the USGS measured depth-integrated suspended-sediment concentration measurements made from October 1, 1947 through September 30, 1975 338

4.2: Model-predicted sediment flux by size class and time within season through the model-predicted cross-section 348

4.3: Model-predicted mean-annual sediment loads of the Paria River for the entire period of gage record and comparison of the model-predicted mean-annual sediment loads with previously published estimates of the mean-annual sediment loads 356

LIST OF SYMBOLS USED IN THE TEXT

$\mathbf{Ri}_g$	gradient Richardson number
D	nominal grain diameter
D_{16}	the 16th percentile particle size in a coarsening sense; in a log-normal distribution, D_{16} is one standard deviation coarser than D_{50}
D_{50}	the 50th percentile particle size in a coarsening sense
D_{84}	the 84th percentile particle size in a coarsening sense; in a log-normal distribution, D_{84} is one standard deviation coarser than D_{50}
F	F-statistic
R^2	multiple squared correlation coefficient
ϕ	units of $-\log_2 D$ (when D is in units of mm)
A_g	area-weighted concentration of gravel at each level z
A_{nozzle}	cross-sectional area of the nozzle on a suspended-sediment sampler
A_s	area-weighted concentration of sand, silt, and clay for a given T_s
$(A_{xy})_n$	bed-parallel area of gravel size-class n
C_D	drag coefficient
DF_{ind}	degrees of freedom associated with the residual sum of squares from individual regression lines fit to each data bin
F_D	drag force
F_1	F-statistic associated with the individual regression line fit to each data bin
F_2	F-statistic associated with the comparison of the regression line fit to the grouped data bins with the regression lines fit to the individual data bins
G_N	normalized number of gravel particles in the bed
G_n	unweighted, normalized number of particles in each gravel size-class n
H	dune height
H_{dn}	elevation of the water surface at the downstream cross-section in the step-backwater calculations
H_{up}	elevation of the water surface at the upstream cross-section in the step-backwater calculations
$H_{v\text{-}dn}$	velocity head at the downstream cross-section in the step-backwater calculations
$H_{v\text{-}up}$	velocity head at the upstream cross-section in the step-backwater calculations

$K(z)$	eddy viscosity at level z
$K(z)_N$	neutral eddy viscosity at level z
$K_\rho(z)$	coefficient of mass diffusion at each level z
$K_\rho(z)_N$	neutral coefficient of mass diffusion at each level z
$L(z)$	local length scale of the turbulence at level z
L_A	downstream advection length of a particle
L_S	settling length scale of a particle
$L_f(z)$	length scale of the turbulence at level z in the Rattray and Mitsuda (1974) 2-part eddy viscosity
L_x	x-direction length scale
L_y	y-direction length scale
L_z	z-direction length scale
M	total number of sand, silt, and clay size-classes m
MS_d	residual mean squares
MS_{diff}	mean squares of the difference between the common regression line fit to the grouped data bins and the individual regression line fit to each data bin
MS_{ind}	residual mean squares from individual regression lines fit to each data bin
MS_r	mean squares due to regression
N	total number of gravel size-classes n
P	pressure
P_n	protrusion height of gravel size-class n
Q	instantaneous fluid discharge in the river
Q_{BF}	bankfull water discharge in the hydraulic geometry model
Q_s	sediment flux or sediment discharge
Q_{sBF}	bankfull sediment load in the hydraulic geometry model
Q_T	total sediment discharge in the river, i.e., total-load flux in the river
S	longitudinal water-surface slope or reach-averaged longitudinal channel slope
S_*	excess shear stress
S_f	frictional slope in the step-backwater calculations
SS_{com}	residual sum of squares from the common regression line fit to the grouped bins of data
SS_d	residual sum of squares

SS_{diff}	sum of squares of the difference between the common regression line fit to the grouped data bins and the individual regression line fit to each data bin
SS_{ind}	residual sum of squares from individual regression lines fit to each data bin
SS_r	sum of squares due to regression
SS_t	total sum of squares
T_*	transport stage
T_s	thickness of the sand, silt, and clay layer
T_{s0}	initial thickness of the sand, silt, and clay layer
U	velocity scale
U_A	velocity scale in the determination of the downstream advection length of a particle
$\underline{U}_m$	velocity tensor of sediment component m
$\underline{U}_w$	velocity tensor of the water component
V_{BF}	bankfull channel volume of a reach
V_b	volume of sediment in the bed
V_{b0}	initial volume of sediment in the bed
V_m	total volume of size-class m in the bed and the flow
V_s	volume of sediment in suspension
$V_{sampler}$	volume of sampled material in a suspended-sediment sampler
W	topwidth of the flow
W_{BF}	bankfull width in the hydraulic geometry model
W_{BANK}	bank width in the hydraulic geometry model
W_{BAR}	bar width in the hydraulic geometry model
W_{TH}	thalweg width in the hydraulic geometry model
X_s	fraction of the bed grain-size distribution that is suspended
c_0	coefficient in the modified Meyer-Peter and Müller bedload equation
c_1	constant in the suspended-load skin-friction roughness parameter equation
ϵ_b	volume concentration of sand, silt, and clay in the bed
ϵ_{gn}	area-weighted concentration of gravel size-class n
ϵ_m	volume concentration of suspended sediment in size-class m at each level z in the flow
$\langle \bar{\epsilon}_m \rangle$	modeled "true" mean concentration of size-class m at a vertical

$(\bar{\epsilon}_m)_{cs}$	modeled "true" mean concentration of size-class m in the cross-section
$(\epsilon_m)_{modeled\ sampler}$	modeled "sampled" mean concentration of size-class m at a vertical
$\left((\epsilon_m)_{modeled\ sampler}\right)_{cs}$	modeled "sampled" mean concentration of size-class m in the cross-section
$(\epsilon_m)_{sampler}$	concentration of each size-class m measured by a depth-integrated suspended-sediment sampler at a vertical
$\left((\epsilon_m)_{sampler}\right)_{cs}$	concentration of each size-class m measured by a depth-integrated suspended-sediment sampler in the cross-section
ϵ_s	volume concentration of suspended sediment at each level z in the flow
ϵ_w	volume concentration of water at each level z in the flow
$(\epsilon_s)_{z_a}$	concentration of suspended-sediment at reference level z_a
$((d_x)_n)_z$	downstream (intermediate) axis of the ellipse formed by gravel size-class n at level z
$((d_y)_n)_z$	cross-stream (major) axis of the ellipse formed by gravel size-class n at level z
f_m	volume fraction of size-class m in the bed
f_{m0}	initial volume fraction of size-class m in the bed
g	gravitational acceleration
h	local flow depth
h_{BF}	maximum bankfull depth in the hydraulic geometry model
h_{BAR}	depth of flow over the bar region in the hydraulic geometry model
h_f	friction loss between cross-sections in the step-backwater calculations
h_s	shock loss between cross-sections in the step-backwater calculations
h_Δ	head loss between cross-sections in the step-backwater calculations
i	smallest gravel size-class n present at level z
j	total number of data in combined data bins
k	von Karman's constant
k_s	bed roughness length
m	number of data bins or sediment size class of sand, silt, or clay
n	number of data or sediment size class of gravel

p	statistical level of significance
Pr	Rouse number
$Pr(D_{50})$	D_{50} Rouse number
q	unit discharge
q_b	unit bedload sediment flux
$(q_b)_m$	unit bedload flux of sediment in size-class m
q_s	unit suspended-load sediment flux
$(q_s)_m$	unit suspended-load flux of sediment in size-class m
q_{sBF}	unit bankfull sediment flux in the hydraulic geometry model
q_T	unit total-load flux
r_c	radius of curvature in the superelevation calculations
s	water surface elevation
t	time or time scale
u	component of velocity in the x-direction or streamwise direction
$\langle u_{fill} \rangle$	vertically averaged sampler filling velocity
u_*	shear velocity
u_{*T}	total shear velocity
$u_{*f}(z)$	local velocity scale of the turbulence at level z
v	component of velocity in the y-direction or cross-stream direction
w	component of velocity in the z-direction
w_m	settling velocity of sediment in size-class m
w_s	settling velocity
$(w_s)_{D_{50}}$	clear-water settling velocity of D_{50} of the bed material
z_a	reference elevation, taken as the top of the bedload layer
z_0	bed roughness parameter
$(z_0)_{sf}$	skin-friction roughness parameter
Δz_s	elevation difference in the water surface across the channel in the superelevation calculations
α	ratio of mass diffusion to momentum diffusion
α_B	bank angle in the hydraulic geometry model
β	constant in the 2-part eddy viscosity of Rattray and Mitsuda (1974)
δ	thickness of the bedload layer
ε	river stage minus bed stage
ϕ_b	nondimensional unit bedload transport rate

ϕ_m	nondimensional shear
ϕ_ρ	nondimensional shear for mass
γ	constant set equal to 0.0045 in the reference concentration equation
$(\gamma_m)_0$	momentum diffusion constant set equal to 5.4
$(\gamma_\rho)_0$	mass diffusion constant set equal to 7.3
μ_f	dynamic viscosity of the fluid (mixture of water plus sediment)
μ_w	dynamic viscosity of water
ν	kinematic viscosity of water
λ	dune wavelength
ρ	density of water
ρ_f	density of the fluid (mixture of water plus sediment)
ρ_s	density of sediment
ρ_w	density of water
σ	standard deviation
τ	stress
τ_*	nondimensional skin-friction shear stress
$(\tau_*)_{cr}$	nondimensional critical shear stress
τ_b	total boundary shear stress
τ_{cr}	critical shear stress
$\tau_D(z)$	gravel form-drag stress resulting from gravel particles protruding through level z
$(\tau_D)_s$	gravel form-drag stress resulting from gravel particles protruding through the water surface
τ_{dd}	dune form-drag component of the stress
τ_f	fluid component of the stress
τ_{gd}	gravel form-drag component of the stress
$(\tau_{gd})_b$	gravel form-drag component of the stress at the bed
τ_{sf}	skin-friction boundary shear stress ($\tau_f(0) = \tau_{sf}$)

NOTE ON NUMERICAL FORMAT

In this dissertation, numbers may be written in four different formats. For example, the number "50,000" may be written as 5.0×10^4, $5\ 10^4$, or 5.0e+4.

ACKNOWLEDGMENTS

I especially want to acknowledge my Ph.D. advisor, Dr. J. Dungan Smith, who provided me with: continual support for the duration of this project, the freedom to pursue a wide variety of research interests, and a constant intellectual challenge. I also want to acknowledge the three most influential people on my development as a scientist, Dr. John Southard, Dr. Joanne Bourgeois, and Dr. J. Dungan Smith. I want to thank Dr. Joanne Bourgeois and Dr. Thomas Dunne for being especially strong advocates of my entrance into the Ph.D. program. I wish to thank the members of my reading committee, Dr. J. Dungan Smith, Dr. Joanne Bourgeois, and Dr. David Montgomery, and also the other members of my advisory committee, Dr. Thomas Dunne, Dr. David McTigue, Dr. Ronald Nece, and Dr. Catherine Petroff. I am also grateful to Dr. Jonathan Nelson for providing a thoughtful review of this dissertation. Numerous conversations with David Mohrig, Jonathan Nelson, Richard McDonald, Mark Schmeeckle, Edmund Andrews, Stephen Wiele, and Randy Parker helped improve the quality of the science in this document.

This research was funded both through the U.S. Geological Survey by Glen Canyon Environmental Studies II of the Bureau of Reclamation and by a National Science Foundation Graduate Fellowship. I thank the National Park Service personnel at Glen Canyon National Recreation Area for easy access to working in the Lees Ferry area. Substantial assistance in the field under difficult working conditions was provided by Susan Millar, Mark Schmeeckle, Richard McDonald, Eleanor Griffin, Peter Furey, and Karen Hardesty. I thank Julia Graf of the Arizona District of the USGS-WRD for providing me with the original suspended-sediment measurement field and laboratory notes for the Paria River. I am grateful to Richard Hereford and Robert Webb of the USGS for providing me with some of the photographs used in this paper. I also thank Bob Gauger, Greg Fisk, Bob Hart, and Frank Brewsaugh at the Flagstaff, AZ office of the Arizona District of the USGS-WRD for allowing me access to their files on the Paria River.

I also thank my fellow graduate students at the University of Washington, especially David Mohrig, Mark Schmeeckle, Marc Hirschmann, Martin Miller, Donna Whitney, Ken MacLeod, Ralph Dawes, Terry Swanson, and Rob Thomas for helping to make graduate school a memorable experience; it was with these people that I grew up as a scientist. I am also indebted to Birgit Müller, who provided me with inspiration during the final days of this project. I also wish to thank my parents for being a constant source of inspiration throughout my life.

DEDICATION

To my parents,

Joseph and Lucy

Chapter 1: INTRODUCTION

Over the last century, the Colorado Plateau has been the focus of extensive research on fluvial channel change in ephemeral alluvial rivers. Beginning with the classic work of Dutton (1882), Dodge (1902), and Bryan (1925), the problem of rapid channel change and the development of arroyos, the so-called "arroyo problem" summarized by W. Graf (1983), has been at the forefront of geomorphologic research. Unfortunately, most of this research has been focused only on temporally correlating observed local changes in channel geometry with various causal mechanisms, e.g., land-use changes, irrigation development, vegetation changes, single catastrophic floods, and climatic change and has not focused on determining the physical linkage between the in-channel physical processes governing flow and sediment-transport and the observed changes in channel geometry. This dissertation, therefore, is aimed at filling this gap in scientific understanding by: (1) thoroughly investigating all hydrologic and channel-geometric data in a rigid, physically based framework from a river system, i.e., the Paria River system, said to have undergone the classic "arroyo-type" channel changes of entrenchment followed by widening and subsequent channel aggradation and narrowing; and (2) developing, testing, and applying a physically based model for flow and sediment transport coupled to the geomorphologic evolution of the Paria River channel during floods.

The river system chosen for this study, the Paria River, has been a major focus of research related to late-nineteenth and twentieth century fluvial channel change in the southwestern United States (e.g., Gregory and Moore, 1931; Bailey, 1935; Gregory, 1951; Hereford, 1983, 1986, 1987a, 1987b , 1989; Webb, 1985; W. Graf, 1987; J. Graf and others, 1991). A conclusion of these studies was that the Paria River was among the channels that incised and widened throughout the southwestern United States in the late 1800's and early 1900's. A conclusion of the more recent, post-1980, work was that the Paria River channel aggraded and narrowed with the formation of new floodplains beginning in 1940 in response to changes in flood magnitude and frequency. Most recently, paleoflood deposits from the Paria River have been used to deduce, in part, climatic trends in the southwest over the last 5000 years (Ely and others, 1993).

The critical item missing from previous work on the Paria River system, and on ephemeral rivers in general, is the investigation of the in-channel mechanics of flow and sediment transport associated with floods. Interpretations of all of the workers mentioned above are based, in part, on assumed behavior, not physically based nor measured behavior, of the Paria River during floods. This dissertation is designed to

address specifically the physics of flow and sediment transport in an ephemeral stream and its physical coupling to cross-section channel adjustment during floods. The Paria River is the ideal choice for such a study because: (1) there is a large quantity of hydrologic data spanning the time period from 1923 to the present, and channel-geometric data spanning the time period from 1872 to the present; (2) previous work uses the Paria River as an example of a river channel that has changed substantially in response to hydrologic changes driven by climatic change over the last century; and, finally, (3) the Paria River has societal relevance in that since the closure of Glen Canyon Dam on March 13, 1963, it is the only remaining major supplier of sand crucial to the riparian environment of the Marble Canyon segment of the Colorado River in Grand Canyon National Park (Figure 1.1).

Prior to the comparison of any model prediction to data, one must insure the quality of the measurements used to test a model. Since this study ultimately involves comparison of model results with data collected over the last century by many different people using many different methodologies in a river system interpreted to have undergone significant changes, the first step in this study was the retrieval and evaluation of all raw hydrologic and channel-geometry data ever collected in the Paria River system. This historically based effort was then combined with an extensive field program in the modern river system so that all aspects of the Paria River system, past and present, could be placed in the same quantitative framework. This work, presented in Chapter 2 of this dissertation, represents not only the most extensive synthesis of hydrologic and channel-geometry data ever assembled, but it also represents the first time that 120 years of channel-change data from an ephemeral river have been placed in a framework that allows the interpretation of all changes in a rigorous, physically based manner.

Chapter 2 is divided into five major sections: (1) a brief description of the Paria River system; (2) a review of past work on the Paria River; (3) a thorough evaluation of the hydrology of the Paria River system that includes the construction and analyses of a 73-year instantaneous discharge time series; (4) assembly and analysis of quantified channel-geometry data covering much of the lower 83% of the river from the 1870's to the present; and (5) placement of the hydrologic and channel-geometry data into a physically based, hydraulic geometry context. Results presented in Chapter 2 show that from 1923 to 1996, the hydrology of the river has been remarkably stable; and, analyses of raw discharge data in Chapter 2 show that trends in the published discharge records of the Paria River used by previous workers to interpret climatic change are, in fact, only due to successive improvements in methodologies used by the U.S. Geological Survey (USGS) to estimate the peak discharge of floods. Furthermore, placement of the channel-geometry data into

Figure 1.1: View of the mouth of the Paria River from the cliff on the east side of the Colorado River. Discharge in the Paria and Colorado rivers is approximately 9 m^3/s and 340 m^3/s, respectively. Earlier in the day, a flood bore traveled down the Paria River increasing the discharge from about 0.3 to about 10 m^3/s over the period of several minutes. Photograph taken by D.J. Topping on May 17, 1993.

the context of the hydraulic geometry model developed in Chapter 2 indicates that the hydraulic geometry of the Paria River has been relatively stable from 1872 to the present and that all past changes in reach-averaged cross-section geometry have been due only to changes in longitudinal slope. Previous workers on ephemeral rivers have mistakenly assumed that a change in the cross-section geometry of a channel required a change in hydrology and sediment transport; in contrast, work presented in Chapter 2 shows that for every steep, wide, braided channel there is a gently sloping, narrow, single-threaded river with an equivalent hydraulic geometry.

Chapter 3 focuses on: (1) the complete evaluation of the grain-size-analyzed suspended-sediment data from the Paria River to determine which grain sizes are in local equilibrium with the hydraulics and supply of sediment on the bed and which grain sizes are advected into a reach from upstream; and (2) development and testing of the geomorphically coupled, flow and sediment-transport model. Two key working hypotheses drive this model: (1) reach averaging removes all convective accelerations due to local irregularities in channel geometry and bed roughness from the problem and results in spatially averaged steady, uniform flow in the reach-averaged cross-section; and, (2) in the reach-averaged cross-section, the mass of each sediment size, including gravel, must be conserved between the bed and the flow, thus providing a direct coupling between the in-channel flow and sediment transport and the geometric response of the channel during floods. Since the Paria River is noted for its extremely high concentrations of suspended sediment (Beverage and Culbertson, 1964), the model includes the physical effects of density stratification due to the high density gradients that typically accompany high concentrations of sand-sized suspended sediment. Prior to its testing against Paria River data in Chapter 4, this model is tested first against the flume data of Kennedy (1961) and Guy and others (1966) and then the Rio Puerco data of Nordin (1963), i.e., the latter the highest suspended-sediment-concentration data set from a natural river for which velocity and sediment concentration profiles were measured.

Finally, since the hydraulic geometry of the Paria River is found to be stable in Chapter 2 indicating that no hidden trends should exist in data from the Paria River, and predictions from the flow and sediment-transport model are found to agree favorably with flume and river data in Chapter 3, the geomorphically coupled, flow and sediment-transport model is finally tested against data from the Paria River in Chapter 4. To this end, seven tests of model predictions against Paria River discharge, channel-geometry and suspended-sediment data are presented. Results from these tests show that the reach-scale mass conservation of each sediment size class between the bed and the flow adequately accounts

for the amount of cross-section enlargement and the amount of sediment in suspension during floods. Furthermore, results from these tests suggest that net lateral advective transport of sediment in a reach is geomorphically important only at high discharges and form drag from channel-scale features is important only at low discharges.

In synopsis, this dissertation is the first study to compile, thoroughly evaluate, and place in a rigorous physically based framework all of the hydrologic, channel-geometry, and suspended-sediment data from an ephemeral river said to have undergone the types of channel changes that compose the "arroyo problem". It is also the first successful attempt to develop and test a flow and sediment-transport model designed to investigate the adjustment of the channel of an ephemeral river during floods. This model successfully predicts the measured amount of channel enlargement during floods and indicates that the only flows that will significantly modify the cross-section shape of a channel are overbank floods. Since data presented in Chapter 2 show that overbank floods only occur 0.021% of the time, results from the geomorphically coupled flow and sediment-transport model show why the hydraulic geometry, not the local geometry, of the Paria River has been so stable over the last 120 years. Finally, this dissertation research illustrates that, in contrast to the assumptions of previous workers, decade-scale climatic variability in the southwestern United States, as inferred from regional tree-ring width data, has only a small impact on the hydrology, geomorphology, and long-term sediment-transport rates in ephemeral-river systems.

Chapter 2: HISTORICAL ANALYSIS OF HYDROLOGY AND CHANNEL GEOMETRY: THE CASE FOR MINIMAL CHANGE IN THE PARIA RIVER FROM 1872 TO 1996

Section 2.1: INTRODUCTION

The major goal of work presented in this chapter is the development of an empirical understanding, in a physically based framework, of the hydrology and fluvial geomorphology of the Paria River system. In this chapter, analyses of all hydrologic and channel-geometry data from the Paria River system are presented in the context of hydraulic geometry; these analyses fully address the nature of the hydrology and channel geometry of the river system from 1872 to 1996. This chapter is organized into six sections: (1) introduction; (2) brief description of the river system; (3) review of previous work on the Paria River system; (4) presentation and analysis of all 1923-1996 hydrologic data from the Paria River; (5) presentation and analysis of all modern and historical channel-geometric data from the Paria River system; and (6) presentation of modern channel geometries and analysis of historical channel-geometric changes in the context of a hydraulic geometry model developed for equilibrium reaches. In this study, an "equilibrium reach" is defined as a reach consisting of a stable alluvial channel and active floodplains, i.e., a reach with a channel and floodplains that have formed in the current hydrologic and sediment-transport conditions. Knowledge of both the long-term mean nature of the river system and the nature of any systematic change in the river system over time, as gleaned from work presented in this chapter, is a prerequisite to the correct formulation, application, testing, and intepretation of results of the geomorphically coupled flow and sediment-transport model developed in Chapter 3 and applied in Chapter 4.

Section 2.2: BRIEF DESCRIPTION OF THE RIVER SYSTEM

The Paria River has a drainage basin of 3730 km^2 and is located in southern Utah and northern Arizona; its headwaters are in the Pink Cliffs of Bryce Canyon National Park from which it flows 157 km south through alternating alluvial and bedrock canyon segments to the Colorado River at Lees Ferry, Arizona (Figure 2.1). It is an ephemeral stream dominated by large floods of short duration. At Lees Ferry, for the period of gage record, i.e., from November 22, 1923 through September 30, 1996, the mean instantaneous discharge was only 0.77 m^3/s, while the mean annual peak discharge was 88 m^3/s, the bankfull discharge was 90 m^3/s, and the largest flood had a peak discharge of 320 m^3/s. To further illustrate the flashy hydrology of the river, though it has a typical return period, the bankfull discharge was equaled or exceeded a total of only 135.3 hours

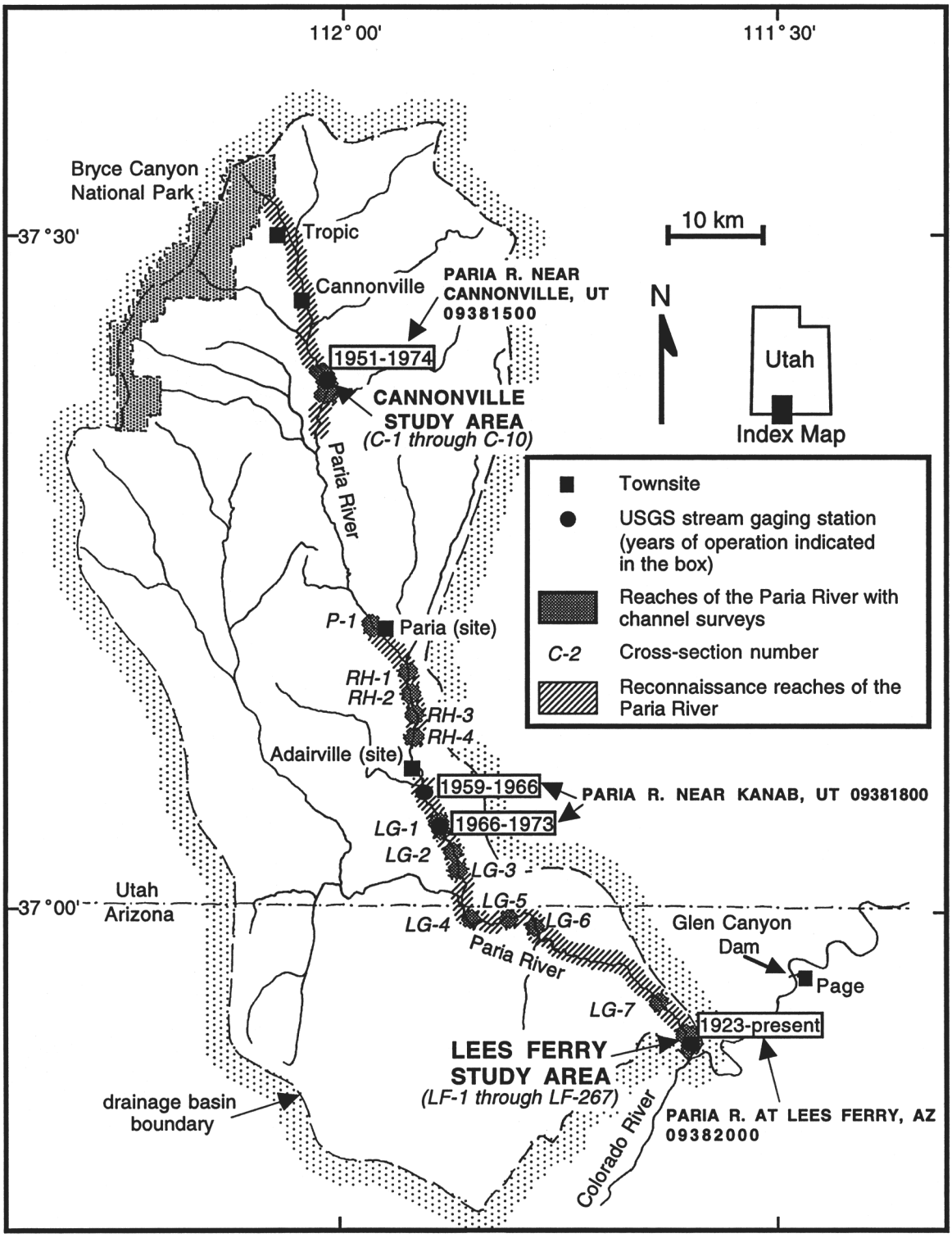

Figure 2.1: Map of the Paria River drainage basin.

in the 72.86 years of gage record, or 0.021% of the time. In addition to its highly variable hydrograph, the river is also noted for its high concentrations of suspended sediment and is the "birthplace" of the term "hyperconcentrated flow" (Beverage and Culbertson, 1964); indeed, the word Paria means "water-muddy" or "water-elk" in the Paiute language (Brian, 1992).

The Paria River is moderately steep, with reach-averaged slopes in excess of 0.008 in the uppermost alluvial reaches and slopes near 0.0035 in the lowermost alluvial reaches near its confluence with the Colorado River (Figure 2.2). The longitudinal profile of the river is fairly smooth (except for minor headcuts in alluvial reaches) regardless of whether the river is flowing through narrow bedrock canyons (the narrowest is only 3.6 m wide; Figures 2.2, 2.3a, & 2.3b) or through wider alluvial valleys. The only bedrock controls in the floor of the lower Paria River occur 20-25 km above the confluence with the Colorado River where the river has cut into the Kayenta Formation (Figures 2.2 & 2.3c). The only major nickpoint in the longitudinal profile occurs 15-20 km above the confluence with the Colorado River where the Paria has cut into the Chinle Formation, causing km^3-scale landslides of the overlying Glen Canyon Group to fill the valley (Figures 2.2 & 2.3d). Numerous lacustrine terraces occur upstream of the landslide dams.

For the alluvial reaches of the river, as the slope decreases in the downstream direction, the bankfull width decreases and the bankfull depth increases. In reaches of 0.008 slope, bankfull widths range from 70 to over 250 m and bankfull depths range from 0.7 to 1.1 m, while in reaches of 0.0035 to 0.004 slope, bankfull widths range from 20 to 40 m and bankfull depths range from 1.5 to 2.0 m. In all surveyed and reconnaissance reaches in the lower 130 km of the 157-km-long river, the floor of the channel is composed of a thin layer of sand, silt, and clay overlying gravel. In this portion of the river, the reach-averaged thickness of this sand, silt, and clay layer is never much more than about 10-15 cm, and the reach-scale average grain-size distribution of the underlying gravel is remarkably constant. Banks of the Paria River are composed of sand, silt, and clay and are lightly vegetated except in reaches that have been heavily colonized by non-native plants, such as tamarisk and Russian olive.

Though the valleys of the Paria River are largely uninhabited today, this was not the case in the late nineteenth century. As with most rivers in southern Utah in the late 1800's, alluvial reaches of the Paria River were intensely developed for agriculture, with complete allocation of water from the Paria River for irrigation. The potential influence of this intensive development of the river on the arroyo-type channel changes that occurred in the late 1800's and early 1900's cannot be ignored. Between 1865 and 1891, the valleys of

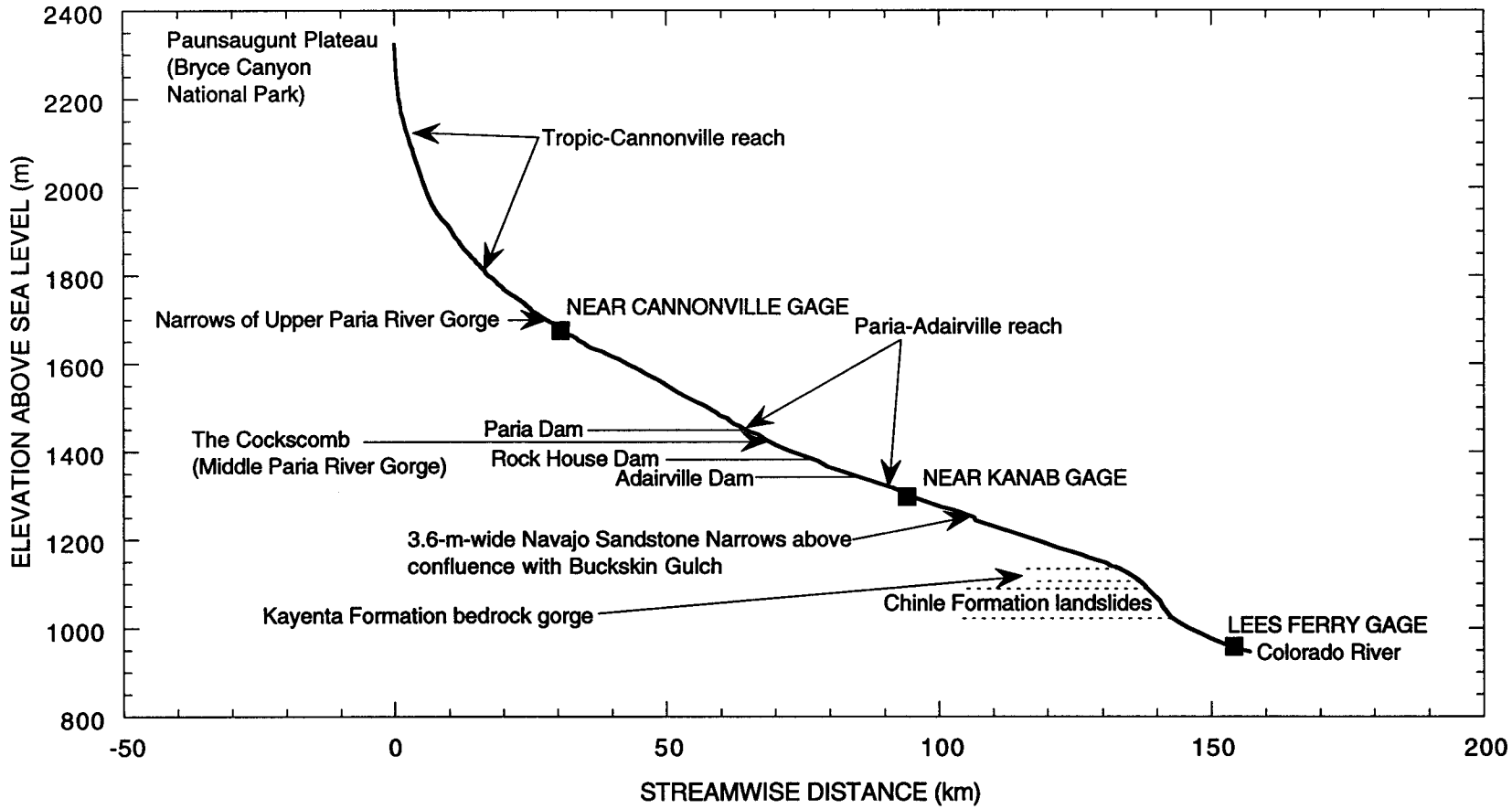

Figure 2.2: Longitudinal profile of the Paria River showing locations of the 3 USGS gaging stations and selected other features.

Figure 2.3: **(a)** Downstream view of the entrance to the narrowest portion of the Lower Paria River gorge. Photograph taken approximately 1 km above the confluence with Buckskin Gulch by D.J. Topping on April 11, 1995. **(b)** Upstream view of the bedrock narrows of the Paria River upstream from the confluence with Buckskin Gulch; narrowest portion of the canyon is 3.6 m at river level. Photograph taken by D.J. Topping on April 11, 1995.

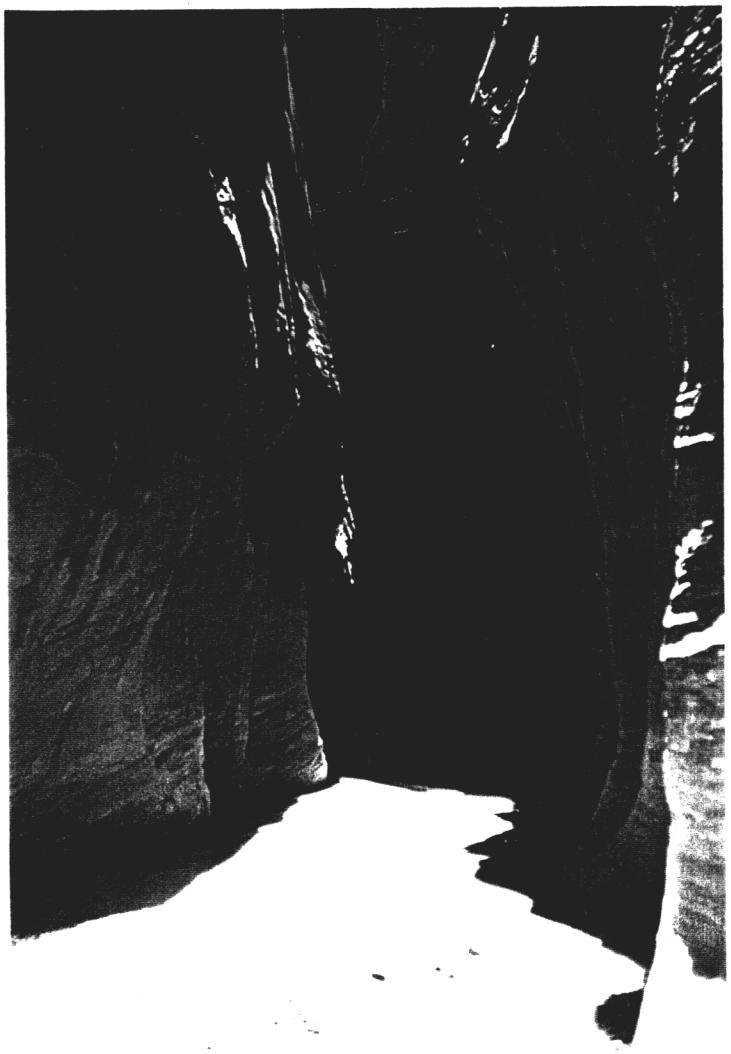

a)

b)

Figure 2.3 (continued): **(c)** Upstream view of bedrock control in the lower portion of the Kayenta Formation bedrock gorge. Camera position in UTM coordinates is approximately 4089650 m north and 435500 m east; photograph taken by D.J. Topping on April 14, 1995. **(d)** April 14, 1995 upstream view of the lower portion of the Chinle Formation landslide complex; the landslides are several hundred meters thick and extend for over 3 km upstream from this point. Camera position in UTM coordinates is approximately 4087950 m north and 440300 m east; photograph taken by D.J. Topping.

c)

d)

the Paria River were fully developed for agriculture and floods that caused the destruction of the irrigated farmland were not synchronous but followed the local initial development of irrigation by about 15 years (Gregory and Moore, 1931; Gregory, 1951).

The lower valley of the Paria River was first settled by Mormon pioneers in December, 1871, at Lees Ferry, AZ by John D. Lee and his family. To irrigate his fields, Lee built a large diversion dam on a meander of the Paria River 2 km above the confluence with the Colorado River. Because of problems with the stability of the channel at the dam site, with numerous dam wash outs, Lee's successor, Warren Johnson, built a new dam 1.6 km upstream in 1875. In about 1900, this dam was probably moved 1.6 km farther upstream, and a tunnel was dug through a portion of the bedrock wall of the canyon to aid in the diversion water from the Paria River to the fields at Lees Ferry (Rusho and Crampton, 1992; unpublished USGS gage technical notes, 1923).

The upper valleys of the Paria River were settled by Mormon pioneers in 1865 at Rock House, located 8.3 km below the future community of Paria (Figure 2.1). In 1871, the settlers at Rock House had diverted part of the Paria River and constructed 2.4 km of irrigation ditches. This settlement was subsequently abandoned in 1874 because of "trouble with the ditches," and the people moved upstream to found the new village of Paria (Gregory and Moore, 1931). In 1873, the community of Adairville was established 6.1 km below Rock House and a dam and 1.3 km of ditches were constructed. This village was abandoned in 1878 because "the water in dry years did not reach their farms," and its residents moved upstream to Paria (Gregory and Moore, 1931).

By 1877, Paria had grown substantially with agriculture occupying the entire floodplain. A large diversion dam had been constructed above the village and a 2.5 km-long ditch ran from the dam along base of the cliffs to the village. Irrigated fields lay between the ditch and the Paria River channel; this diversion also powered a grist mill and a sorghum mill in the village (Bailey and Burrill, 1877). The population of Paria reached a peak of 130 in 1884; however, large floods of unknown magnitude occurred in 1883 and 1884, washing away the irrigated fields on the floodplain and converting the narrow, meandering stream to a wide, straight wash, causing the ultimate abandonment of Paria in 1885. Initially, 12.2 km^2 of the floodplain were irrigated at Paria and all but about 0.2 km^2 were lost to the river as it straightened and widened (Gregory and Moore, 1931).

In the uppermost Paria River valley, the village of Cannonville was founded in 1875, Clifton in 1876, Henrieville in 1878, and Georgetown in 1886. All of these villages had extreme difficulty in controlling the intakes of irrigation ditches and maintaining the canals across the floodplains due to the highly variable flows in the river. Of the initial

20.3 km^2 of land under irrigation around Cannonville and Henrieville, 33% was lost to the Paria River during floods beginning in 1890 (Gregory and Moore, 1931). Since the water of the Paria was both fully allocated for irrigation by 1890 and somewhat unpredictable in quantity, the village of Tropic was developed above Cannonville in 1891 by virtue of importing water from the Sevier River via a ditch across the present day Bryce Canyon National Park (Gregory, 1951).

During the twentieth century, to monitor Paria River flows, the USGS has maintained as many as three gages simultaneously on the mainstem, one below Cannonville, UT from 1951 to 1974, one east of Kanab, UT from 1959 to 1973, and one near the confluence with the Colorado River at Lees Ferry, AZ from November 22, 1923 to the present. The gage near Cannonville was a continuous-stage-recorder gage from 1951 to 1955 and was reactivated as an annual-crest stage gage from 1959 to 1974. The gage near Kanab was only an annual-crest stage gage. The gage at Lees Ferry was initially a staff gage read several or more times a day by an observer; it became a continuous-recorder stage gage on September 12, 1929. Much of the large quantity of data presented and analyzed in this paper is from reaches of the Paria River in which these USGS stream gages are or were located.

Section 2.3: PREVIOUS WORK

Previous work on the Paria River can be divided into two categories, (1) work focused on observed channel-geometric changes in the late 1800's and early 1900's: Gregory and Moore (1931), Bailey (1935), and Gregory (1951); and (2) work focused on perceived hydrologic and channel-geometric changes in the early 1940's: Hereford (1983, 1986, 1987a, 1987b, 1989), W. Graf (1987), Andrews (1990), and J. Graf and others (1991). Research in category one was completed during the time of observed channel enlargement in the early part of the twentieth century and relied largely on direct observation of channel geometric change, while research in category two was initiated at least 40 years after the major channel geometric changes in the early 1940's were thought to have occurred and relied on indirect methodologies to reconstruct inferred channel geometric change.

Gregory and Moore (1931), Bailey (1935), and Gregory (1951) used a combination of field work in the Paria River valley during the time of channel enlargement and of research based on historical accounts of Mormon settlers to characterize changes in the Paria River channel during the early twentieth century. Gregory and Moore (1931) and Gregory (1951) concluded that a major cause of stream widening in the late 1800's and

early 1900's was the intensive development of the Paria River for irrigation. Bailey (1935) concluded that settlement and the resulting heavy denudation of the native plant cover were responsible for the geomorphic changes observed in the late 1800's and early 1900's since both entrenchment of alluvium and widening of channels were occurring only in areas that were heavily developed for irrigated farming and grazing about 10 years prior to the observed changes.

Based on field mapping of floodplains and terraces, stratigraphy of floodplain sections dated by tamarisk annual growth rings, repeat photography, and some analysis of the Paria River gage records and published annual-maximum flood series, Hereford (1983, 1986, 1987a, 1987b) determined that the channel of the Paria River had changed substantially beginning in about 1940 by the deposition of new floodplains on the floor of the wide channel that existed after channel enlargement in the late 1800's and early 1900's. Over the entire basin, Hereford (1987b) calculated that 4×10^7 m^3 of sediment were stored in post-1940 floodplains covering a total area of 20 km^2. Hereford (1986) concluded that: (1) post-1940 sediment accumulation in the Paria River valley was chiefly by vertical accretion without significant lateral migration of the channel; (2) post-1940 aggradation over the entire length of the Paria River was isochronous; and (3) the Paria River began to reincise the post-1940 alluvium during erosive floods in 1980. Specifically in the Lees Ferry reach, he found that, prior to 1939, the channel of the Paria River was wider than at present and lacked a floodplain; and, beginning in 1939, as new floodplains started to form, the hydraulic geometry of the channel at the gage changed through both channel-floor aggradation and channel narrowing. Hereford (1986, 1987a) attributed these changes in channel geometry to a change in climate on the Colorado Plateau in the early 1940's.

Using information from both repeat photography and seven cross-sections surveyed in the Paria River valley in the early 1980's, W. Graf (1987) determined that, in the upper 140 km of the Paria River valley, 1.97×10^7 m^3 of new floodplain alluvium had accumulated from 1943±5 to 1980. As these new floodplains were forming, Andrews (1990), by virtue of an analysis of the annual-maximum flood series at the Lees Ferry, AZ gage, determined that the mean annual flood of the Paria River decreased by about 50% in the early 1940's. Finally, J. Graf and others (1991) investigated the correlations of suspended-sediment load, flow volume, and flood characteristics at the Lees Ferry, AZ gage and estimated that the annual sediment loads in the Paria River decreased by about 67% in 1940 as the new floodplains started to form.

Section 2.4: PARIA RIVER HYDROLOGY

2.4a: Introduction

Since a complete understanding of the hydrology of the Paria River system over the past century is a prerequisite to correct interpretation of any changes in channel geometry or sediment transport that may have occurred, the first step in this study was the retrieval of all raw hydrologic data collected at the three USGS stream gages that have operated along the mainstem of the Paria River. This step was followed by: (1) a thorough evaluation of all of the measurements of stage and discharge from these three stations; (2) reconstruction of the instantaneous discharge time series for the period of November 22, 1923 through September 30, 1996 at Lees Ferry, AZ; (3) trend analyses of the annual flow volume, instantaneous discharge, flood-peak discharge, flood volume, and flood duration at Lees Ferry, AZ; (4) flood-frequency analyses of both the annual-maximum and partial-duration series at Lees Ferry, AZ; (5) flow-duration analyses at Lees Ferry, AZ; (6) analysis of the behavior of flood peaks traveling down the lowermost 127 km of the river, i.e., the segment of the river monitored by the three gaging stations; and (7) comparison of the flood-frequency distributions at the three stations. This portion of Chapter 2 presents the history of stream gaging on the Paria River, the type and quality of data collected at each gaging station, and a brief presentation of results from the analyses introduced above.

2.4b: History of stream gaging on the Paria River by the U.S. Geological Survey

As many as three stream gaging stations have been operated simultaneously by the U.S. Geological Survey on the mainstem of the Paria River, one below Cannonville, UT (station no. 09381500), one near Kanab, UT (station no. 09381800), and one above the confluence with the Colorado River at Lees Ferry, AZ (station no. 09382000) progressively located 30, 94, and 155 km below the headwaters of the river (Figure 2.1). Of these three stations, the Lees Ferry gage has the longest period of record, with 73 years, while the gages near Cannonville and Kanab have 21 and 15 years of record, respectively. The three gaging stations with the type and quality of data collected at each station are described in detail below.

2.4b-1: Lees Ferry, AZ - Station 09382000

The Lees Ferry, AZ gaging station was installed by the USGS on November 22, 1923 on a cliff on the right bank of the Paria River 2.4 km above the post-1909 low-water confluence with the Colorado River and 1.9 km above the post-1909 high-water confluence

with the Colorado River (Figure 2.4). As used in this paper, "post-1909 low-water confluence" refers to the location of the confluence of the Paria and Colorado Rivers during times of relatively low flow, i.e., discharges less than 1100 m^3/s, in the Colorado River; and, "post-1909 high-water confluence" refers to the location of the confluence of the Paria and Colorado Rivers during times of high flow, i.e., discharges greater than 1100 m^3/s, in the Colorado River. This original gage was a staff gage that was read by a local ranch resident twice daily during relatively steady flows and more frequently during floods such that a detailed graphical record of each flood could be constructed. After a meander cutoff that resulted in the abandonment of the channel near the gage during a flood on October 5, 1925, the staff gage was replaced on October 13, 1925 by a new staff gage (with a new datum) located 497 m downstream on the left bank against a cliff on the outside of a meander. On September 11, 1929, this second staff gage was ultimately replaced by a new continuous-recorder stage gage located 9 m upstream with a datum 0.046 m lower than the second staff gage. This continuous-recorder stage gage is still used today and consists of a stilling well containing a float on a cable assembly attached to a continuous stage recorder graph. Throughout this paper, the gage at the original location is referred to as "the 1923-1925 gage" and the gage at the second location is referred to as either "the post-1925 gage" or, simply, "the gage". In the fall of 1984, a system was installed to record river stages every 15 minutes and automatically transmit these stage data via satellite to the USGS Arizona District computer system.

1923-1996 discharge measurements

From November 1923 through September 1996, USGS personnel have made approximately 2670 discharge measurements to relate the measured stage at the gage to the fluid discharge in the river. (The terms "fluid discharge" and "discharge" are used interchangeably in this paper in reference to the discharge of water plus suspended-sediment; the term "sediment discharge" is used in reference to sediment discharge alone.) Of these measurements, all but nine were made by sounding the depths and measuring the mean or surface velocities across the channel with either a Price AA current meter or by the timing of floating debris; in this study, both of these types of measurements are termed standard discharge measurements. The other 9 discharge measurements are termed "float-area measurements" and were made by timing as little as one piece of floating debris down the center of the channel, assuming a vertical and lateral distribution of velocity in the channel, and surveying the cross-section area of the channel at a lower stage when it could be easily waded. Depending on both the validity of the assumed velocity distribution in the

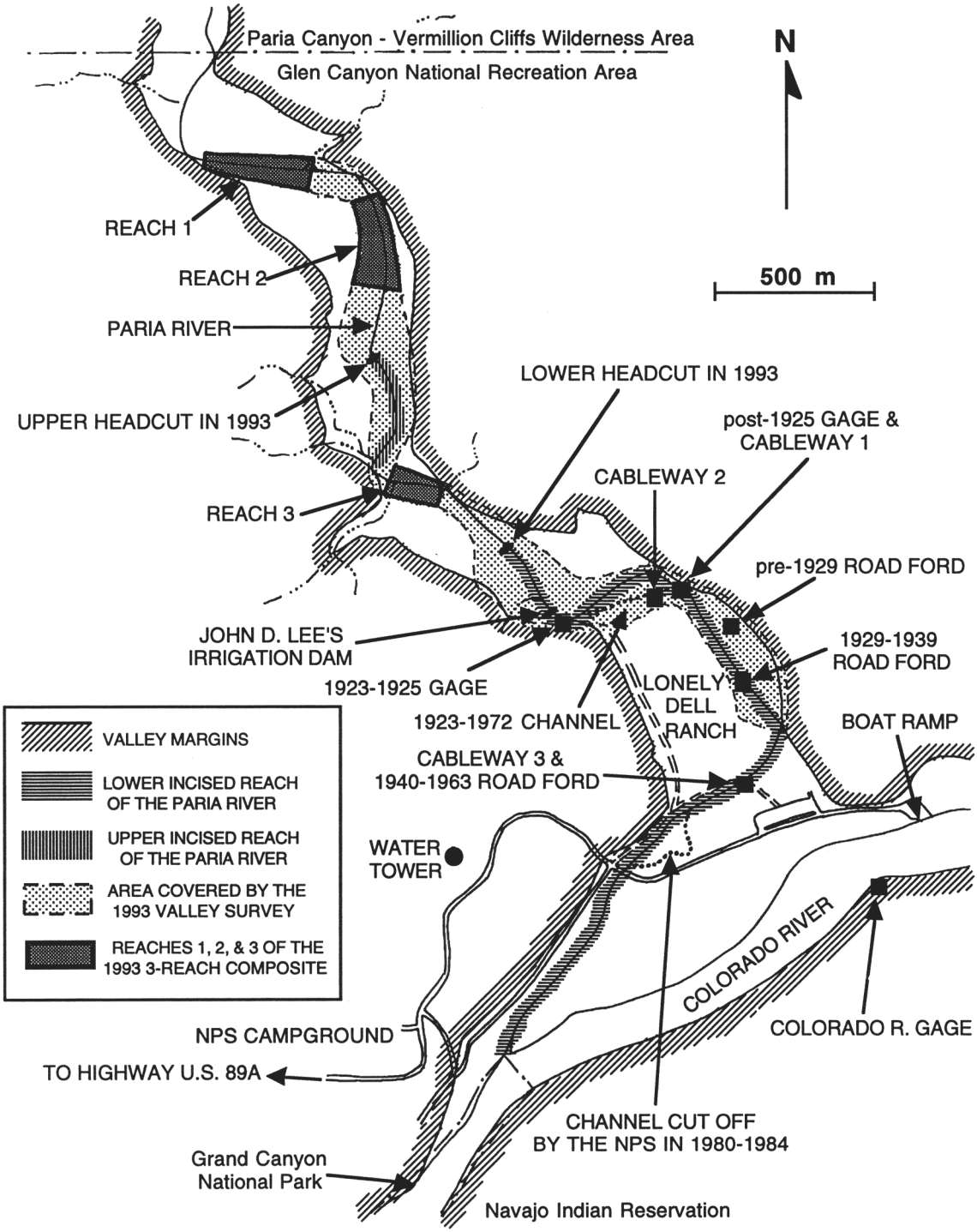

Figure 2.4: Map of the Lees Ferry, AZ study area.

channel and the amount of change in the channel cross-section area between the measurement times of float velocity and cross-section area, large errors can be obtained by the float-area method. Unfortunately, only 13 of the 2670 "direct" measurements of fluid discharge have been made at discharges over 40 m^3/s, and, of these, 5 are float-area measurements.

Discharge measurements during floods

Prior to 1947, measurement of discharge during floods was problematic and could only be achieved either by the float-area method or by wading with a Price AA current meter at the widest, shallowest cross-section on the river. To provide for measurements at higher discharges, on October 1, 1947, the USGS installed the first of three measurement cableways (Figure 2.4). This first cableway, termed "Cableway 1" in this study, was located 23 m above the gage at the apex of the meander at what was described by USGS technicians Johnson and Klohr on August 5, 1948, and Klohr on September 29, 1949, as a poor measuring section because of extreme channel curvature, irregular bed topography, and the tendency for debris to accumulate in the cross-section (unpublished USGS discharge measurement field notes, 1948, 1949). To facilitate better measurements, the cableway was moved to a position 82 m above the gage in April 1953 to a straight and slightly narrower reach (Figure 2.4).[1] This second cableway, termed "Cableway 2" in this study, collapsed during lateral channel migration sometime between February 24 and March 5, 1980, and was reinstalled in September 1984 at a location 0.7 km downstream of the gage near the site of an old road ford used from 1940 to 1963 (Figure 2.4); this third cableway is termed "Cableway 3" in this study.

These three cableways have made measurements at higher flows possible, but have not aided in the measurement of discharge during extreme events. With the exception of one flood (i.e., the flood of October 5, 1925 during which a poor float-area measurement was made), the highest flows on the Paria River have always been determined via indirect methods; and over most of the discharge range in the river, discharges have been calculated by interpolating along stage-discharge rating curves constructed from measured discharges below 20 m^3/s and indirectly determined flood peak discharges in excess of 200 to 300 m^3/s. Unfortunately, large, systematic, nonrandom errors in these rating curves are

---

[1]Analysis of a USGS air photo from October 8, 1952 (U.S. Geological Survey, 1952) indicates that the new cableway site was 25% narrower than the 1947-1953 cableway site at the bankfull level; the apparent change in width corresponding to the movement of the cableway was misinterpreted in Figure 11 of J. Graf and others (1991) as a decrease in channel width at one location.

present because methods for determining peak discharges have not been consistent through time, but rather have evolved over time and have only been relatively consistent at the Lees Ferry gage from September 1963 to the present.

The three different indirect methods used by the USGS to estimate peak flood discharges

Three very different methods have been used by the USGS to determine peak flood discharges. Prior to 1941, the USGS employed what is referred to in this study as the old-style slope-area method. This method consisted simply of: (1) surveying high-water marks and channel cross-sections down a reach of the river after a flood had receded; (2) determining the longitudinal slope of the water surface from the surveyed high-water marks; (3) determining the area and hydraulic radius for each cross-section; (4) assuming steady-uniform flow between each cross-section, assuming a roughness, and applying Manning's equation to determine the mean velocity in either each cross-section individually or the average of several cross-sections; and (5) determining the average discharge for the reach from the mean velocity and area for each cross-section and then averaging the discharge values for each cross-section. This method, because it excluded effects of nonuniform flow due to reach-scale expansions and contractions, consistently overpredicted peak discharges by 25 to 120% (as shown below in Section 2.4c-1). Thus, the old-style slope-area method discharge computations that were done following floods on September 13, 1927, August 2, 1929, September 8, 1929, September 13, 1939, September 6, 1940, September 14, 1940, and September 18, 1940 were all too high, as will be shown in Section 2.4c.

From 1941 to 1963, peak discharges on the Paria River were estimated indirectly by the differential method. This method involved determining the discharge of the Colorado River below the confluence of the Paria and Colorado Rivers and subtracting the discharge of the Colorado determined above the confluence at the Colorado River gage at Lees Ferry, AZ, thus backcalculating the discharge of the Paria River. (See Figure 2.32a below in Section 2.5a-3 for the location of the Colorado River gage.) To facilitate this method, on March 27, 1941, the USGS installed a staff gage 1.2 km below the post-1909 low-water confluence on the right bank of the Colorado, and a stage-discharge rating curve was developed for this staff gage using measured Colorado River discharges from the cableway above the confluence when the Paria River was low. Unfortunately, as the USGS determined in 1963, the stage-discharge relationship at the new staff gage on the Colorado River below the Paria was not stable because no stable hydraulic control existed in that reach. During floods on the Paria, large amounts of sediment transported into the

Colorado by the Paria would be deposited in the pool at the staff gage and thus significantly decrease the cross-section area of the Colorado River, adversely affecting the stage-discharge relationship such that the discharge in the Colorado below the Paria River appeared to be too high (unpublished USGS station analysis, 1963). Therefore, the backcalculated discharge determined for the Paria River by the differential method would be too high. USGS personnel first recognized this potential problem with the differential method during the Paria River flood of September 12, 1958, when 1.5 m of fill in the pool near the staff gage was observed (unpublished USGS annual technical file, 1958). The potentially larger magnitude of fill in this pool was later documented following a Paria River flood on August 23, 1992 (J. Graf and others, 1995). During Paria River floods in 1963, the USGS determined that this method overpredicted Paria River discharges by an unknown amount and discarded the method (unpublished USGS station analysis, 1963). The full magnitude of the error present in the differential method was never fully evaluated by the USGS, and the largest flood peak determined by this methodology, 538 m^3/s on September 12, 1958, was downgraded to 297 m^3/s merely by using stage-discharge ratings set by the old-style slope-area method. Peak discharges of the other floods determined by the differential method, however, were never reevaluated by the USGS; these floods, occurring on October 19, 1943, July 25, 1946, and August 24, 1946, defined the upper portions of the 1943-1963 stage-discharge rating curves. Calculations conducted as part of my study (using the Grand Canyon backcalculation method described below) show that: (1) the 1958 flood peak was no larger than 175 m^3/s, indicating that error in the differential method could be as high as +200% for extreme flood events; and (2) errors in the differential method for the lower discharge peaks of October 1943, July 1946, and August 1946 were found to be about +100%.

Finally, the flood of September 1, 1963 marked the first application of the modern slope-area method at the Lees Ferry, AZ gage on the Paria River. (This method was subsequently used to calculate the discharge for floods on September 18, 1963 and September 9, 1980 and, defines the upper end of the current rating curve in use by the USGS.) The modern slope-area method adequately incorporates the effects of flow nonuniformity in the computation of discharge and is described in detail in Dalrymple and Benson (1967). After applying this method to the September 1, 1963 flood, USGS technicians found that this calculation produced a major shift in the rating curve previously defined mainly by both the differential and old-style slope-area methods; however, no attempt was made to correct the previous discharge records by recomputing discharges for the old slope-area surveys with the modern method. Thus, the published discharge record

for the Paria River, like that of most ephemeral rivers in the southwestern United States, includes large systematic, nonrandom errors that reflect improvements over time in techniques used by the USGS to estimate peak flood discharges.

Suspended-sediment and bed-sediment measurements

Lees Ferry, AZ has also been a long-term USGS suspended-sediment and bed-sediment sampling station; these measurements will be presented in detail in Chapter 3. From October 1, 1947 through September 30, 1976, quasi-daily suspended sediment samples were collected at this site; a subset of this data set, 145 samples collected from July 7, 1954 through September 26, 1976 were analyzed by the USGS for the distribution of sediment grain sizes. Another quasi-daily set of 81 suspended sediment samples was collected from July 1, 1983 through December 12, 1983 by the USGS and analyzed for grain-size distribution by the Bureau of Reclamation (Garrett and others, 1993). In addition to the suspended-sediment data, from 1958 to 1971, 21 samples of bed material were collected at this site and analyzed for grain size by the USGS.

2.4b-2: Near Cannonville, UT - Station 09381500

The near Cannonville, UT gaging station was installed by the USGS in December, 1950 on a cliff on the left bank of the Paria River 12 km below the village of Cannonville, UT. From December, 1950 through September 1955, this gage was a continuous-recorder stage gage similar to that at Lees Ferry, consisting of a stilling well, float assembly, and continuous stage recorder graph. Between December 29, 1950 and October 5, 1955, the USGS conducted 81 wading discharge measurements in the reach near this gage with the highest being at a discharge of only 2.78 m^3/s. Three modern slope-area method computations were completed following floods on May 18, 1951, August 3, 1951, and September 21, 1952. A final wading discharge measurement was made at the highway bridge 7.4 km above the gage on October 25, 1957. This gage was discontinued as a continuous-recorder stage gage in October 1955 and replaced in 1959 with an annual-crest stage gage at the same location and datum; the gage was removed in 1974. Annual-crest stage gages record only the stage of the largest flood of the year and, since no clock is present in these gages, unlike continuous-recorder stage gages, witnesses must identify the date of the flood. Thus, some error may be associated with the dates of floods recorded by annual-crest gages. Also, on July 14, 1958, the grain-size distributions of one bed sample of gravel and one bed sample of sand, silt, and clay were analyzed at the near Cannonville gage (Iorns and others, 1964).

2.4b-3: Near Kanab, UT - Station 09381800

The near Kanab, UT gaging station was installed by the USGS on July 31, 1959 at the new highway bridge on U.S. highway 89 east of Kanab, UT and west of Page, AZ. Throughout its period of record, this gage was operated as an annual-crest gage only. Because the alluvial channel at the highway bridge was laterally unstable, in 1966, the gage was moved to a new location 6 km downstream on the left bank against a cliff in a stable bedrock-walled reach. The lower portion of the stage-discharge relation at this gage was defined by several discharge measurements each year. At lower flows, discharge measurements were made by wading in the reach near the gage and, at higher flows, discharge measurements were made from the highway bridge. The highest portion of the stage-discharge relation was extrapolated from a curve drawn through the low-flow discharge measurements and through several modern slope-area discharge computations made at discharges near 30 m^3/s. This gage was removed in 1974.

2.4c: Methodology for discharge recomputation

2.4c-1: Lees Ferry, AZ

The first step in construction of an instantaneous discharge record for the Paria River at Lees Ferry, AZ was to retrieve all available USGS data for the gage from: the Arizona District offices in Flagstaff and Tucson, AZ and the Federal Records Centers in Lakewood, CO and Laguna Niguel, CA. These data consisted of: (1) USGS gage observers' notebooks from November 22, 1923 through September 30, 1934; (2) the gage construction report from September 1929; (3) annual gage technical files and station histories from 1924 through 1992; (4) stage recorder graphs from September 11, 1929 through September 30, 1984 (recorder graphs from October 1, 1975 through September 30, 1977 were not found); (5) 15-minute stage measurements from October 1, 1984 through September 30, 1996; (6) 2670 USGS discharge measurement field notes from discharge measurements made from November 11, 1923 through October 4, 1996; and (7) slope-area channel surveys following floods on October 5, 1925, September 13, 1927, August 2, 1929, September 8, 1929, September 13, 1939, September 6, 1940, September 6, 1940, September 14, 1940, September 18, 1940, September 1, 1963, September 18, 1963, and September 9, 1980.

The second step in construction of an instantaneous discharge record involved checking all of the retrieved data for errors and converting the discharge measurements to a standard format. Given that a velocity profile is quasi-logarithmic in shape in steady, uniform flow, the mean velocity in the vertical will occur at approximately 40% of the flow

depth. Since velocities measured at depths other than at 40% of the flow depth, e.g., surface velocities, were sometimes used by the USGS to compute discharges of the Paria River, some of the discharges in the 2670 discharge measurement data set needed to be recomputed to be compatible with the rest of the data set. This was accomplished by converting velocities measured at anything other than 40% of the flow depth to velocities at 40% of the flow depth by assuming a quasi-logarithmic velocity profile constructed from the 2-part eddy viscosity of Rattray and Mitsuda (1974).

Following retrieval of the data and checking for errors, the third step was to convert all of the analog measurements into a digital format. This involved: (1) entering all measurements of stage, discharge, channel geometry, and water temperature as a function of time from the 2670 discharge measurement field notes into an ascii computer file; (2) entering the 3552 observations of river stage as a function of time from the gage observers' notebooks for the period from November 22, 1923 through September 11, 1929 into an ascii computer file (this exercise also involved using a digitizing table to digitally record information from the graphical sketches of gage height during floods found in these notebooks); (3) digitizing 394431 stage measurements as a function of time from the stage-recorder graphs for the period from September 11, 1929 through September 30, 1984 to characterize information on these charts at 10-minute precision in time and 3 mm precision in stage; and (4) converting all of the surveyed channel topography and high-water elevation measurements from the USGS slope-area surveys into a single Cartesian coordinate system.

After the four preliminary steps listed above, construction of the instantaneous discharge record involved five final steps: (1) computation of statistically significant stage-discharge rating curves for the discharge range covered by the standard and float-area measurements during the period of gage record; (2) reevaluation of peak discharge of the largest floods during the period of record with redundant modern methods to remove trends in the stage-discharge relation caused by the evolving methods described in Section 2.4b-1; (3) recomputation through inclusion of stage-discharge information from all discharge measurements and recomputed flood peaks of new stage-discharge rating curves for the discharge range covering the entire range of flows during the period of gage record; (4) applying stage shifts as a function of time to the computed stage-discharge rating curves for the period of record; and, finally, (5) computation of instantaneous discharge for the entire period of record. Detailed description of my methodology to reconstruct the instantaneous discharge record at Lees Ferry, AZ is the subject of a forthcoming manuscript and only the summary is included below.

The three initial stage-discharge rating curves

Because of large shifts in the bed elevation at the Lees Ferry gage, the USGS has used more than 20 different stage-discharge rating curves over the period of gage record. Very few of these curves have any statistical significance, especially in the higher discharge portions, since very few discharge measurements are made at higher discharges. To construct an accurate instantaneous discharge record, it was desirable to improve the accuracy of the stage-discharge relations by first removing the effect of the bed-elevation changes on the stage, and then collapsing as much of the stage-discharge data onto as few stage-discharge rating curves as possible. This was possible because the shape of the cross-section at the post-1925 gage has been relatively stable over much of the period of record independent of changes in bed elevation until the passage of a headcut by the gage on August 14, 1972 (see Figure 2.27 in Plate 1 below in Section 2.5a-3).

The first step in the construction of these three stage-discharge rating curves was to subtract the minimum bed elevation from the stage of each non-ice affected, standard and float-area discharge measurement, thus relating each measured discharge to ε, i.e., the river stage minus the bed stage. Bed stage as a function of time was defined both from measurements of the point of zero flow at the gage and also from minimum river stage as recorded in the gage observers' notebooks and stage-recorder graphs. Finally, three regressions of the form $Q = (a\varepsilon)^b$, where a and b are regression constants, were fit to data from : (1) the 1923-1925 gage for the period November 22, 1923 to October 5, 1925; (2) the post-1925 gage for the period from October 5, 1925 to August 14, 1972; and (3) the post-1925 gage for the period from August 15, 1972 to September 30, 1996.

Because the highest discharge measurement in each of the three periods was made at a discharge less than bankfull, discharges for overbank flows still needed to be determined to adequately define the final stage-discharge rating curves for the entire range of discharges in each of the three time periods; these three final stage-discharge rating curves are determined below. Thus, peak discharges for the nine largest events and five smaller floods during the period of gage record were determined by as many as three different methods, such that the results for each flood-peak discharge recomputation could be independently confirmed (Table 2.1). These three methods are the Grand Canyon backcalculation method, the step-backwater method, and the superelevation method.

Grand Canyon backcalculation method

The Grand Canyon backcalculation method, first presented by Topping and Smith (1993), was used to determine peak discharges for floods occurring on 10-5-25, 9-13-27,

Table 2.1: Flood rankings with past and present methodologies of peak-discharge determination for the ten largest Paria River floods of the 20th century.

FLOOD RANK	FLOOD RANK DURING PERIOD OF GAGE RECORD	DATE OF FLOOD PEAK	USGS PUBLISHED PEAK DIS. (m^3/s)	METHOD USED BY USGS FOR DETER-MINING PEAK DIS.	PEAK DISCHARGES DETERMINED BY METHODS USED IN THIS STUDY			**VALUE USED IN THIS STUDY (m^3/s)**
					GRAND CANYON BACK-CALC. (m^3/s)	STEP-BACK-WATER (m^3/s)	SUPER-ELEV-ATION (m^3/s)	
1	---	1st week of Sept. 1909	---	---	---	---	---	**400***
2	1	Sept. 13, 1927	405	OLD S-A	320	320	---	**320**
3	2	Sept. 6, 1940	396†	OSA EX	310	310	330	**310**
4	3	Oct. 5, 1925	456§	S-FLOAT	270	270	230	**270**
5	4	Sept. 9, 1980	241	S-A	240**	240	---	**240**
6	5	Aug. 2, 1929	340	OLD S-A	210	210	---	**210**
7	6	Sept. 1, 1963	202	S-A	200	200	210	**200**
8	7	Sept. 13, 1939	278	OLD S-A	180	180	190	**180**
9	8	Sept. 12, 1958	538††	DIFF	175	---	---	**175**
10	9	Aug. 8, 1932	297	RATING	160	---	---	**160**

Notes:

OLD S-A = Old-style slope-area computation
OSA EX = Extrapolation based on old-style slope-area method computations
S-FLOAT = Float-area computation based on a single float velocity
S-A = Modern slope-area method
DIFF = Differential method
RATING = Rating-curve extrapolation

* This value was determined from extrapolation of Ratings A & B based on descriptions of the flood by Jerry Johnson (as described in the text).

† After surveying the channel near the gage, USGS personnel determined that "impossible conditions" (unpub. USGS gage tech. file, 1940) existed in the reach above the gage for a slope-area computation and calculated this peak by extrapolating the rating curve based on peak discharges determined by the old slope-area method for floods on 9-13-39, 9-14-40, and 9-18-40.

§ In computing this discharge, a single float (surface) velocity of 5.1 m/s measured by Jerry and W.E. Johnson in the center of the channel was used as the only basis for determining the mean velocity for both the channel and overbank portions of the flood (unpub. USGS discharge measurement field notes, 1925).

** This value was backcalculated from Colorado River discharges using the wave model of Wiele and Smith (1996).

†† The discharge of this peak was later downgraded by the USGS to 326 m^3/s.

8-2-29, 8-8-32, 9-13-39, 9-6-40, 9-1-63, and 9-18-63. A modified version of this method applying the model of Wiele and Smith (1996) was used to determine the peak discharge for the flood on 9-9-80. By conserving the mass of water in the Grand Canyon, the Grand Canyon backcalculation method simply involves, for a fixed time period, determining the volume of water passing the Colorado River gage near Grand Canyon, AZ and, after correcting for appropriate travel times between gages, subtracting the volumetric input of water from the Colorado River at Lees Ferry, AZ, the ungaged spring inflow in Marble and upper Grand Canyons, and the Little Colorado River to backcalculate the volume of water being added by the Paria River during a flood (Figure 2.5). Once the volume of water added by the Paria River is known, the overbank portion of the Paria River stage-discharge rating curve is determined by shooting for the correct volume.

In the three paragraphs below, the Paria River flood of September 6, 1940 is used to illustrate the five steps of the Grand Canyon backcalculation method (Figure 2.6). **(STEP 1)** For the time period bracketing the Paria River flood, instantaneous discharge at the Colorado River gages near Grand Canyon and at Lees Ferry, the Little Colorado River gage at Grand Falls, and Moenkopi Wash gage near Tuba City (Figure 2.5) are reconstructed by digitizing the instantaneous stage data from the stage-recorder graphs and applying the stage-discharge rating curves and shifts used during this time period by the USGS. (After 1946, combined instantaneous discharges of the Little Colorado River and Moenkopi Wash were computed from records of the Little Colorado River gage near Cameron, thus simplifying this step.) **(STEP 2)** Initial and final times of integration at the Colorado River gage near Grand Canyon gage are chosen such that: (a) these times bracket the passage of the flood wave originating from the Paria River, (b) flows in the Colorado River at the near Grand Canyon gage are steady, and (c) the flows at the upstream gages on the Colorado River at Lees Ferry, Paria River at Lees Ferry, Little Colorado River at Grand Falls, and Moenkopi Wash near Tuba City are all steady at the initial and final times of integration at the Colorado River near Grand Canton gage minus the discharge travel times from each gage to the near Grand Canyon gage. (Appropriate discharge travel times to the Colorado River gage near Grand Canyon from each upstream gage were determined empirically for the complete discharge range at each site.) **(STEP 3)** The volume of water passing the Grand Canyon gage for the time period bracketing the Paria River flood is then computed by integrating discharge with respect to time from the chosen initial to final times of integration (Figure 2.6a).

Initial and final times of integration, $t_{initial}$ and t_{final}, for the September 6, 1940 Paria River flood at the Colorado River gage near Grand Canyon were chosen as 13:41 on

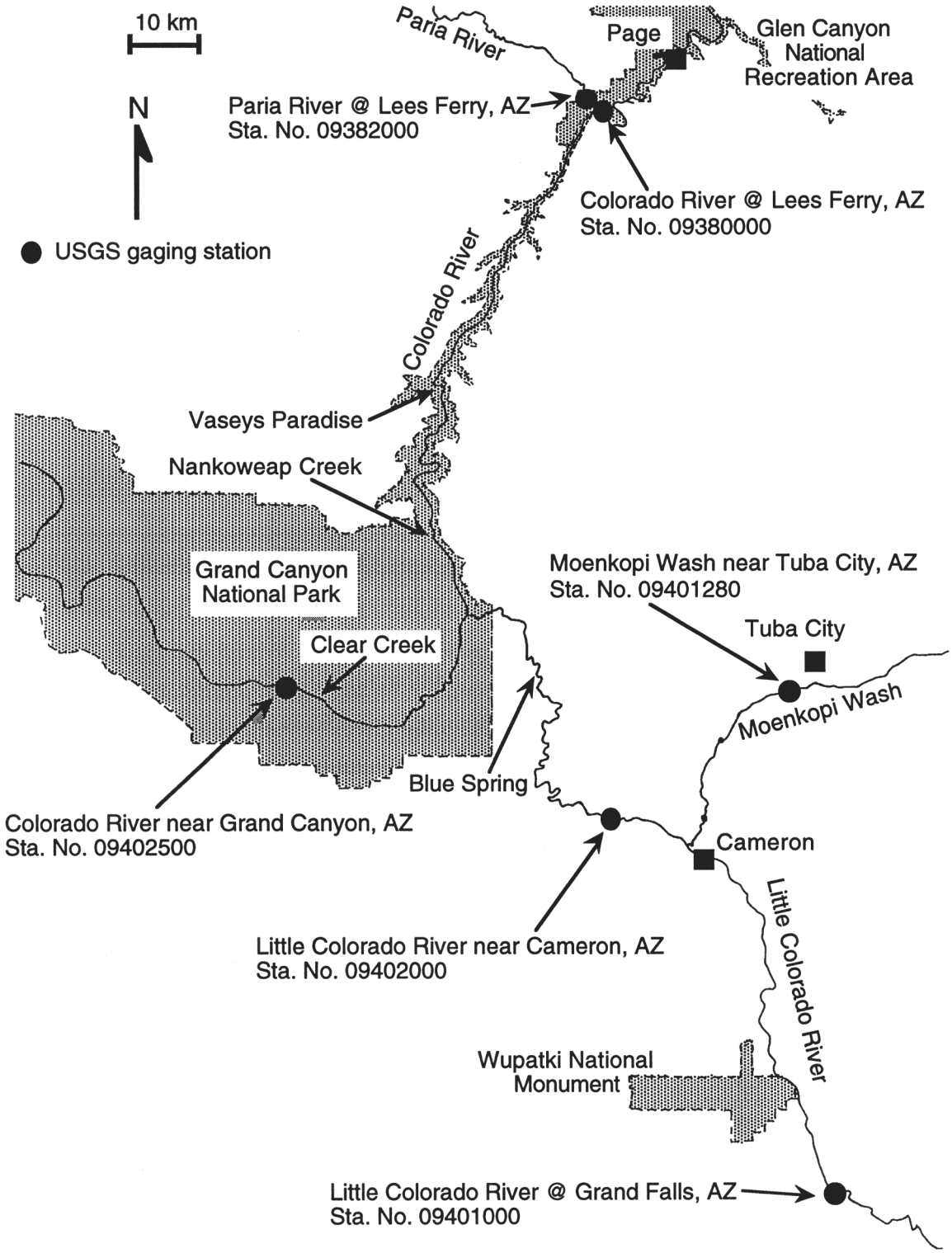

Figure 2.5: Map of the eastern Grand Canyon region showing the locations of the USGS gages used in the Grand Canyon backcalculation method.

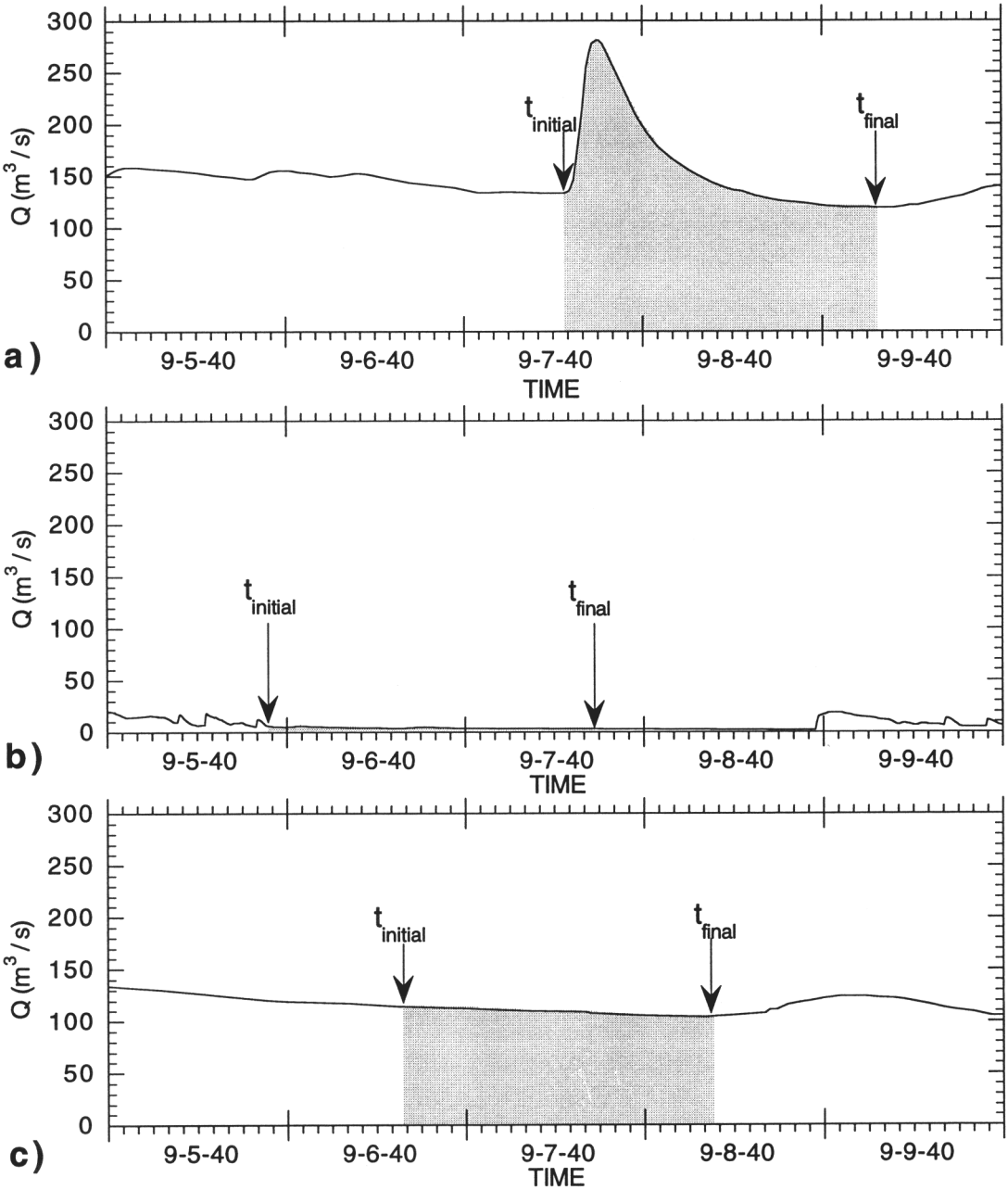

Figure 2.6: **(a)** Instantaneous discharge at the Colorado River near Grand Canyon, AZ gage for the time bracketing the September 6, 1940 Paria River flood (region of integration is shaded). **(b)** Instantaneous discharge at the Little Colorado River at Grand Falls, AZ gage for the time bracketing the September 6, 1940 Paria River flood (region of integration is shaded). **(c)** Instantaneous discharge at the Colorado River at Lees Ferry, AZ gage for the time bracketing the September 6, 1940 Paria River flood (region of integration is shaded).

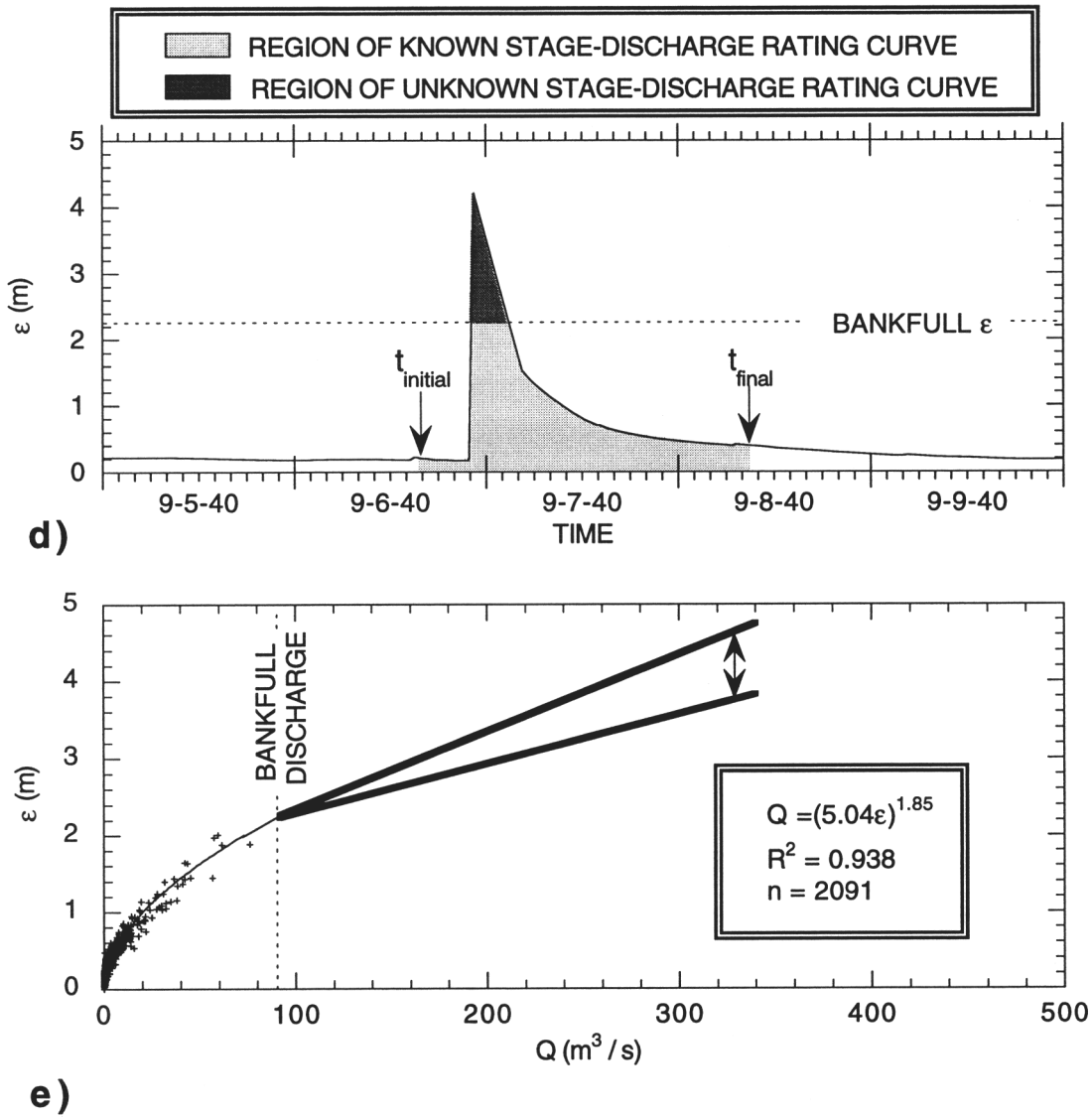

Figure 2.6 (continued): **(d)** Instantaneous stage at the Paria River at Lees Ferry, AZ gage for the time bracketing the September 6, 1940 Paria River flood showing the region of the "known stage-discharge rating curve" below bankfull stage and the region of the "unknown stage-discharge rating curve" above bankfull stage. **(e)** Initial stage-discharge rating curve for the Paria River used in step 4 of the Grand Canyon backcalculation method; the "known stage-discharge rating curve" shown by the solid thin line is fixed by the 2091 discharge measurements made at discharges below bankfull; the "unknown stage-discharge rating curve" shown by the solid thick line is the linear extension of the "known stage-discharge rating curve" and is iteratively determined by the shooting method (schematically indicated by the double arrow).

9-7-40 and 7:26 on 9-9-40 resulting in a calculated water volume of 2.41×10^7 m^3 passing this site (Figure 2.6a). Given that the independently determined discharge travel time from both the Little Colorado River at Grand Falls and Moenkopi Wash near Tuba City gages to the Grand Canyon gage is similar at approximately 40.08 hours, 21:36 on 9-5-40 and 15:22 on 9-7-40 were chosen for the initial and final times of integration, respectively, resulting in a calculated water volume input of 6.21×10^5 m^3 from the Little Colorado River and 2.71×10^4 m^3 from Moenkopi Wash (Figure 2.6b). Since the independently determined discharge travel times from the gages on the Colorado and Paria Rivers at Lees Ferry to the Colorado River gage near Grand Canyon are equal at 22.08 hours, 15:36 on 9-6-40 and 9:22 on 9-8-40 were chosen as the initial and final times of integration, respectively (Figures 2.6c & 2.6d). Discharge of the ungaged spring inflow below these gages and above the Grand Canyon gage, i.e., discharge mainly from Blue Spring, Vaseys Paradise, Nankoweap Creek, and Clear Creek (Figure 2.5), was determined by subtracting the cumulative discharge of Moenkopi Wash, the Little Colorado River, the Colorado and Paria Rivers at Lees Ferry from the discharge of the Colorado River near Grand Canyon for the chosen beginning and ending times of integration at each gage. For the time period of the 1940 Paria River flood, the ungaged spring inflow was calculated by this method to be a constant 12.7 m^3/s resulting in a cumulative volume of 1.91×10^6 m^3. Since the volume input by the Colorado River at Lees Ferry was 1.64×10^7 m^3, the backcalculated volume of water input by the Paria River was found to be 5.14×10^6 m^3.

(STEP 4) After the backcalculated volume of Paria River water is known, the overbank portion of the Paria River stage-discharge rating curve, i.e. the "unknown stage-discharge rating curve" in Figures 2.6d & 2.6e, is computed by iteratively shooting for the rating curve that computes discharges that integrate to the correct volume of water (Figures 2.6d & 2.6e). For the 1940 example, in each iteration, the stage-discharge rating curve for discharges less than bankfull, i.e. the "known stage-discharge rating curve" in Figures 2.6d & 2.6e, was fixed by regression through the 2091 ice-free standard and float-area discharge measurements made from November 1925 to August 1972. The overbank portion of the stage-discharge rating curve was determined by iteratively shooting for the linear extension of the rating curve required by conservation of mass so that the integrated volume of water passing the Paria River gage from the initial to final times of integration equaled that backcalculated from the other gages, specifically 5.14×10^6 m^3. **(STEP 5)** Finally, a peak discharge for the flood can be determined from the overbank extension of the stage-discharge rating curve that satisfies conservation of mass among the gages. For

the September 6, 1940 flood, a peak fluid discharge of 310 m^3/s was calculated by this method (Table 2.1).

Step-backwater method

The second method for determining Paria River peak discharges, the step-backwater method, consists of a modified version of the standard step-backwater computation described by Chow (1959). This method was used to calculate peak discharges for Paria River floods with USGS slope-area channel surveys, i.e., floods on 10-5-25, 9-13-27, 8-2-29, 9-8-29, 9-13-39, 9-6-40, 9-14-40, 9-18-40, 9-1-63, 9-18-63, and 9-9-80. The step-backwater method used in this study iteratively shoots for a discharge that produces the best agreement between the calculated water-surface profile and the surveyed high-water marks in the reach. Because all Paria River flows in reaches surveyed for slope-area measurements were subcritical, solution of the standard step-backwater energy equation is accomplished in the upstream direction, ultimately marching upstream in a stepwise fashion through all of the surveyed cross-sections. A modification to the step-backwater method used in this study uses the roughness parameter, z_0, instead of the standard Manning's n to characterize roughness in the channel. The rationale for making this modification is discussed below.

The standard step-backwater energy equation that is solved from cross-section to cross-section is:

$$H_{up} = H_{dn} + H_{v\text{-}dn} + h_{\Delta} - H_{v\text{-}up}, \tag{2.1}$$

where H_{up} is the elevation of the water surface at the upstream cross-section, H_{dn} is the elevation of the water surface at the downstream cross-section, $H_{v\text{-}dn}$ is the velocity head at the downstream cross-section and is equal to the square of the mean velocity in the downstream cross-section divided by the acceleration of gravity, $H_{v\text{-}up}$ is the velocity head at the upstream cross-section and is equal to the square of the mean velocity in the upstream cross-section divided by the acceleration of gravity, and h_{Δ} is the head loss between the two cross-sections and is set equal to h_f+h_s, i.e., the friction loss plus the shock loss. As is the convention, for expanding reaches, the shock loss, h_s, is defined as $(H_{v\text{-}up} - H_{v\text{-}dn})/2$ and, for contracting reaches the shock loss is set equal to 0. The friction loss, h_f, between the two cross-sections is calculated as the mean of the frictional slopes for steady, uniform flow at each of the two cross-sections divided by the longitudinal distance between the two cross-sections. Since Manning's equation is not used in this particular step-backwater model, the friction loss cannot be solved analytically but must be

calculated by shooting for the frictional slope at each cross-section that produces the input discharge.

The roughness parameter, z_0, was chosen to characterize bed roughness because it has greater physical meaning than Manning's n, i.e., z_0 can be directly related to the gravel grain-size distribution present on the bed and is unaffected by flow depth relative to particle size. Manning's n is difficult to use because it cannot be directly related to a fixed length scale on the bed, and it varies significantly with changes in flow depth relative to a fixed bed grain-size distribution (Wiberg and Smith, 1991; Wiele and Smith, 1996). For example, the Manning's n for a 3-m deep flow over 10-cm diameter particles is considerably lower than the value of Manning's n for a 0.5-m deep flow over 10-cm diameter particles, while z_0 does not depend on flow depth and would be the same for both cases (Wiberg and Smith, 1991).

To determine the mean velocity at each iteration in each cross-section, the mean velocity multiplied by the depth at closely spaced verticals is integrated across the channel and divided by the cross-section area. The vertically averaged mean velocity, $\langle u \rangle$ at each vertical is found by the relationship:

$$\langle u \rangle = \frac{\sqrt{ghS_f}}{k} \ln\left(\frac{0.48h}{z_0}\right), \tag{2.2}$$

where g is the acceleration of gravity, h is the local flow depth at each vertical, S_f is the frictional slope, ρ is the density of water, and k=0.408 is von Karman's constant as determined by Long and others (1993). The constant 0.48 is the analytically determined constant for a quasi-logarithmic velocity profile constructed using the 2-part eddy viscosity of Rattray and Mitsuda (1974); for purely logarithmic profiles, the appropriate constant would be 0.37 (Wiberg and Smith, 1991). For low transport stages, that is, transport stages less than or equal to 2.0 in the thalweg, z_0 was set equal to $0.1D_{84}$, where D_{84} is the 84th percentile grain size in a coarsening sense, as found by Dietrich and Whiting (1989), Wiberg and Smith (1991), and Pitlick (1992). Since the mean value of D_{84} in the Lees Ferry reach of the Paria River is 10 cm, z_0 for low transport stages was set equal to 1 cm. Transport stage is defined as the boundary shear stress divided by the critical shear stress for D_{50}. For transport stages from 2.0 to 3.5, z_0 was set equal to $0.5D_{84}$ as indicated by the measurements of Pitlick (1992). This higher roughness is interpreted to result from the breakup of the stable gravel pavement on the floor of the channel and the initiation of gravel bedforms at these higher transport stages.

Figure 2.7 compares the peak discharges determined by the various methods of the USGS to those predicted by the modified step-backwater method for all of the floods for

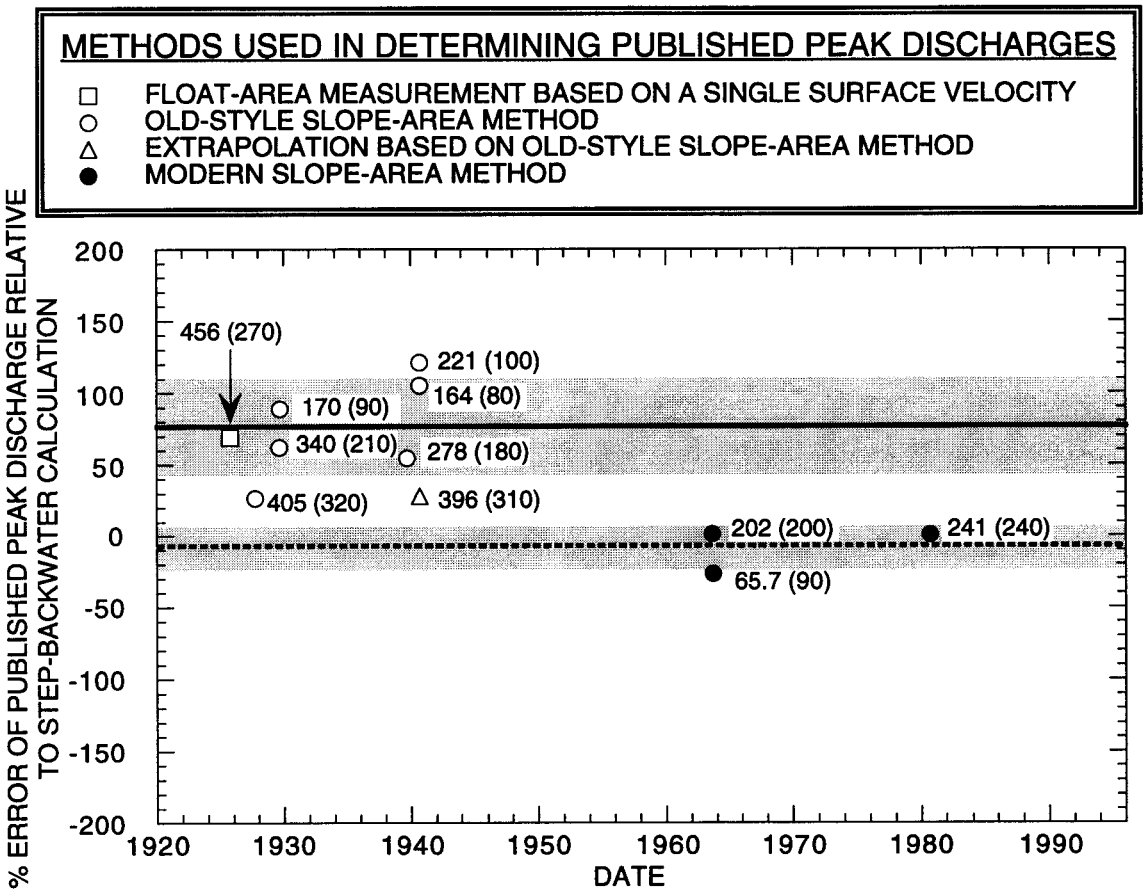

Figure 2.7: Percent error of the USGS published peak flood discharges of the Paria River at Lees Ferry, AZ (determined by various methods) relative to peak flood discharges calculated by the step-backwater method; values in parentheses are the flood peak discharges computed by the step-backwater method; values outside parentheses are the published flood peak discharges; solid thick line indicates the mean percent error of the old-style slope-area method relative to the step-backwater method; dotted thick line indicates the mean percent error of the modern slope-area method relative to the step-backwater method; shaded areas indicate the regions within one standard deviation of the mean percent error associated with either the old-style or the modern slope-area methods relative to the step-backwater method.

which slope-area channels surveys are available. The solid thick line and surrounding shaded region indicates the mean ± 1 standard deviation percent error of the old-style slope-area method relative to the step-backwater method; the dotted thick line and surrounding shaded region indicates the mean ± 1 standard deviation percent error of the modern slope-area method relative to the step-backwater method. The main source of error in the old-style slope-area measurements is not the choice of roughness, but, rather, the exclusion of the effects of the expansions and contractions on the head loss through a reach. This exclusion neglects both velocity-head terms and the shock-loss term in equation 2.1 making the energy slope equal to the frictional slope through a reach, a condition that exists only for steady, uniform flow. As is obvious in Figure 2.7, this exclusion has a greater impact on the calculated results for the lower discharge floods. These lower discharge floods are characterized by relatively more nonuniformity in flow, that is, the expansions and contractions in cross-section area are larger with respect to the mean cross-section area.

Superelevation method

The third and simplest method for determining Paria River peak discharges is the superelevation method. This method calculates the mean velocity of the river passing the post-1925 gage by relating the mean velocity in the cross-section to the superelevation of the water surface across the meander. The key assumptions used in the superelevation method are that the flow was both steady and uniform in the streamwise direction while the high-water marks were created by the flood. Superelevation of the water surface across the meander was determined from measured high-water marks from the slope-area channel surveys following the floods of 10-5-25, 9-13-39, 9-6-40, 9-14-40, 9-18-40, 9-1-63, and 9-18-63. Mean velocity calculated from the superelevation was then multiplied by the cross-section area of the channel at the gage to compute the peak discharge of the flood. As noted previously, since the cross-section at the gage has been relatively stable over the period from 1925 to 1972, the cross-section area for all floods was calculated by shifting the zero bed elevation of the cross-section measured on October 15, 1963 to the appropriate zero bed elevation for each flood. The equation that relates the superelevation to the cross-sectionally and vertically averaged streamwise velocity $\langle\langle u \rangle\rangle$ of water flowing through a meander for steady, streamwise-uniform flow, as first derived by Leliavsky (1955), is:

$$\langle\langle u \rangle\rangle = \sqrt{\frac{\Delta z_s}{W} r_c g}\,, \tag{2.3}$$

where Δz_s is the elevation difference in the water surface across the channel, W is the width of the channel, and r_c is the radius of curvature of the channel centerline through the

meander. As determined from the slope-area channel surveys, the radius of curvature of the Paria River meander above the post-1925 gage was approximately 50 m from at least 1939 to 1963.

The three final stage-discharge rating curves and shifts

Following determination of the best value of the peak discharge for each of the 14 overbank floods, it was now possible to construct statistically significant stage-discharge rating curves that cover the full discharge range of the Paria River at Lees Ferry, AZ. Thus, final stage-discharge rating curves were determined for each of the three time periods of November 22, 1923 through October 5, 1925, October 5, 1925 through August 14, 1972, and August 15, 1972 through September 30, 1996 by regression through all of the values of Q as a function of ε (Figure 2.8). Also shown in Figure 2.8 are the number of points included in each regression and the multiple-squared correlation coefficient for each regression.

The final step prior to computing the instantaneous discharge time series for the entire period of record involved applying the correct shifts in stage for the time of each discharge measurement and the time of each of the 14 investigated flood peaks. These shifts are equivalent to the negative of the residual in ε relative to the regression for each discharge measurement and correct for all deviation in ε from the stage-discharge rating curve determined by regression; shifts between discharge measurements are assumed to vary linearly with time. This method of applying shifts is identical to the shifting control method used by the USGS at the Lees Ferry gage over the period of record. Absolute values of the shifts are much less than 20 cm for the times of the vast majority of discharge measurements and reflect minute changes in channel geometry in the gage cross-section not accounted for by the measured changes in bed stage.

Finally, the instantaneous discharge time series for the Paria River at Lees Ferry, AZ could now be computed by applying the three final stage-discharge rating curves and the shifts to the instantaneous stage data from November 22, 1923 through September 30, 1996; this time series is presented in Section 2.4d below.

2.4c-2: Near Cannonville, UT

The first step in the evaluation of the discharge record from the Paria River gage near Cannonville, UT was to retrieve all available USGS data for the gage from: the Utah District offices in Cedar City and Salt Lake City, UT and the Federal Records Center in Lakewood CO. These data consisted of: 82 USGS discharge measurement field notes

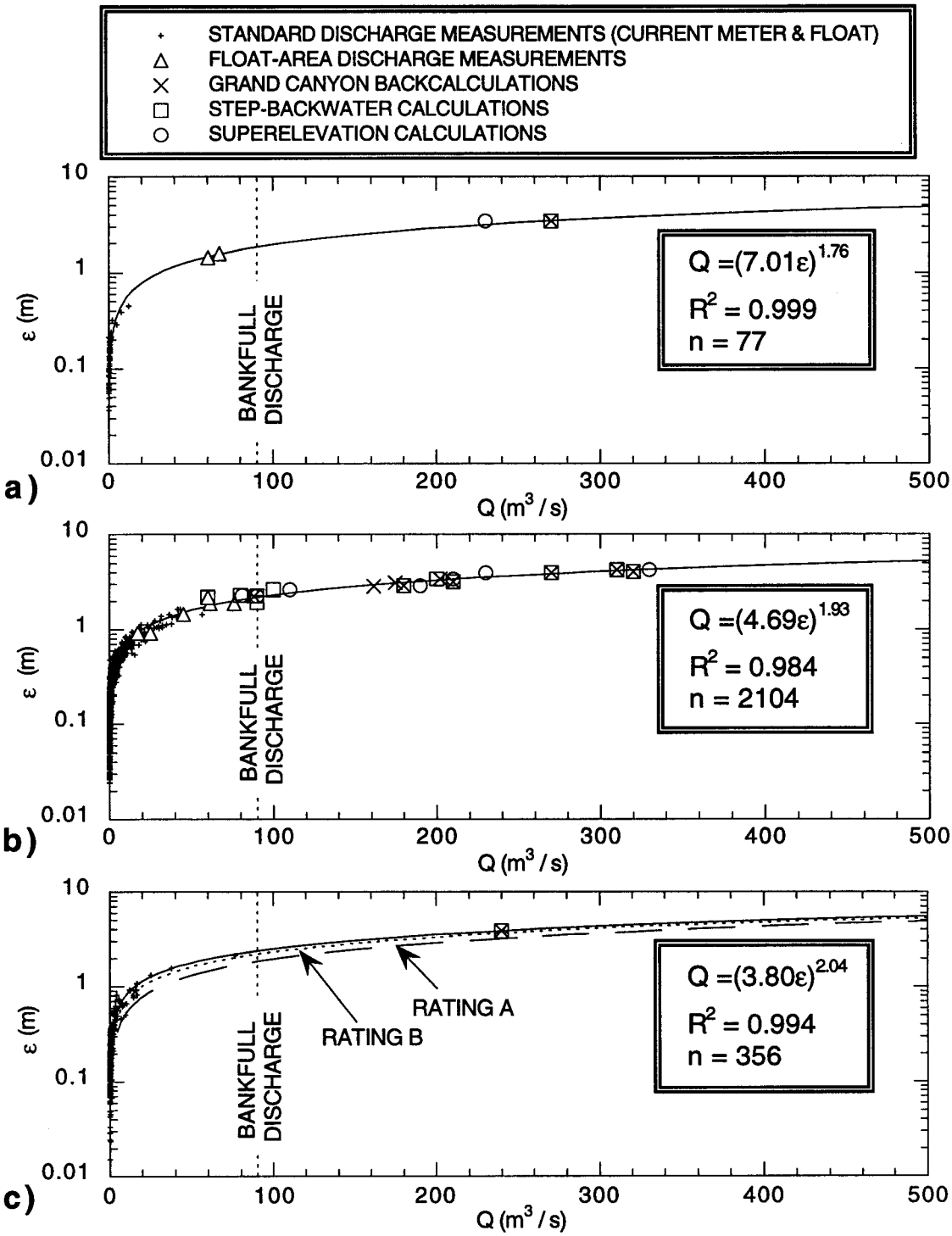

Figure 2.8: **(a) Rating A**, the final stage-discharge rating curve at the 1923-1925 gage for the period from November 22, 1923 to October 5, 1925. **(b) Rating B**, the final stage-discharge rating curve at the post-1925 gage for the period from October 5, 1925 to August 14, 1972. **(c) Rating C**, the final stage-discharge rating curve at the post-1925 gage for the period from August 15, 1972 to September 30, 1996.

from discharge measurements made from December 29, 1950 through October 25, 1957, and the slope-area channel surveys following floods on May 18, 1951, August 3, 1951, and September 21, 1952. The stage-recorder graphs from 1951 to 1955 could not be found.

Even though the stage-discharge rating curve is constrained by only 82 standard discharge measurements and 3 modern slope-area discharge computations, the discharge record for this site is relatively free of the errors that dominate the published historical record from the Lees Ferry, AZ gage, for two reasons. First, this site is at the upstream end of a bedrock-walled reach with a stable mixed sand and gravel bed; the bed at the gage has not experienced more than 20 cm of elevation change since 1951 making the stage-discharge relation for this site extremely stable. Second, the peak flows that define the upper portion of the stage-discharge rating curve were all determined using the modern slope-area method and not the (incorrect) old-style slope-area or differential methods that were used at Lees Ferry, AZ. Thus, in this study, the discharge record from the near Cannonville, UT gage was used as published by the USGS with no revisions.

2.4c-3: Near Kanab, UT

To evaluate the discharge records from the annual-crest gage near Kanab, UT, all of the limited data stored at the Utah District office in Cedar City, UT were retrieved. No records from this site could be found at either the Salt Lake City, UT office or the Federal Records Centers. Data from this site consisted of: notes indicating the installation date of the gage on 7-31-59, a report describing moving the gage from the highway bridge downstream in 1966, level notes indicating the elevation of reference marks at the post-1966 site relative to the gage datum in 1970, notes summarizing the nine wading discharge and four point-of-zero-flow measurements from October 19, 1971 to April 24, 1974 , and notes showing the results from two modern-slope area discharge computations following floods on August 4, 1970 and August 18, 1970.

Like the near Cannonville, UT gage, the published discharge record this site was determined to be free of large errors, at least from 1966 to the end of record in 1974, largely because the post-1966 reach is a bedrock-walled reach with a stable sand and gravel bed. Only 9 cm of bed elevation variation occurred from April 18, 1971 to April 24, 1974, and a resurvey of this site on April 10, 1995, as part of this study, indicated that only 1.5 cm of bed elevation change has occurred at the gage since 1974, indicating that the stage-discharge relation at this site is extremely stable. Moreover, discharges near 30 m^3/s determined by the modern slope-area method constrain the upper portion of the rating

curve, so none of the errors from changing methodologies of the type from Lees Ferry, AZ are present at the near Kanab, UT gage. The only revision of discharge records from this gage as part of this study was downgrading the published flood peak of 436 m^3/s on August 31, 1963 to 300 m^3/s by a log-linear regression using all of the other stage-discharge data from this site. This revision had the effect of making the peak discharge of the 1963 flood at this site intermediate with respect to the upstream peak discharge of 330 m^3/s at the near Cannonville, UT gage and the downstream peak discharge of 200 m^3/s at the Lees Ferry, AZ gage.

2.4d: The Paria River instantaneous discharge time series at Lees Ferry, AZ

The computed instantaneous discharge time series for the Paria River at Lees Ferry, AZ is shown in Figure 2.9a. As previously mentioned, the stage recorder graphs from October 1, 1975 through September 30, 1977 were not found; thus, instantaneous flows for these two years were approximated using the published mean daily discharges and peak discharges for this period. Discharge of the bankfull flow, 90 m^3/s, is shown by the horizontal dotted line Figure 2.9a; the bankfull flow is defined as the discharge at which the channel is filled with water to the elevation of the active floodplain. For the Lees Ferry, AZ reach, the elevation of the floodplain was determined from channel surveys that were conducted in 1925, 1939, 1940, 1963, and 1993 in equilibrium reaches with longitudinal bed slopes within 15% of 0.0035 (the rationalization for this will be described in subsequent sections of this chapter). Discharge at the bankfull stage was determined from standard discharge measurements, step-backwater measurements, and the flow and sediment-transport model developed in Chapter 3 and applied to the Paria River in Chapter 4.

Also shown in Figure 2.9a is the most likely peak discharge, with the appropriate range of uncertainty, of the largest known post-1880 flood. According to USGS interviews with Jerry Johnson in 1944, this flood occurred during the first week of September 1909. Johnson, born at Lees Ferry in about 1880, when asked about the elevation of his new irrigation flume on March 16, 1944 by USGS technician Frank Dodge, stated, "Well, it is above all except one flood." In this interview, Johnson also mentioned that this event flooded the ranching area opposite the gage and carried a third more water than any succeeding flood. Johnson continued by saying that his flume was under the high-water mark, but still "12 feet plus" [3.7 m] above the present [1944] elevation of the water surface. In a later interview on April 7, 1944, Johnson told Dodge

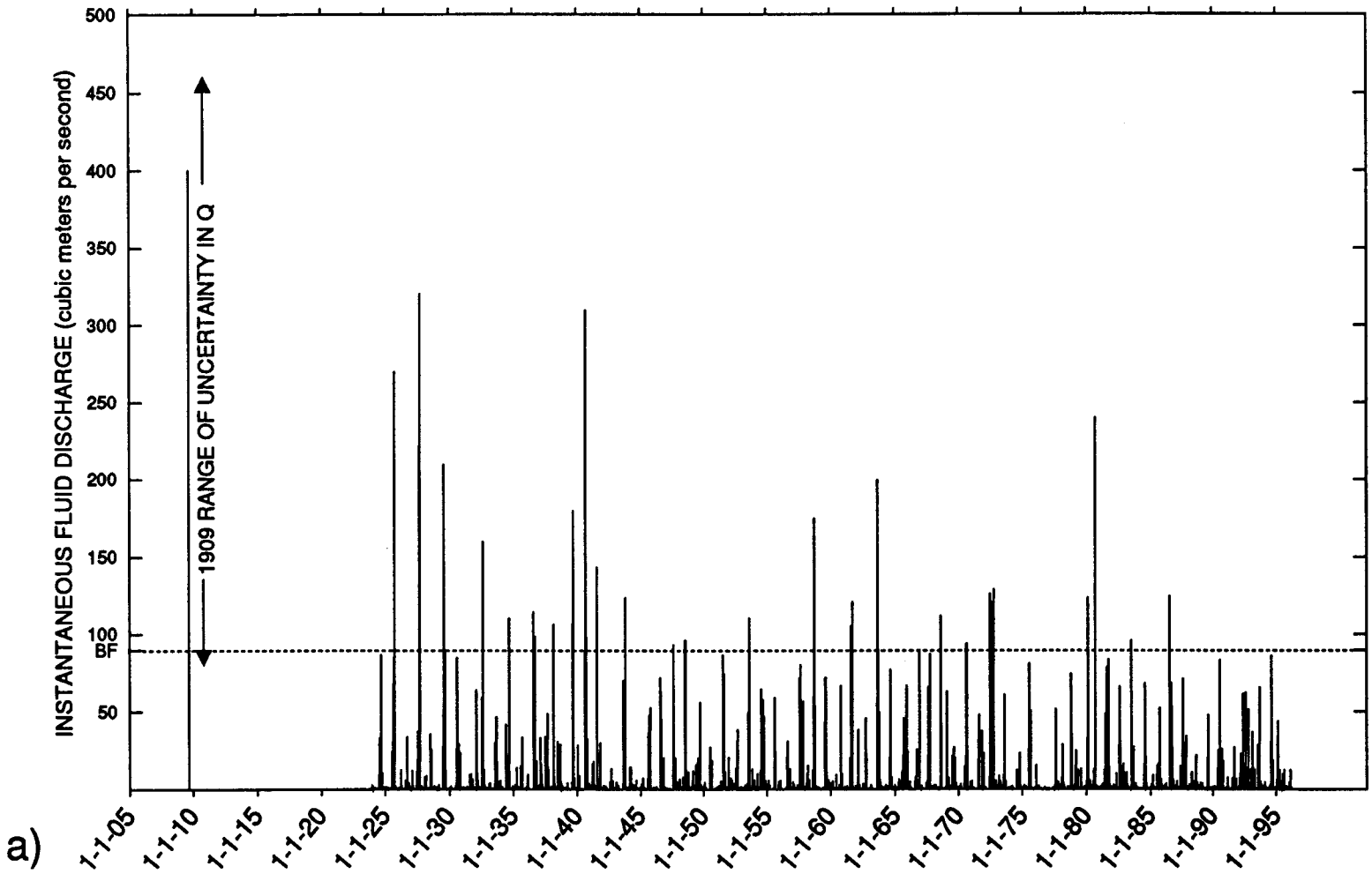

Figure 2.9: **(a)** The instantaneous discharge time series of the Paria River at Lees Ferry, AZ; the magnitude of the bankfull discharge, abbreviated as BF on the y-axis, is indicated by the dotted line.

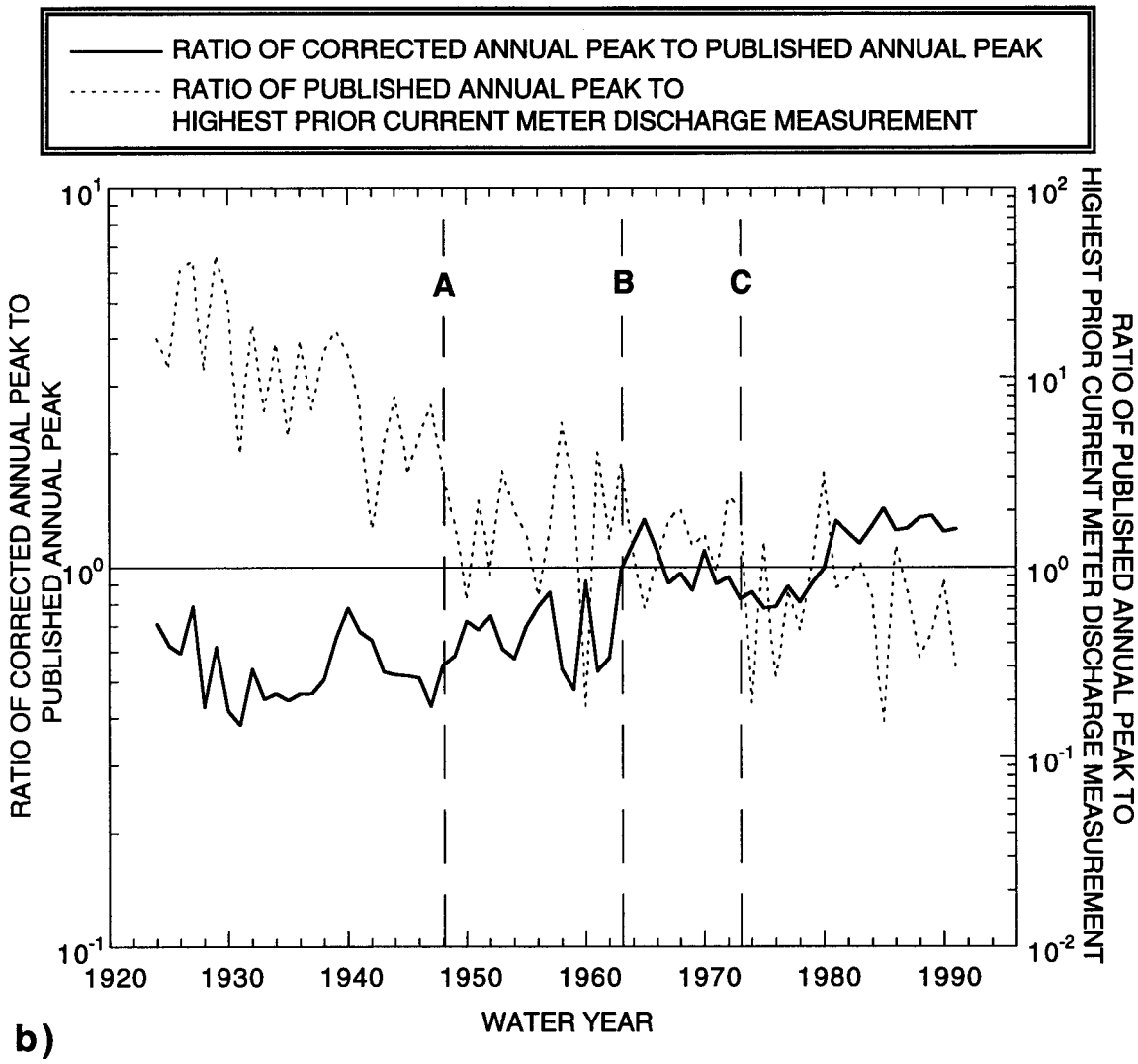

Figure 2.9 (continued): (b) Ratio of the corrected annual-maximum flood peak discharge to the USGS published annual-maximum flood peak discharge for water years 1924-1991 and the ratio of the USGS published annual-maximum flood peak discharge to the highest discharge current-meter discharge measurement made prior to that time for water years 1924-1991. (A water year is inclusive of the time from October 1 of the preceding calendar year through September 30 of the current calendar year.) The letter **A** indicates the time of installation of the first discharge measurement cableway, Cableway 1; the letter **B** indicates the time of the first USGS indirect discharge measurement made by the modern slope-area method; and, the letter **C** indicates the time of the last standard discharge measurement made at a discharge in excess of 17 m^3/s.

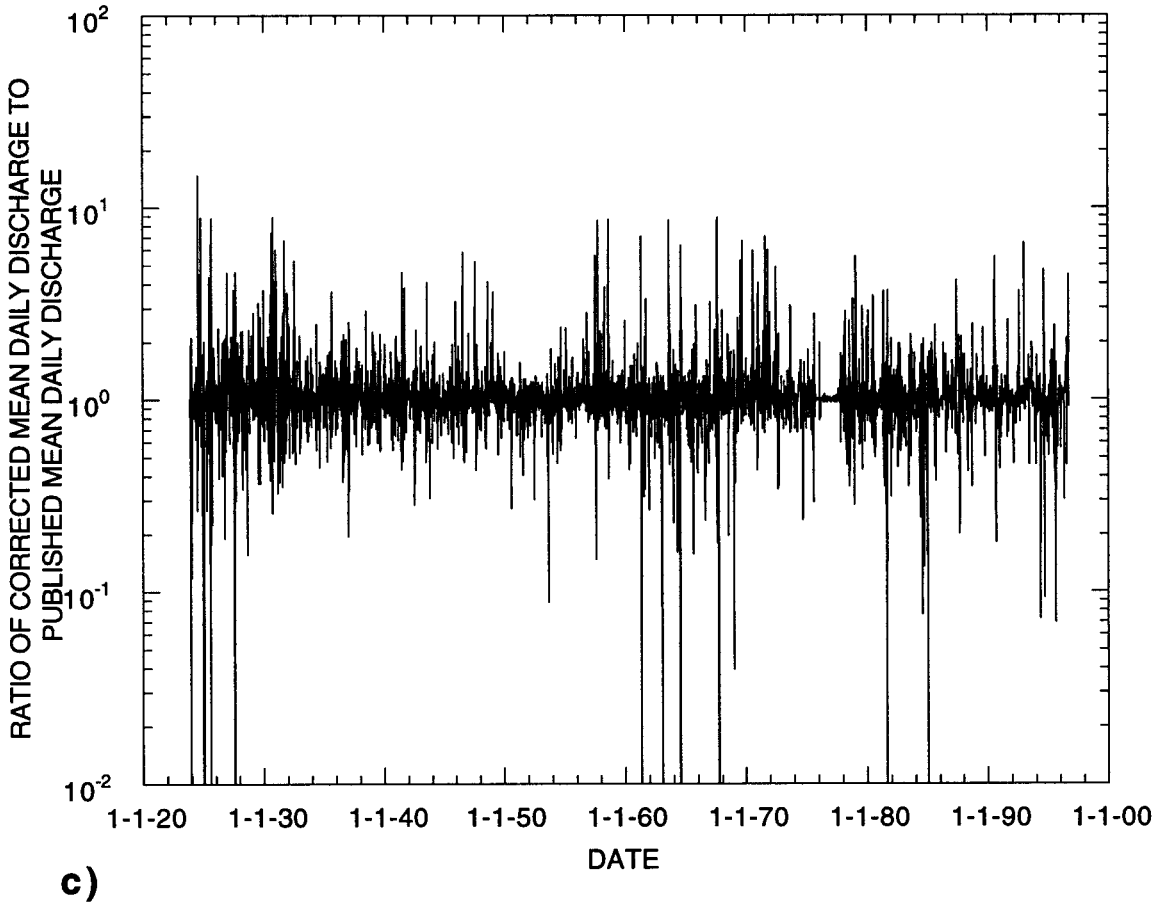

Figure 2.9 (continued): (c) Ratio of the corrected mean daily discharge to the USGS published mean daily discharge for the period from November 22, 1923 through September 30, 1996.

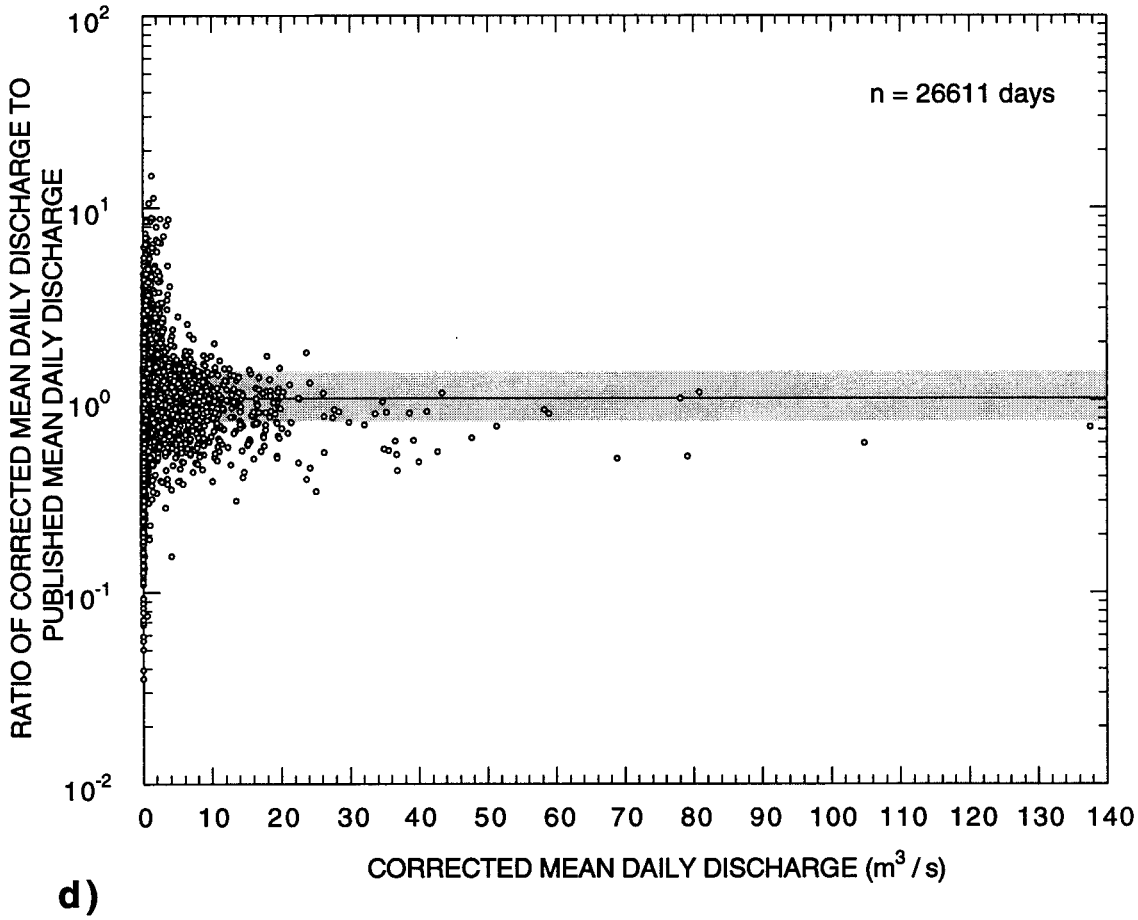

Figure 2.9 (continued): (d) Ratio of the corrected mean daily discharge to the USGS published mean daily discharge as a function of the corrected mean daily discharge for the period from November 22, 1923 through September 30, 1996; shaded area indicates region within one geometric standard deviation of the log-transformed mean ratio for all the data.

that he thought the stage of the 1909 flood was 4 feet [1.2 m] above the October 5, 1925 flood during which Johnson made a float-velocity measurement, but that the flood merely "came up to about" the level of the field across from the post-1925 gage site and did not flood it. By using both rating curves A and B (shown in Figure 2.8), and assuming no bed elevation change between 1909 and 1925 at the old and post-1925 gage sites, I calculated the peak discharge for the 1909 flood is calculated to be 460 m^3/s. Therefore, the peak discharge for the 1909 flood would have been 44% larger than the second largest subsequent flood, the September 13, 1927 flood.

A peak discharge of 460 m^3/s may be too high for the 1909 flood, however, because of the high likelihood of post-1909 channel incision at the future gage sites. Given that the effective base level at the high-water confluence of the Paria and Colorado Rivers permanently decreased by about 3.6 m during the course of the 1909 flood (as described Section 2.5a-3 below), probably initiating incision of the lowermost Paria River, the assumption that no decrease in bed elevation occurred between 1909 and 1925 at the future gage sites may not be valid. For example, if 3 m of bed degradation at either gage site occurred between 1909 and 1925, the value of ε used in the calculation of discharge using rating curves A and B would have to be decreased by 3 m, making the peak discharge of the 1909 flood as little as 80 m^3/s. However, since Johnson thought the 1909 flood was about a third larger than any subsequent flood, and because some portion of the incision due to the 1909 base level drop probably occurred at the gage sites during the course of the 1909 flood, it is likely that the discharge of the 1909 flood was closer to 460 than 80 m^3/s; the most probable discharge, at 1 significant figure given the large uncertainty, is 400 m^3/s.

Evaluation of error in published discharge records

Figure 2.9b provides a useful illustration of the sources of error in the USGS published discharge record of the Paria River at Lees Ferry, AZ. In this figure, both the ratio of the corrected discharge of the annual-maximum flood peak (computed in this study) to the published discharge of the annual-maximum flood peak and the ratio of the published discharge of the annual-maximum flood peak to the discharge of the highest prior current-meter discharge measurement are shown. Because of the old-style slope-area and differential methods used to define the highest portion of the pre-1948 rating curve, the corrected annual peak discharge is only, on average, 55% of the published annual peak discharges for this time period. After the installation of Cableway 1 and feasibility of higher-flow standard discharge measurements, this average improves to 66% for the period from 1948 to 1963. Finally, after the introduction of the modern slope-area methodology

at Lees Ferry, AZ in 1963, the corrected peak discharges are, on average, 108% of the published peak discharges, i.e., within 8% of the published peak discharges. The upward-creeping ratio of corrected to published peak discharges for the post-1980 era is explained by modern USGS stage-discharge rating curves containing no higher-flow standard discharge measurements because the USGS discontinued its program of a resident technician living at Lees Ferry on August 4, 1976 (the last standard discharge measurement over 17 m^3/s on the Paria River was made in 1972).

The necessity of reevaluating and recomputing the discharges as done in this study is perhaps best illustrated by the ratio of the published discharge of the annual-maximum flood peak to the discharge of the highest prior current-meter discharge measurement in Figure 2.9b. Prior to the construction of Cableway 1, each year, the published annual peak was on average 1420% of the highest current meter discharge measurement made prior to that time. This improved dramatically after construction of the cableway, when the published annual peak was on average only 148% of the highest current meter discharge measurement made prior to that time.

Comparison of recomputed mean daily discharges to published mean daily discharges

Figure 2.9c compares the ratio of the mean daily discharges computed in this study to the USGS published mean daily discharges at the Lees Ferry, AZ gage for the 26611 days from November 22, 1923 through September 30, 1996. This ratio is log-normally distributed with the geometric mean and standard deviations equal to $10^{0.0092}$ and $10^{0.13}$, respectively. Since the peak flows with the highest errors in the published discharge record are of extremely short duration and do not have a tremendous impact on the mean daily discharges, the mean daily discharges computed in this study are still in excellent agreement with the USGS published mean daily discharges and are 102% of these values, i.e., within 2% of these values. Figure 2.9d indicates, as expected, for the higher-discharge days, the computed mean daily mean discharges are on average slightly below the USGS published mean daily discharges. Unexpectedly, Figure 2.9d indicates that the greatest disagreement between the computed mean daily discharges in this study and the published mean daily discharges in Figure 2.9c occurs on days with mean daily discharges less than 20 m^3/s.

2.4e: Hydrologic-trend analyses at Lees Ferry, AZ

Since trends in the published discharge records of the Paria River have been used by Hereford(1986, 1987a), Webb(1985), Andrews (1990), and J. Graf and others (1991) as partial evidence of a significant climate change occurring on the Colorado Plateau in the

early 1940's, it was necessary to address what the nature of this hydrologic change was by using the more complete instantaneous discharge time series constructed in Section 2.4d. This task had to be completed before investigating the geomorphology and sediment transport of the system so that any geomorphic or sediment-transport changes could be placed in the appropriate hydrologic context. F-statistic trend analyses were, therefore, conducted on the annual flow volume, instantaneous discharge, flood-peak discharge, flood volume, and flood duration .

Results of the hydrologic-trend analyses are presented in Table 2.2. Of the twelve analyzed quantities, only two have trends significant at the 0.05 level; these are the instantaneous discharge and flood peak discharge that decrease 0.049 m^3/s and 7.1 m^3/s, respectively, over the period of gage record. The trend in peak discharges, as explained below, is completely due to only 3 out of the 1308 floods that have occurred over the 72.86-year period of record. As shown in Table 2.2, if the three floods responsible for the trend are excluded, the trend in the peak flood discharge is not significant.

Annual flow volume

Figure 2.10a illustrates the annual flow (i.e., runoff) volume of the Paria River at Lees Ferry, AZ for each water year from November 22, 1923 through September 30, 1996. The F-statistic associated with the linear regression through these data indicate that the variance about the regression is significantly different than the variance in the data at the 0.830 level of significance and, therefore, as first shown by Webb (1985), no trend is present in the annual flow volume data for the Paria River. However, though there is no trend in annual flow volume with time, years with larger peak flows still have a substantially larger annual volume of water, as seen in Figure 2.10b. The F-statistic associated with the linear regression in Figure 2.10b is equal to 38.8, thus, the trend of increasing annual flow volume with increasing annual peak discharge is significant at the 2.94×10^{-8} level .

In contrast to the conclusion of Webb (1985) that there is no significant correlation between annual runoff volume and the peak discharge of large floods, the Paria River data clearly show that the annual flow volume is substantially larger during years with extreme events. The physical reason for this is obvious; that is, the volume of extreme events is a considerable fraction of the annual flow volume. As shown in Table 2.2, the volume of floods with overbank peaks is $5.2 \times 10^6 \pm 4.16 \times 10^6$ m^3, and the annual flow volume is $2.44 \times 10^7 \pm 9.05 \times 10^6$ m^3. Thus, the mean overbank flood volume is 21% of the mean

Table 2.2: Summary of hydrologic-trend analyses.

ANALYZED QUANTITY	F	n	LEVEL OF SIGNIFICANCE, *p*, AT WHICH NULL HYPOTHESIS OF NO TREND IN DATA CAN BE REJECTED	IS THERE A TREND AT THE $p = 5\%$ LEVEL OF SIGNIFICANCE?	MEAN±1σ OF QUANTITY OVER DATES IN FIRST COLUMN (RATE OF CHANGE IN PARENTHESES)
11-22-23 TO 10-1-96 ANNUAL FLOW VOLUME (m^3)	0.0465	73	0.830	**NO**	$2.44 \times 10^7 \pm 9.05 \times 10^6$ m^3
11-22-23 to 10-1-96 INSTANTANEOUS (15 -MINUTE) DISCHARGE	58.1	2,610,372	2.49×10^{-14}	YES, DECREASING	0.774±3.02 m^3/s (-1.85×10^{-6} $m^3/s/day$)
11-22-23 to 10-1-96 PEAK DISCHARGES FOR FLOODS WITH PEAK DISCHARGES > 3.79 m^3/s	7.21	1308	0.00734	YES, DECREASING*	16.6±27.1 m^3/s (-2.67×10^{-4} $m^3/s/day$)
11-22-23 to 10-1-96 PEAK DISCHARGES FOR FLOODS WITH PEAK DISCHARGES > 3.79 m^3/s & BANKFULL (90 m^3/s)	0.165	1275	0.685	**NO**	13.3±15.3 m^3/s
11-22-23 to 10-1-96 PEAK DISCHARGES FOR FLOODS WITH PEAK DISCHARGES > 3.79 m^3/s & 2x BANKFULL (180 m^3/s)	2.67	1302	0.103	**NO**	15.5±21.4 m^3/s
11-22-23 to 10-1-96 PEAK DISCHARGES FOR FLOODS WITH PEAK DISCHARGES > 3.79 m^3/s & 2.8x BANKFULL (252 m^3/s)	2.57	1305	0.109	**NO**	15.9±23.5 m^3/s

Table 2.2 (continued): Summary of hydrologic-trend analyses.

ANALYZED QUANTITY	F	n	LEVEL OF SIGNIFICANCE, *p*, AT WHICH NULL HYPOTHESIS OF NO TREND IN DATA CAN BE REJECTED	IS THERE A TREND AT THE *p* = 5% LEVEL OF SIGNIFICANCE?	MEAN±1σ OF QUANTITY OVER DATES IN FIRST COLUMN (RATE OF CHANGE IN PARENTHESES)
9-12-29 to 10-1-96 FLOOD VOLUME FOR FLOODS WITH PEAK DISCHARGES > 3.79 m^3/s	2.42	1308	0.120	**NO**	$4.79 \times 10^5 \pm 1.23 \times 10^6$ m^3
11-22-23 to 10-1-96 FLOOD VOLUME FOR FLOODS WITH PEAK DISCHARGES > BANKFULL (90 m^3/s)	0.158	33	0.694	**NO**	$5.20 \times 10^6 \pm 4.16 \times 10^6$ m^3
9-12-29 to 10-1-96 FLOOD DURATION FOR FLOODS WITH PEAK DISCHARGES > 3.79 m^3/s	0.186	1308	0.666	**NO**	12.0±21.2 hours
11-22-23 to 10-1-96 FLOOD DURATION FOR FLOODS WITH PEAK DISCHARGES > BANKFULL (90 m^3/s)	1.53	33	0.225	**NO**	53.0±53.9 hours
11-22-23 to 10-1-96 PEAK DISCHARGES FOR FLOODS WITH PEAK DISCHARGES > BANKFULL (90 m^3/s)	1.80	37	0.188	**NO**	143±61.1 m^3/s
11-22-23 to 10-1-96 DURATION OF OVERBANK FLOWS (>90 m^3/s) FOR FLOODS WITH PEAK DISCHARGES > BANKFULL (90 m^3/s)	2.59	37	0.117	**NO**	3.66±5.42 hours

Notes:
* The 3 floods of 10-5-25, 9-13-27, and 9-6-40 are solely responsible for this significant trend.

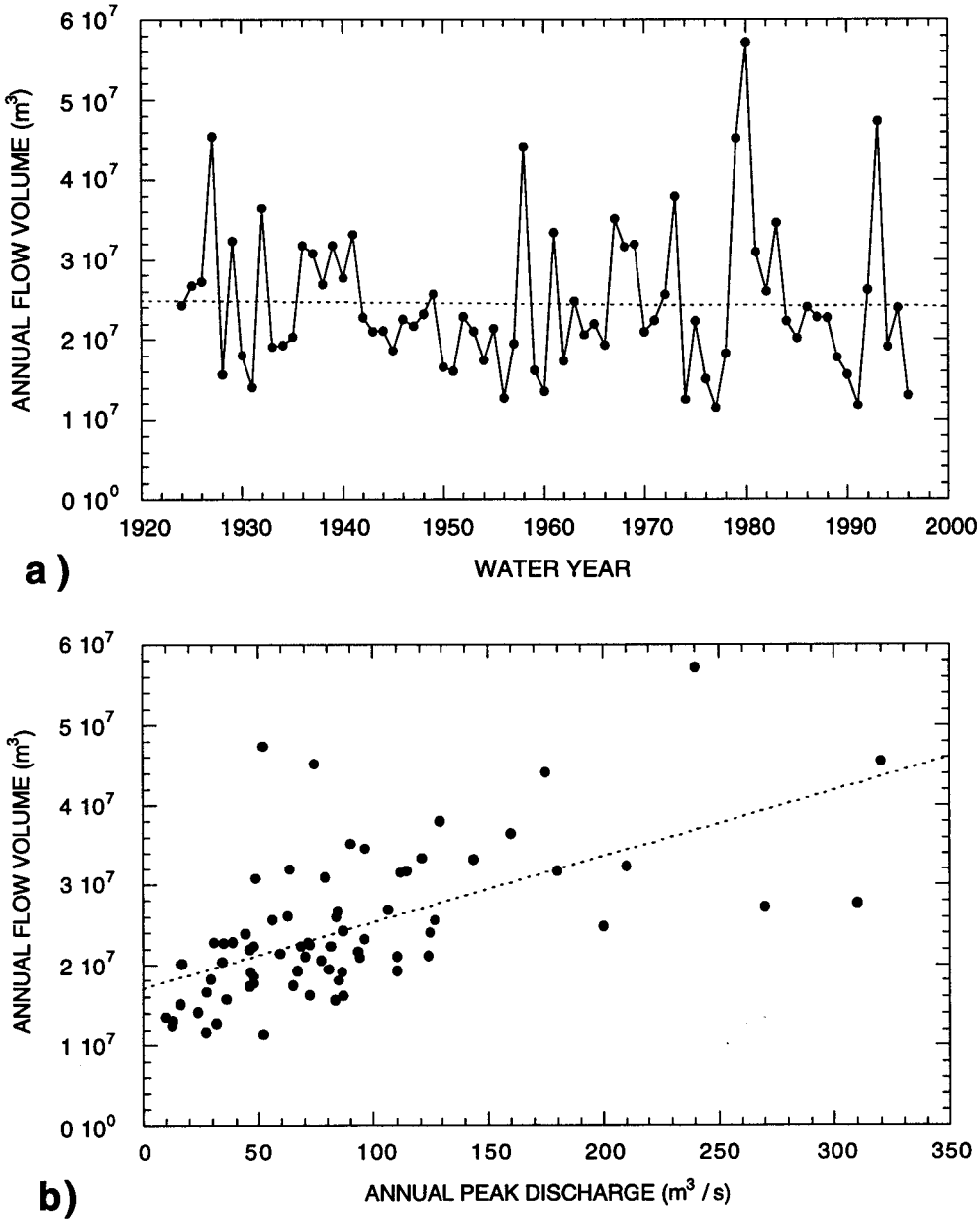

Figure 2.10: **(a)** Annual flow volume as a function of water year for water-years 1924 through 1996; dotted line is the best-fit linear regression through the data. **(b)** Annual flow volume as a function of the annual-maximum peak flood discharge; dotted line is the best-fit linear regression through the data.

annual flow volume, and the mean-plus-one-standard-deviation overbank flood volume is 61% of the mean-minus-one-standard-deviation annual flow volume.

Instantaneous discharge, peak flood discharge, flood volume, and flood duration

For the instantaneous discharge trend analysis, discharges were interpolated at equally spaced, 15-minute intervals resulting in a time series with 2,610,372 equally spaced discharge data. Over the entire period of gage record at Lees Ferry, the mean instantaneous, i.e. 15-minute, discharge is 0.77 m^3/s and the standard deviation is 3.02 m^3/s. Because of the large number of points in the linear regression, the decrease in instantaneous discharge over the 73 year period of record is significant, though not physically important. From November 22, 1923 through September 30, 1996, the instantaneous discharge decreases at the 2.49×10^{-14} level of significance at a rate of 1.85×10^{-6} $m^3/s/day$. This decrease is not physically important since it is only 6% of the long-term mean, i.e., 0.049 m^3/s, over the period of record.

Four trend analyses were conducted on the peak discharges of the 1308 individual floods that occurred from November 22, 1923 through September 30, 1996. The base flow that defines a flood in these analyses was chosen to be one standard deviation above the mean instantaneous discharge, i.e., 3.79 m^3/s. As mentioned, there is a significant decrease in peak flood discharges over the period of record at the 0.00734 level of significance, but it is due to only 3 out of 1308 events. As shown in Table 2.2, there is no trend with respect to time for peak flood discharges equal to or below the bankfull discharge (1275 events), equal to or below twice (i.e., 2x) the bankfull discharge (1302 events), or equal to or below 2.8x the bankfull discharge (1305 events). The significant decreasing trend in the peak flood discharge with respect to time exists only because of the three floods on October 5, 1925, September 13, 1927, and September 6, 1940 (Figure 2.11a). So, with the exception of the three largest floods in 73 years of gage record, the distribution of peak discharge with respect to time is stationary.

Similar trend analyses were conducted for flood volume and flood duration with respect to time. Flood volume is defined as the integrated volume of water in a flood over the time discharge exceeds the chosen base flow, which for these four analyses was 3.79 m^3/s. Flood duration is defined as the time discharge in a flood exceeds the chosen base flow. For the 1308 floods with peak discharges greater than 3.79 m^3/s, no significant trend in flood volume or flood duration with respect to time was found (Figures 2.11b & 2.11d). Moreover, for the largest events, that is, the 33 floods over the base flow of

Figure 2.11: **(a)** Peak flood discharge as a function of time for the period of November 22, 1923 through September 30, 1996; solid thin line is the best-fit linear regression through all the data; circled data are the 3 flood peaks solely responsible for the significance (at the 0.05 level) of the decreasing trend in the linear regression through all the data; dotted thin line is the best-fit linear regression through all but the circled data, i.e., all floods with peak discharges less than 2.8x bankfull. **(b)** Flood volume as a function of time for the period of November 22, 1923 through September 30, 1996; solid thin line is the best-fit linear regression through all the data. **(c)** Volume of floods with overbank peak discharges as a function of time for the period of November 22, 1923 through September 30, 1996; solid thin line is the best-fit linear regression through all the data.

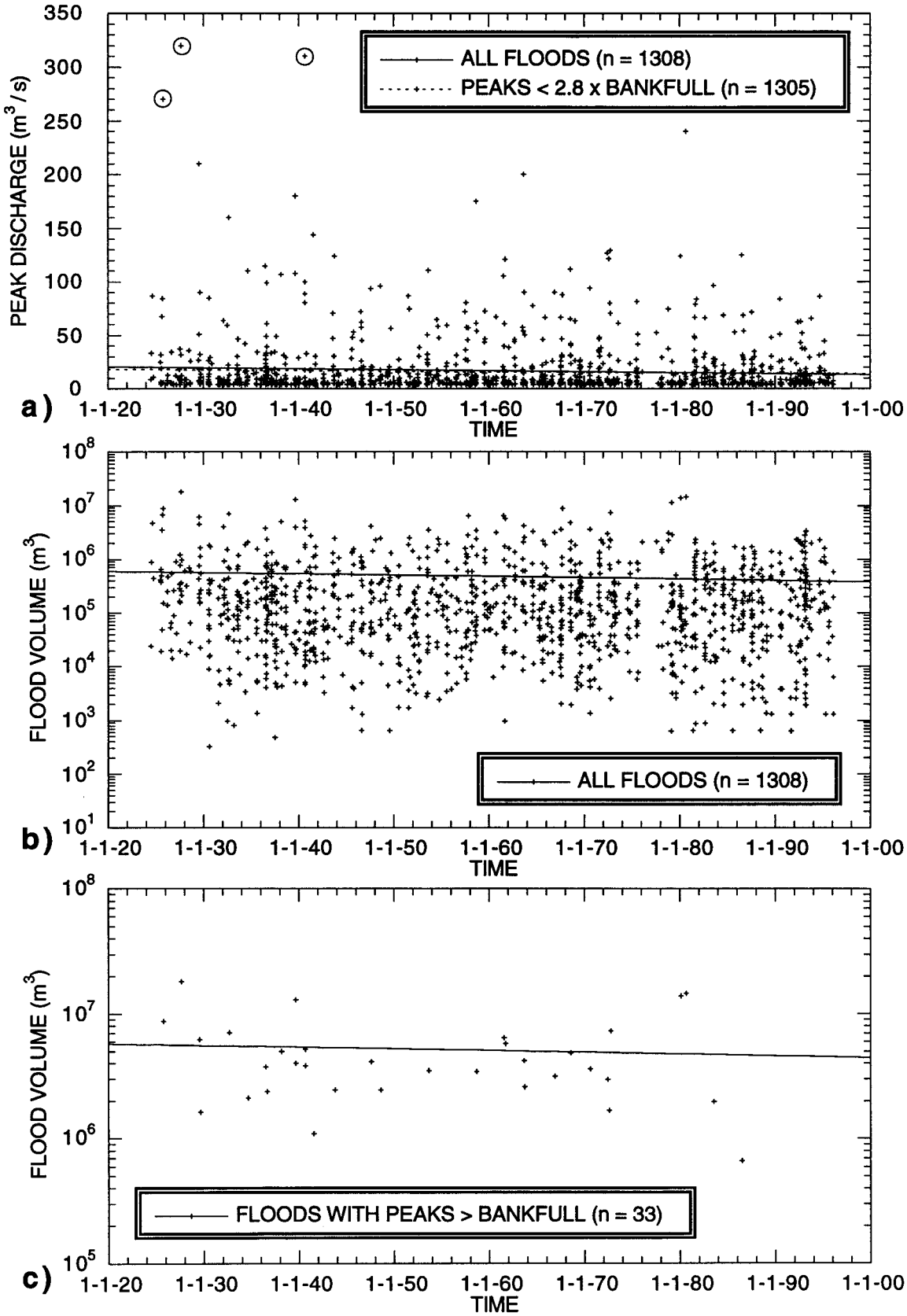
a)
PEAK DISCHARGE (m³/s)
350
300
250
200
150
100
50
0
ALL FLOODS (n = 1308)
PEAKS < 2.8 x BANKFULL (n = 1305)
1-1-20
1-1-30
1-1-40
1-1-50
1-1-60
1-1-70
1-1-80
1-1-90
1-1-00
TIME
b)
FLOOD VOLUME (m³)
10⁸
10⁷
10⁶
10⁵
10⁴
10³
10²
10¹
ALL FLOODS (n = 1308)
1-1-20
1-1-30
1-1-40
1-1-50
1-1-60
1-1-70
1-1-80
1-1-90
1-1-00
TIME
c)
FLOOD VOLUME (m³)
10⁸
10⁷
10⁶
10⁵
FLOODS WITH PEAKS > BANKFULL (n = 33)
1-1-20
1-1-30
1-1-40
1-1-50
1-1-60
1-1-70
1-1-80
1-1-90
1-1-00
TIME

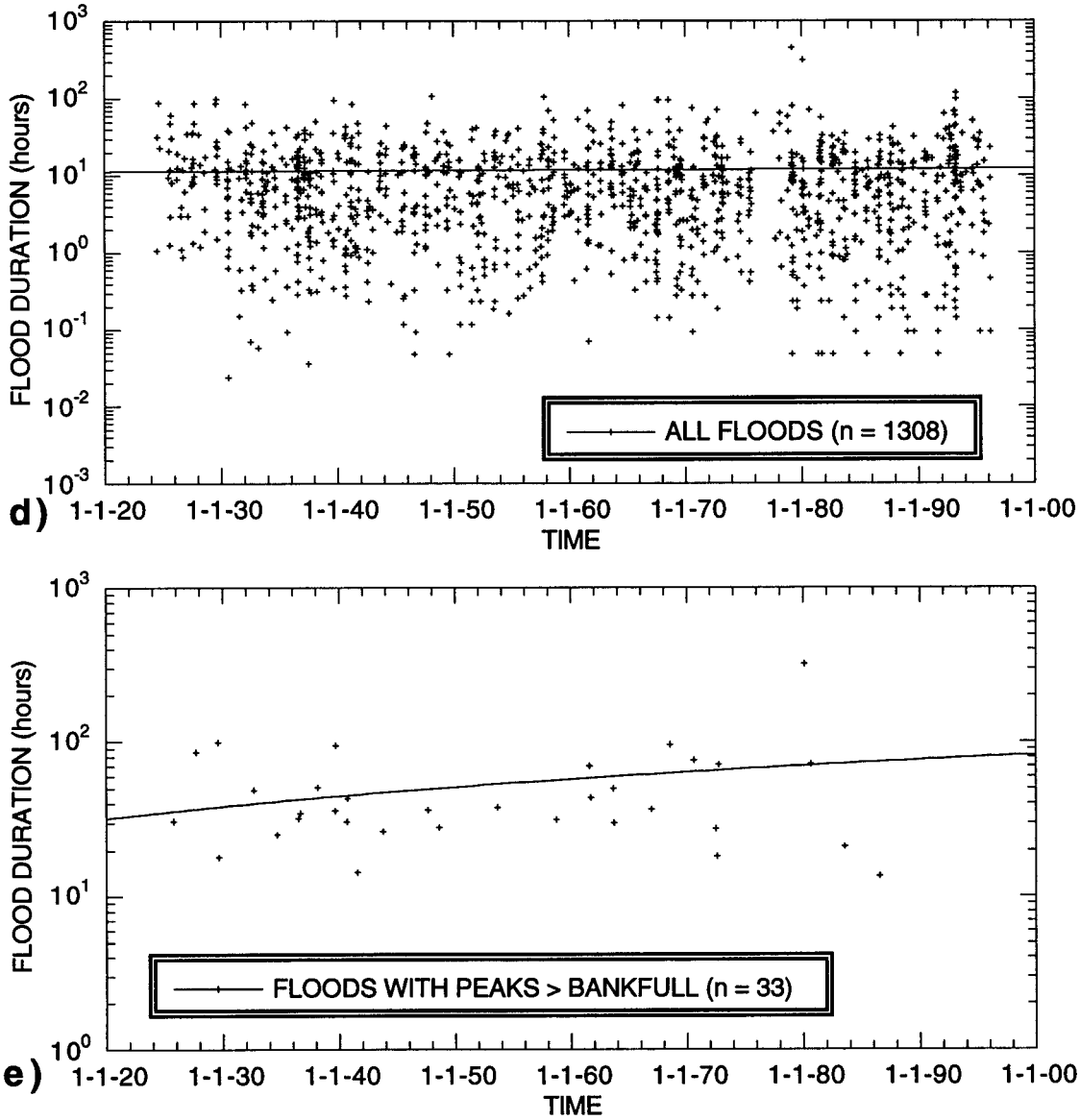

Figure 2.11 (continued): **(d)** Flood duration as a function of time for the period of November 22, 1923 through September 30, 1996; solid thin line is the best-fit linear regression through all the data. **(e)** Duration of floods with overbank peak discharges as a function of time for the period of November 22, 1923 through September 30, 1996; solid thin line is the best-fit linear regression through all the data.

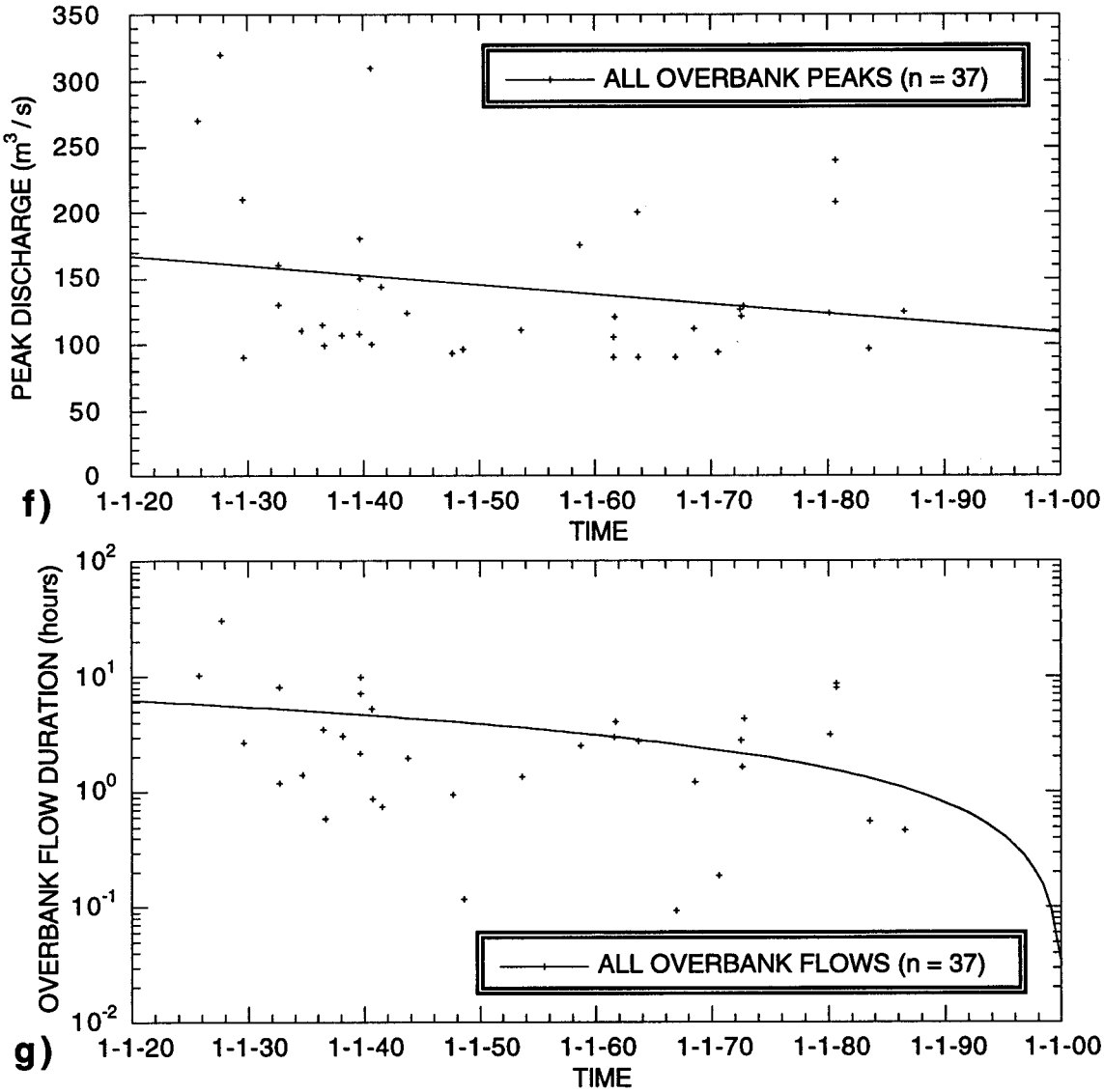

Figure 2.11 (continued): **(f)** Peak flood discharge of all overbank peaks as a function of time for the period of November 22, 1923 through September 30, 1996; solid thin line is the best-fit linear regression through all the data. **(g)** Duration of overbank flows as a function of time for the period of November 22, 1923 through September 30, 1996; solid thin line is the best-fit linear regression through all the data.

3.79 m^3/s that had overbank peak discharges, no significant trend in flood volume or flood duration with respect to time was found (Figures 2.11c & 2.11e). So, over the period of record, the distributions of flood volume and duration have been stationary with respect to time and have respective means of 4.79×10^5 m^3 and 12.0 hours (Table 2.2). Also, the flood volume and duration of floods with overbank peaks have been stationary with respect to time and have respective means of 5.20×10^6 m^3 and 53.0 hours (Table 2.2).

Discharge of overbank peaks and duration of overbank flows

Two last trend analyses were designed to examine only the largest flows and were conducted using a base flow equal to the bankfull discharge of 90 m^3/s (Figure 2.11f and 2.11g). Because some of the 33 overbank floods over the period of gage record have multiple peaks with trough discharges less than bankfull, the choice of bankfull as the base flow for the analyses yielded 37 instead of 33 peaks. Over the period of record, with the use of a bankfull base flow, the distributions of peak discharge and overbank-flow duration have been stationary with respect to time and have respective means of 143 m^3/s and 3.66 hours (Table 2.2). For the 37 overbank peaks, the trend in peak discharge with respect to time is significant only at the 0.188 level and, therefore, not significant. Also, for the 37 overbank peaks, the duration of overbank flow as a function of time is significant at the 0.117 level and, therefore, is not significant. As will be shown below in the flow-duration analysis, duration of overbank flows on the Paria River is extremely short with the mean being only 3.66 hours and the cumulative time of overbank flows being only 135.42 hours over the 73 years of record or 0.021% of the time.

2.4f: Flood-frequency analyses at Lees Ferry, AZ

In conjunction with the above hydrologic-trend analyses, comprehensive flood frequency analyses were conducted on both the annual-maximum flood series (containing 73 floods) and the partial-duration series (containing 1308 floods over 73 years) both to calculate the flood-frequency distribution for the Paria River at Lees Ferry, AZ and to determine if any shift in the flood-frequency distribution has occurred during the period of gage record as suggested by Andrews (1990) and J. Graf and others (1991). For the entire period of record, peak discharge as a function of return period for both the partial-duration series and annual-maximum series is shown in Figure 2.12a. Also shown in Figure 2.12a, is the log-Pearson Type III fit to the annual-maximum series and the associated 95% confidence limits. The log-Pearson Type III fit to the annual-maximum series was

calculated for this and subsequent flood-frequency analyses by the method described by the Interagency Advisory Committee on Water Data (1982); for the 73-year period of record at Lees Ferry, AZ, the weighted skew coefficient was -0.286. Over the period of record, the mean annual flood, 88±65 m^3/s has been approximately equal to the bankfull flow, 90 m^3/s, and the bankfull flow has been equaled or exceeded on average every 2.2 years in the partial-duration series and 2.9 years in the annual-maximum series. So, although the duration of overbank flows has been short, i.e., 0.021% of the time, compared to non-ephemeral rivers (e.g., Emmett, 1975; Leopold, 1994), the recurrence interval of the bankfull flow on the Paria River has been fairly typical compared to any river (e.g., Dunne and Leopold, 1978; Williams, 1978).

To address the conclusions of Andrews (1990) and J. Graf and others (1991) that the flood-frequency distribution on the Paria River changed in the earliest 1940's, the annual-maximum and partial-duration series analyses were recomputed for the separate periods from November 22, 1923 through September 30, 1939 and October 1, 1939 through September 30, 1996. Results from these analyses are shown in Figures 2.12b and 2.12c. The break between water years 1939 and 1940 was chosen because Hereford (1986) chose 1940 as the year new floodplains were initiated in the Lees Ferry reach in response to a decline in large floods; the issue of new versus old floodplains will be addressed in subsequent sections of this chapter.

As noted by Andrews (1990) and J. Graf and others (1991) there is an apparent difference between the mean flood-frequency curves calculated for the annual-maximum series before and after 1940. Also, in general agreement with Andrews (1990), the discharge of the mean annual flood of the Paria River did decrease by 34% in 1940. Nevertheless, the difference in the mean flood-frequency curve in the earliest 1940's is only an apparent difference, and not a statistically significant difference. Part of the difference between the results of Andrews (1990) and J. Graf and others (1991) and the results from this study is due to the use of the published annual peaks by Andrews (1990) and J. Graf and others (1991) and use of the recomputed annual peaks in this study; however, the results of neither Andrews (1990) nor J. Graf and others (1991) can truly be evaluated since they did not include the confidence limits in their flood-frequency distribution plots. As can be seen in Figure 2.12b, there is substantial overlap at the 95% confidence (i.e., 0.05 significance) level in the flood-frequency curves for the water-year 1924-1939 and 1940-1996 analyses (the weighted skew coefficients for the 1924-1939 analysis was -0.052 and for the 1940-1996 analysis was -0.387). Thus, the apparent

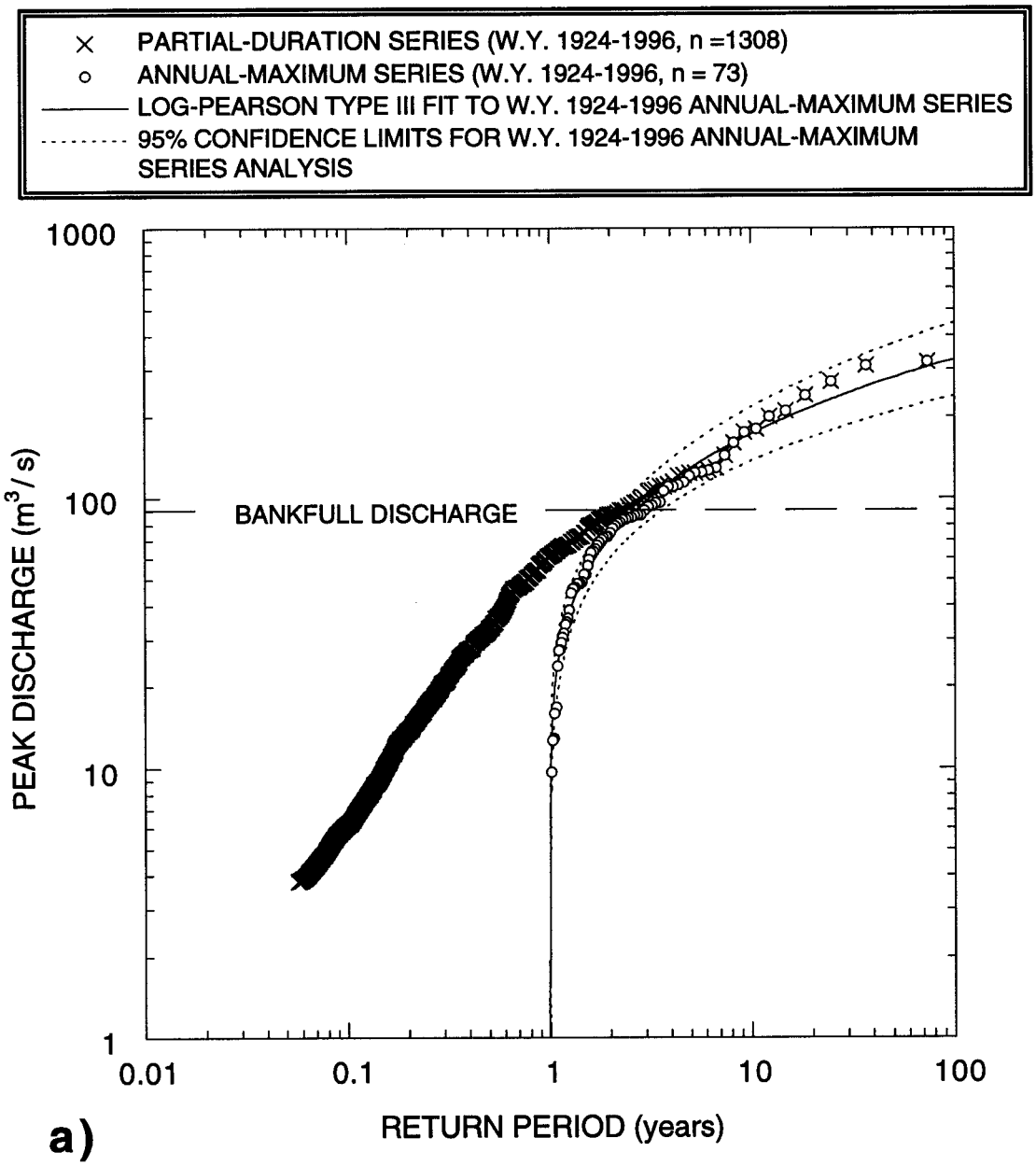

Figure 2.12: **(a)** Peak flood discharge as a function of return period for the partial-duration and annual-maximum flood series of the Paria River at Lees Ferry, AZ for the period of November 22, 1923 through September 30, 1996.

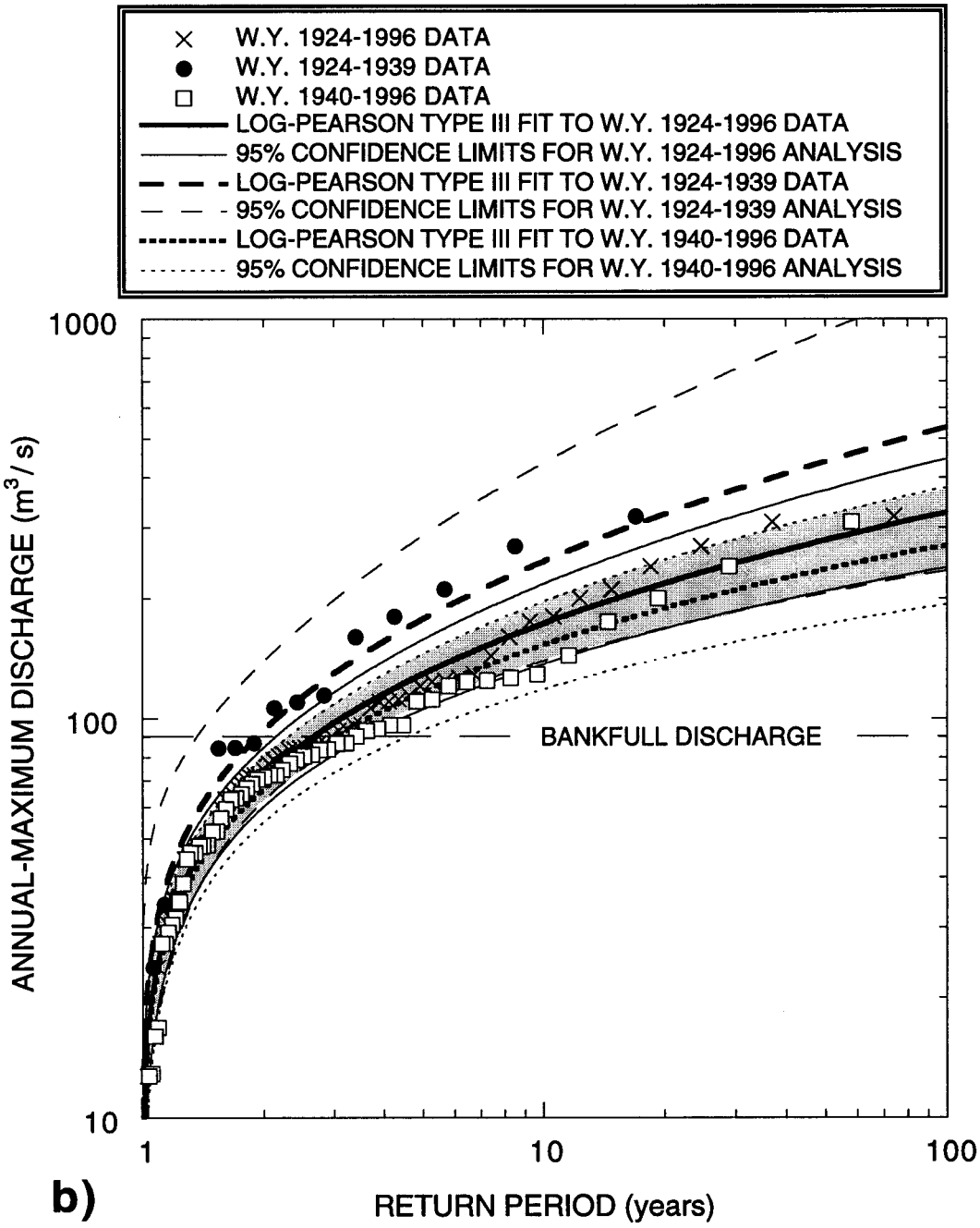

Figure 2.12 (continued): **(b)** Peak flood discharge as a function of return period for the annual-maximum flood series of the Paria River at Lees Ferry, AZ for the periods of November 22, 1923 through September 30, 1996, November 22, 1923 through September 30, 1939, and October 1, 1939 through September 30, 1996.

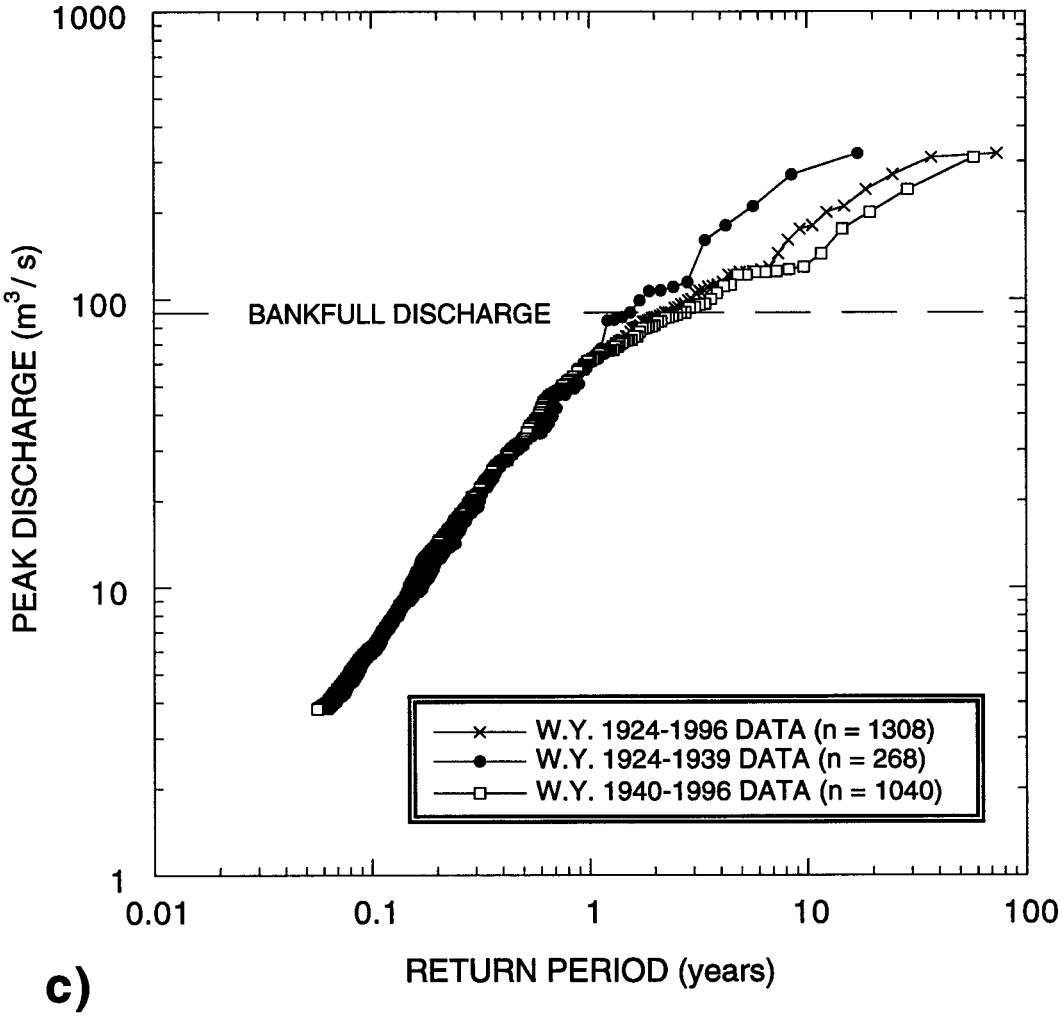

Figure 2.12 (continued): (c) Peak flood discharge as a function of return period for the partial-duration flood series of the Paria River at Lees Ferry, AZ for the periods of November 22, 1923 through September 30, 1996, November 22, 1923 through September 30, 1939, and October 1, 1939 through September 30, 1996.

difference in the mean curves noted by Andrews (1990) and J. Graf and others (1991) is merely the artifact of comparing a long period with a shorter period containing a clustering of a few large floods.

Figure 2.12c shows peak discharge as a function of return period for the partial-duration flood series for water years 1924-1996, 1924-1939, and 1940-1996. As with the annual-maximum series, a slight shift in the flood frequency of overbank events occurs between the 1924-1939 and 1940-1996 periods and is due to a clustering of larger floods in the 1920's. Both periods have identical flood-frequency distributions, however, for all floods with peak discharges less than 70 m^3/s. Importantly, this discharge range for which the flood-frequency distributions are identical includes the vast majority of all the floods that have occurred on the Paria River. Ninety-five percent of all the floods occurring during the period from November 22, 1923 through September 30, 1939, and 97% of all the floods occurring during the period from October 1, 1939 through September 30, 1996, had peak discharges less than 70 m^3/s.

2.4g: Flow-duration analysis at Lees Ferry, AZ

Figure 2.13 shows the results from the flow-duration analysis that was conducted on the instantaneous discharge time series for the Paria River at Lees Ferry, AZ. As with the flood-frequency analyses, flow duration is presented for the time periods of November 22, 1923 through September 30, 1996, November 22, 1923 through September 30, 1939 and October 1, 1939 through September 30, 1996. Also shown is the time period of November 22, 1923 through September 30, 1939 minus the time associated with the two largest floods that occurred during this time period on October 5, 1925 and September 13, 1927; this was computed to show that much of the difference in flow duration for the higher flows between water years 1924-1939 and 1940-1996 is due to only two events.

The truly ephemeral nature of the Paria River is perhaps best illustrated by comparing the partial-duration flood-frequency analysis with the cumulative flow-duration analysis for the period of gage record at Lees Ferry, AZ. Peaks equal to the mean instantaneous discharge of 0.77 m^3/s occur, by extrapolation of the partial-duration flood-frequency curve, about every 3.7 days, but the mean instantaneous discharge is equaled or exceeded only 20.6% of the time. Also, as already mentioned, the bankfull discharge occurs every 2.2 years, but is equaled or exceeded only 0.021% of the time. So, higher flows above base flow may occur frequently, but are of very short duration.

Like the flood-frequency distribution curves, the major differences in the flow-duration curves between the periods of water years 1924-1939 and 1940-1996 are

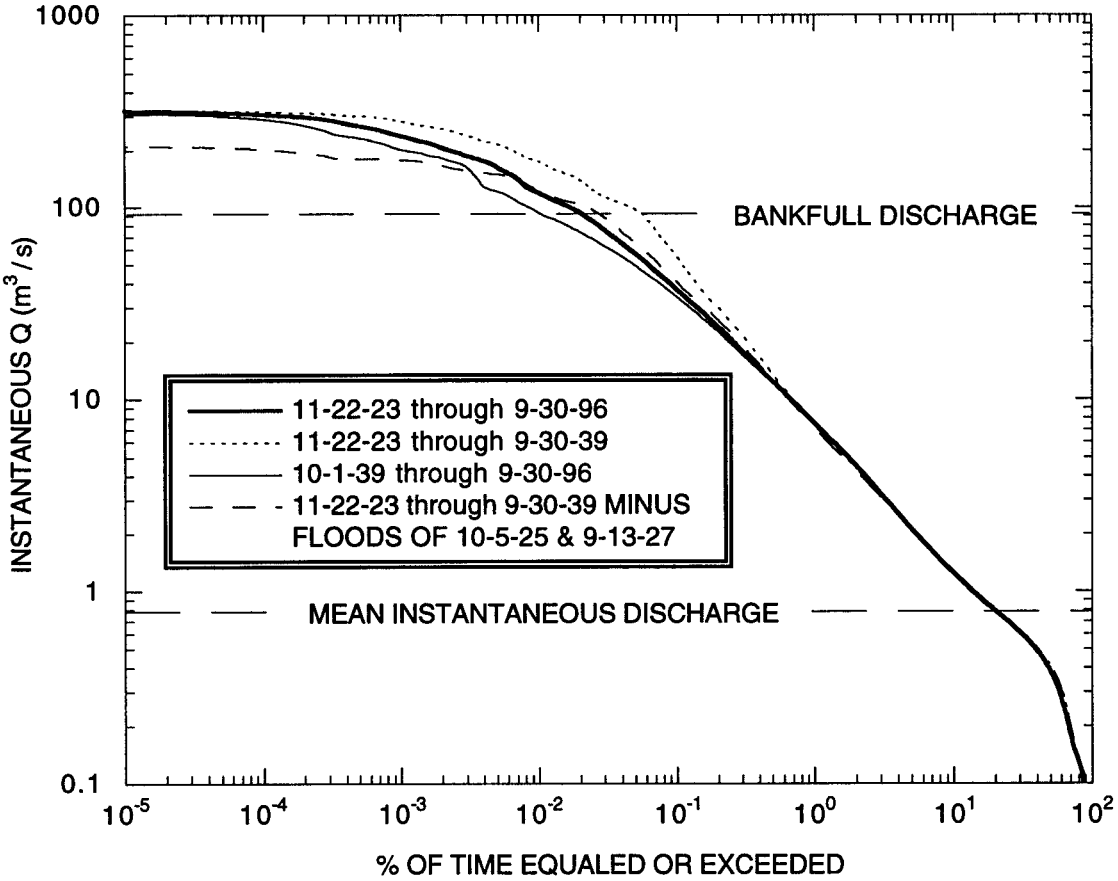

Figure 2.13: Flow-duration curves for the Paria River at Lees Ferry, AZ. These are modified versions of the standard flow-duration curves used by most hydrologists; in this graph, instantaneous fluid discharge, not mean daily discharge, is shown as a function of the percent of the time that a given flow is equaled or exceeded. Use of the mean daily discharge instead of the instantaneous discharge has the adverse effect of artificially decreasing the time a flow is equaled or exceeded; this effect is especially large for the higher flows.

restricted to the highest flows, i.e., flows that are equaled or exceeded less than 0.5% of the time (29 days out of the 15.86 years of the first period or for 104 days out of the 57 years of the second period). In the entire 72.86 years of gage record, the bankfull flow was equaled or exceeded only 0.021% of the time, or 135.42 hours. In the 15.86 years of the first period, the bankfull flow was equaled or exceeded only 0.058% of the time, or 80.55 hours; and, in the 57 years of the second period, the bankfull flow was equaled or exceeded only 0.011% of the time, or 54.87 hours. After excluding the 2 largest floods, in the 15.85 years of the first period, the bankfull flow was equaled or exceeded only 0.029% of the time or 39.66 hours. In any case, the differences in flow duration between the periods from November 22, 1923 through September 30, 1939 and October 1, 1939 through September 30, 1996 are small.

2.4h: Comparison of peak flood discharge and flood-frequency analyses at the three gages

Bankfull discharges at the Lees Ferry, near Cannonville, and near Kanab gages are virtually identical. The bankfull discharges at the two upstream gages were determined by: (1) tracing the high-water marks of bankfull flows from alluvial reaches immediately above the near Cannonville and near Kanab gages into the reaches at these gages; (2) determining the stage of these flows at the gages; and (3) using the USGS stage-discharge rating curves for these two gages. The bankfull discharge determined by this method using the higher portion of the rating curve in use from 1951 to 1974 at the near Cannonville, UT gage is 98 m^3/s and by using the 1970 rating curve at the near Kanab, UT gage is 89 m^3/s. Both of these discharges are, within measurement error, identical to the 90 m^3/s bankfull discharge at the Lees Ferry, AZ gage.

Similarity of bankfull discharges at the three gages is to be expected in a river like the Paria River because most floods are caused by intense summer precipitation in the uppermost 14% of the drainage basin, i.e., that portion of the drainage basin above the near Cannonville gage (Topping, in prep.). These floods are typically conveyed down the river from Cannonville to Lees Ferry with little modification. On average, peak discharges of larger floods traveling down the Paria River decrease by less than 33% between the gage near Cannonville, UT and the gage at Lees Ferry, AZ (Figure 2.14). Figure 2.14a illustrates the behavior of the peak discharges of floods between the near Cannonville and Lees Ferry gages as constrained by all floods from the periods from 1951 through 1955 and from 1959 through 1974 that had peak discharges greater than 5.66 m^3/s at the near Cannonville, UT gage. Figure 2.14b illustrates the behavior of the peak discharges of

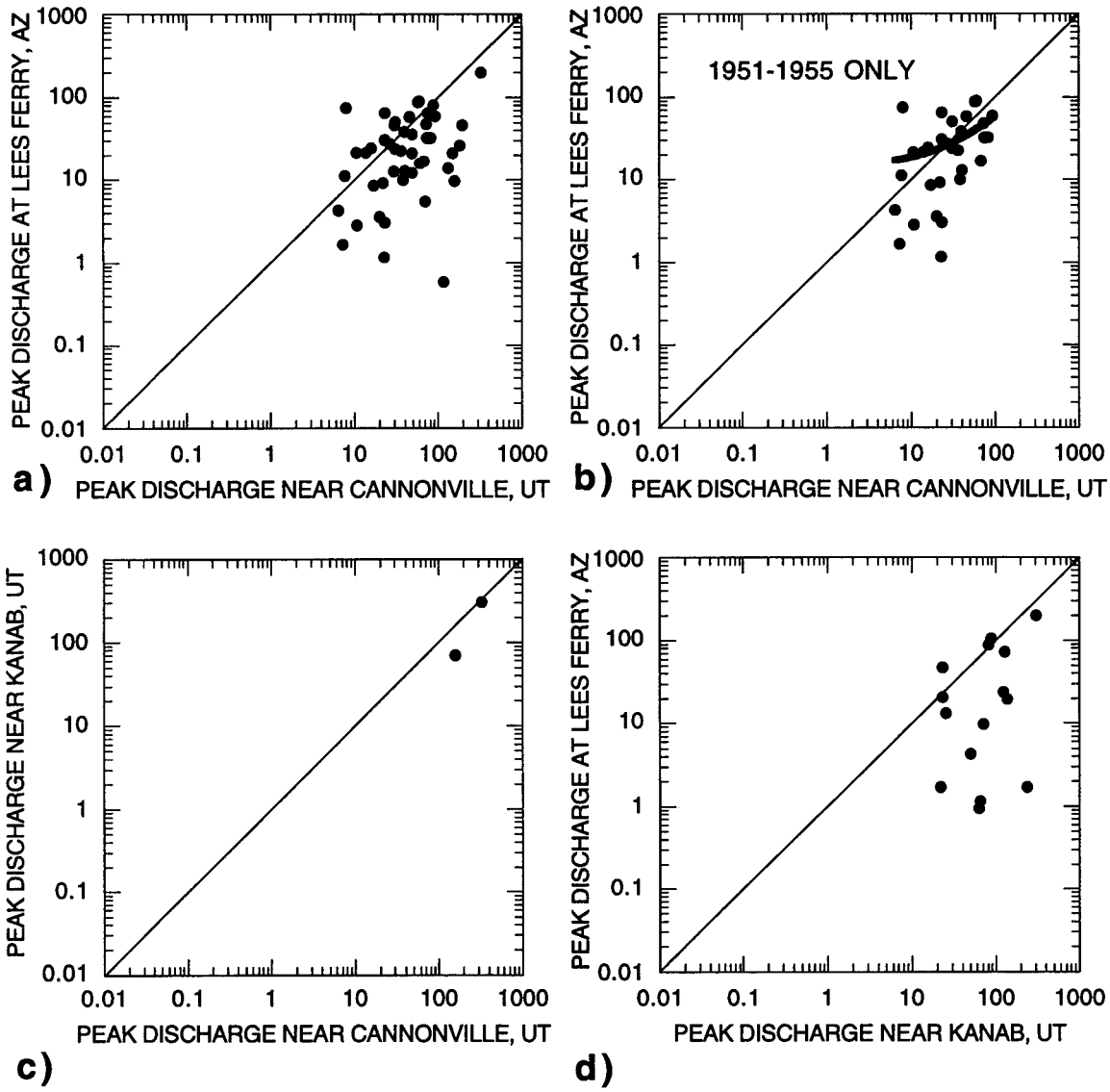

Figure 2.14: **(a)** For the same flood, peak discharge at the Lees Ferry, AZ gage as a function of peak discharge at the near Cannonville, UT gage (for floods passing the 1951-1955 continuous-recorder stage gage and the 1959-1974 annual-crest gage). **(b)** For the same flood, peak discharge at the Lees Ferry, AZ gage as a function of peak discharge at the near Cannonville, UT gage (for floods passing the 1951-1955 continuous-recorder stage gage only); solid thick line is the best-fit linear regression to the data. **(c)** For the same flood, peak discharge at the near Kanab, UT gage as a function of peak discharge at the near Cannonville, UT gage. **(d)** For the same flood, peak discharge at the Lees Ferry, AZ gage as a function of peak discharge at the near Kanab, UT gage.

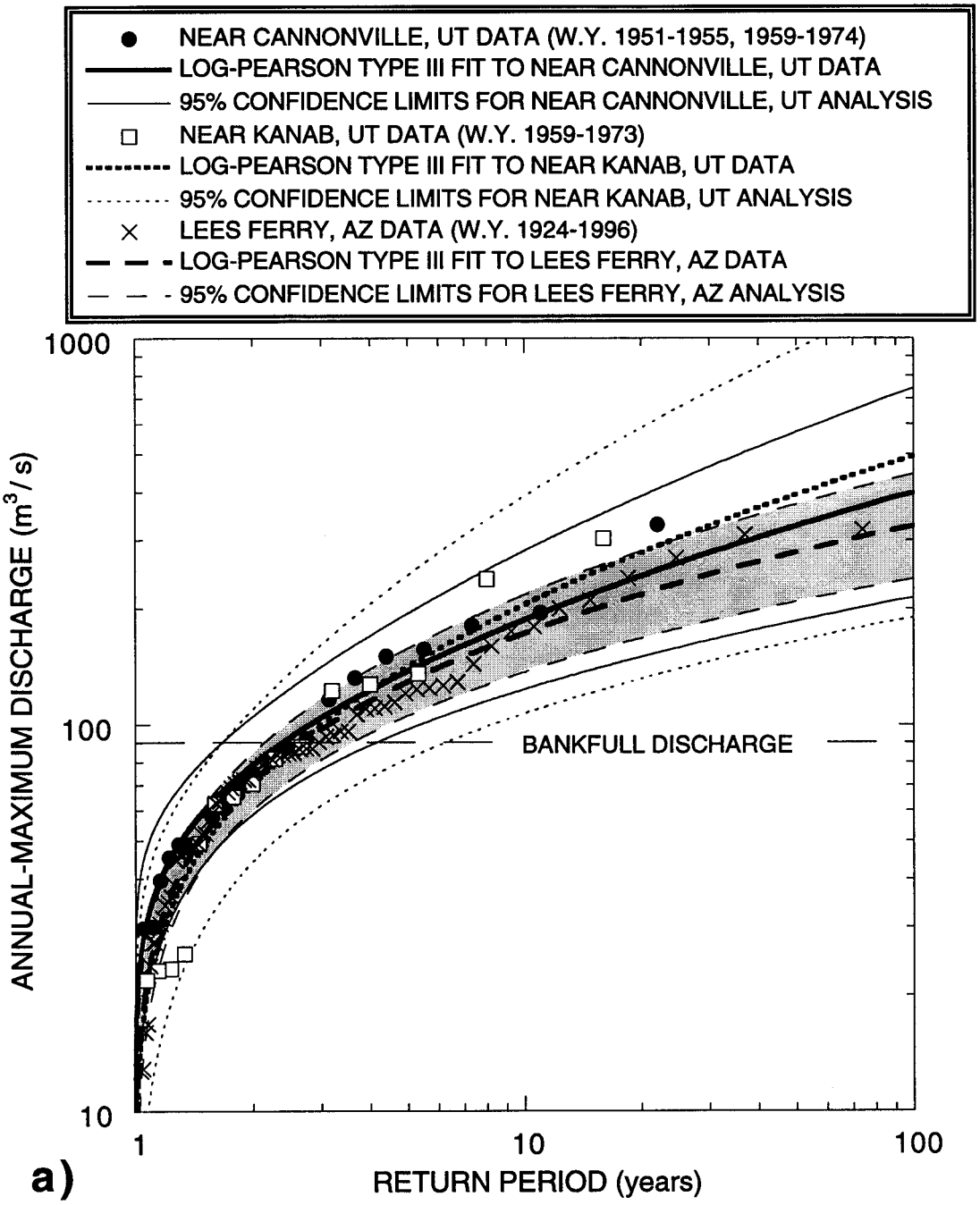

Figure 2.15: **(a)** Peak flood discharge as a function of return period for the annual-maximum flood series of the Paria River near Cannonville, UT, near Kanab, UT, and at Lees Ferry, AZ.

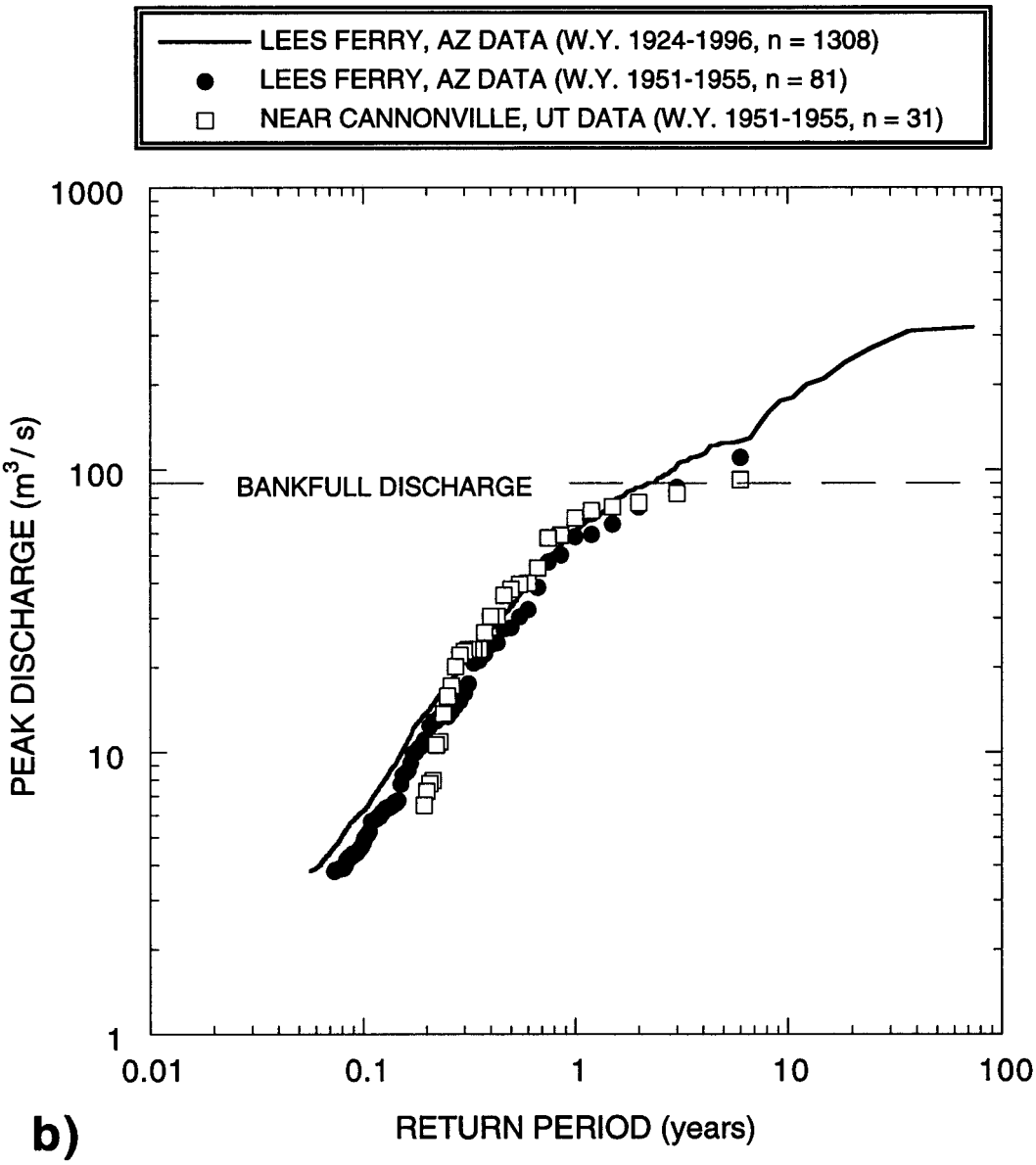

Figure 2.15 (continued): **(b)** Peak flood discharge as a function of return period for the partial-duration flood series of the Paria River near Cannonville, UT and at Lees Ferry, AZ.

floods between the two gages for the best subset of the data in Figure 2.14a, i.e., the floods that passed the near Cannonville gage between 1951 and 1955 while it was a continuous-recorder stage gage. These data are better than the 1959-1974 data because they do not have the large uncertainties in the day of flood occurrence found with data from the annual-crest gage. The linear regression in Figure 2.14b shows that the higher peak discharges decrease by less than 33% and the lower peak discharges may increase by as much as 300% between Cannonville and Lees Ferry.

Figure 2.14c illustrates the behavior of the peak discharges between the near Cannonville and Kanab gages. In only two cases from 1959 through 1973 were the annual peak discharges at the two gages associated with the same flood, hence only the two points in Figure 2.14c. The apparent large decreases in peak flood discharge between the near Kanab gage and the Lees Ferry gage in Figure 2.14d are probably the result of the large uncertainty associated with the day of occurrence of the annual-maximum flood at the near Kanab, UT annual-crest gage.

Given that the bankfull discharges are identical at the three gages, and the flood peaks do not decrease substantially between the near Cannonville, UT gage and the Lees Ferry, AZ gage, one would expect similar flood frequency distributions at the three gages. Comparison of flood-frequency curves for the annual-maximum flood series at the three gages is shown in Figure 2.15a. The gray shaded region indicating the region of overlap between the three flood-frequency distributions at the 95% confidence level or 0.05 level of significance in Figure 2.15a illustrates that the differences between flood-frequency distributions at the three gages are not statistically significant. (The weighted skew coefficients for the near Cannonville, UT and near Kanab, UT analyses were 0.199 and 0.024, respectively.) Likewise, Figure 2.15b shows that the flood-frequency distributions for the partial-duration flood series at the near Cannonville, UT and Lees Ferry, AZ gages are identical within error. In this figure, the peak discharge as a function of the return period for the partial duration-series at both gages for water years 1951 through 1955 are shown, as is the peak discharge as a function of the return period for the partial duration-series at the Lees Ferry, AZ gage for water years 1924 through 1996.

2.4i: Hydrologic summary with climatic implications

The Paria River is an ephemeral river with infrequent large floods of very short duration. For the period November 22, 1923 through September 30, 1996, at Lees Ferry, AZ, the mean instantaneous discharge, mean annual discharge , bankfull discharge, and largest peak flood discharge have been 0.77 m^3/s, 88 m^3/s, 90 m^3/s, and 320 m^3/s,

respectively. Because the Paria River is ephemeral, the mean instantaneous discharge has been equaled or exceeded only 20.6% of the time, and although the bankfull discharge has occurred every 2.2 years, it has been equaled or exceeded only 0.021% of the time. From about 1880 to 1996, the largest known flood occurred in 1909 and had a peak discharge only about 25% larger than largest flood that occurred during the period of gage record at Lees Ferry, AZ. Over the period of gage record, no significant trend exists in the annual flow volume; however, years with higher peak discharges have significantly larger annual flow volumes.

Only two significant trends in the Paria River hydrologic data are present for the period from November 22, 1923 through September 30, 1996: the mean instantaneous discharge has decreased by 6% or 0.049m^3/s; and the peak discharges of floods have decreased. Exclusion of the floods of October 5, 1925, September 13, 1927, and September 6, 1940 from the analysis completely removes the trend in peak discharges, however, indicating that the distribution of peak flood discharges less than 2.8x bankfull (99.8% of all floods) has been stationary with respect to time. No trends are present in either flood volume or flood duration for either the entire set of 1308 floods or the 33 floods with overbank peaks. Moreover, no trends are present in the duration of overbank flows. Thus, the distribution of flood volumes, flood durations, and overbank flow durations have all been stationary with respect to time. Though, as shown by Andrews (1990), the mean annual flood for the period from 1924 through 1939 was higher than for the post-1939 period, at the 0.05 level of significance, no statistically significant change occurred in the flood-frequency distribution for the annual-maximum flood series in the earliest 1940's. Analysis of the partial-duration flood series indicates that no change in the flood-frequency distribution occurred in 1940 for flows less than about 70 m^3/s. Furthermore, analysis of flow duration indicates that no change in the duration of flows less than 12 m^3/s has occurred over the period of gage record, that is, no change in discharges that have been equaled or exceeded more than all but 0.5% of the time has occurred from November 22, 1923 through September 30, 1996.

Bankfull discharges of the Paria River at the three gaging stations are the same within error, thus, the bankfull discharge is constant over at least the lowermost 127 km of the 157-km long river. Furthermore, analysis of the peak discharge of floods traveling down the river past the three gaging stations indicates that, on average, the peak discharge of floods does not change substantially down the Paria River. Peak discharges of the larger floods may decrease by about 33% and peak discharges of smaller floods may increase by as much as 300% between the near Cannonville, UT and Lees Ferry, AZ

gages. Also, flood-frequency distributions at the three gages are statistically indistinguishable. The channel of the Paria River, therefore, for more than 81% of its total length, is merely a conveyance system that transports flood waters derived from the uppermost 14% of the drainage basin.

Lack of major hydrologic trends in the Paria River indicates that the impact of postulated 20th century climate change, such as that as suggested by tree-ring width data (Figure 2.16), on the hydrology of the Paria River has been small. Anomalies in the annual tree-ring width index have been extensively used to reconstruct climatic variation in the southwestern United States (e.g. Dean and others, 1985; Webb, 1985; Webb and others, 1991; and Hereford and others, 1996); however, there is great uncertainty as to how changes in tree-ring width index reflect actual hydrologic change. From 1500 to the present, the only four statistically significant anomalies in the annual tree-ring width index, that is, anomalies for which the absolute value of the standard deviation has been smaller than the absolute value of the tree-ring width index minus unity, have been the negative anomalies of 1575-1589 and 1732-1734 and the positive anomalies of 1910-1921 and 1983-1986. Moreover, the magnitude of the peak for the positive anomaly of 1910-1921 is the largest since 309 A.D. (not shown in Figure 2.16), suggesting that the possible climate change associated with the 1910-1921 anomaly should have a significant hydrologic impact. Though the Paria River gage record begins on the falling limb of the 1910-1921 anomaly, some effect of the possible change in climate associated with this anomaly should still be present in the instantaneous discharge time series, allowing potential evaluation of the hydrologic effect of the largest tree-ring width index anomaly in 1700 years. Given that the Paria River hydrology has been fairly stable for the period of gage record, and the flood peak discharge distribution has also been stationary with respect to time (with the possible exception of the floods of October 5, 1925, September 13, 1927, and September 6, 1940), however, the apparent hydrologic impact reflected by even large anomalies in the tree-ring width index seems to be quite small.

Section 2.5: MODERN AND HISTORICALLY BASED RESEARCH IN THE PARIA RIVER SYSTEM

To determine the modern distribution of channel and sediment types in the Paria River system, an extensive program of field work was conducted from January 1993 through April 1996. This field program consisted of comprehensive topographic surveys of large sections of river valley, measurements of gravel and sand grain-size distributions, and inventories of sand, silt, and clay volumes in the channel and floodplains. The primary

Figure 2.16: 1200-1986 A.D. portion of the 0-1986 A.D. regional (i.e., northern Arizona and Southern Utah) composite of tree-ring width data from as many as 74 separate stands of Ponderosa Pine, Pinyon, Douglas Fir, Engelmann Spruce, Juniper, Rocky Mountain Bristlecone Pine and Great Basin Bristlecone Pine; in compositing the data, the mean tree-ring width index for the years from 1770 through 1962, i.e., the years of data overlap for all 74 stands, was set equal to unity for each stand. Data from the 74 stands are from 19 different sources (Laboratory of Tree-Ring Research, University of Arizona, 1990); individual sources are as follows: (1) 1 chronology by F. Biondi; (2) 3 chronologies by R.M. Bradfield; (3) 2 chronologies by K. Briffa and F.H. Schweingruber; (4) 4 chronologies by J.S. Dean; (5) 13 chronologies by J.S. Dean and D.O. Bowden; (6) 1 chronology by J.S. Dean and V.C. Lamarche; (7) 3 chronologies by J.S. Dean and W.J. Robinson, (8) 3 chronologies by J.S. Dean and R.L. Warren; (9) 1 chronology by J.S. Dean, W.J. Robinson, and D.O. Bowden; (10) 1 chronology by J.S. Dean, B.T. Burns, W.J. Robinson, and D.O. Bowden; (11) 2 chronologies by J.S. Dean, W.J. Robinson, and others; (12) 13 chronologies by D.A. Graybill; (13) 2 chronologies by T.P. Harlan; (14) 1 chronology by J.B. Harsha and C.W. Stockton; (15) 1 chronology by E. Schulman, D.O. Bowden, and J.S. Dean; (16) 3 chronologies by C.W. Stockton; (17) 5 chronologies by M.A. Stokes; (18) 14 chronologies by M.A. Stokes and T.P. Harlan; and (19) 1 chronology by C.E. Young.

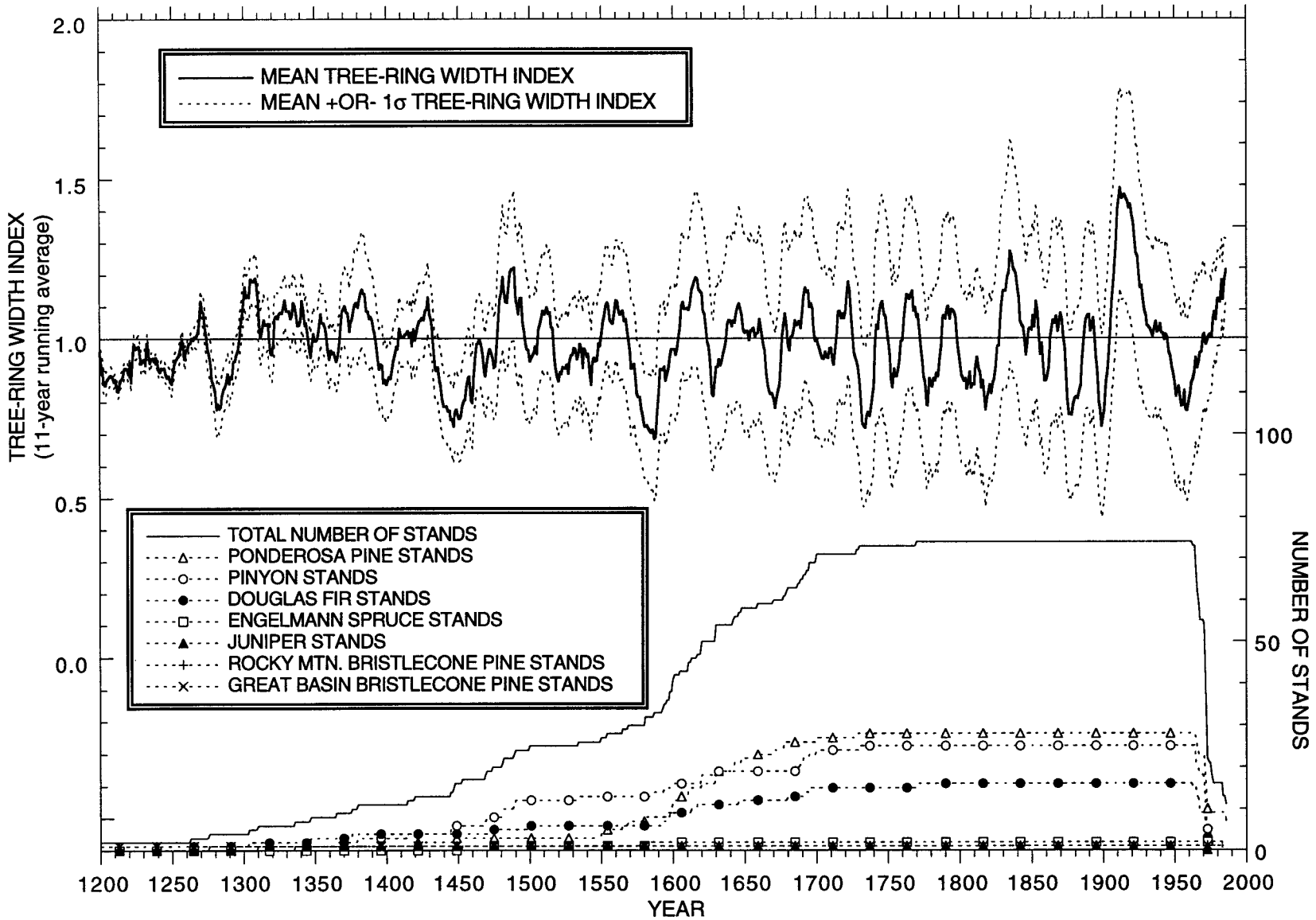
MEAN TREE-RING WIDTH INDEX
MEAN +OR- 1σ TREE-RING WIDTH INDEX
TOTAL NUMBER OF STANDS
PONDEROSA PINE STANDS
PINYON STANDS
DOUGLAS FIR STANDS
ENGELMANN SPRUCE STANDS
JUNIPER STANDS
ROCKY MTN. BRISTLECONE PINE STANDS
GREAT BASIN BRISTLECONE PINE STANDS
TREE-RING WIDTH INDEX
(11-year running average)
2.0
1.5
1.0
0.5
0.0
NUMBER OF STANDS
100
50
0
1200
1250
1300
1350
1400
1450
1500
1550
1600
1650
1700
1750
1800
1850
1900
1950
2000
YEAR

study site for this research was chosen as the segment of the Paria River above Lees Ferry, AZ because of its location at the bottom of the basin, its extensive data set of historical flow, channel geometry, and sediment-transport, and its being the focus of previous work. Secondary study sites were the segment in the vicinity of the near Cannonville, UT gage; the segment including the townsites of Paria, Rock House, and Adairville, UT; and the segment of the Paria River in the Lower Paria River Gorge below the near Kanab, UT gage. This section of this chapter presents results from both the 1993-1996 field program and analyses of the 1872-1994 historical data set of channel geometric measurements from these four segments of the river.

2.5a: The Paria River at Lees Ferry, AZ in 1993

The 1993 field program

The goal of the 1993 field program at Lees Ferry, AZ was a complete topographic and sedimentologic characterization of the lowermost modern Paria River system. To accomplish the first part of this goal, 3.3 km of the valley in the vicinity of the USGS gaging station were surveyed with a Nikon Model DTM-A10 total station during January 16-18, March 5-17, May 15-18, and November 13-14, 1993. The upper end of this surveyed reach is 2.8 km above the USGS gaging station and extends downstream to a position 1.4 km above the low-water confluence of the Paria River with the Colorado River (Figure 2.4). During the course of the four 1993 field excursions, 267 cross-sections were surveyed across the valley encompassing a total of 8755 individual locations surveyed to 0.5 cm precision; these cross-sections were variably spaced in the streamwise direction to capture all macroscopic geometric variability in the channel and floodplain.

The second part of the 1993 field program focused on measurement of: locations of various sediment types (e.g., gravel, sand, silt, and clay) in the system, volumes of each sediment type at each location, and grain-size distributions of each sediment type at each location. The channel floor and floodplain of the Paria River consists of a relatively thin, 0-2 m thick, layer of sand, silt, and, clay overlying a thicker layer of gravel. From March 21 to April 4, 1993, 599 measurements of sand, silt, and clay thickness to 1-cm precision were obtained in the lower 1.95 km of the 3.3 km surveyed reach with a 2-m-long pole subdivided at 1-mm increments to determine the local volume of sand, silt, and clay overlying the gravel in the channel and channel-margin portions of the floodplain. Grain-size distributions of the sand, silt, and clay in the system were determined by the collection and dry-sieve analysis (at 0.5 ϕ intervals from -6 to 4 ϕ) of 94 samples from surveyed locations in the channel, floodplain, and terraces. Grain-size distributions of the

underlying gravel in the lower 1.95 km of the 3.3 km reach were constructed from 43 subsets of 3938 individual measurements of clast-size determined by the method of Wolman (1954) to cm precision. Since pebble counts typically underrepresent the finest sizes of gravel on the bed, gravel grain-size distributions were modeled as log-normal distributions weighted toward the coarsest 90% of the sample.

Detailed description of the Lees Ferry study area in 1993

In 1993, the 3.3 km Lees Ferry study area consisted of approximately 1.4 km of river channel in local hydraulic equilibrium with an active floodplain and two deeply incised reaches (Figure 2.17) of 0.5 and 1.35 km length, respectively. These incised reaches are entrenched 1-2 m into fluvial terraces that were formerly active floodplains of the river. Two headcuts, i.e., the upper and lower headcuts, bordering the upper ends of these two incised reaches were 1.85 and 0.85 km above the gage, respectively, in 1993. As will be illustrated in a subsequent section of this paper, the lower headcut is a relatively new feature of the river and is due to a lowering of the base level at the mouth of the Paria in 1963 as a result of the closure of Glen Canyon Dam, and the upper headcut is an older feature that has been located near its present position since at least 1929 and is probably due to a change in the base level at the mouth of the Paria resulting from an avulsion in 1909. In the equilibrium reaches, i.e., reaches with active floodplains and net constructional banks, the Paria River has a mean longitudinal slope of 0.004, a mean bankfull width of 23 m, a mean bankfull depth of 1.8 m, and a mean bank-slope angle of 15 degrees. In the incised reaches, i.e., reaches entrenched into formerly active floodplains (that are now terraces) with net erosional banks, bankfull widths cannot be easily defined, but the channel tends to have steeper banks and be about 20 to 30% narrower than in the equilibrium reaches. The widest parts of the Paria River tend to occur immediately upstream of the headcuts, where the bankfull widths may be as great as 45 m. In the equilibrium reaches, the width of the floodplain bordering the channel is highly variable, ranging from as little as 20 m to more than 100 m. Colluvium from the margins of the canyon, alluvial fans derived from tributary canyons, and older Paria River fluvial terraces typically rise 0.5 to 1 m above the floodplain sediments.

In both the equilibrium and incised reaches, the floor of the channel of the Paria River is composed of ellipsoidally shaped gravel (Figure 2.18) overlain by variable thicknesses of sand, silt, and clay. Over the 1.95 km of the Lees Ferry reach in which pebble counts were conducted, a correlation exists between the coarseness of the gravel on the bed and the local longitudinal bed slope. Three gravel grain-size distributions were

Figure 2.17: **(a)** Upstream view of the equilibrium channel of the Paria River above the upper headcut. Photograph taken 6 km above the Paria River gage by D.J. Topping on January 23, 1993. **(b)** Upstream view of the incised channel of the Paria River below the gage. Photograph taken 250 m below the gage by D.J. Topping on July 6, 1992.

a)

b)

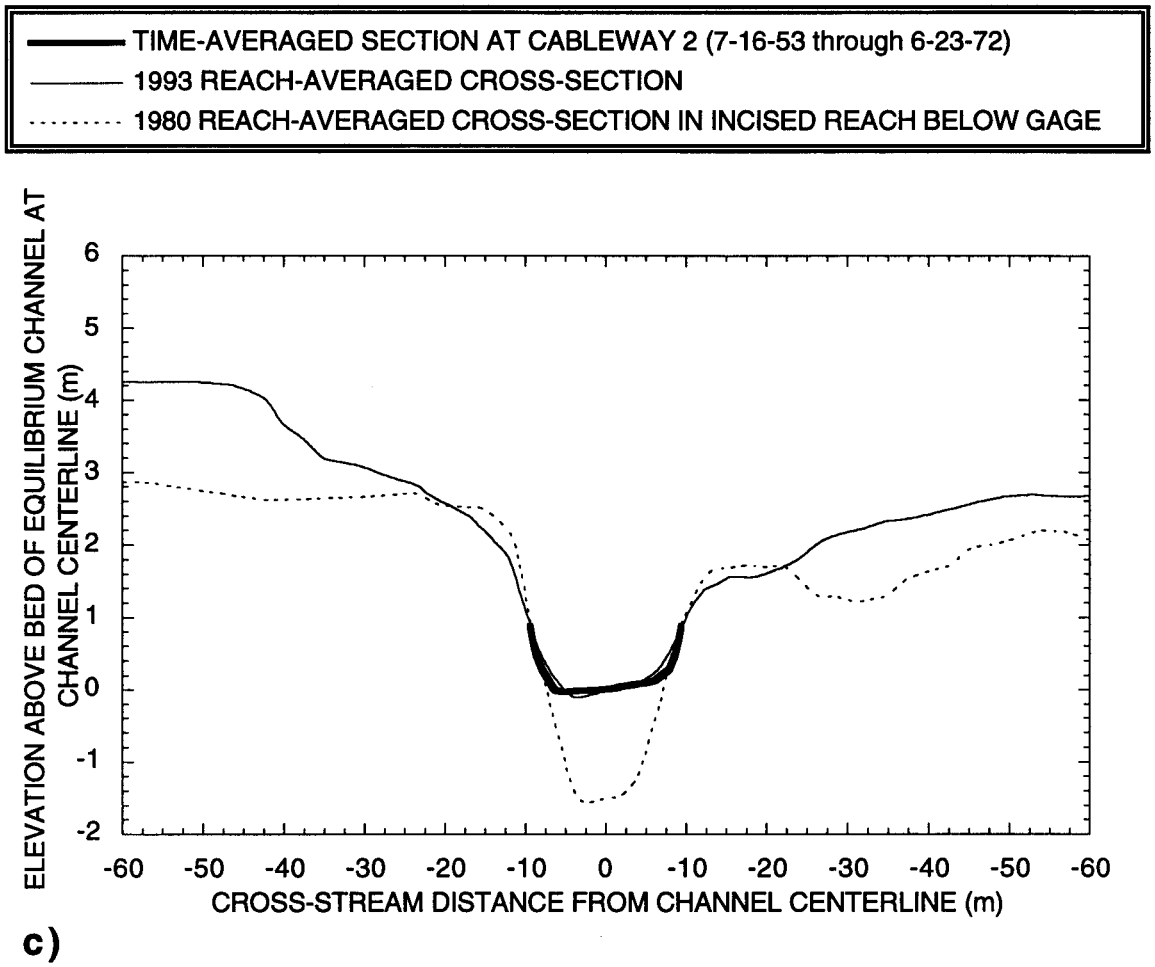

c)

Figure 2.17 (continued): **(c)** Comparison of the geometry of: (1) the time-averaged cross-section at Cableway 2 from 7-16-53 through 6-23-72; (2) the 1993 reach-averaged cross-section (described in detail below); and (3) the 1980 reach-averaged cross-section from the incised reach below the gage. Zero elevation of each cross-section is defined as the elevation of the bed of the equilibrium channel at the channel centerline; thus, 1.5 m of elevation have been subtracted from the 1980 reach-averaged cross-section to account for the channel incision. The convention used for all cross-sections in this study, unless otherwise stated, is that "left" in the cross-section corresponds to the left bank of the river when facing downstream. The 1980 reach-averaged cross-section was constructed from the USGS slope-area survey of October 30-31, 1980 following the September 9, 1980 flood; the time-averaged cross-section at Cableway 2 and the reach-averaged 1980 cross-section have been reversed to match the geometric asymmetry of the 1993 reach-averaged cross-section.

defined on the basis of the local longitudinal bed slope and a fourth was defined for an equilibrium reach of the river (Figure 2.19).

"Gravel grain-size distribution 1" comprises the bed of the 0.6 km reach above the lower headcut and is defined by measurements of the nominal diameter of 2082 individual particles; this reach has a mean longitudinal bed slope of 0.003 and includes the lower portion of the upper incised reach. D_{50} and D_{84} determined from the raw data are equal to 5 and 12 cm, respectively; and D_{50} and D_{84} determined from the log-normal fit to the data are 5.1 and 11.3 cm, respectively.

"Gravel grain-size distribution 2" comprises the bed of the 0.85 km reach below the lower headcut and above the gage and is defined by measurements of the nominal diameter of 1693 individual particles; this reach has a mean longitudinal bed slope of 0.006. D_{50} and D_{84} determined from the raw data are equal to 8 and 25 cm, respectively; and D_{50} and D_{84} determined from the log-normal fit to the data are 7.6 and 20.9 cm, respectively.

"Gravel grain-size distribution 3" comprises the bed in the 0.5 km reach below the gage and is defined by measurements of the nominal diameter of 163 individual particles; this reach is deeply incised and has a mean longitudinal bed slope of only 0.002. D_{50} and D_{84} determined from the raw data are equal to 3 and 9 cm, respectively; and D_{50} and D_{84} determined from the log-normal fit to the data are 3.3 and 8.0 cm, respectively.
"Gravel grain-size distribution 4" comprises the bed in the 162-m equilibrium reach, known as "Reach 3", located between the 2 meander bends above the lower headcut (Figure 2.4). Reach 3 is part of a three-reach composite described below and consists of a relatively straight section of equilibrium channel bordered by active floodplains and having a longitudinal bed slope of 0.004. Gravel grain-size distribution 4 is defined by measurements of the nominal diameter of 842 individual particles. For this fourth grain-size distribution, D_{50} and D_{84} determined from the raw data are equal to 4 and 10 cm, respectively; and D_{50} and D_{84} determined from the log-normal fit to the data are 4.3 and 8.8 cm, respectively.

Unlike the coarseness of the gravel in the bed, the average thickness of the sand, silt, and clay layer burying the gravel is similar in both the equilibrium and incised reaches. In the 0.6 km reach above the lower headcut, at low flows, sand, silt, and clay cover 73% of the bed with gravel comprising the remainder of the bed surface. Thickness of the sand, silt, and clay layer as defined by 130 measurements in this reach is 20±18 cm over the 73% of the bed in which the gravel is buried translating into an average thickness of 15 cm over the entire bed. In the 1.35 km reach below the lower headcut, at low flows, sand, silt, and clay cover 57% of the bed. Thickness of the sand, silt, and clay layer as defined

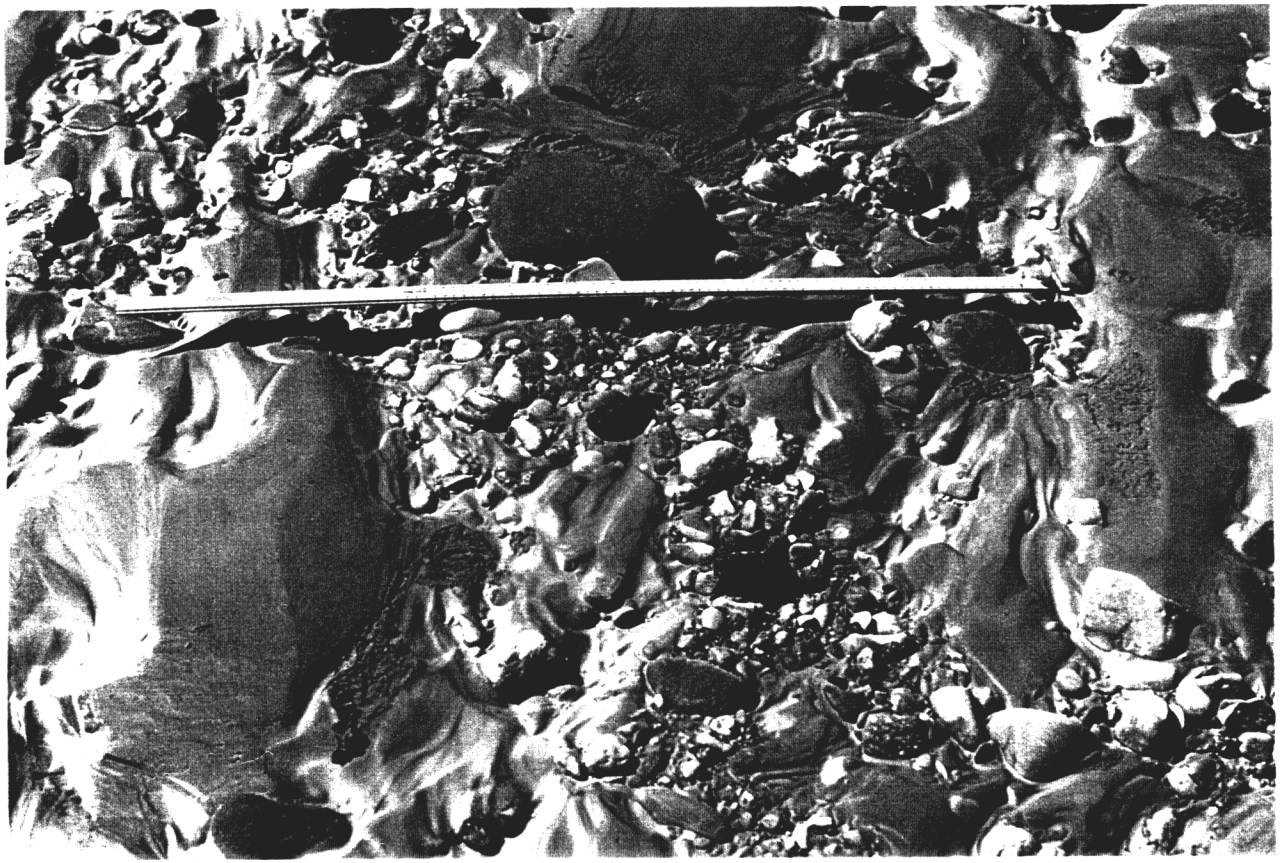

Figure 2.18: Photograph illustrating a typical portion of the Paria River bed; meter stick for scale. The downstream direction is toward the top of the photograph. Photograph taken by D.J. Topping 1.5 km above the gage on March 21, 1993.

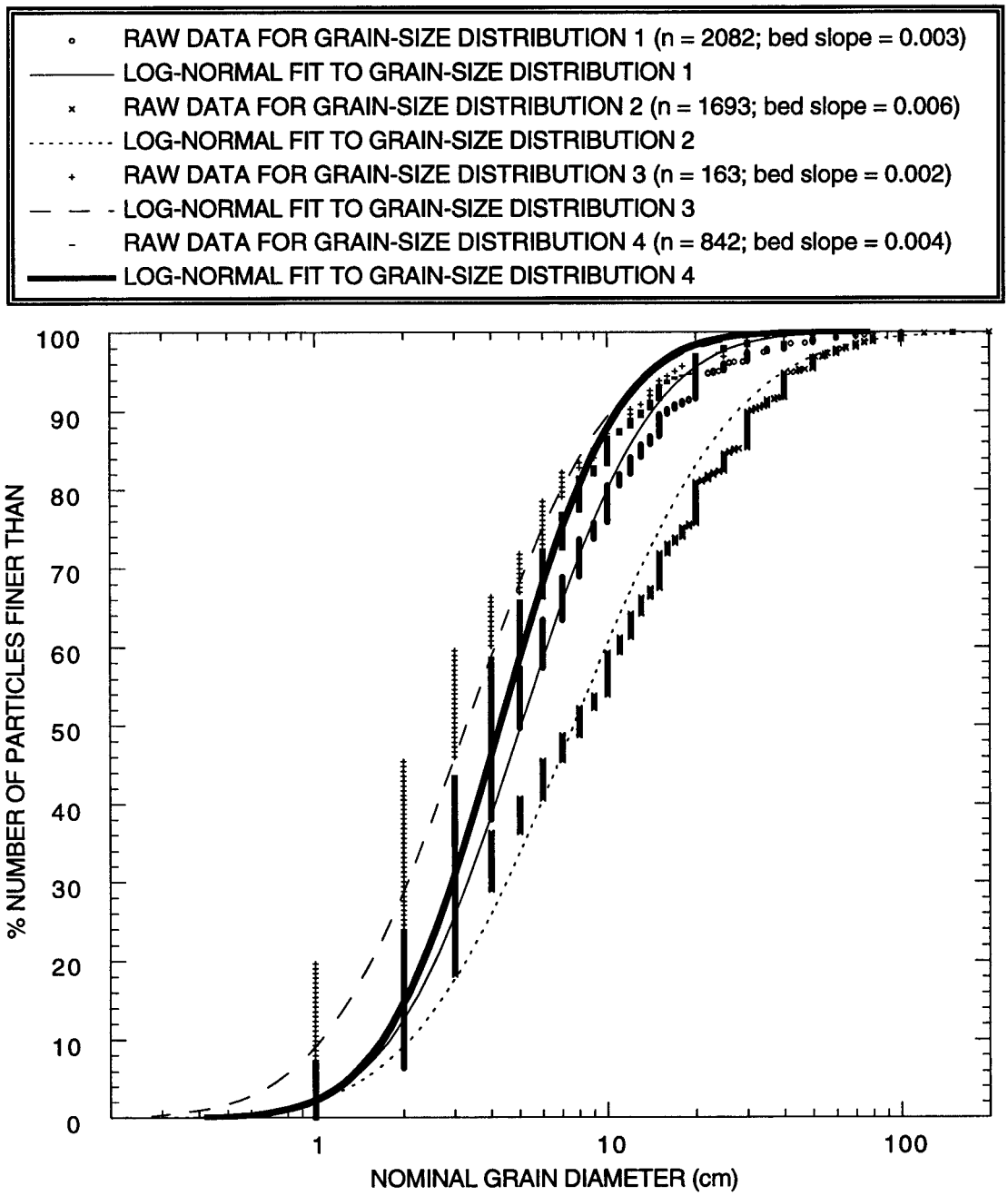

Figure 2.19: Cumulative grain-size distributions of the four gravel grain-size distributions that comprise the bed of the Paria River in the Lees Ferry study area.

by 469 measurements in this reach is 22±25 cm over 57% of the bed in which the gravel is buried translating into an average thickness of 13 cm over the entire bed.

Four types of grain-size distributions of sand, silt, and clay are present in the Lees Ferry reach, as determined from the 94 grain-size analyses of the 94 bed material samples collected in 1993. These four grain-size distributions comprise four different sediment environments: the channel thalweg (composed of Type 1 sediment), the channel bar tops and banks (composed of Type 2 sediment), the floodplains (composed of Type 3 sediment), and the terrace surfaces (composed of Type 4 sediment). Figure 2.20 indicates the relative positions of these four sediment environments in the 1993 reach-averaged cross-section (defined in the subsequent section); Table 2.3 lists the mean volume fractions and standard deviations among samples for each 1/2-ϕ size class for each of the four types of sediment.

In the sandy portions of the channel, four bed configurations can be present the Paria River depending on the flow conditions: ripples, dunes, upper-plane bed, and antidunes. Along the margins of the channel, and in other portions of the channel where the boundary stress is low, the bed is typically covered by ripples. In the main channel, in flows less than 30 cm in depth, dunes form on those portions of the bed where the gravel is effectively buried, i.e., where D_{84} of the gravel is buried by the sand, silt, and clay layer. The dunes wash out and the bed becomes planar (upper-plane bed) at slightly higher flows. At flows between about 30 and 60 cm in depth, the Froude number in the thalweg increases to the critical value of 0.844 (Kennedy, 1963), and antidunes develop on the portions of the bed where D_{84} of the gravel is buried by the sand, silt, and clay layer (Figure 2.21a). These antidune fields typically occupy the main thalweg and have not been observed to develop on the low-amplitude bar surfaces (where the sand, silt, and clay layer is typically thinner). At flows greater than 60 to 80 cm in depth, the surface waves over the antidunes die out indicating that the antidunes on the bed are gone; presumably, this occurs when most of the sand, silt, and clay overlying the gravel has gone into suspension and the bed has become starved of sand. Observations of the water surface during higher flows indicate that the bed remains planar after the antidunes die out. A photograph, taken by USGS technician W.T. Stuart on September 13, 1939, of the planar water surface indicates that antidunes are not present at near-bankfull flows, i.e., flows approximately 1.6-2.0 m in depth (Figure 2.21b). During the highest flows, when the transport stage of the gravel exceeds 2, gravel dunes probably develop on the bed (as previously discussed in Section 2.4c-1).

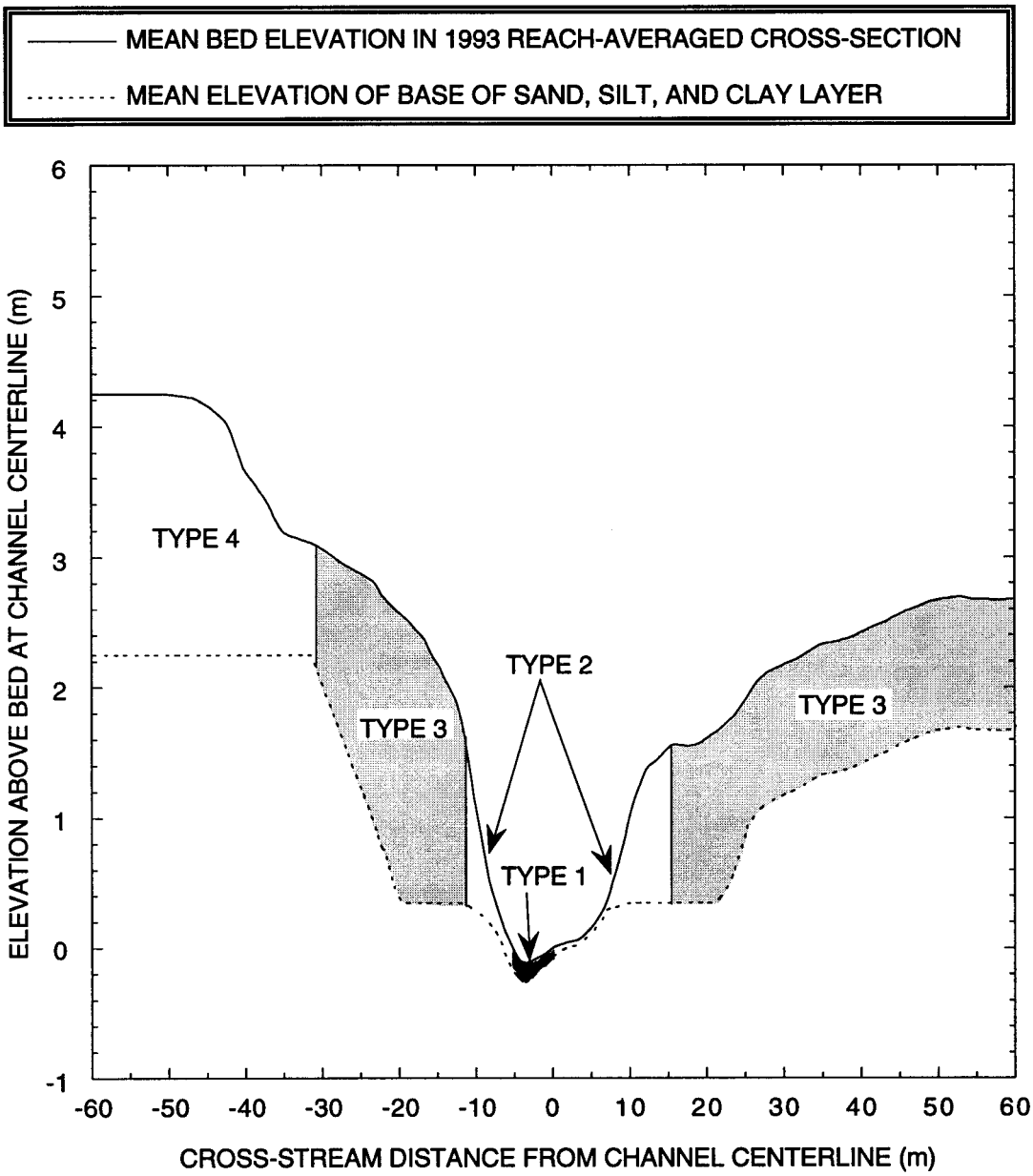

Figure 2.20: Locations of the four sediment environments in the 1993 reach-averaged cross-section.

Table 2.3: Mean and standard deviation of the volume fraction in each size class for the four types of sediment overlying gravel in the Paria River; n indicates the number of individually analyzed samples comprising each sediment type. Distributions are truncated at -1.0 ϕ.

SEDIMENT SIZE CLASS (inclusive of finer bound and exclusive of coarser bound)		**TYPE 1 SEDIMENT** (n = 66)		**TYPE 2 SEDIMENT** (n = 4)		**TYPE 3 SEDIMENT** (n = 14)		**TYPE 4 SEDIMENT** (n = 10)	
ϕ	mm	MEAN (%)	STD. DEV. (%)	MEAN (%)	STD. DEV. (%)	MEAN (%)	STD. DEV. (%)	MEAN (%)	STD. DEV. (%)
-0.5 to -1.0	1.41 to 2.0	13.4	15.9	0.0620	0.0573	0.0997	0.112	0.663	1.65
0.0 to -0.5	1.00 to 1.41	4.87	5.13	0.0691	0.0655	0.205	0.349	0.424	0.975
0.5 to 0.0	0.71 to 1.00	3.15	2.86	0.0995	0.101	0.695	1.01	0.672	1.34
1.0 to 0.5	0.50 to 0.71	6.62	4.28	0.131	0.111	2.68	3.75	1.85	2.16
1.5 to 1.0	0.35 to 0.50	17.0	9.25	0.0802	0.0274	6.01	6.06	5.94	3.83
2.0 to 1.5	0.25 to 0.35	27.7	15.2	0.232	0.129	14.1	9.64	21.8	11.0
2.5 to 2.0	0.177 to 0.25	15.1	9.51	1.87	0.609	24.8	8.97	29.9	9.43
3.0 to 2.5	0.125 to 0.177	7.99	6.51	31.9	10.0	28.7	11.5	21.8	7.49
3.5 to 3.0	0.088 to 0.125	2.69	1.85	18.4	0.897	8.33	2.77	6.96	2.73
4.0 to 3.5	0.0625 to 0.088	1.01	0.912	21.3	4.10	6.18	2.15	4.74	1.68
<4.0	<0.0625	0.477	1.15	25.9	6.54	8.20	4.66	5.24	2.73

Figure 2.21: **(a)** Breaking wave over antidune in Paria River; meter stick for scale (0.8 m is protruding from the sand). Mean flow depth in the antidune field is approximately 40 cm. Photograph taken by D.J. Topping 1.3 km above the gage on March 22, 1993.
(b) Upstream view of Paria River at near-bankfull stage; photograph taken by W.T. Stuart 500 m below the gage on September 13, 1939. Save for the surface waves against the outside bank of the meander in the foreground, the water surface is relatively planar.

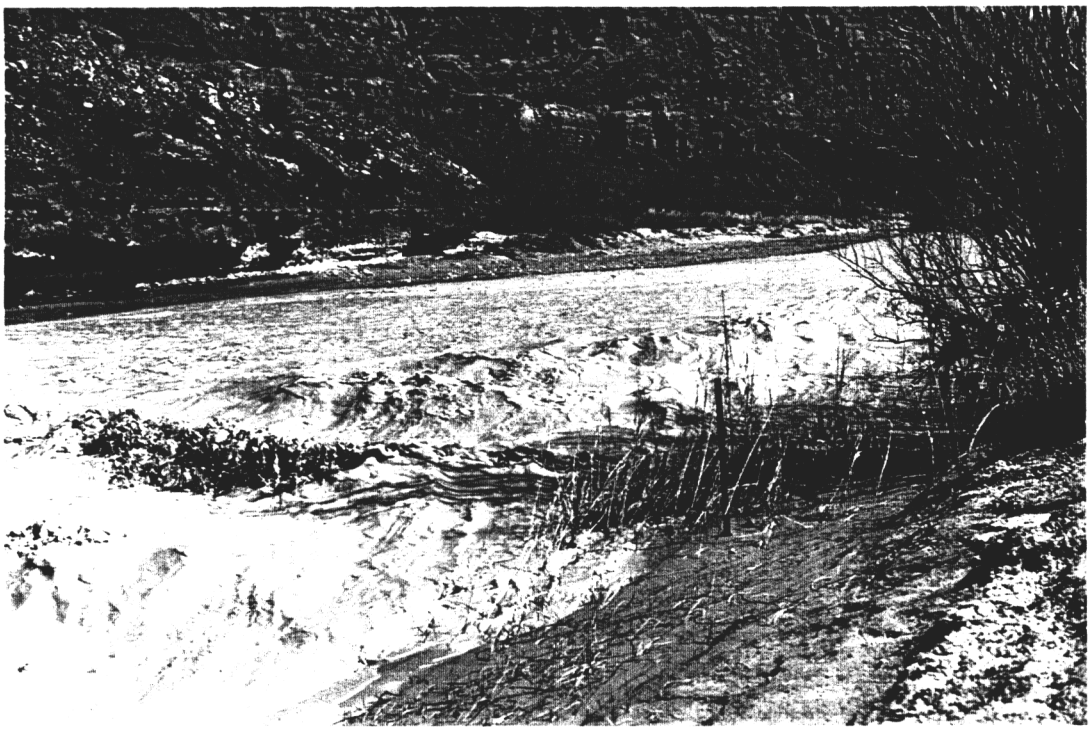

a)

b)

2.5a-1: The 1993 Lees Ferry 3-reach composite and reach-averaged cross-section

The best approach to comparing the channel geometries of present and past reaches of a river is through the construction of reach-averaged cross-sections; this approach allows the direct comparison of both the reach-scale mean and variance in topography between either spatially or temporally distinct reaches of a river. Likewise, an extremely useful approach to modeling the reach-scale geomorphic adjustment of a channel during floods is through reach averaging, in which all convective accelerations driven by local variability in topography and roughness are removed from the problem and all reach-scale channel changes are related to the reach-averaged, uniform flow field (this physical simplification is developed in detail in Chapter 3). Thus, in order to compare modern equilibrium channel shapes to past channel shapes, and to convert field measurements into a useful format for input into a reach-averaged, geomorphically coupled flow and sediment-transport model (developed in Chapter 3), the topographic, sedimentologic, and roughness information from a characteristic portion of the Paria River was collapsed onto a single reach-averaged cross-section.

That portion of the Paria River in the Lees Ferry study area chosen to be the most representative of alluvial portions of the Paria River in the 10 km above its confluence with the Colorado River was a 762-m composite of 3 individual equilibrium reaches, termed "Reach 1", Reach 2", and "Reach 3", that are located on Figure 2.4. Because the goal of constructing the reach-averaged cross-section was to collapse all information from equilibrium alluvial channel segments onto a single reach-averaged cross-section, apexes of meanders (typically located against bedrock cliffs) and regions of local channel instability, i.e., the reaches including the upper headcut and the entire reach below the lower headcut, were excluded from the segment of the river to be reach-averaged. Furthermore, since one of the major goals of this study was to develop and test a reach-averaged, geomorphically coupled, flow and sediment transport model (described in Chapters 3 and 4), these three reaches were chosen to construct a reach-averaged cross-section (to be used as input into the model) also because they were similar to the reach in which most of the historical discharge and suspended-sediment measurements were made by the USGS (Figure 2.22), measurements that will be used to test the model in Chapter 4.

Respective lengths of Reaches 1, 2, and 3 were 304 m, 296 m, and 162 m in 1993 and the mean channel longitudinal bed slope for this 3-reach composite was 0.004. Each reach consisted of a relatively straight channel, with low-amplitude bars and parallel constructional banks (not erosional banks), bordered by a well-defined, flat floodplain.

Figure 2.22: **(a)** Upstream oblique view of the reach immediately upstream of the gage at Cableway 2; photograph taken sometime between 1964 and 1968. This reach is the reach in which most of the historical discharge and suspended-sediment measurements were made by the USGS. Photograph from USGS-WRD Arizona District files, Flagstaff, AZ. **(b)** Downstream oblique view of Reach 2 of the 1993 3-reach composite used in constructing the 1993 reach-averaged cross-section. Photograph taken by D.J. Topping on November 15, 1993.

a)

b)

Not only were these reaches in apparent vertical and lateral equilibrium with the floodplain in 1993, but they had been relatively stable since about 1927-1929, as indicated by the results of analyses presented in the next section of this paper. Though some local lateral accretion of floodplain sediment had occurred (most notably in the lower section of Reach 2), no notable channel-bed aggradation or incision had occurred in this portion of the river since 1929.

Method for constructing a reach-averaged cross-section

The method for constructing a reach-averaged cross-section for each reach is a four-step process: **(STEP 1)** the channel centerline is defined at the bankfull elevation; **(STEP 2)** zero elevation in each cross-section is defined as the elevation of the bed at the channel centerline; **(STEP 3)** measurements of the: (a) local bed elevation, (b) local thickness of sand, silt, and, clay, (c) local sand, silt, and clay grain-size distribution, and (d) local gravel grain-size distribution at each point in each cross-section are weighted by 1/2 the distance between that cross-section and the next cross-section upstream plus 1/2 the distance between that cross-section and the next cross-section downstream; and **(STEP 4)** mean values and standard deviations of these measurements at each point on each cross-section are calculated along the direction of the channel centerline.

The 1993 reach-averaged cross-section

In the 1993 survey, each cross-section contained approximately 50-80 topographic measurement points in the channel, floodplain, and terrace environments. The mean and mean ± 1 standard deviation of bed elevation for the reach-averaged cross-sections for Reaches 1, 2, and 3 are illustrated in Figure 2.23. These three reach-averaged cross-sections were then weighted by the lengths of each reach and combined to form the "1993 reach-averaged cross-section" depicted in Figure 2.24.

Since Reaches 1 and 2 are above the 1.95-km reach of intensive measurements of sand, silt, and clay layer thicknesses, sand, silt, and clay grain-size distributions, and gravel grain-size distributions, measurements from only Reach 3 were used to define these properties for the 1993 reach-averaged cross-section (this approximation was checked in the field in November 1993 and found to be adequate). For each channel cross-section point in Reach 3, the thickness of the sand, silt, and clay layer overlying the gravel was determined by interpolation from three measurements made across the channel at each cross-section. Thickness of the sand, silt, and clay layer in the floodplains and terraces was extrapolated from the channel with the aid of local measurements from shallow

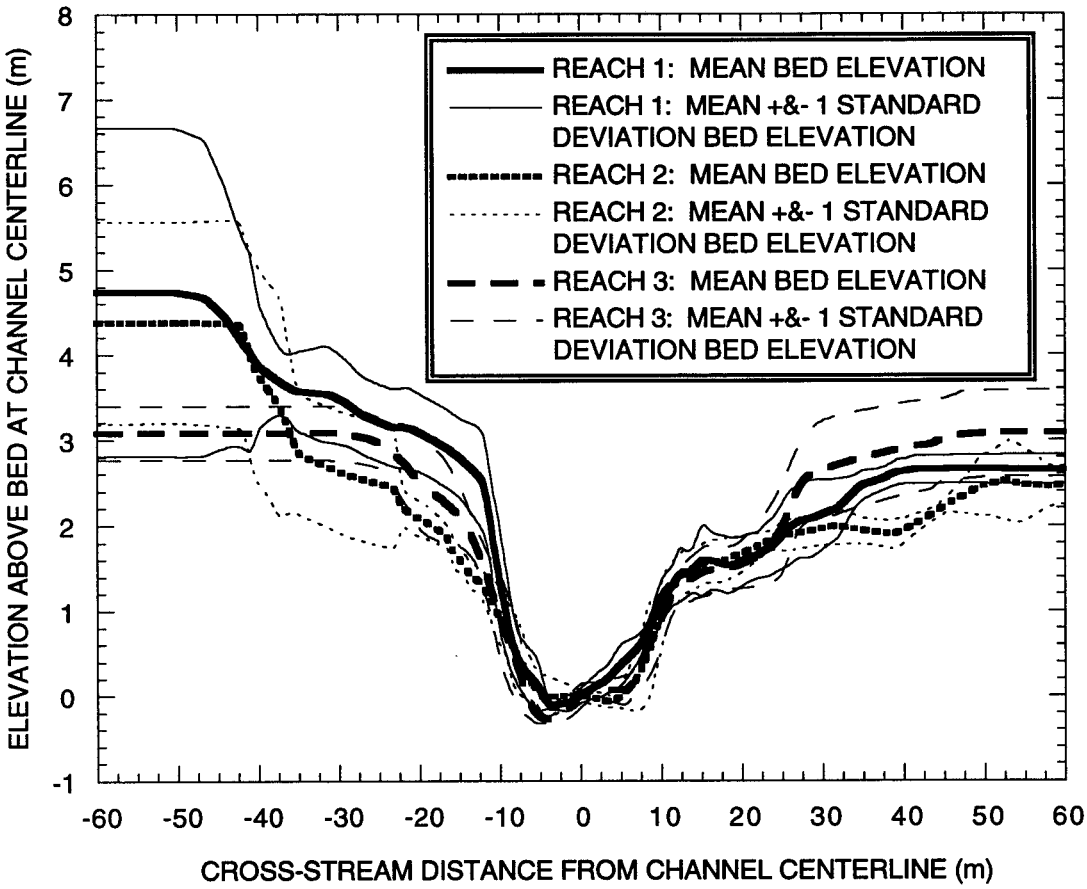

Figure 2.23: Mean, mean plus one standard deviation, and mean minus one standard deviation bed elevation as a function of cross-stream position in the reach-averaged cross-sections from Reaches 1, 2, and 3 of the 1993 3-reach composite.

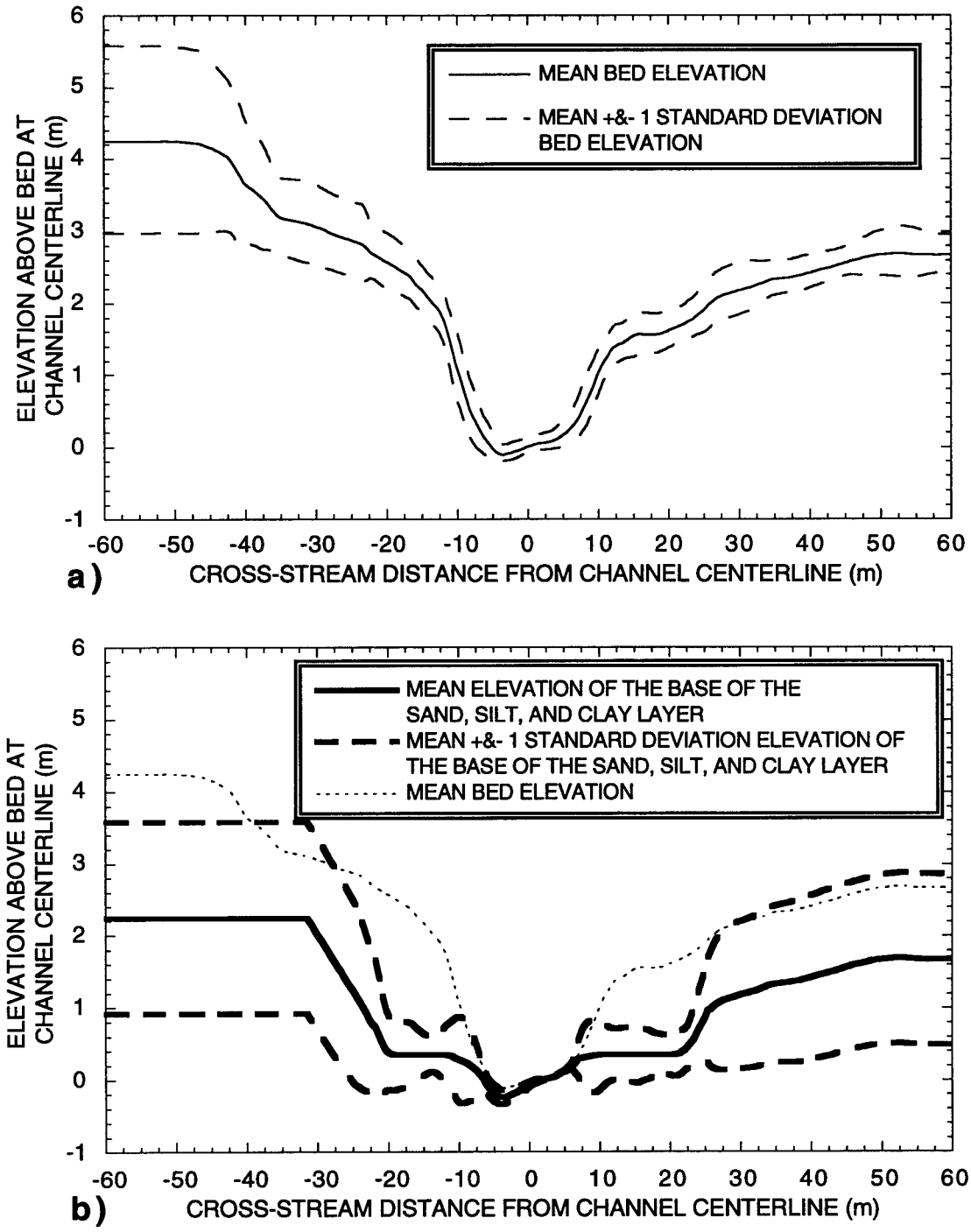

Figure 2.24: **(a)** Mean, mean plus one standard deviation, and mean minus one standard deviation bed elevation as a function of cross-stream position in the 1993 reach-averaged cross-section. **(b)** Mean, mean plus one standard deviation, and mean minus one standard deviation of the elevation of the base of the sand, silt, and clay layer as a function of cross-stream position in the 1993 reach-averaged cross-section; for reference, the mean bed elevation as a function of cross-stream position in the 1993 reach-averaged cross-section is also shown.

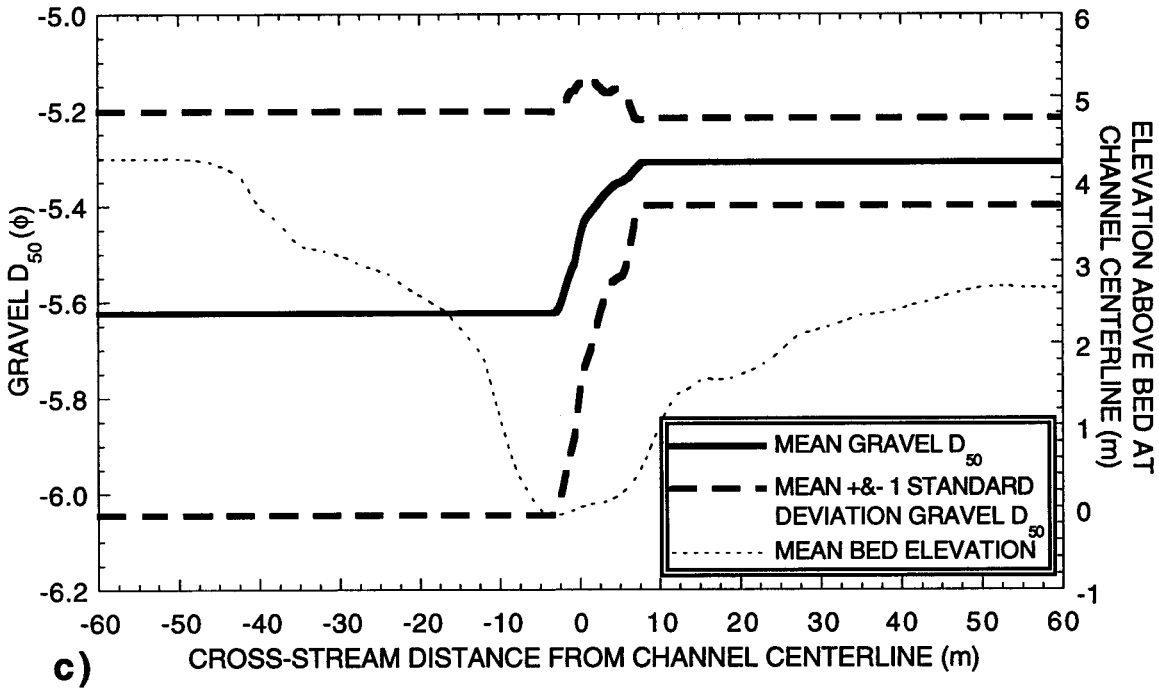

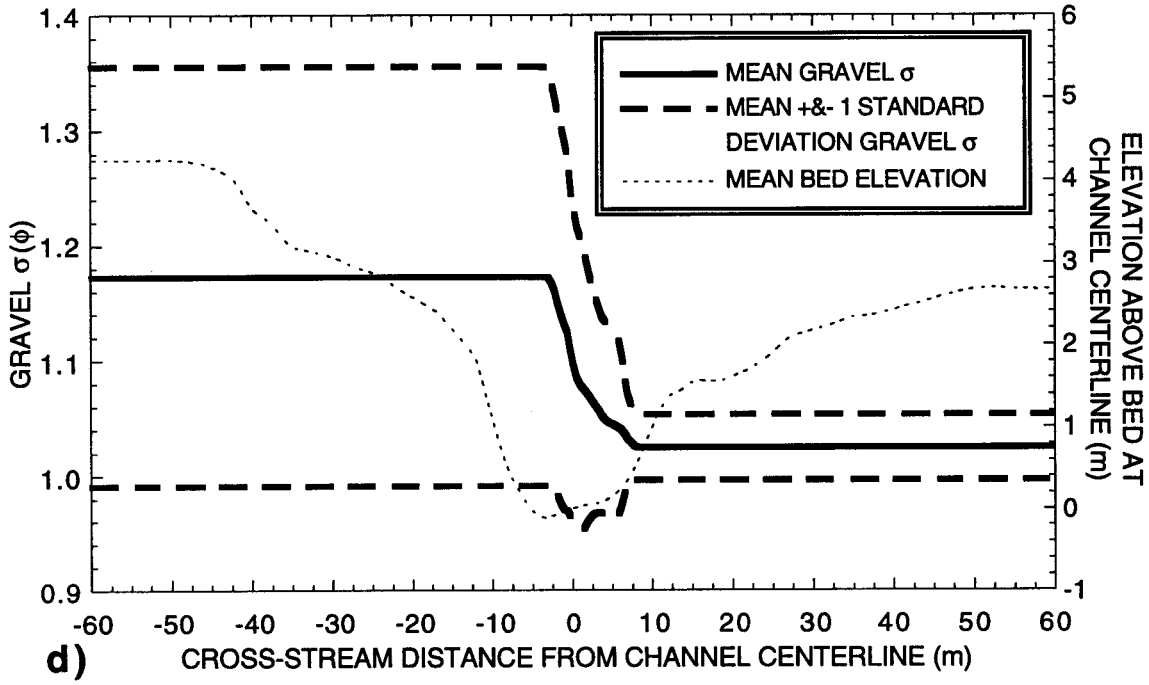

Figure 2.24 (continued): **(c)** Geometric mean, geometric mean plus one standard deviation, and geometric mean minus one standard deviation of the gravel D_{50} as a function of cross-stream position in the 1993 reach-averaged cross-section; for reference, the mean bed elevation at each cross-stream position is also shown. **(d)** Geometric mean, geometric mean plus one standard deviation, and geometric mean minus one standard deviation of the gravel σ as a function of cross-stream position in the 1993 reach-averaged cross-section; for reference, the mean bed elevation at each cross-stream position is also shown.

trenches and from pre-existing cuts made by tributary channels. The gravel grain-size distribution at each channel cross-section point in Reach 3 was determined from four individual Wolman pebble counts (combined into one pebble count in Figure 2.19) that were conducted in the thalweg and bar environments of this reach. Gravel grain-size distributions under the sand, silt, and clay layer in the floodplain and terraces were extrapolated from measured grain-size distributions at the margins of the channel.

2.5b: The Paria River at Lees Ferry, AZ from 1872 to 1994

All channel geometry data collected in the Lees Ferry reach from 1872 to 1994 were compiled and analyzed in order to: place the above 1993 spatial analysis of the Lees Ferry reach of the Paria River in a broader historical context, to address whether changes in channel geometry reported by Hereford (1986, 1987a) and J. Graf and others (1991) are merely local changes or really reach-scale changes, and to correctly interpret any temporal trends in the 1947-1983 suspended-sediment data collected in the Lees Ferry reach. The following section of this chapter is thus organized into six subsections: (1) presentation and evaluation of the seven different types of data used to characterize channel geometry; (2) reconstruction of the lateral position of the channel from 1872 to 1994; (3) reconstruction of the vertical position of the channel bed from 1872 from 1994; (4) reconstruction of reach-averaged channel cross-section geometry from 1872 to 1994; (5) analysis of changes in the amount of sediment stored in the Lees Ferry since 1925; and (6) comparison of the historical and 1993 measured grain-size distributions of sand, silt, and clay on the bed of the channel.

The following are the results from this aspect of the study. During the period from 1872 to 1994, the Lees Ferry reach of the Paria River has experienced both vertical and lateral changes in the position of the channel, mainly in response to changes in base level at the confluence with the Colorado River. From 1939 to 1993, the largest changes in the vertical position of the channel were limited to the reach within 1.8 km of the historical high-water confluence with the Colorado; and, from about 1872 to 1993, all significant changes in the vertical position of the Paria River channel were limited to the reach within about 3.4 km of the historical high-water confluence with the Colorado River.

In contrast to the conclusions of Hereford (1986, 1987a) and J. Graf and others (1991), no net formation of new floodplain volume has occurred since 1939 in this reach. Regardless of changes in the lateral and vertical position of the channel, for reaches of a fixed reach-averaged longitudinal bed slope (within 15% of 0.0035), the cross-section channel geometry has not changed since 1872. Since 1963, however, the lowermost 2.3

km of the Paria River above the historic high-water confluence have incised by as much as 1.5 m, in response to the new base level at the confluence resulting from the closure of Glen Canyon Dam on the Colorado River. Effect of the incision first reached the gage in 1972; after 1980, the channel in the reach near the gage was 30-40% narrower than the non-incised, equilibrium channel that occupied this reach prior to 1972. Above the lower incised reach near the gage, however, the cross-section geometry of the river in 1993 was identical to the cross-section geometry that existed for longitudinal bed slopes near 0.0035 in the gage reach from about 1872 to 1972. The only universal change that has affected the entire lowermost Paria River is not a geomorphic change, but rather, a botanical change; this change is the dense colonization, by the nonnative tamarisk and Russian olive, of floodplains that were only lightly to moderately vegetated prior to the mid-1960's.

Comparison of the inferred positions of channel and floodplain surfaces in the dated stratigraphic section of Hereford (1986, 1987a) with surveyed positions of these features in cross-sections from 1939, 1963, and 1993 that intersect the location of his stratigraphic section indicates that the stratigraphic methods that have previously been used to estimate the volume and age of floodplain sediment in the Paria River basin by Hereford (1986, 1987a, 1987b) and W. Graf (1987) can be misleading. In fact, little significant sediment storage, as indicated by surveyed cross-sections, has occurred in the Paria River above the gage since 1925-1929. However, the amounts of net sediment storage and erosion over time have been very large in the reach within 1.8 km of the historic high-water confluence with the Colorado River, i.e., the reach with the largest historic changes in the vertical and lateral position of the channel. In this lowermost reach, net erosion occurred from 1925-1929 to 1939-1943, net deposition occurred from 1939-1943 to 1963, and net erosion occurred from 1963 to 1993. Finally, the size distributions of the sand, silt, and clay on the bed and banks of the Paria River have not changed over the last 40 years and can thus be treated as invariant with respect to time.

2.5b-1: Source and evaluation of information comprising the 1872-1994 channel geometry data set

The 1872-1994 Lees Ferry channel geometry data set was compiled from seven different types of measurements (listed in order of relative usefulness): (1) USGS slope-area topographic channel surveys; (2) larger-scale topographic surveys made by the National Park Service (NPS) and the Bureau of Reclamation (USBR); (3) USGS discharge measurement field notes; (4) aerial photographs; (5) the 1927 General Land Office cadastral survey of the Lees Ferry area (Gould, 1928); (6) written descriptions of the channel made

by John D. Lee in 1872 and by USGS resident technicians from 1923 to 1975; and (7) ground-based photographs of the river and valley from various sources taken in 1873, 1911, 1915, 1921, 1929, 1931, 1935-1938, 1939, 1951, 1960, 1961, 1963, 1964-1968, 1970, 1972, 1973, 1976, 1979, 1980, 1981, 1982, 1983, 1984, 1986, 1987, 1988, 1992, 1993, 1994, and 1995.

USGS slope-area surveys

The first source of data, the USGS slope-area surveys from 1925, 1927, 1929, 1939, 1940, 1963, 1980, and 1992, was, by far, the most useful and precise; these surveys typically resolve 3-dimensional channel geometric properties at the 2- to 10-cm scale over cumulative streamwise distances of several hundred meters. Moreover, some of the USGS slope-area surveys, specifically those from 1939, 1963, and 1980, include photographs of the surveyed reaches, thus permitting the evaluation of the seventh source of data, ground-based photography. In this study, USGS slope-area surveys were used to reconstruct the lateral and vertical positions of the channel as well as the local and reach-averaged cross-section channel geometry.

NPS and USBR topographic surveys

The larger-scale topographic surveys of the NPS in 1975 (National Park Service, 1975) and USBR in 1990 (Bureau of Reclamation, 1990) are the second most useful and precise source of information since they permit 10- to 50-cm scale resolution of 3-dimensional topography, albeit over greater streamwise distances than the USGS slope-area surveys. In this study, the NPS and USBR surveys were used to reconstruct the lateral and vertical positions of the channel as well as the local cross-section channel geometry.

USGS discharge measurement field notes

The third most useful source of data, measured cross-sections from the USGS discharge measurement field notes from 1923 to 1994, permit cm-scale resolution of 2-dimensional, i.e. vertical and cross-stream, channel features. In this study, measured cross-sections from the USGS discharge measurement field notes were used to reconstruct both local cross-section geometry and the time-averaged cross-section geometry at Cableway 2, and also were used in a statistical analysis of channel cross-section geometry. Furthermore, streamwise locations of discharge-measurement cross-sections that were

measured at the upstream margin of the Colorado River backwater in the mouth of the Paria River were used to reconstruct changes in the vertical position of the Paria River channel.

Aerial photographs

Aerial photographs are the fourth most useful source of information as only m-scale 2-dimensional, i.e. streamwise and cross-stream, information can be obtained. In this study, four aerial photographs from the USGS (U.S. Geological Survey, 1951; 1952; 1977; 1980), 1963 and 1972 aerial photographs from Turner and Karpiscak (1980), and one 1984 aerial photograph from the USBR were used to reconstruct the lateral position of the channel and to reconstruct changes in channel width at Cableway 2 .

General Land Office cadastral surveys

The fifth most useful source of information was the 1927 cadastral survey made by the General Land Office. Cadastral surveys are useful for reconstructing the position of river channels where crossed by surveyed section lines and are useful in reconstructing the position of the bank tops only where the bank tops are explicitly surveyed, as in the case of the right bank of the Colorado River in 1927. Unfortunately, cadastral surveys are not useful for reconstructing the widths of ephemeral streams because the widths measured by the land surveyors where the section lines cross the channel are not the bankfull channel widths, but merely the widths of the low-flow water surface. For example, the measured width of the Paria River water surface in the March 1927 Lees Ferry cadastral survey of Gould (1928) is 13.1±2.6 m (based on four section-line crossings), whereas the measured bankfull widths from USGS slope-area surveys and discharge measurements range from 20 to 40 m for the same time period. Cadastral surveys are also of limited use in documenting changes in channel width for this reason.

In the reach near Paria and Adairville, UT (discussed below in Section 2.5d), where dramatic channel widening occurred from 1884 to 1917, as documented by field work conducted by Gregory and Moore (1931) in 1917, cadastral resurveys (Bailey and Burrill, 1877; Thoma and Rathbone, 1917) of the same section lines in March 1877 and March 1917 indicated no change in river width. Bankfull width of this segment of the Paria River increased by at least a factor of 3 during the interval between these cadastral surveys, but the width of the low-flow water surface did not. At six section-line crossings in alluvial reaches below the townsite of Paria, UT, the water-surface width in March 1877 was 11.3±2.0 m. and in March 1917 was 13.1±9.3 m. Hence, the method of reconstructing channel geometry from cadastral surveys, as used by Webb (1985) and

Webb and others (1991), can be misleading; and, in this study, cadastral surveys are only used to reconstruct the lateral position of the channel.

Written descriptions of the channel

The sixth most useful source of channel geometry information is historical written descriptions of the channel; these are most useful in cases where dimensions of the channel are given. In the Lees Ferry reach, the earliest "measurement" of channel dimensions comes from the personal diary of Mormon pioneer John D. Lee, in which he describes the dimensions of the irrigation dam he constructed from June 12 through June 22, 1872:

> "Now begins the Tug of War. A Dam 8 foot deep & 7 Rods long to make, besides heavy repairs on the ditch, before the water can be brought to revive the now dyeing crops, vines, and trees" (Cleland and Brooks, 1983).

Combination of these dimensions with the elevation of the intake to his irrigation ditch, as surveyed in March 1993, allowed the reconstruction of the bankfull width and depth below the June 1872 floodplain. Entries in gage station histories by USGS gage observers were also found to be useful in reconstructing the bed elevation of the lowermost Paria River from 1921 through 1957. Thus, in this study, written descriptions were used both to reconstruct local cross-section geometry and to reconstruct the vertical position of the channel.

Ground-based photographs

Surprisingly, the least useful source of channel geometry data and potentially the most misleading was found to be the source of data most commonly used by previous workers on the Paria River, i.e., ground-based photography. Accuracy of repeat ground-based photography has previously been assumed by other workers. Repeat photography has been used in recent years to document vegetation changes by Turner and Karpiscak (1980) and Melis and others (1996), and to document channel-shape changes by Burkham (1972), Williams and Wolman (1984), Webb (1985, 1996), Hereford (1986, 1989, 1993), W. Graf (1987), Webb and others (1991, 1996), Hereford and others (1996), and Melis and others (1996). However, ground-based photographs can be misleading and should only be used to determine channel dimensions in cases where the dimensions of photographed channel features can be independently determined from objects of known dimension within the field of view [as in the usage of this method by Webb (1996) and Webb and others (1996)].

Figure 2.25 illustrates the potential problem with repeat photography. Figures 2.25a and 2.25b are two downstream views taken from near the same location on October 25 or 27, 1939 and October 15, 1963 in the reach above the Lees Ferry gage; these photographs were both taken about a month after comparably sized floods. The impression one gets from the photographs is that the channel geometry in both views is about the same; this impression is, however, incorrect. In 1939, this portion of channel was about 40 m wide and had a longitudinal bed slope of 0.006, while in 1963, it was only 20 m wide and had a longitudinal bed slope of only 0.003. Figure 2.25c shows the streamwise-averaged surveyed topography in the field of view in the two photographs ("left" in the cross-sections corresponds to "left" in the photographs).

Figures 2.25d through 2.25i are photographs of reaches that appear quite different from one another but, in fact, all have the same cross-section geometry. Figures 2.25d and 2.25e are two downstream views (one taken obliquely above and one from within the channel) of the reach below the Lees Ferry gage taken on September 13, 1939. Figure 2.25f and 2.25g are two upstream views (again, one taken obliquely above and one taken from within the channel) of the reach above the Lees Ferry gage taken on September 18, 1963, and Figures 2.25h and 2.25i are two downstream views (again, one taken obliquely above and one taken from within the channel) of a portion of Reach 2 of the 1993 3-reach composite taken on November 15, 1993. All three photographed reaches look different mainly because of vegetation, but, in fact, all have the same longitudinal bed slopes (0.003) and the same mean cross-section geometry. Figure 2.25j shows the streamwise-averaged surveyed topography in the field of view of the photographs of the three reaches (again, "left" in the cross-sections corresponds to "left" in the photographs). None of the vegetation in the 1939 photographs is nonnative, the bushes on the left side of the 1963 photographs are nonnative (tamarisk), and almost all of the vegetation along the banks in the 1993 photographs is nonnative (tamarisk and Russian olive). Repeat photography clearly illustrates changes in vegetation through time, but does not necessarily allow the accurate reconstruction of changes in channel topography.

In this study, ground-based photographs were only used when no other source of data was available; in these cases, photographs were used reconstruct lateral positions of the channel and were used to reconstruct local cross-section channel geometry only when dimensions of features in the field of view could be independently checked by either subsequent survey or estimates of the size of "standard-sized" features. For example, surveyed distances between photographed large rocks, trees, or terrace margins whose positions had not moved between the time of the photograph and the time of the survey

Figure 2.25: **(a)** Downstream view of the reach above the gage on October 25 or 27, 1939; gage stilling well is visible against the cliff in the distance. Photograph taken by W.T. Stuart. **(b)** Downstream view of the reach above the gage on October 15, 1963; gage stilling well is visible against the cliff in the distance. Photograph taken by R.H. Roeske; camera is approximately 50 m closer to the gage than in Figure 2.25a.

a)

b)

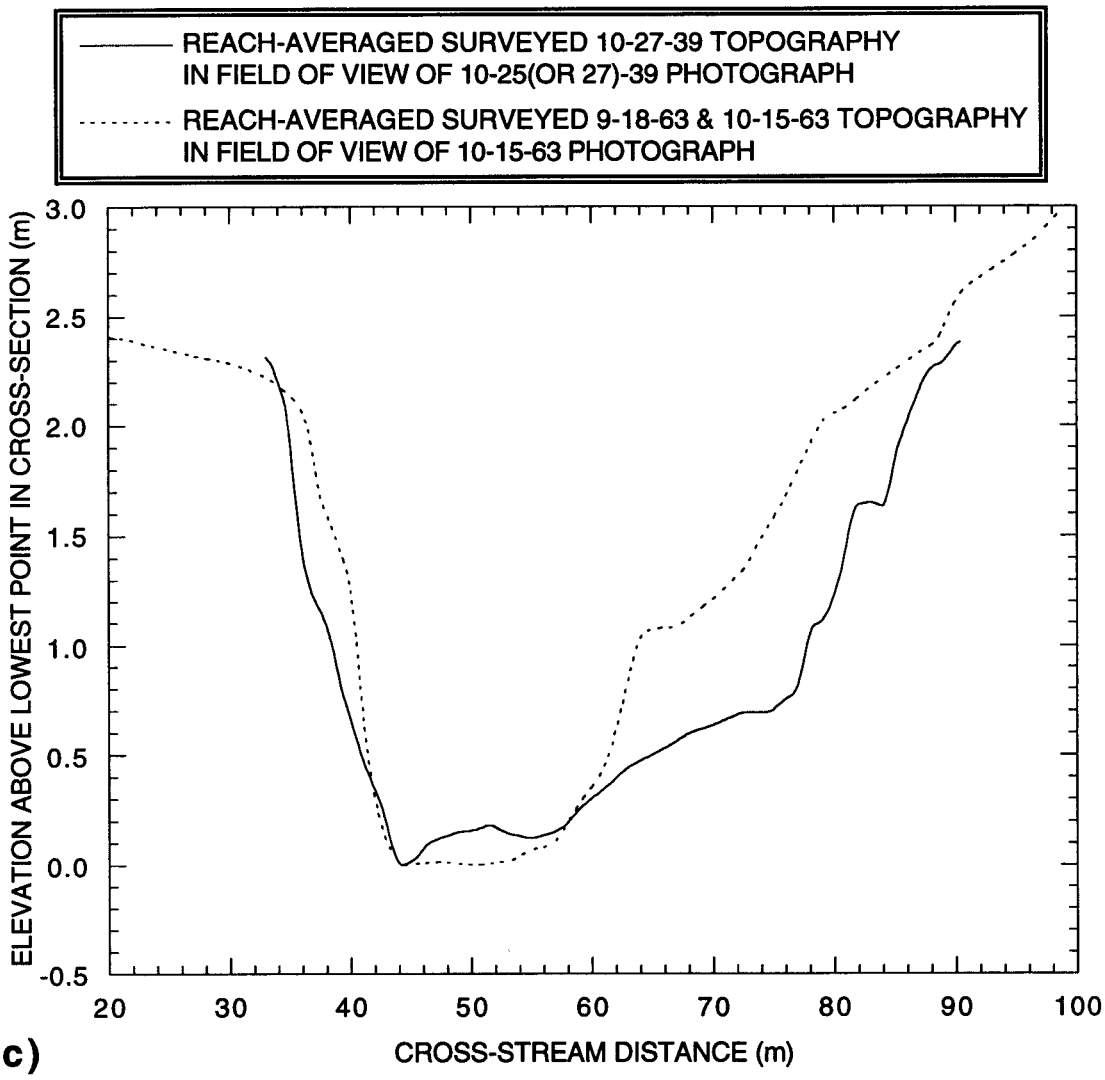

Figure 2.25 (continued): (c) Reach-averaged surveyed topography in the fields of view of Figures 2.25a & 2.25b; "left" in this figure corresponds to "left" in Figures 2.25a & 2.25b.

Figure 2.25 (continued): (d) Downstream view from obliquely above of the reach below the gage on September 13, 1939; photograph taken by W.T. Stuart. The Paria River is at near-bankfull stage in this view. **(e)** Downstream view from floodplain level of the view in Figure 2.25d; photograph taken by W.T. Stuart on September 13, 1939.

d)

e)

Figure 2.25 (continued): **(f)** Upstream view from above of the reach above the gage on September 18, 1963; photograph taken by R.H. Roeske. **(g)** Upstream view from channel level of the view in Figure 2.25f; photograph taken by R.H. Roeske on September 18, 1963.

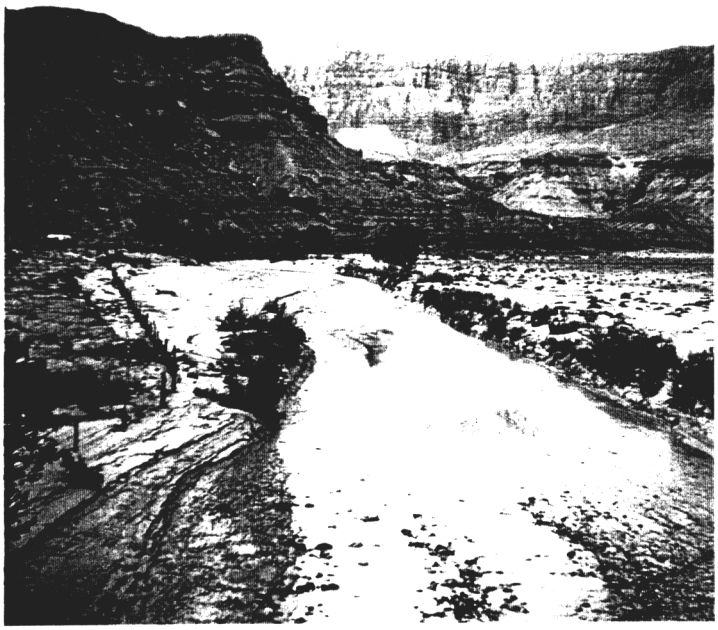

f)

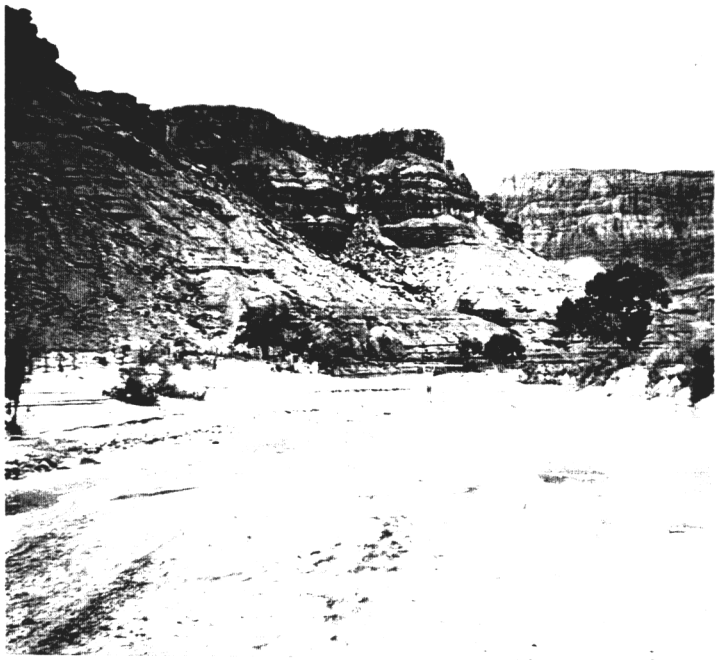

g)

Figure 2.25 (continued): (h) Downstream view from above of Reach 2 of the 1993 3-reach composite. Camera is located 2.6 km above the gage; photograph taken by D.J. Topping on November 15, 1993. **(i)** Downstream view from channel level of the view in Figure 2.25h; photograph taken by D.J. Topping on November 15, 1993.

h)

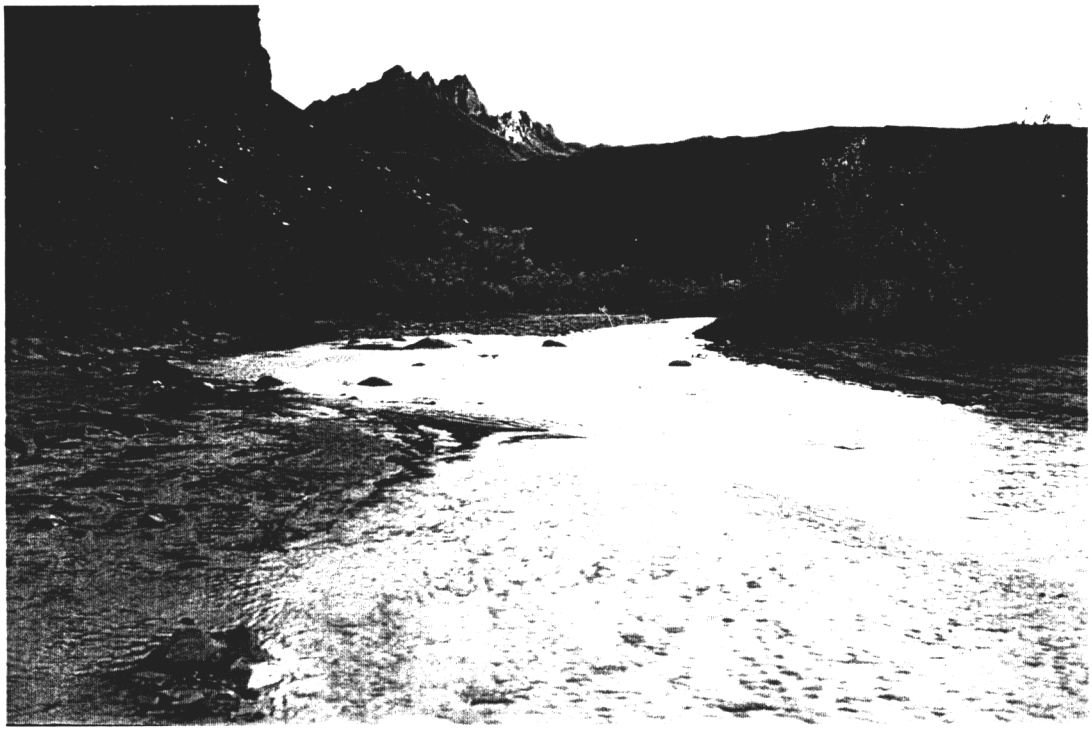

i)

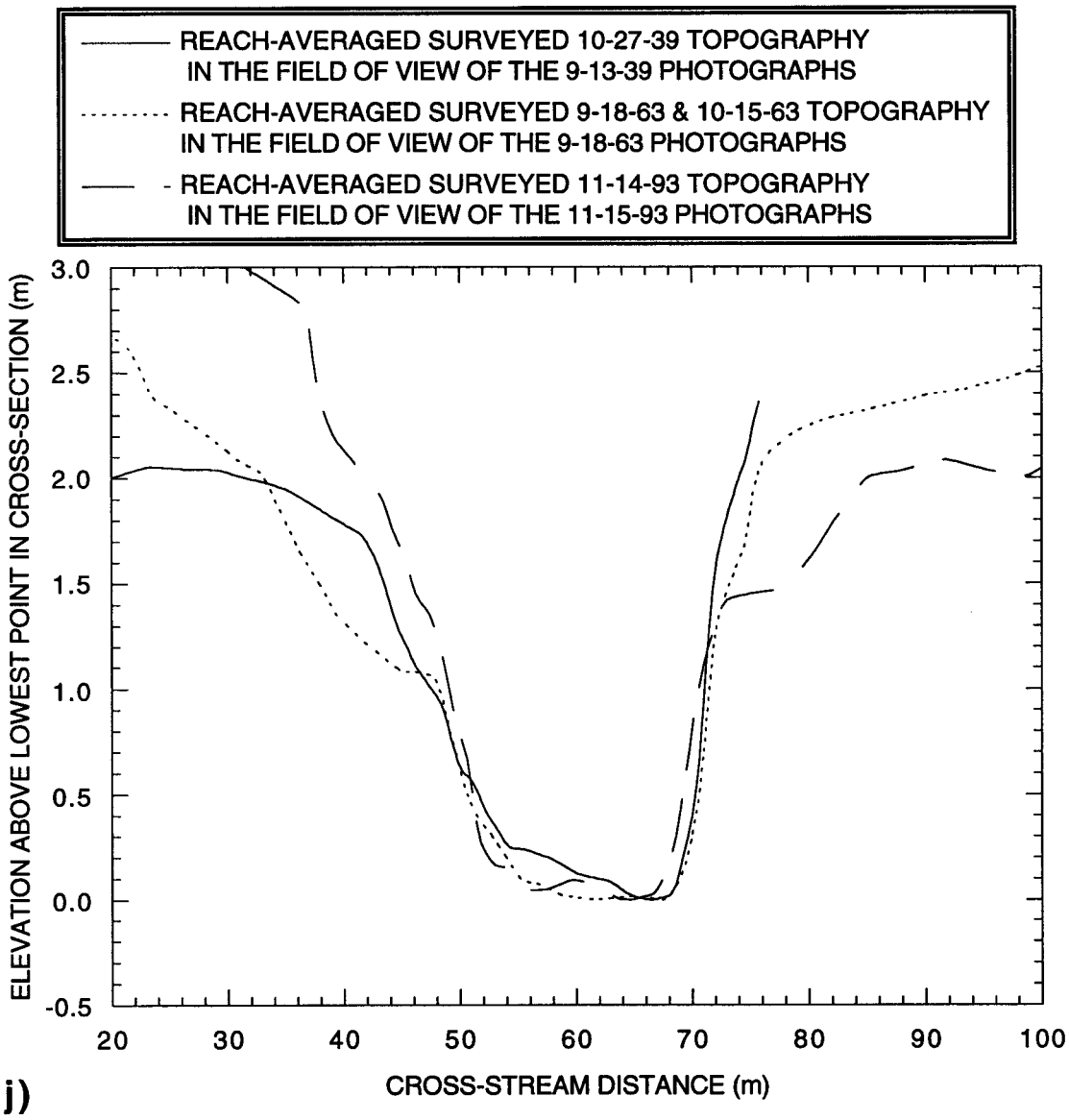

Figure 2.25 (continued): (j) Reach-averaged surveyed topography in the fields of view of Figures 2.25d & 2.25e, Figures 2.25f & 2.25g, Figures 2.25h & 2.25i; "left" in this figure corresponds to "left" in Figures 2.25d & 2.25e, Figures 2.25f & 2.25g, Figures 2.25h & 2.25i.

were used to determine channel width. Also, the size of "standard-sized" features, e.g., the width of a wagon or the width between wagon-wheel ruts, that are adjacent to the channel were used to reconstruct channel widths from photographs.

2.5b-2: Changes in the lateral position of the channel

Over the period from 1873 to 1994, the lateral position of the lowermost 2 to 2.5 km of the Paria River channel changed substantially; and, over the period 1927 to 1994, the lateral position of the 0.5 km reach of the Paria River in the vicinity of the upper headcut also changed substantially. With the exception of these two portions of the channel, however, the remainder of the river in the Lees Ferry study area, including the three reaches in the 1993 3-reach composite, has been laterally stable (Figure 2.26). Featured in Figure 2.26 are the lateral positions of the channel for various time periods, locations of Reaches 1, 2, and 3 of the 1993 3-reach composite, positions of the upper and lower headcuts in 1993, position of the confluence of the Paria and Colorado Rivers from 1873 to 1909, and position of the post-1909 high-water confluence of the Paria and Colorado Rivers.

As shown in Figure 2.26, the channel of the Paria River has migrated across large portions of the valley floor over the period from 1872 to 1994, in direct contrast to the conclusion of Hereford (1986, 1987a) that channel-shape changes have occurred without significant lateral migration of the channel. In the reach including the post-1925 USGS gaging station and the dated floodplain stratigraphic section of Hereford (1986, 1987a), the channel has laterally migrated over 100 meters, resulting in the erosion of pre-existing floodplain and terrace sediment and deposition of new floodplain sediment. As will be shown in Sections 2.5b-3 & 2.5b-4, the two reaches of the Paria River in the Lees Ferry study area with the greatest lateral instability, i.e., the 2-km-long reach above the high-water confluence with the Colorado River and the reach near the upper headcut, are also the reaches with the greatest vertical instability and in which dramatic cross-section geometric changes have accompanied changes in longitudinal bed slope.

The episode which preceded the single greatest avulsion in the lower Paria River was the growth of a meander from 1873 to 1909 in the reach immediately above the confluence with the Colorado River (Figure 2.26). During the September 1909 flood on the Paria River, the Paria cut through the outside of this new meander and entered the Colorado River at a new position downstream of the old confluence (Rusho and Crampton,

Figure 2.26: Lateral positions of the Paria River channel in the Lees Ferry study area through time. The 1993 position of the channel is shown by the solid line; the past positions of the channel, for the years indicated in the boxes, are shown by dashed lines. Paved roads are shown by double, solid lines; gravel roads are shown by double, dashed lines. In the reach between the post-1925 gage site and the confluence, the lateral positions of the channel are shown in color for 5 key time periods: (1) the **1873** position is shown in **pink**; (2) the position immediately prior to the **1909** avulsion is shown in **light blue**; (3) the **1911-1927** position is shown in **yellow**; (4) the position after the August 2, **1929** flood is shown in **orange**; and (5) the position after the September 13, **1939** flood is shown in **light green**. Sources of information used in constructing this map were: (1) the 1993 survey of the study area; (2) USGS slope-area surveys from 1925, 1927, 1929, 1939, 1940, 1963, and 1980; (3) the 1927 General Land Office survey of Gould (1928); (4) 1951, 1952, 1977, and 1980 USGS aerial photographs, the 1984 USBR aerial photograph, and the 1965 and 1973 aerial photographs published in Turner and Karpiscak (1980); (5) 1952 and 1977 USGS topographic quadrangles; (6) the 1975 National Park Service survey and the 1990 Bureau of Reclamation survey; and (7) 1873 Wheeler Expedition photograph in Figure below, the 1909? A.H. Jones photograph on page 118 of Rusho and Crampton (1992), the 1911 Kolb photograph in Figure 2.37b below, the 1915 and 1921 E.C. LaRue photographs in Figures 2.37c & 2.33d below, four 1915 H.E. Gregory photographs (2 of which appear as Figure 2.33a below), and the late 1930's high-water photograph of the confluence in Figure 2.32b below. All of the historically surveyed cross-sections from the USGS slope-area surveys, cross-sections constructed from the 1975 National Park Service survey, and a subset of the 267 cross-sections surveyed during 1993 are presented in Figure 2.27 (Plate 1).

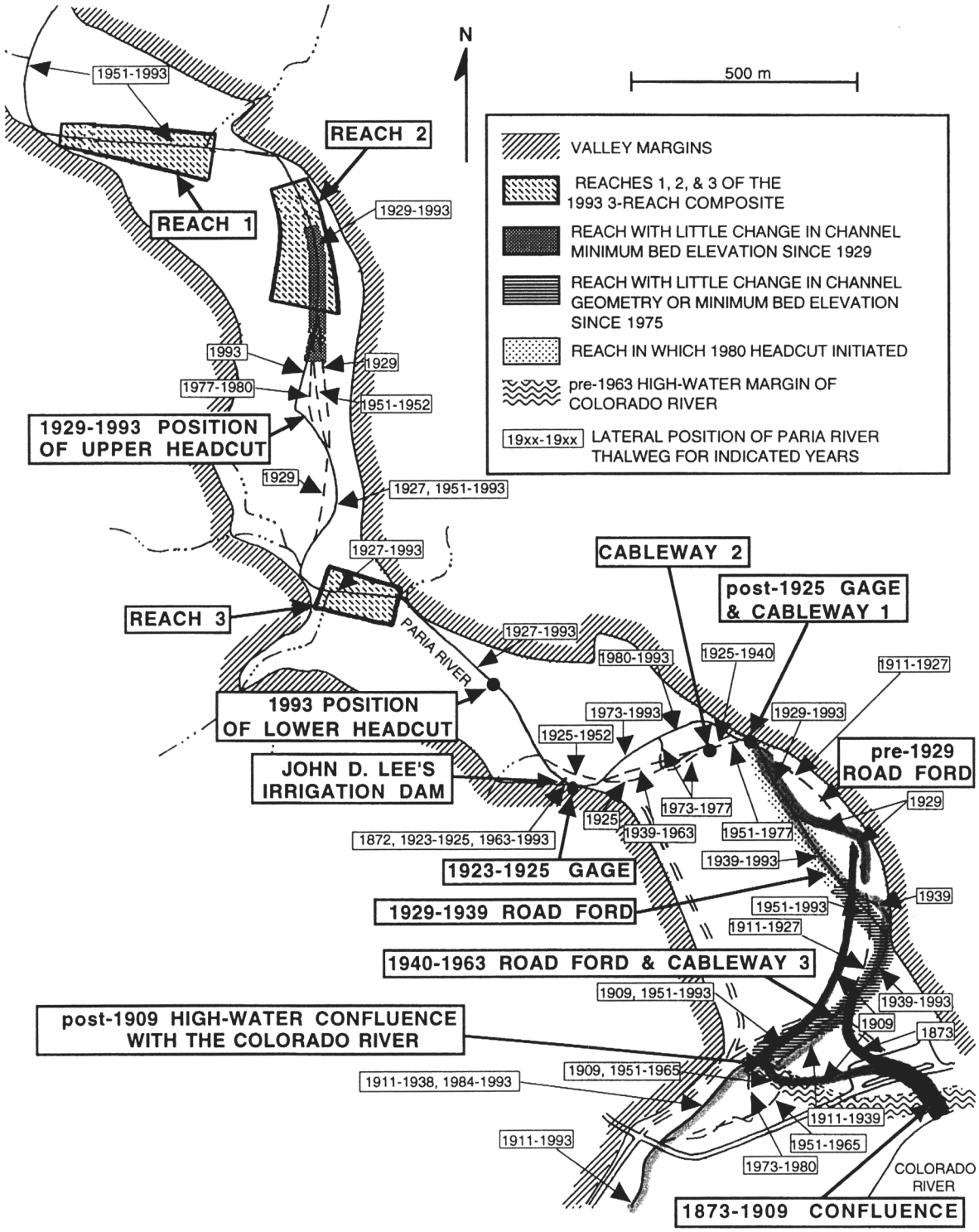
N
500 m
VALLEY MARGINS
REACHES 1, 2, & 3 OF THE 1993 3-REACH COMPOSITE
REACH WITH LITTLE CHANGE IN CHANNEL MINIMUM BED ELEVATION SINCE 1929
REACH WITH LITTLE CHANGE IN CHANNEL GEOMETRY OR MINIMUM BED ELEVATION SINCE 1975
REACH IN WHICH 1980 HEADCUT INITIATED
pre-1963 HIGH-WATER MARGIN OF COLORADO RIVER
19xx-19xx LATERAL POSITION OF PARIA RIVER THALWEG FOR INDICATED YEARS
REACH 1
REACH 2
REACH 3
1951-1993
1929-1993
1993
1929
1977-1980
1951-1952
1929-1993 POSITION OF UPPER HEADCUT
1929
1927, 1951-1993
1927-1993
PARIA RIVER
1927-1993
1993 POSITION OF LOWER HEADCUT
JOHN D. LEE'S IRRIGATION DAM
CABLEWAY 2
post-1925 GAGE & CABLEWAY 1
1980-1993
1925-1940
1911-1927
1973-1993
1929-1993
1925-1952
pre-1929 ROAD FORD
1929
1973-1977
1925
1939-1963
1951-1977
1872, 1923-1925, 1963-1993
1923-1925 GAGE
1939-1993
1929-1939 ROAD FORD
1939
1951-1993
1911-1927
1940-1963 ROAD FORD & CABLEWAY 3
1909, 1951-1993
1939-1993
1909
1873
post-1909 HIGH-WATER CONFLUENCE WITH THE COLORADO RIVER
1911-1938, 1984-1993
1909, 1951-1965
1911-1939
1911-1993
1951-1965
1973-1980
COLORADO RIVER
1873-1909 CONFLUENCE

1992; unpublished March 16, 1944 USGS interview with Jerry Johnson).[2] At discharges less than about 1100 m^3/s on the Colorado River, this new confluence was located 800 m downstream along the Colorado River at an elevation 5 m below the 1873-1909 confluence; at discharges greater than about 1100 m^3/s on the Colorado River, this new confluence was located 400 m downstream along the Colorado River and at an elevation 1.8 m below the 1873-1909 confluence. This avulsion lowered the elevation of the high-water confluence by about 1.8 m while shortening the length of the Paria River channel by 500 m, resulting in a net base level drop of 3.6 m assuming a slope of 0.0035 (see Section 2.5b-3) for the 500 m of Paria River channel that were abandoned. Therefore, this avulsion is interpreted to have initiated much of the channel incision (described in Section 2.5b-3) that by 1929 had affected 3.4 km of the Paria River channel above the post-1909 high-water confluence.

Other major episodes of meander migration in the reach below the post-1925 gage occurred during the flood of August 2, 1929, in which as much as 30 m of bank erosion occurred (unpublished USGS gage technical notes, 1929), and the September 13, 1939 flood, in which about 10 m of bank erosion occurred (unpublished USGS slope-area survey, 1939). These two events are notable in that they both caused major relocations of the road ford that crossed the Paria River. After the 1939 flood, a new, partially concrete-surfaced road ford was built on January 23-26 1940, to be used as the road crossing until the construction of the highway bridge by the National Park Service in 1963. The only recent meander cutoff that has occurred in the reach below the post-1925 gage was caused by the artificial straightening of a section of the channel sometime between 1980 and 1984 by the National Park Service. This was done to prevent the meander from migrating through the new road that they had built in 1963 on the previous high-stage floor of the Colorado River.

In the reach immediately above the post-1925 gage, one major meander cutoff and one major avulsion have occurred since 1925. The meander cutoff occurred during the October 25, 1925 flood, in which the meander at the 1923-1925 gage was cut off, causing the abandonment of that gage by the USGS. The avulsion was more gradual and occurred over the period from about August 15, 1972 through September 9, 1980. During this time period, new meanders developed in the reach above the post-1925 gage in response to a steepening of the reach resulting from the retreat of headcuts into this reach (described in detail in Section 2.5b-3). The first headcut that destabilized the reach above the gage

---

[2]The time of this avulsion was incorrectly reported to have occurred in 1917 by Rusho and Crampton (1992).

initiated at the confluence in about 1963 and retreated past the gage on August 14-15, 1972. This avulsion was completed during the September 9, 1980 flood, in which a second headcut initiated in the 300-m long reach below the gage and retreated into the reach above the gage.[3] Between 1972 and 1980, during the course of the avulsion, the section of channel above the post-1925 gage lengthened by 30 m.

As mentioned, the last major episode of lateral channel migration in the Lees Ferry study area has occurred in the vicinity of the upper headcut. Between the time of the March 1927 cadastral survey of Gould (1928) and the USGS slope-area survey following the August 2, 1929 flood, this section of channel straightened. Then, beginning after the August 2, 1929 flood and continuing to the present, new meanders have developed in the immediate vicinity of the upper headcut resulting in 120 m of channel lengthening. During this episode of meander migration, considerable amounts of sediment have been eroded from both floodplains and terraces in this reach.

2.5b-3: Changes in the vertical position of the channel; the base-level control of the Colorado River on the Paria River

Between 1873 and 1993, the lowermost 3.5 km of the Paria River above the high-water confluence have been subjected both to: major episodes of channel entrenchment in response to base level lowering at the confluence in both 1909 and 1963, and to subsequent base level fluctuations related to the stage of the Colorado River during large sediment transporting events in the Paria River. Longitudinal profiles of the Paria River from 1872 to 1993 indicate that the section of the river affected by these episodes of entrenchment and aggradation is localized near the confluence and does not extend more than 3.5 km above the post-1909 high-water confluence (Figure 2.28). Based on his stratigraphic work in the reach near the 1925-present gage, Hereford (1986, 1987a) interpreted pre-1940 channel entrenchment, post-1939 channel-bed aggradation, and renewed channel entrenchment beginning in 1980 to be universal features of the Paria River. As will be shown in Sections 2.5c, 2.5d, and 2.5e, and lending further support to the local nature of channel entrenchment and aggradation in the Paria River system, the elevation of the Paria River channel at the gage below Cannonville, UT has not changed since 1951, the elevation of the channel above the townsite of Paria, UT has not changed since 1877, and the elevation of the channel at the gage near Kanab, UT has not changed since 1971.

---

[3]Both of these headcuts have since coalesced into what is termed the lower headcut (Figure 2.26).

1872-1993 longitudinal profiles of the Paria River in the Lees Ferry study area

The influence of the Colorado River on the longitudinal profile of the lowermost Paria River is illustrated in Figure 2.28. Figure 2.28 is a compilation of Paria River channel and terrace longitudinal profiles for the period from 1872 to 1993. The 1990-1993 bed profile shown in Figure 2.28 was constructed by combining the minimum bed elevations from the 267 cross-sections of the 1993 survey with those from the 1990 Bureau of Reclamation survey. The 1993 "high" and "low" terrace profiles were constructed from surveyed terrace elevations in a subset of the 1993 cross-sections; at many of these cross-sections, there were two identifiable terraces, hence the distinction between "high" and "low" terraces. The 1921-1929, 1939-1940, and 1957-1963 bed profiles were constructed both from: the minimum bed elevations from USGS slope-area survey cross-sections, and from USGS measurements of the extent and depth of the Colorado River backwater in the lowermost channel of the Paria River (using the information in Figure 2.33). The 1872-1873 bed profile was approximated by a linear regression fit to the bed elevation at John D. Lee's irrigation dam in June 1872 and the bed elevation of the Paria River at the confluence determined from the 1873 photograph taken by T.H. O'Sullivan of the Wheeler Survey (see Figure 2.37a below). Bed elevation of the center channel of the Colorado River (see Figure 2.32a below) was determined from the National Park Service and Bureau of Reclamation surveys.

Four important features to note in Figure 2.28 are: (1) the 1872-1873 bed profile is parallel to and approximately 2 m below the 1990-1993 "high" terrace profile; (2) the elevation of the Paria River bed has not changed since 1872-1873 in the reach in excess of 2 km above the 1925-present USGS gage and 3.9 km above the current, post-Glen Canyon Dam confluence with the Colorado River, (3) the 1939-1940, 1957-1963, and 1990-1993 bed profiles converge 350 m above the gage, thus, indicating that no major change in bed elevation since 1939 has occurred in excess of 350 m above the gage, and (4) the temporal variability of the bed elevation of the Paria River channel increases toward the confluence with the Colorado River. These features suggest that the 1990-1993 "high" terrace was the active floodplain prior to the September 1909 avulsion that lowered the base level at the confluence, and that all changes in the bed elevation of the Paria River channel that have occurred within 3.9 km of the current, post-Glen Canyon Dam confluence with the Colorado River since 1872-1873 are due to base level changes at the confluence.

Figure 2.28: Longitudinal bed and terrace profiles of the Paria River in the Lees Ferry study area. Bed profiles are shown for five different time periods; the thin **red** lines are the best-fit linear regressions through the 1990-1993 "high" and "low" terrace profiles. Also shown are: (1) locations of Reaches 1, 2, and 3 of the 1993 3-reach composite **(in orange)**; (2) the range of bed elevations at the post-1925 gage; (3) the 1872 crest elevation of John D. Lee's irrigation dam **(in brown)**; (4) peak stages of the backwater in the lowermost Paria River from the two largest known Colorado River floods during the period from 1872 to 1993, the 8500 m^3/s 1884 flood and the 6300 m^3/s 1921 flood **(in brown)**; (5) the mean annual peak stage of the Colorado River **(in brown)**; and (6) elevations of the stage of the Colorado River backwater in the lowermost channel of the Paria River during the six largest Paria River floods during the period from 1923 to 1996, i.e., the floods of 1925, 1927, 1939, 1940, 1963, and 1980 **(in dark blue)**. Stage of the Colorado River backwater in the lowermost channel of the Paria River was determined from the information in Figure 2.33 below.

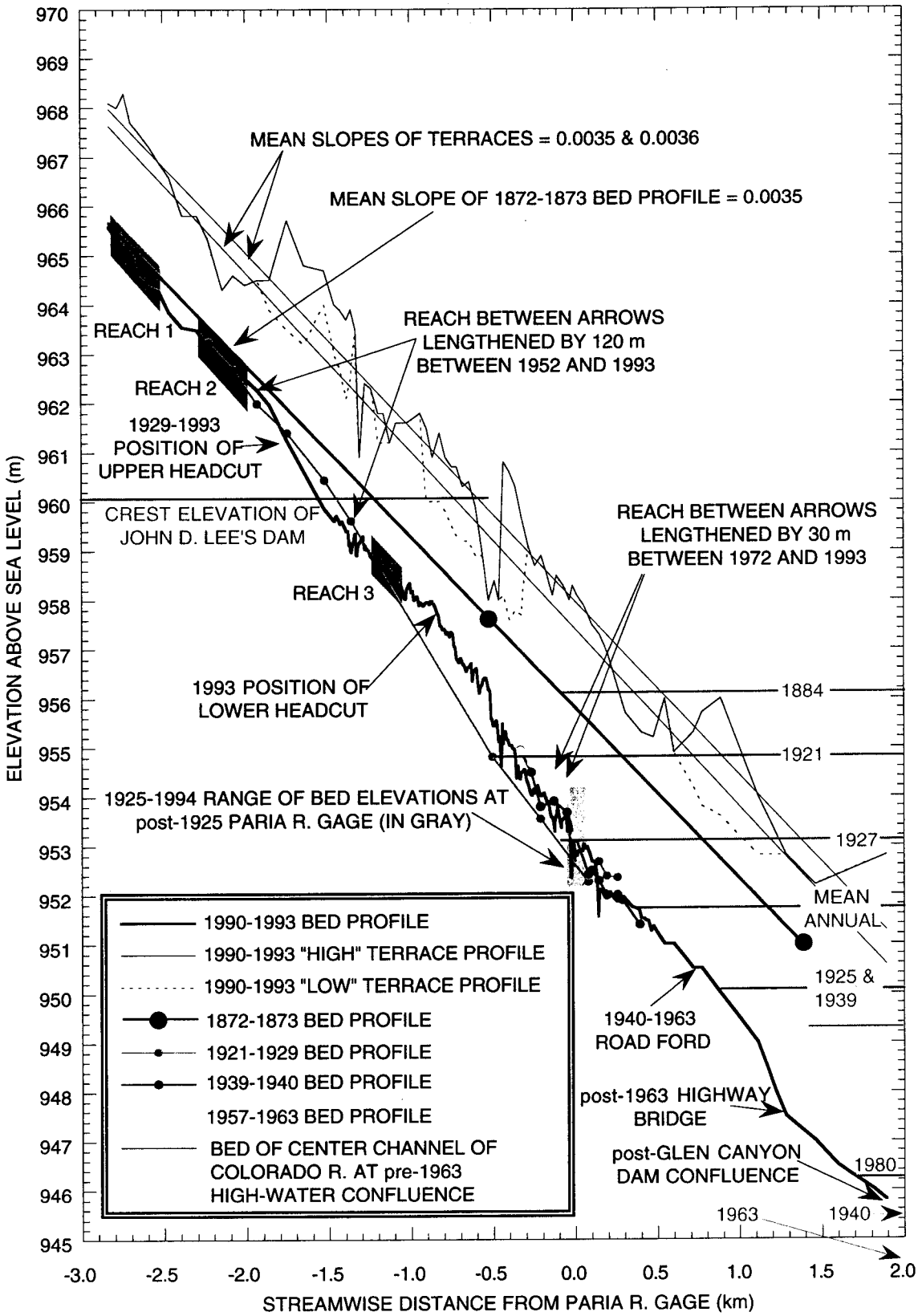
MEAN SLOPES OF TERRACES = 0.0035 & 0.0036
MEAN SLOPE OF 1872-1873 BED PROFILE = 0.0035
REACH BETWEEN ARROWS LENGTHENED BY 120 m BETWEEN 1952 AND 1993
REACH 1
REACH 2
1929-1993 POSITION OF UPPER HEADCUT
CREST ELEVATION OF JOHN D. LEE'S DAM
REACH BETWEEN ARROWS LENGTHENED BY 30 m BETWEEN 1972 AND 1993
REACH 3
1993 POSITION OF LOWER HEADCUT
1884
1921
1925-1994 RANGE OF BED ELEVATIONS AT post-1925 PARIA R. GAGE (IN GRAY)
1927
MEAN ANNUAL
1925 & 1939
1940-1963 ROAD FORD
post-1963 HIGHWAY BRIDGE
post-GLEN CANYON DAM CONFLUENCE
1980
1963
1940
1990-1993 BED PROFILE
1990-1993 "HIGH" TERRACE PROFILE
1990-1993 "LOW" TERRACE PROFILE
1872-1873 BED PROFILE
1921-1929 BED PROFILE
1939-1940 BED PROFILE
1957-1963 BED PROFILE
BED OF CENTER CHANNEL OF COLORADO R. AT pre-1963 HIGH-WATER CONFLUENCE
ELEVATION ABOVE SEA LEVEL (m)
STREAMWISE DISTANCE FROM PARIA R. GAGE (km)
970
969
968
967
966
965
964
963
962
961
960
959
958
957
956
955
954
953
952
951
950
949
948
947
946
945
-3.0
-2.5
-2.0
-1.5
-1.0
-0.5
0.0
0.5
1.0
1.5
2.0

Local nature of Paria River channel bed aggradation and degradation over time

The local nature of Paria River channel bed aggradation and incision over time in the reach near the gage is illustrated in Figure 2.29 (Plate 1). As shown in Figure 2.29, the "system-wide" bed aggradation occurring between 1939 and 1980 that was reported to be a general feature of the Paria River system by Hereford (1986, 1987a) and J. Graf and others (1991) is merely a local feature. This post-1939, pre-1980 aggradation only affects the channel from 210 m above the post-1925 gage to the confluence with the Colorado River (Figure 2.29). Furthermore, no major change in minimum bed elevation has occurred from 1929 to 1993 in the reach of the channel extending from 2.2 to 1.8 km above the post-1925 gage; and, as already stated in the previous section, no change in minimum bed elevation has probably occurred from 1872-1873 to 1993 in the reach 2 km above the post-1925 gage. Over the entire period from 1872 to 1993, the most striking change in bed elevation in the Lees Ferry reach is the 3 m of incision that occurred sometime between 1872 and 1921 at the site of John D. Lee's irrigation dam. Since the influence of this incision quickly diminishes in the upstream direction and does not extend more than 1.5 km above the dam site (Figure 2.27), this episode of entrenchment is interpreted to be largely the result of the 3.6 m base level drop at the confluence during the September 1909 flood.

The most complete, though not longest, record of change in minimum bed elevation (Figure 2.29) is found at the post-1925 gage. At the gage, the following provide a complete record of bed elevation change from 1922 to 1994: 413 measurements of the "point of zero flow", 1 extrapolation of the bed elevation from the elevation of the 1922 Colorado River backwater 100 m below the gage site, 213 supplemental bed elevations determined from the records of river stage, and the bed elevation curve that collapses all non-ice affected discharge measurements made from 1925 to 1994 onto 2 single rating curves (as previously described in Section 2.4c-1). Over this period, the largest changes in bed elevation at the gage have been: (1) 1 m of incision that occurred between 1922 and 1925 (interpreted to have occurred during the 1925 flood that caused a meander cutoff near the 1923-1925 gage); (2) subsequent rapid aggradation of the channel bed to its former elevation by 1930; (3) continued slow bed aggradation from 1940 to 1972; (4) passage of the first of two headcuts related to the 1963 change in base level at the confluence during a flood on August 14, 1972 , (5) passage of the second of two headcuts related to the 1963 change in base level at the confluence during a flood on September 9, 1980; and (6) continued slow incision from 1980 to 1994.

The second most complete record of change in minimum bed elevation (Figure 2.29) is found at the 1940-1963 road ford. At this ford, located 720 m below the gage, no net change in bed elevation had occurred from 1948 to 1963, though seasonal 0.6 m fill by the Colorado River and subsequent incision by the Paria River had periodically occurred (this process is documented below). From 1963 to 1975, the bed at the ford degraded by 1.5 m and then remained stable from 1975 to 1993. The 1963 bound of this entrenchment is set by the fact that the floor of the channel at the ford was 1.5 m higher while the road ford was used, prior to the construction of the highway bridge across the Paria River in 1963.

In summary, the longitudinal bed and terrace profiles in Figure 2.28 and the measurements of minimum bed elevation in Figure 2.29 show that: channel aggradation and incision in the lowermost Paria River is localized, and that the longitudinal bed profile of the lowermost Paria River is controlled by the base level set by the Colorado River. During the period from 1872 to 1993, two major decreases in the mean base level of the Paria River at the confluence with the Colorado River occurred, one during 1909 and one in 1963. During the Paria River avulsion in September 1909, the mean base level at the confluence decreased by 3.6 m; and, by 1929, this base level drop had affected 3.4 km of Paria River above the post-1909 high-water confluence, i.e., the entire reach below the 1993 position of the upper headcut. The second major decrease in mean base level (described in detail below) occurred as a result of the closure of Glen Canyon Dam on the Colorado River in 1963; and, by 1993, this second base level drop had affected 2.3 km of the Paria River above the old post-1909 high-water confluence.

Post-1963 channel entrenchment and the pre-1963 seasonal interplay of the Paria and Colorado rivers at the confluence

Starting between 1963 and 1972, several headcuts have retreated up the Paria River channel from the confluence with the Colorado River, resulting in 1.5 m of entrenchment on average over the reach of the Paria River below the gage; this incision was misinterpreted by Hereford (1986, 1987a) and J. Graf and others (1991) as climate driven. As seen in Figure 2.29, the first of these headcuts passed the gage during a flood on August 15, 1972, resulting in 0.4 m of incision at the gage. During the flood of September 9, 1980, the second of these headcuts initiated in the 350-m-long reach below the gage (Figure 2.29) and passed the gage, resulting in 0.7 m of incision at the gage. Entrenchment of the reach below the gage proceeded in a headward fashion, with the bulk the incision 350 to 720 m below the gage occurring from 1963 to 1975 and the bulk of the incision 0 to 350 m below the gage occurring from 1975 through the time of the 1980 flood

(Figure 2.29). Though the potential pitfalls of repeat photography have already been discussed, the qualitative changes in: the elevation of the channel bed with respect to the floodplain, and the shape of the channel in the reach above the 1940-1963 road ford are shown in Figure 2.30. In both the 1939 and 1960 photographs, the channel is broad and shallow with well-defined floodplains on both margins, while in the 1995 photograph, the channel is deeply incised into a terrace that was the former floodplain.

To interpret correctly the post-1963 channel incision, it is essential to understand the effect of the historic interplay between floods on the Colorado and Paria rivers on the reach below the gage. Unpublished USGS records from the Lees Ferry gage on the Colorado River from 1948, 1949, 1952, 1957, and 1963 indicate that prior to the closure of Glen Canyon Dam, the Colorado River would, at discharges of 600-900 m^3/s, begin flowing over the bar at the confluence of the two rivers and typically occupy the left, i.e., main, channel, the center channel across the bar, and the lowermost 0.5 km of the Paria River channel; and, at discharges of approximately 1100-1400 m^3/s, the Colorado River would occupy the left, center, and right channels across the bar, and the lowermost 0.9 km of the Paria River channel (Figures 2.31 & 2.32). These high flows of the Colorado River seasonally filled the lower Paria River channel with sediment. Then, during monsoon-season floods, occurring from July through October, the Paria River would recut a channel in a headward fashion from the confluence. A short historical account of this natural interplay between the Colorado and Paria rivers is presented in Table 2.4.

Over the period of record, the range of Paria River minimum bed elevation at the post-1925 gage has been set by the fluctuating base level set by the interplay of the Paria and Colorado rivers (Figure 2.33). The elevation of the backwater of the Colorado River in the lowermost channel of the Paria River during Colorado River floods from 1884 to 1929 is shown in this figure. Limits on the elevation of the bed of the Paria River at the post-1925 gage correlate well with the elevation of the mean peak annual stage of the Colorado River on the lower bound, and correlate well with the probable equilibrium, i.e., 0.0035, slope of the Paria River channel between the post-1925 gage and the post-1909 high-water confluence on the upper bound. This lends support to the hypothesis that the changes in minimum bed elevation at the post-1925 Paria River gage over the period of record have been the result of the fluctuating base level set by the Colorado River. In other words, the data in Figure 2.33 suggest strongly that over the period of record, the lower Paria River channel could not cut to an elevation below the peak annual stage of the Colorado River, nor could it aggrade to an elevation such that, at the probable equilibrium

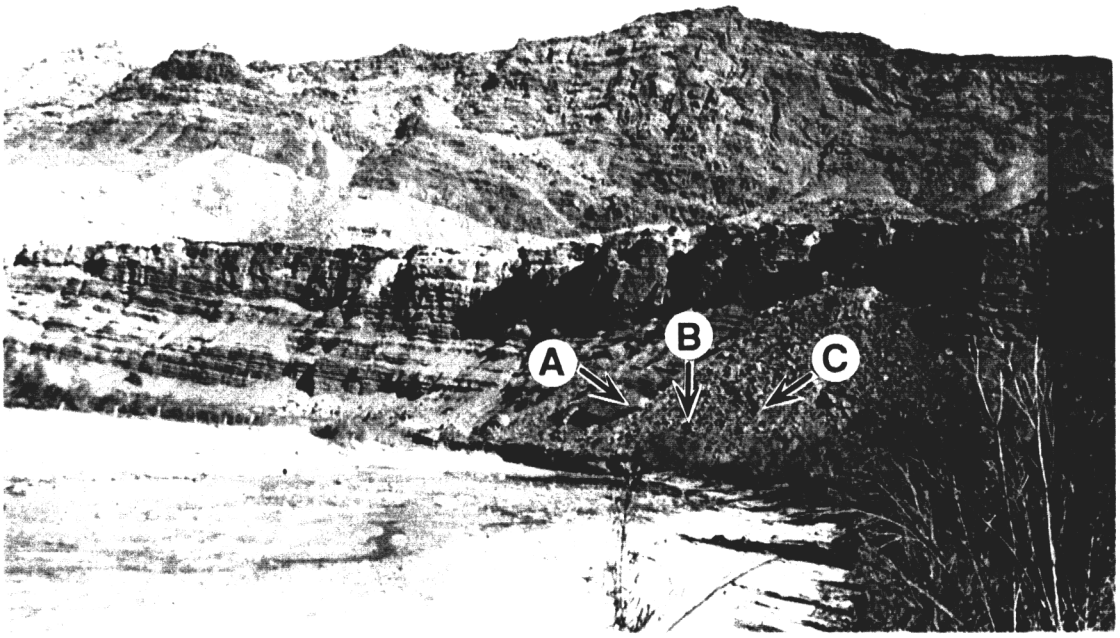

a)

Figure 2.30: **(a)** November 20, 1939 upstream view of the lower Paria River channel from a position near the post-1909 high-water confluence with the Colorado River and 150 m below the 1940-1963 road ford; photograph taken by J.S. Gatewood. The letters **A**, **B**, and **C** show the location of talus boulders that can be identified for scale and orientation in Figures 2.30b & 2.30c.

Figure 2.30 (continued): **(b)** May 5, 1960 upstream view of the lower Paria River channel; photograph from USGS-WRD Arizona District files, Flagstaff, AZ. Photograph was taken from the left bank of the Paria River at the 1940-1963 road ford. The letters **A**, **B**, and **C** show the location of talus boulders that can be identified for scale and orientation in Figures 2.30a & 2.30c. **(c)** April 15, 1995 upstream view of the incised lower Paria River channel; this portion of the channel has incised 1.5 m between 1963 and 1975. Photograph taken by D.J. Topping from the same position as Figure 2.30b. The letters **A**, **B**, and **C** show the location of talus boulders that can be identified for scale and orientation in Figures 2.30a & 2.30b.

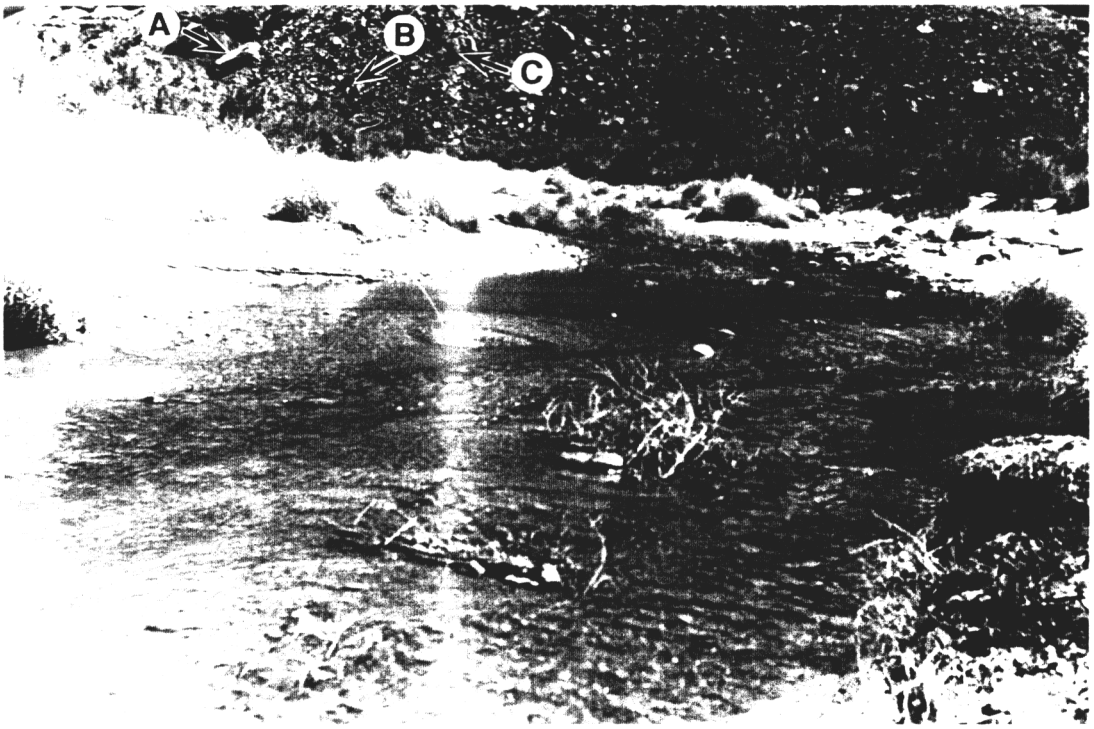

b)

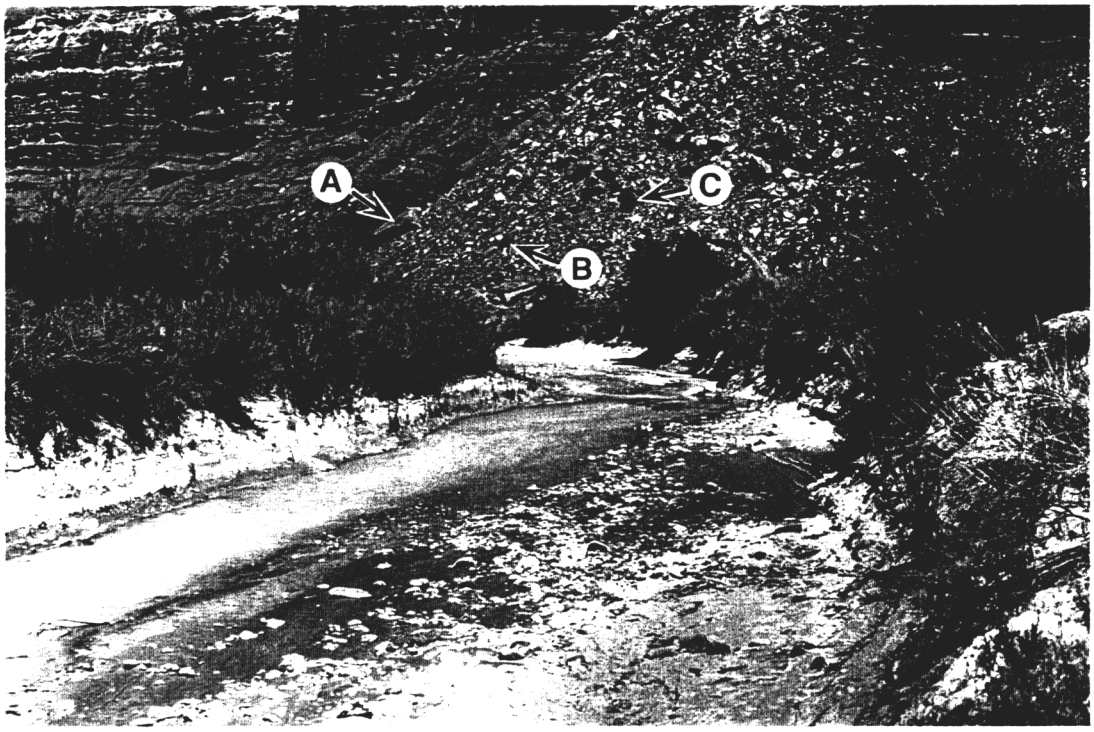

c)

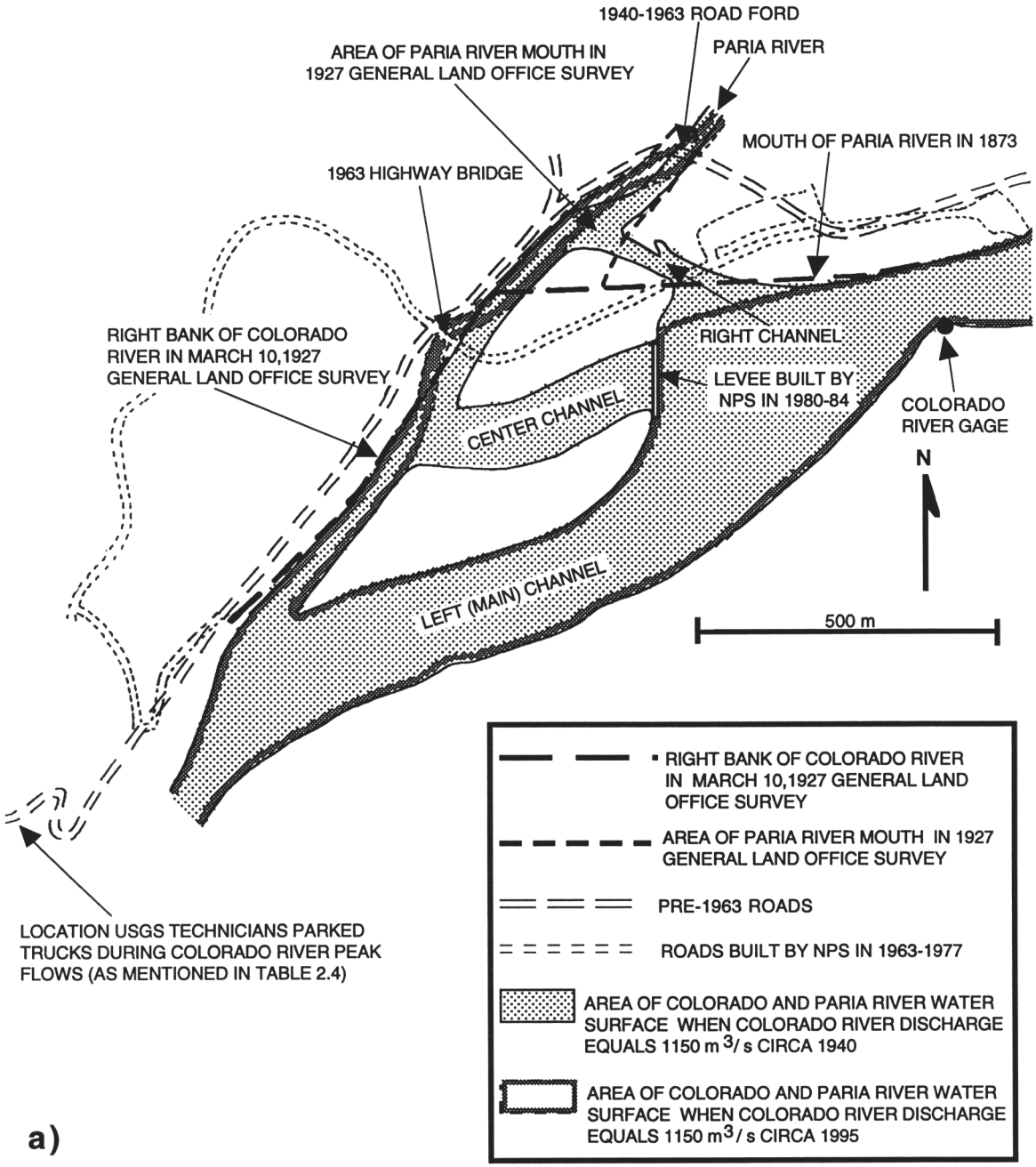

Figure 2.31: **(a)** Map showing the natural (circa 1940) geometry and the post-Glen Canyon Dam and post-National Park Service development (circa 1995) geometry of the confluence of the Paria and Colorado rivers with the discharge of the Colorado River approximately equal to 1150 m^3/s (constructed from USGS gage records, photographs, topographic surveys, and the 1927 cadastral survey of Gould (1928).

Figure 2.31 (continued): (b) Upstream view of the high-water confluence of the Paria and Colorado rivers in the 1930's. Discharge in the Colorado River is approximately 2600-2800 m^3/s; note the substantial Colorado River backwater in the mouth of the Paria River. View is from the old dugway on the left bank of the Colorado River. Photograph taken from unpublished USGS "Supplement to station description, Colorado River at Lees Ferry, AZ, September 1, 1938". **(c)** May 17, 1993 upstream view of the bar at the confluence of the Paria and Colorado rivers. Discharge in the Colorado River is 350 m^3/s. View is from the old dugway on the left bank of the Colorado River at a position 500 m downstream from the camera position in Figure 2.31b. The letter **A** indicates the position of the high-water confluence of the Paria River and Colorado rivers in Figure 2.31b; the letter **B** indicates the position of the levee across the head of the bar constructed by the National Park Service; the letter **C** indicates the position of the Paria River meander cut off by the National Park Service; the letter **D** indicates the position of the new Paria River channel dug by the National Park Service. Photograph by D.J. Topping.

b)

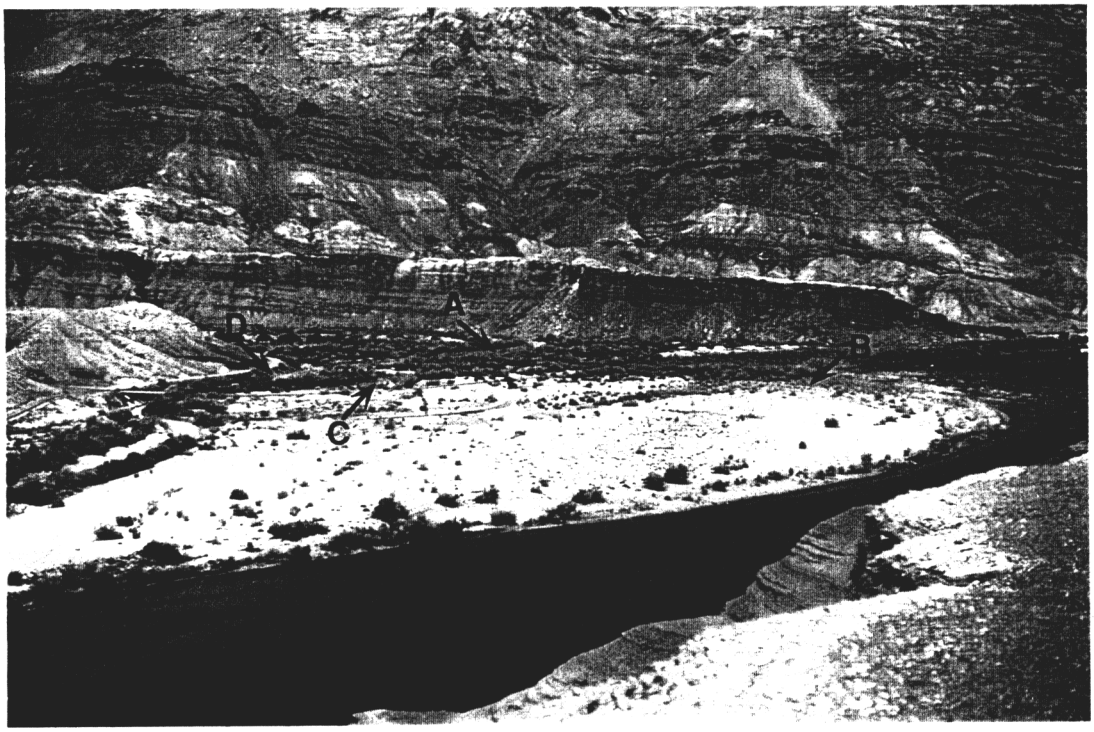

c)

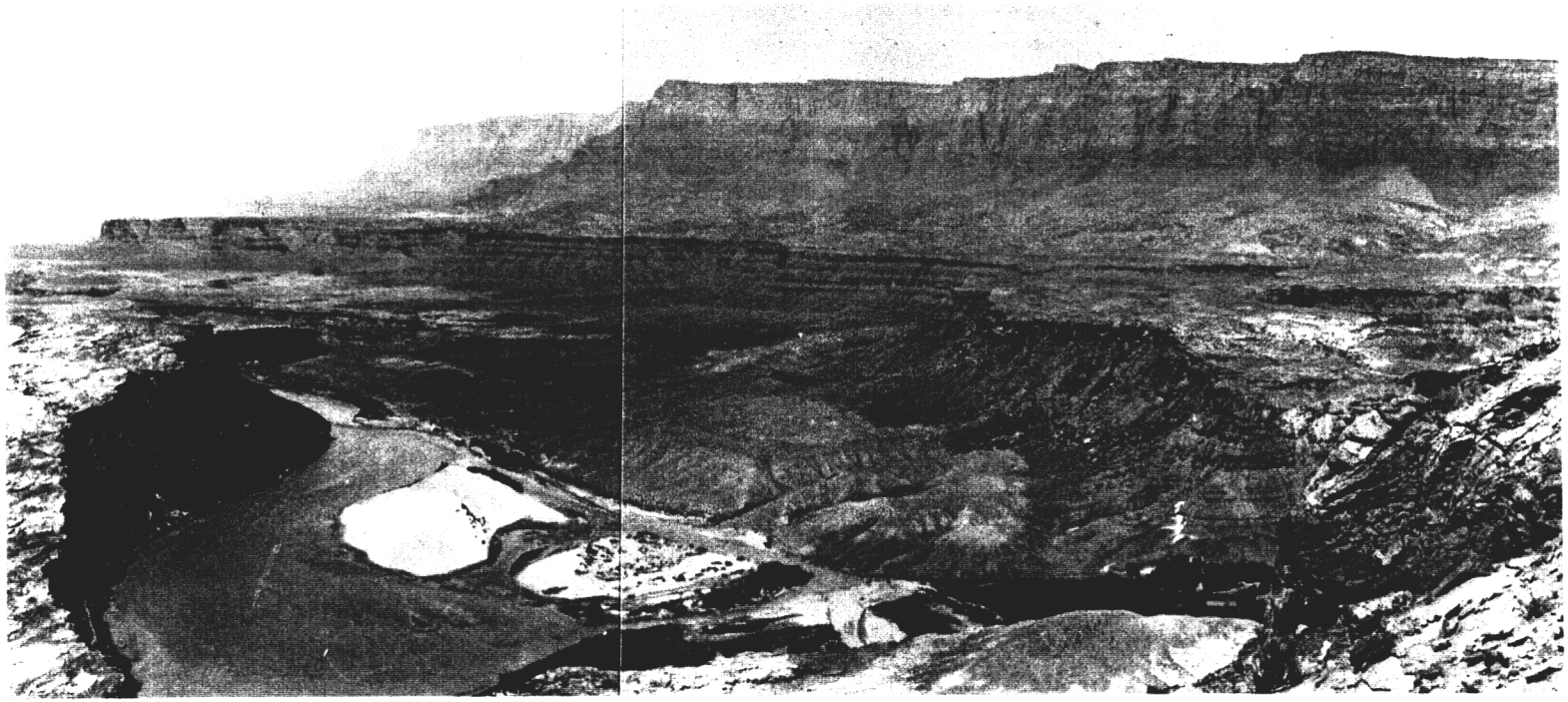

a)

Figure 2.32: **(a)** Composite photograph of the confluence of the Paria and Colorado rivers taken by H.E. Gregory in June 1915 from a position approximately 1/2 of the way up the Spencer Trail north of Lees Ferry, AZ. Because of its higher suspended sediment concentrations, the water in the Paria River appears to be a lighter shade of gray than the Colorado River water. Estimated discharge in the Colorado River is 1300-1500 m^3/s.

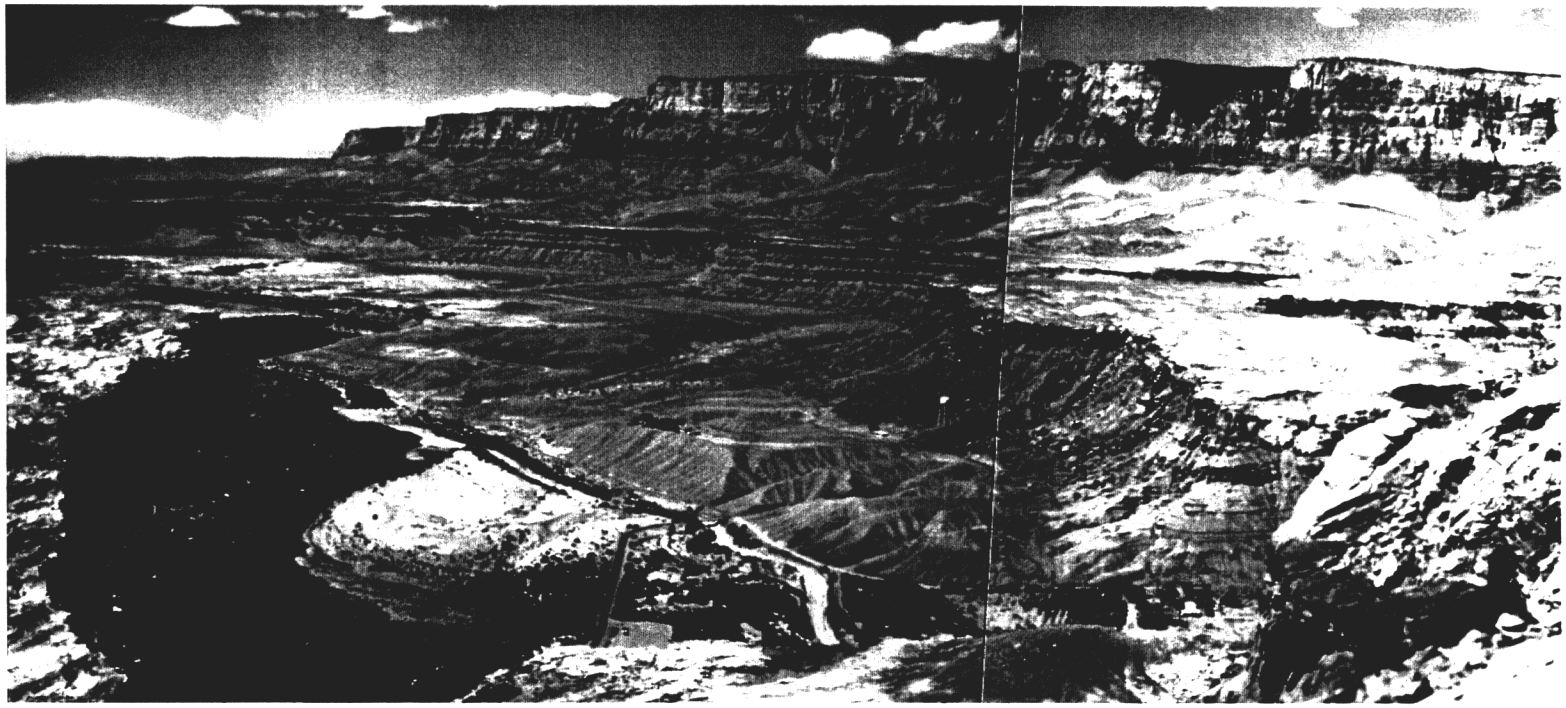

b)

Figure 2.32 (continued): (b) Composite photograph of the confluence of the Paria and Colorado rivers taken by D.J. Topping on April 15, 1995 from the same position as the photograph in Figure 2.32a. Discharge in the Colorado River is 270 m^3/s.

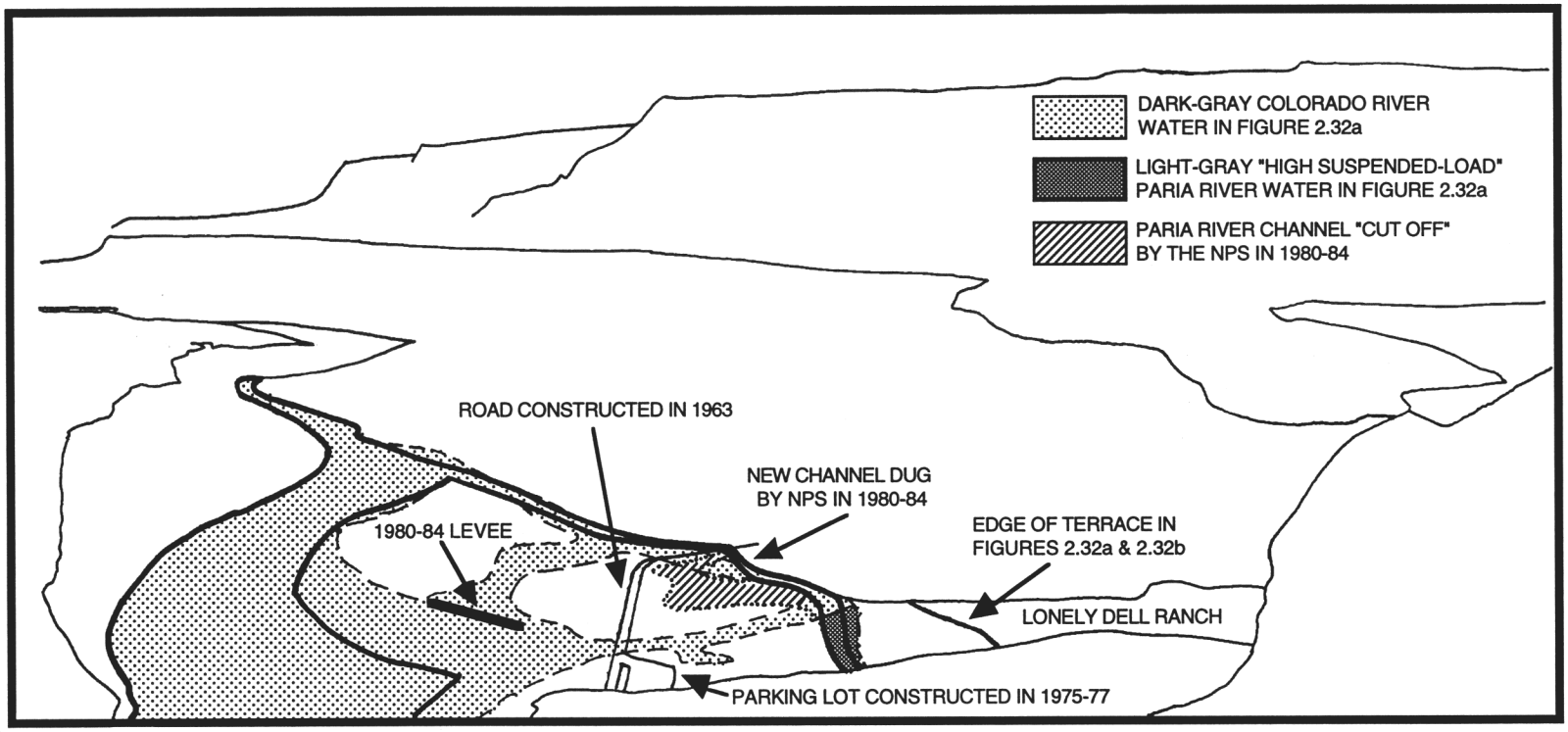

c)

Figure 2.32 (continued): (c) Line drawing of the views in Figures 2.32a & 2.32b illustrating the human-induced changes in the confluence geometry. Dashed thin lines indicate the edges of water in Figure 2.32a and solid thick lines indicate the edges of water in Figure 2.32b.

d)

Figure 2.32 (continued): (d) Photograph of the confluence of the Paria and Colorado rivers taken by E.C. LaRue on May 19, 1921 from a position at the top the Spencer Trail north of Lees Ferry. Discharge in the Colorado River is 1400 m^3/s. Apart from vegetational differences on the Paria River floodplain above the confluence, and the right channel of the Colorado River across the confluence bar being filled with sand, the confluence appears approximately the same as in Figure 2.32a.

Table 2.4: Colorado River backwatering events on the Paria River as described by James E. Klohr, USGS Resident Engineer, in the 1948, 1949, and 1952 USGS Station Histories of the Colorado River gage at Lees Ferry, Arizona.

4-20-48	Sand waves [antidunes] today at gage-house section of the Colorado River indicating silt [and sand] load working over control [bar at mouth of Paria].
4-23-48	Heavy winds and cloudiness. Small side-channel starts through Paria riffle at gage height 13.0 [feet, discharge 40,000 cubic feet per second (cfs) or 1130 cubic meters per second (m^3/s)].
4-26-48	Colorado River falling stage.
5-1-48	[Colorado] River rising today.
5-21-48	Large side channel through Paria bar and considerable backwater and drift in backwater of Paria mouth. Paria backed up to present road crossing today at gage height 15.6 [feet].
5-22-48	Considerable drift in Colorado River.
5-23-48	Backwater approximately 2.0 feet [0.6 m] deep on Paria [road] crossing.
5-24-48	Colorado River backwater drowns out Paria River crossing.
5-27-48	Backwater recedes at gage height 17.0 [feet]. Crossing fordable. [The USGS surveyed backwater curve of relation in Figure 4 indicates 2 feet (0.6 m) of bed aggradation at the road ford between 5-21-48 and 5-27-48].
5-28-48	Slight rise in Paria River [on] account [of] thundershowers at headwaters...Paria flow very muddy.
6-1-48	Paria flash flood silts up crossing.
6-15-48	Colorado River slowly falling
6-23-48	Paria bar normal. No side channels. [Gage height 12.5 feet, discharge 36,000 cfs (1020 m^3/s).]
3-19-49	Colorado River starts rising slowly. Paria River very muddy account melting snow in upper reaches of stream.
4-27-49	Small side channel [right channel] starts flowing through Paria bar at gage height 12.5 [feet, 36,000 cfs (1020 m^3/s)]. Considerable backwater in mouth of Paria River. No effect on [Paria] gage.
6-18-49	[Colorado River] backwater over Paria crossing. Crossing not passable by car. Flash floods in Paria.
6-19-49	Very muddy flash flood in Paria last night and today.
6-19-49	Paria crossing filled in with mud from flash flood on [top of] backwater from Colorado River.
6-20-49	Backwater [continues] over Paria crossing.
6-21-49	Backwater in Paria to approximately 300 feet below [Paria] gage. Colorado River peak gage height 20.2 [feet] and discharge 122,000 [cfs (3450 m^3/s)].
6-22-49	Backwater in Paria drops off considerably [as Colorado River stage drops].
6-25-49	Paria crossing impassable by automobile.
6-30-49	Conditions normal past three days. [Colorado] River falling steady. Paria River crossing not passable by auto at end of month [on] account [of] deep silt deposited by [Colorado River] backwater and [Paria River] flash floods.
7-2-49	Made crossing of Paria by auto today, but muddy and bad crossing. Crossing cannot be improved until heavy flash flood [in Paria River] scours out silt deposited by recent backwater from Colorado River.

Table 2.4 (continued):	
5-7-52	Colorado River water backed up a block beyond our Paria River crossing. [Crossing] now impassable by car. We have one truck on far side of the Paria. [Records indicate that the elevation of the bed at the ford is 0.5 m higher than it was on 6-18-49].
5-8-52	Colorado River measurement made today at 107,000 cfs [3030 m^3/s]. [We are] using our second boat to cross Paria River. Truck on far side of the Paria River now moved to the top of the hill approximately 2 miles from station on account of water [from Colorado River] backing up into side washes.
5-9-52	[Colorado River] now on downgrade.
5-21-52	Colorado River measured at 82,800 cfs [2340 m^3/s]. Paria now crossable by car again.
5-31-52	Colorado River now on the rise [again].
6-6-52	Paria River ford not crossable by car. Took truck on top of hill two miles from here for fear of high water blocking road.
6-12-52	Colorado River peaked at mean gage height 21.18 [feet] at 3:00 a.m., discharge 124,000 cfs [3510 m^3/s].
6-21-52	Colorado River measurement at 76,700 cfs [2170 m^3/s]. Paria River ford left with about 2 feet [0.6 m] of slop after Colorado River receded. Will need a Paria River rise to wash it out.
6-30-52	Cleaned mud out of Paria crossing with the aid of two men from Cliff Dwellers Lodge, [crossing] now crossable by car.

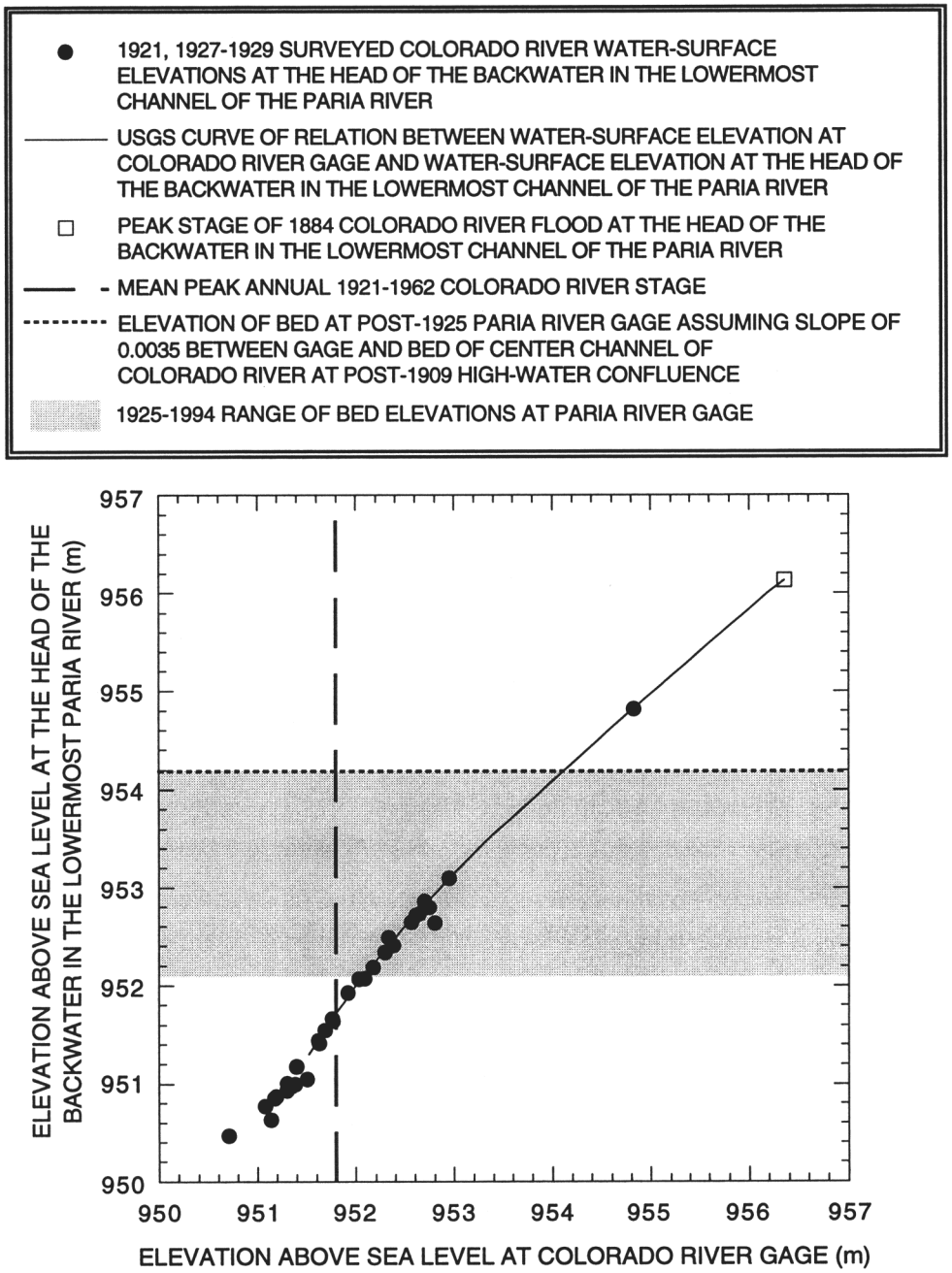

Figure 2.33: Elevation of the Colorado River water surface at the head of the backwater in the lowermost Paria River channel as a function of the elevation of the Colorado River water surface at the Colorado River gage at Lees Ferry, AZ. The USGS curve of relation was fitted to the 1921 and 1927-1929 data by the USGS (unpublished USGS report, 1938). Also presented are: (1) the 1925-1994 range of minimum bed elevations at the Paria River gage, (2) the elevation of the water surface for the 1921-1962 mean peak annual Colorado River flood at the Colorado River gage, and (3) the elevation of the bed at the Paria River gage given a longitudinal bed slope equal to 0.0035, i.e., a slope equal to the slope of the 1990-1993 terraces and the 1872-1873 bed of the channel, between the post-1925 Paria River gage and the post-1909 high-water confluence with the Colorado River.

slope of 0.0035, the projected mouth of the Paria River would be above the elevation of the post-1909 high-water confluence with the Colorado River.

The seasonal interplay between the Colorado and Paria rivers that set the fluctuating base level of the Paria River is now gone as a result of the 1963 closure of Glen Canyon Dam on the Colorado River 26 km above the confluence. Not only has the dam closure prevented the seasonally high, sediment-rich Colorado River flows that filled the channel of the lowermost Paria River with sediment, but it has also caused major changes in the channel of the Colorado River. Since the closure of the dam has cutoff the upstream supply of sediment, the reach of the Colorado River above the confluence with the Paria River has incised substantially; between the initiation of dam construction in 1956 and the 1975 survey by Pemberton (1976), approximately 9.87×10^6 m^3 of bottom sediment had been removed from the reach between the dam and the mouth of the Paria (Turner and Karpiscak, 1980), corresponding to between 1.6 and 7.0 m of maximum bed incision at each measurement section, with most of the incision occurring prior to 1965 (Williams and Wolman, 1984). Moreover, the high-discharge releases from Glen Canyon Dam in 1965, the first high-discharge releases after dam closure, caused up to 5 meters of permanent bed incision in the pool of the Colorado River at the Lees Ferry gage (Burkham, 1986).

Even if the high, sediment-rich flows of the Colorado River were not stopped by the closure of Glen Canyon Dam, the same range of flows that historically transported sediment across the bar via the center and right channels into the lowermost channel of the Paria River would have been prevented by the development of the bar area by the National Park Service starting in 1963 (Figures 2.31 & 2.32). The right channel across the bar that was occupied by the Colorado River at about 1100-1400 m^3/s has not been flooded by the Colorado River since construction of a bridge and elevated road across the bar in 1963 by the NPS; a flow of 2700 m^3/s would now be required to overtop this artificial barrier. Also, since the NPS constructed a levee across the head of the bar in 1980-1984, the Colorado River now only flows through the left, i.e. main, channel at 600 m^3/s and no longer occupies the center channel across the bar until about 1200 m^3/s. (This levee was barely overtopped by the experimental 1275 m^3/s Grand Canyon flood of March-April 1996; partial fill of the lowermost Paria River channel with sand and gravel was observed in April 1996 following recession of this flood).

<u>Pre-1963 seasonally fluctuating base level of the Paria River</u>

As mentioned, in addition to the two major drops in mean base level in 1909 and 1963, seasonal base level fluctuations due to the interplay of floods on the Colorado and

Paria rivers prior to 1963 heavily influenced the bed elevation at the Paria River gage. In the 1920's, USGS personnel were concerned that the post-1925 Paria River gage was too close to the mouth and would be adversely affected by its proximity to the Colorado River. USGS engineer D.A. Dudley in 1925 indicated that the location of the gage was unfavorable since "high water in the Colorado River would cause backwater at the gage" (unpublished USGS Paria River gage at Lees Ferry, AZ annual technical file, 1926). Indeed, as already shown in Figure 2.28 the backwater from the largest Colorado River floods would typically inundate the site of the post-1925 Paria River gage.

Since June 1921, the Colorado River has inundated the post-1925 gage site 3 times (unpublished USGS report on Colorado River flood stages, 1925; unpublished USGS Paria River gage at Lees Ferry, AZ annual technical file, 1927): (1) on June 18, 1921, the Colorado River backwater extended 0.5 km above the post-1925 gage site; (2) on July 1, 1927, the backwater from the Colorado River inundated the bed at the post-1925 gage site by 0.4 m; and (3) on September 13, 1927, a 3400 m^3/s Colorado River flood inundated the bed at the post-1925 gage site by 0.6 m while the Paria River was also in flood. The September 13, 1927 event is unique in the period from 1923 through 1996 in that it is the only coincidence of extreme floods on both rivers; this event caused 0.6 m of permanent aggradation at the post-1925 gage. Following the aggradation that occurred during the September 1927 flood, the backwater from four subsequent 3400 m^3/s Colorado River floods in 1941, 1949, 1952, and 1957 would extend to within 150 m of the post-1925 Paria River gage but would not inundate it (unpublished USGS Paria River discharge field notes, 1949, 1957; unpublished USGS Colorado River gage at Lees Ferry annual technical file, 1941, 1949, 1952, 1957). Likewise, the backwater from the 3400 m^3/s Colorado River flood of 1922 did not inundate the post-1925 gage site, but only extended to within 100 m of it (unpublished USGS Colorado River gage at Lees Ferry annual technical file, 1922), thus indicating that, prior to the incision of the lower Paria River during the October 5, 1925 flood, the bed at the post-1925 gage site was at about the same elevation that it reattained after the September 1927 flood.

Changes in minimum bed elevation at the Paria River gage do not always correlate with either the stage of the Colorado River during a Paria River flood or the size of Paria River flood, however. Of the six largest Paria River floods during the period of record, significant bed aggradation at the post-1925 gage site accompanied only the largest, the September 13, 1927 flood that occurred during the backwater of the gage site by the Colorado River. Significant incision of the bed only accompanied the third largest (the 270 m^3/s October 5, 1925 flood) and fourth largest (the 240 m^3/s September 9, 1980) flood,

during which 1.0 m and 0.7 m of incision occurred, respectively. During both of these Paria River floods, the stage of the Colorado River was low. No appreciable change in bed elevation at the post-1925 gage site accompanied the second largest (the 310 m^3/s September 7, 1940) flood, the fifth largest (the 200 m^3/s September 31, 1963), and the sixth largest (the 180 m^3/s September 13, 1939) Paria River floods that occurred when the stages of the Colorado River were also relatively low. Furthermore, seven cross-sections surveyed in the reaches above and below the gage before and after the September 6, 1940 flood indicate that no channel bed elevation or channel shape change occurred in either of these reaches during the second largest flood during the period of record (Figure 2.27).

Causes of other changes in minimum bed elevation at the post-1925 gage site

Finally, not all changes in bed elevation in the Paria River channel at the gage result from hydraulic processes intrinsic to the Paria and Colorado rivers. Other changes in minimum bed elevation have been historically the result of external forcing mechanisms, e.g., gage maintenance, or rock falls from the cliff above the gage. For example, 0.2 m of bed aggradation occurred between August 31 and September 7, 1929, as the result of rock being removed from the cliff and dumped in the channel by USGS personnel installing a gage stilling well on August 24-26 and September 1 and 4, 1929 (Figure 2.34a). Also, 0.2 m of incision occurred on March 25, 1973, as the result of a USGS worker lowering the bed of the Paria River at the gage with a tractor and grading blade in order to reconnect the gage stilling well to low flow in the river (Figure 2.33b). Additionally, 0.1 m of bed aggradation resulted from the largest historical rockfall, measuring 12 m^3 in volume, on July 5, 1929 (unpublished USGS discharge measurement field notes, 1929). These are only a few examples; numerous other episodes of gage maintenance and natural rock fall have influenced the elevation of the bed at the gage during the period of record.

2.5b-4: Reach-averaged cross-section channel geometry from 1872 to 1994

After the lateral and vertical positions of a channel, the third, and most important, aspect of channel geometry is the reach-averaged cross-section channel geometry. As will be shown in Section 2.6, for a given reach-averaged longitudinal slope and bed roughness, changes in the hydrology and sediment transport must be reflected in changes in the cross-section geometry of the channel. Because Hereford (1986, 1987a) concluded that the cross-section geometry of the Lees Ferry reach of the Paria River began to change after 1939 (with development of new floodplains as the channel narrowed and aggraded), thus

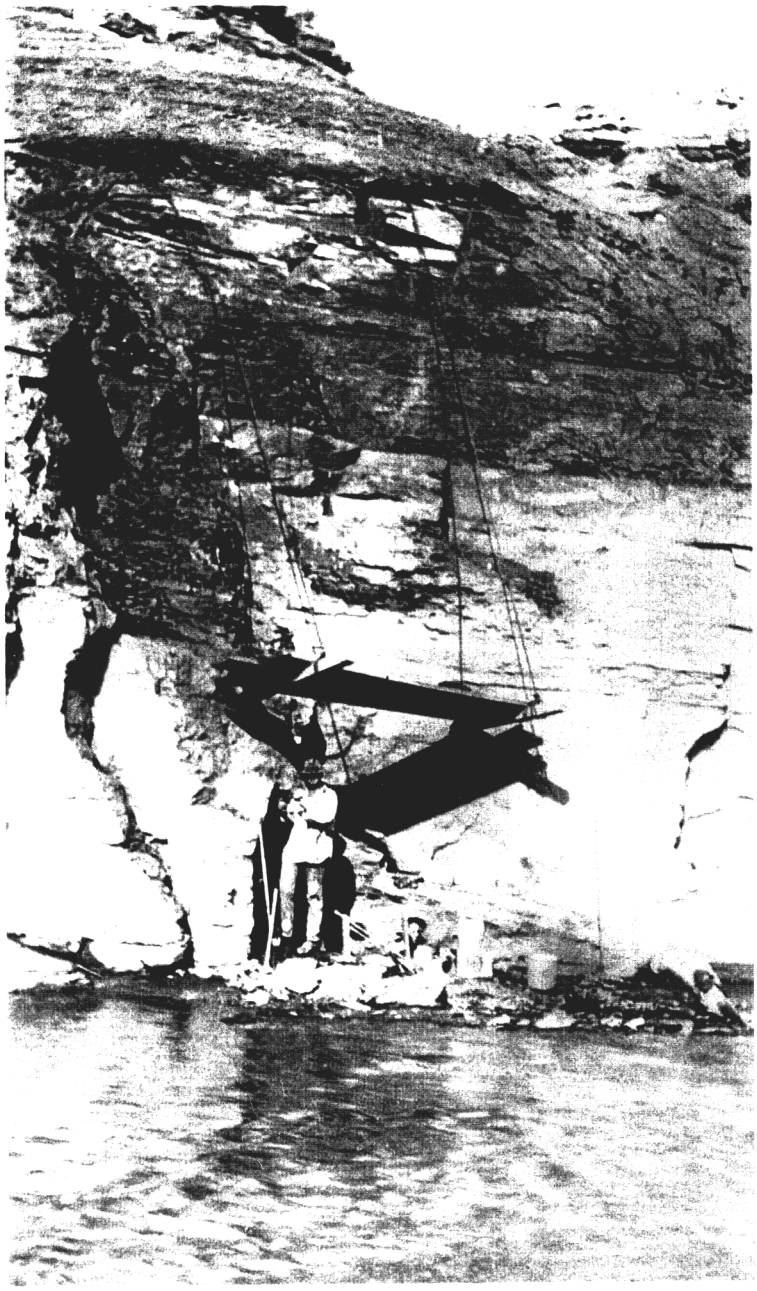

a)

Figure 2.34: **(a)** Paria River continuous-recorder stage gage during construction on August 27 or 28, 1929; USGS personnel excavating for lower end of gage stilling well. The rock in the channel was removed from the overhanging cliff behind the USGS workers on August 24-26, 1929. More rock was removed on September 1 and 4, 1929 such that the cliff would be vertical for the installation of the gage stilling well. Photo taken from the unpublished USGS "Report of Construction for Paria Gaging Station on Paria River at Lees Ferry, Arizona" submitted by J.A. Baumgartner, Assistant Engineer, on January 1930.

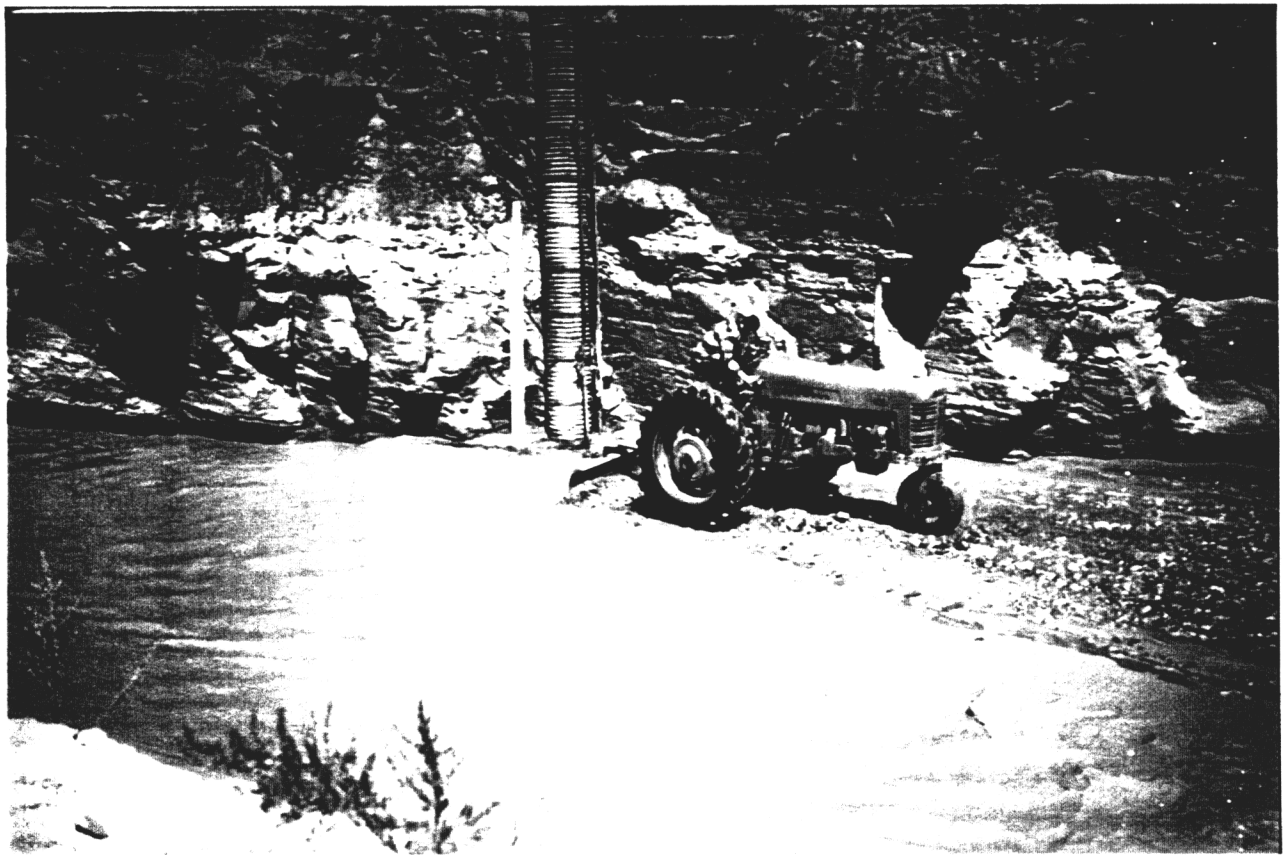

b)

Figure 2.34 (continued): (b) USGS worker lowering the bed of the Paria River at the gage with a tractor and grading blade on March 25, 1973 in order to reconnect the gage well to the flow in the river. Photograph from USGS-WRD Arizona District files, Flagstaff, AZ.

implying that the hydrology and sediment transport of the system changed after 1939, great care was taken in this study to investigate fully the channel cross-section geometries present in the Lees Ferry reach for the period from 1872 to 1994. Investigation of channel cross-section geometries in the Lees Ferry reach was divided into two parts. First, to eliminate the influence of changes in the longitudinal channel bed slope on the cross-section channel geometry, comparisons of reach-averaged cross-section channel geometry for the period from 1872 to 1993 were conducted for reaches of similar longitudinal slope. Second, in order to determine the significance of any changes in channel geometry, a statistical analysis of cross-section channel geometry, as defined by the 2445 ice-free discharge measurements made in the Lees Ferry reach from 1923 to 1994, was also conducted.

2.5b-4a: Comparative analysis of reach-averaged Paria River cross-section geometry

The first approach used to determine the long-term mean of, and to detect any systematic changes in, the reach-averaged cross-section geometry of the river was to compare reach- or time-averaged channel geometries determined from channel surveys, high-flow discharge measurements, a written description of channel dimensions, and ground-based photographs (when no other data for a certain time period were available). Sources of data for this part of this investigation were: the 3.5-km 1993 valley survey completed as part of this study (described previously in Section 2.5a-1); USGS slope-area surveys from 1925, 1927, 1929, 1939, 1940, and 1963; two cross-sections surveyed as parts of USGS float-area discharge measurements from 1924 and 1925; 65 cross-sections measured as parts of the USGS discharge measurements made at Cableway 2 from 1953 to 1972; the journal entry of John D. Lee describing the dimensions of his irrigation dam in 1872; and five ground-based photographs, with objects of known dimension in the field of view, from 1873, 1911, 1915, and 1921. These data were then reach-averaged or time-averaged, if possible, and grouped into two categories: (1) data from reaches with either reach-averaged longitudinal bed slopes within 15% of 0.0035 or no bed-slope data; and (2) data from reaches with reach-averaged longitudinal bed slopes greater than 0.004 or less than 0.002. The value of 0.0035 was chosen as the mean slope for the data of Category 1 because it is equal to the most probable equilibrium bed slope for the lowermost Paria River for the following reasons: it is equal to the mean 1990-1993 terrace slope (Figure 2.28), i.e. likely 1872-1873 floodplain slope; it is equal to the inferred 1872-1873 channel bed slope (Figure 2.27); is within 15% of the reach-averaged bed slope of the 3-reach composite used to construct the 1993 reach-averaged cross-section, i.e. within 15% of

0.004; and is within 5.5% of the lowest longitudinal slope in the lowermost 25 km of the Paria River determined from the USGS 7.5-minute topographic quadrangles (Figure 2.2), i.e. within 5.5% of 0.0037.

The rationale for breaking the data into two categories is further developed in Section 2.6. Simply stated, for a given reach-averaged longitudinal bed slope and bed-sediment size distribution, and given no major hydrologic or sediment transport changes with respect to time, the equilibrium alluvial cross-section geometry of a reach should be invariant with respect to time. Therefore, the reach-averaged cross-section geometry data comprising Category 2 should be distinct from those comprising Category 1. Results of this comparative analysis of cross-section geometry will be presented below, followed by detailed descriptions of the data used in the analysis.

Data from reaches with longitudinal bed slopes approximately equal to the equilibrium bed slope of 0.0035 (Category 1 data)

For reaches with known reach-averaged longitudinal bed slopes within 15% of 0.0035 (specifically the 1925 reach above the gage, the reach below the gage in 1939-1940, the reach above the gage near Cableway 2 from 1953 to 1972, the reach above the gage in 1963, and the 1993 3-reach composite), the reach-averaged cross-section geometry has been invariant with respect to time from at least 1925 to 1993 (Figure 2.35). Furthermore, reaches with unknown reach-averaged longitudinal bed slopes, but slopes probably close to 0.0035 (specifically the reach 500 m above the gage in 1872, the reach near the confluence with the Colorado in 1873, the reach between the gage and the confluence from 1911 to 1921, the reach 458 m above the gage in 1924, and the reach 183 m below the gage in 1925), all have channel dimensions or channel cross-section geometries that are compatible with the those of reaches with slopes known to be within 15% of 0.0035 (Figure 2.35).

The cross-section geometry data comprising Category 1 are compared in Figure 2.35a; for those data that were reach- or time-averaged, the mean reach- or time-averaged bed elevation at each cross-stream position for each reach- or time-averaged cross-section is shown in this figure. The magnitude of the standard deviation in bed elevation at each cross-stream position for each reach- or time-averaged cross-section is shown is illustrated in Figure 2.35b; the mean plus and the mean minus one standard deviation bed elevation at each cross-stream position for the reach- or time-averaged cross-section geometry data of Category 1 are shown in this figure. Overlap at one standard deviation of the reach- or time-averaged cross-section geometries in Figure 2.35b indicates that the differences in

Figure 2.35: **(a)** Mean bed elevation as a function of cross-stream position in the October 10, 1924 cross-section, the August 29, 1925 cross-section, the November 4, 1925 average cross-section for the reach above the post-1925 gage, the 1939-1940 reach-averaged cross-sections for the reach below the gage, the 1953-1972 time-averaged cross-section at Cableway 2, the 1963 reach-averaged cross-section in the reach above the gage, and the 1993 reach-averaged cross-section; left and right in the November 4, 1925 average cross-section, the 1939-1940 reach-averaged cross-section, and the 1953-1972 time-averaged cross-section have been reversed to match the geometric asymmetry of the 1963 and 1993 reach-averaged cross-sections. Also shown are the top endpoints of John D. Lee's irrigation dam in 1872 and the positions of the bankfull channel margins at the river mouth in 1873 and the reach below the gage in 1911-1921. Differences that exist in cross-section geometry above the bankfull level in Figure 2.35a are of no consequence since they merely reflect differences in terrace geometry in each of the compared reaches. **(b)** Mean plus and mean minus one standard deviation bed elevation as a function of cross-stream position in the 1939-1940 reach-averaged cross-section for the reach below the gage, the 1953-1972 time-averaged cross-section at Cableway 2, the 1963 reach-averaged cross-section for the reach above the gage, and the 1993 reach-averaged cross-section. For this comparison, left and right in the 1939-1940 reach-averaged cross-section and the 1953-1972 time-averaged cross-section have been reversed to match the geometric asymmetry of the 1963 and 1993 reach-averaged cross-sections.

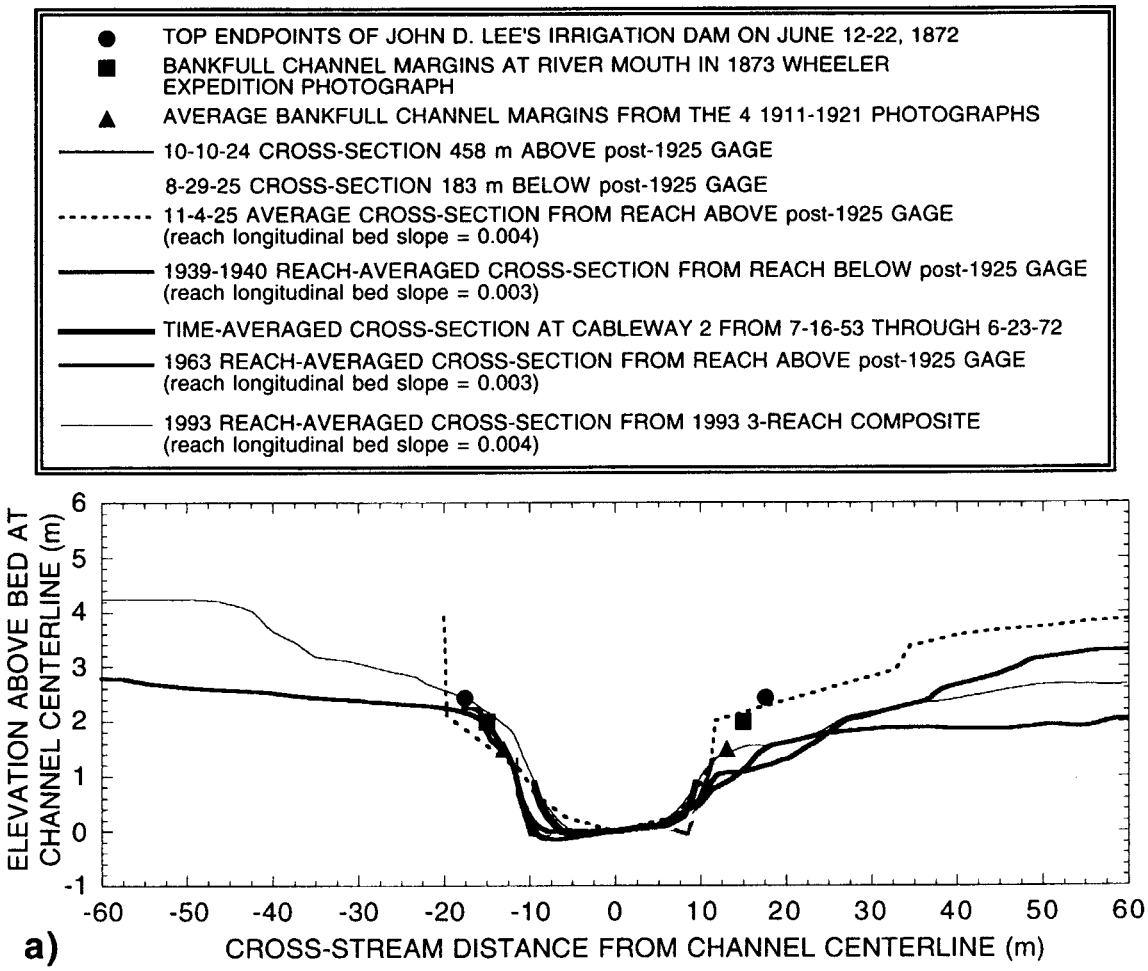
TOP ENDPOINTS OF JOHN D. LEE'S IRRIGATION DAM ON JUNE 12-22, 1872
BANKFULL CHANNEL MARGINS AT RIVER MOUTH IN 1873 WHEELER EXPEDITION PHOTOGRAPH
AVERAGE BANKFULL CHANNEL MARGINS FROM THE 4 1911-1921 PHOTOGRAPHS
10-10-24 CROSS-SECTION 458 m ABOVE post-1925 GAGE
8-29-25 CROSS-SECTION 183 m BELOW post-1925 GAGE
11-4-25 AVERAGE CROSS-SECTION FROM REACH ABOVE post-1925 GAGE (reach longitudinal bed slope = 0.004)
1939-1940 REACH-AVERAGED CROSS-SECTION FROM REACH BELOW post-1925 GAGE (reach longitudinal bed slope = 0.003)
TIME-AVERAGED CROSS-SECTION AT CABLEWAY 2 FROM 7-16-53 THROUGH 6-23-72
1963 REACH-AVERAGED CROSS-SECTION FROM REACH ABOVE post-1925 GAGE (reach longitudinal bed slope = 0.003)
1993 REACH-AVERAGED CROSS-SECTION FROM 1993 3-REACH COMPOSITE (reach longitudinal bed slope = 0.004)
ELEVATION ABOVE BED AT CHANNEL CENTERLINE (m)
6
5
4
3
2
1
0
-1
-60
-50
-40
-30
-20
-10
0
10
20
30
40
50
60
a)
CROSS-STREAM DISTANCE FROM CHANNEL CENTERLINE (m)

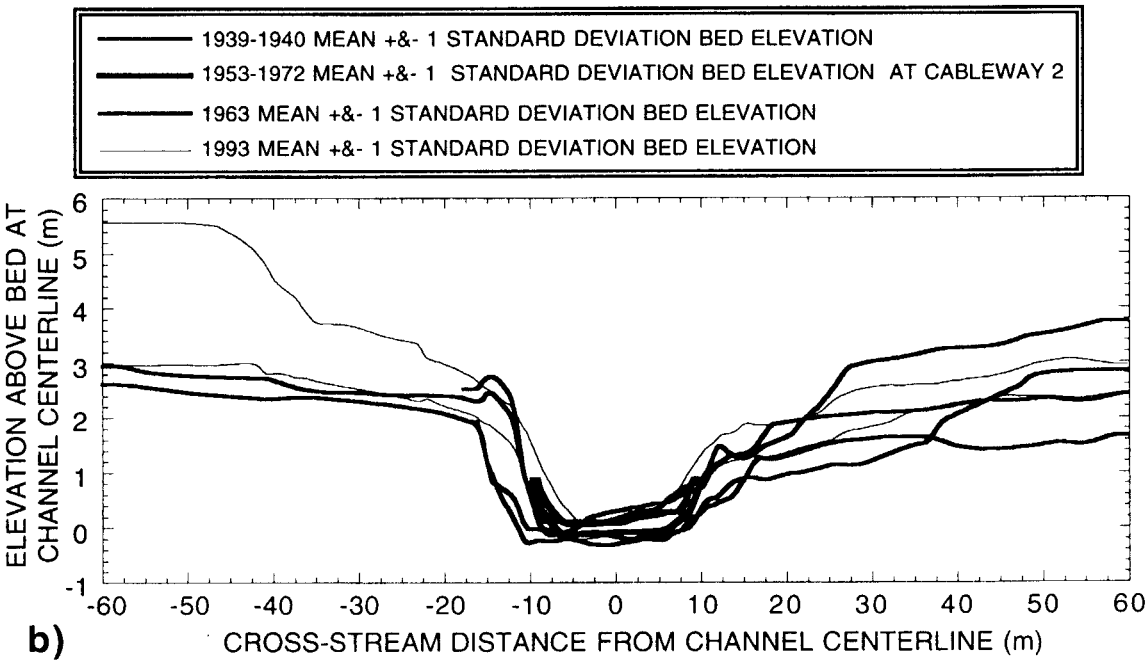
1939-1940 MEAN +&- 1 STANDARD DEVIATION BED ELEVATION
1953-1972 MEAN +&- 1 STANDARD DEVIATION BED ELEVATION AT CABLEWAY 2
1963 MEAN +&- 1 STANDARD DEVIATION BED ELEVATION
1993 MEAN +&- 1 STANDARD DEVIATION BED ELEVATION
ELEVATION ABOVE BED AT CHANNEL CENTERLINE (m)
6
5
4
3
2
1
0
-1
-60
-50
-40
-30
-20
-10
0
10
20
30
40
50
60
b)
CROSS-STREAM DISTANCE FROM CHANNEL CENTERLINE (m)

reach-averaged cross-section geometry between the reaches comprising Category 1 are insignificant. Furthermore, if the magnitudes of the standard deviations in Figure 2.35b are used to infer the magnitude of standard deviations for the data in Figure 2.35a without known standard deviations, the cross-section geometries of all reaches comprising Category 1 (i.e., all reaches with longitudinal bed slopes within 15% of the equilibrium bed slope), spanning the time period from 1872 to 1993 are identical within error.

Data from reaches with longitudinal bed slopes greater than 0.004 or less than 0.002 (Category 2 data)

As will be shown in Section 2.6, by virtue of conservation of water and sediment mass, for channels with identical bankfull discharges, bankfull sediment loads, and identical grain-size distributions on the bed, the equilibrium cross-section geometry for a reach with a steep longitudinal bed slope must be much broader and shallower than a reach with a more gentle longitudinal bed slope. Thus, it makes sense that the steeper 1929 and 1939 reaches from Category 2 are much broader and shallower than the reaches comprising Category 1 (Figure 2.36). The lone outlier to this channel geometry framework, the low-sloping, broad reach below the gage in 1927, is interpreted to be not representative of the equilibrium channel shape, and rather to be the result of deposition of sediment in this reach during the backwatering event by the Colorado River; this interpretation is based on the observation that the bed of the Paria River at the gage aggraded by 0.6 m while being backwatered by the Colorado River.

Stability of the reach-averaged Paria River cross-section geometry during extreme events

The final point to be made with regard to reach-averaged cross-section geometry is that, for reaches of similar longitudinal bed slope, the reach-averaged cross-section geometry surveyed immediately after an extreme event is identical (at an overlap of one standard deviation) to the reach-averaged cross-section geometry surveyed as many as 13 years after the last major flood. For example, the reach-averaged cross-section geometry surveyed 1-2 months after either the second (the 1940 flood), third (the 1925 flood), sixth (the 1963 flood), or seventh (the 1939 flood) largest floods during the period of gage record, is indistinguishable from the reach-averaged cross-section geometry surveyed in 1993, 13 years after the fourth largest flood during the period of gage record (the 1980 flood). So, regardless of changes in the lateral or vertical position of the channel, the reach-averaged cross-section geometry for a fixed longitudinal bed slope has, indeed, been stable from 1872 to 1993. These observations indicate that the long-term hydraulic

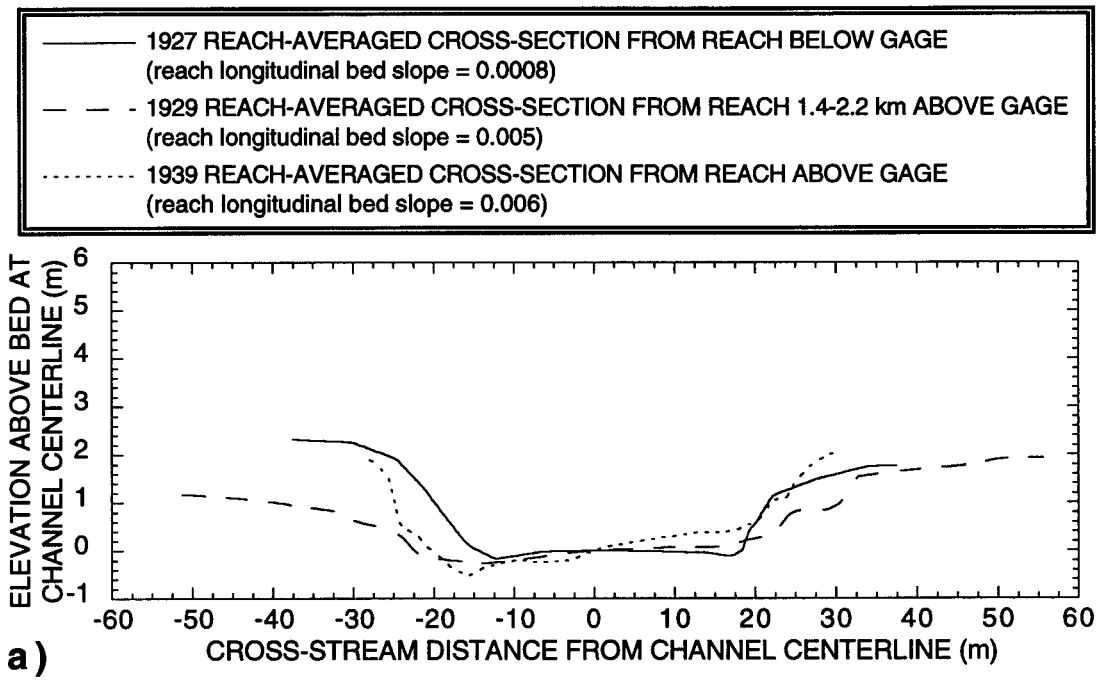

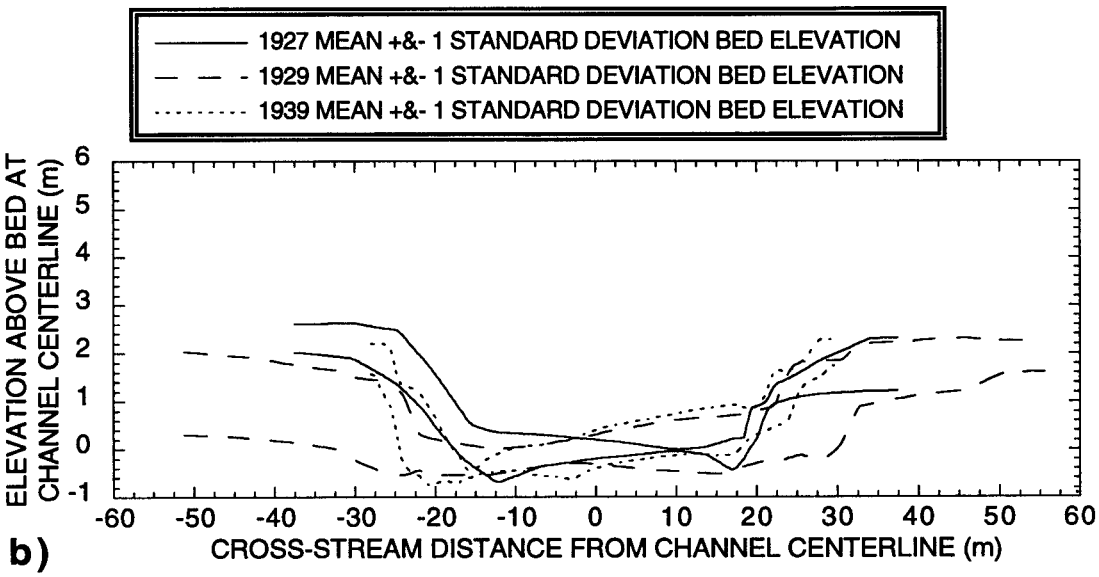

Figure 2.36: **(a)** Mean bed elevation as a function of cross-stream position in the reach-averaged cross-sections for the October 2, 1927 reach below the gage, the September 10, 1929 reach 1.4-2.2 km above the gage, and the October 27, 1939 reach above the gage. **(b)** Mean plus and mean minus one standard deviation bed elevation as a function of cross-stream position in the reach-averaged cross-sections for the October 2, 1927 reach below the gage, the September 19, 1929 reach 1.4-2.2 km above the gage, and the October 27, 1939 reach above the gage.

geometry (see Section 2.6) of the lowermost Paria River has been invariant, and suggest that the hydrology and sediment transport of the Paria River have been relatively stable from 1872 to the present.

Detailed descriptions of the data used in the comparative analysis of reach-averaged Paria River cross-section geometry

Detailed descriptions of the thirteen measurements of cross-section geometry appearing in Figures 2.35 and 2.36 are presented below. The oldest measurement of channel cross-section geometry (Figure 2.35a) is from a published description of an irrigation dam. On June 6, 1872, a flood washed out the irrigation dam John D. Lee had built about 500 m above the post-1925 gage site and 10 m upstream from the 1923-1925 gage site (Figures 2.4 & 2.26). This description, appearing above in Section 2.5b-1, indicates that the channel at the dam site was 2.4 m deep in the center and 35.2 m wide at the crest of the dam; the top endpoints of the dam, assuming that the dam was symmetric about the channel centerline, are indicated on Figure 2.36a. The reach-averaged longitudinal bed slope associated with this measurement is unknown.

The second measurement of channel cross-section geometry (Figure 2.35a) is from analysis of a photograph taken of the mouth of the Paria River in 1873 by T.H. O'Sullivan, photographer with the Wheeler Survey (Figure 2.37a). By using the width of a wagon (labeled **A** in Figure 2.37a) as a scale (the distance from the camera to both the wagon and the mouth of the Paria River is equivalent), the estimated bankfull width (labeled **B** in Figure 2.37a) of the Paria River is 30 m and the bankfull depth is 2 m. Positions of the bankfull channel margins (30 m wide at 2 m above the bottom of the channel) appear in Figure 2.35a. The reach-averaged longitudinal bed slope associated with this measurement is unknown.

The third measurement of channel cross-section geometry (Figure 2.35a) is the result of averaging four determinations of bankfull widths and depths from 4 photographs taken from 1911 through 1921 in the reach below the post-1925 gage.[4] The first photograph used in the average was taken by the Kolb brothers in 1911 (Figure 2.37b). By using the 1975 National Park Service Survey (National Park Service, 1975) and the 1993 valley survey (described in Section 2.5a-1) to determine the distance between the terrace margin (labeled **C** in Figure 2.37b) appearing in the center of the photograph and

---

[4]The photograph taken by A.H. Jones (p. 118 of Rusho and Crampton, 1992), which was used to identify the 1909 position of the thalweg in Figure 2.27, was not used in this average because no identifiable features on the left bank of the Paria River channel could be used for scale.

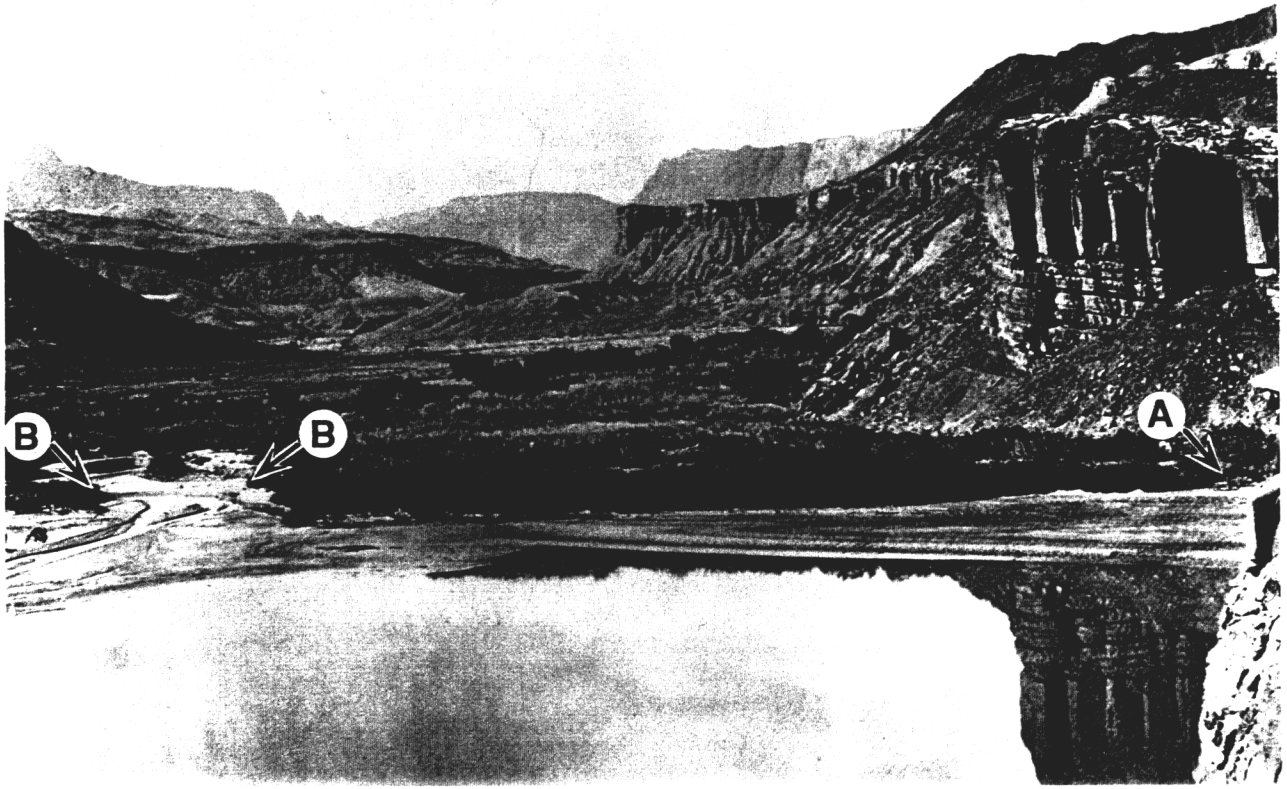

a)

Figure 2.37: **(a)** View of the mouth of the Paria River from high on the left bank of the Colorado River in 1873; photograph taken by T.H. O'Sullivan of the Wheeler Survey. The letter **A** indicates the position of the wagon used for scale in determining the bankfull width and depth of the Paria River; the letters **B** indicate the positions of the bankfull channel margins used in the bankfull width determination.

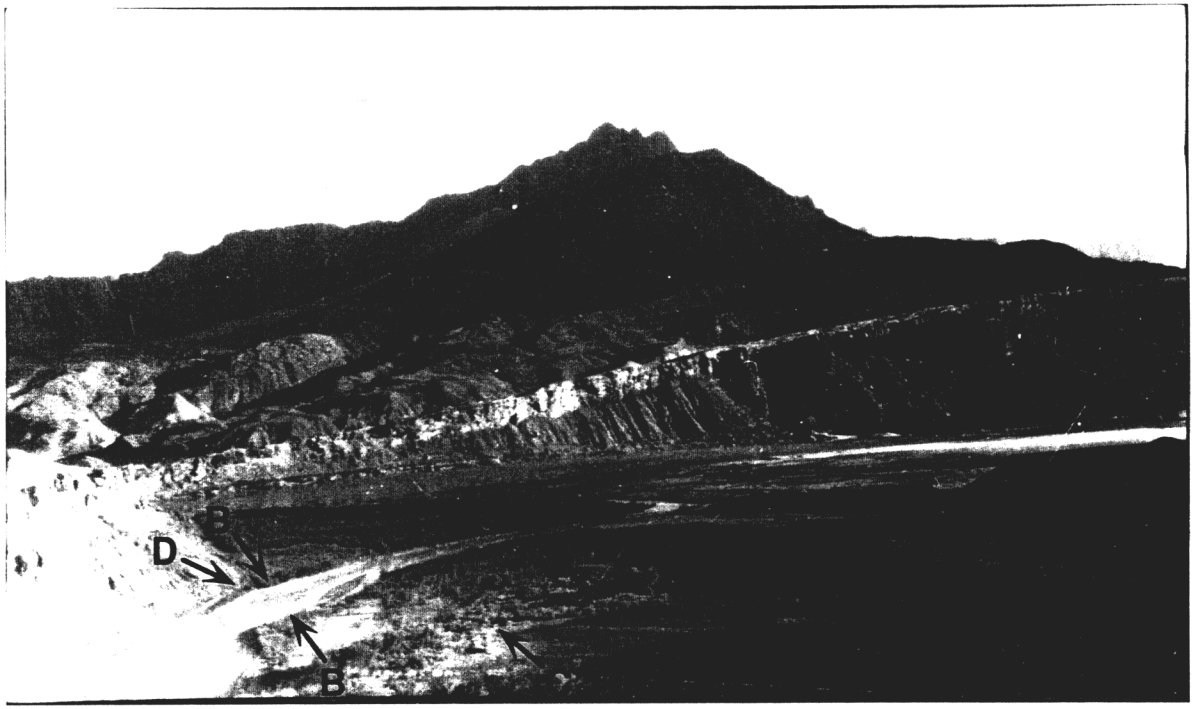

b)

Figure 2.37 (continued): (b) Down-valley view of the lowermost Paria River in 1911; photograph taken by the Kolb brothers. The letters **B** indicate the positions of the bankfull channel margin used in the bankfull width determination; the letter **C** indicates the position of a bend in the margin of the terrace located in the 1975 National Park Service survey and my 1993 survey; the letter **D** indicates the position of the "nose" of the talus located in the 1975 National Park Service survey and my 1993 survey. The surveyed distance between the features marked by letters **C** and **D** is 200 m.

c)

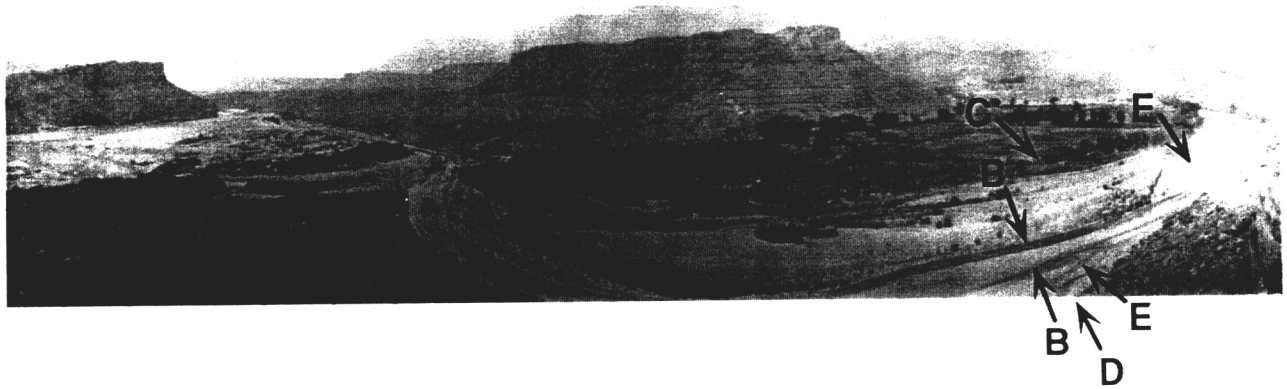

Figure 2.37 (continued): **(c)** View of the lowermost Paria River on September 1, 1915; photograph taken by E.C. LaRue with a panorama lens. The letters **B** indicate the positions of the bankfull channel margins used in the bankfull width determination (in approximately the same location as in Figure 2.37b); the letter **C** refers to the same feature as in Figure 2.37b; the letter **D** refers to the same feature as in Figure 2.37b (which is just below the bottom of the view in this photograph); the letters **E** indicate the position of the line of wagon tracks used as a "backup" scale. The letter **F** indicates the position of the Paria River channel prior to the September 1909 avulsion; the downstream direction in this old channel was toward the camera.

the base of the talus (labeled **D** in Figure 2.37b) appearing on the left in the photograph, bankfull width (labeled **B** in Figure 2.37b) in the left portion of this photograph is estimated to be 30 m. The second photograph used in the 1911-1921 average was taken by H.E. Gregory in June 1915 and appears above as Figure 2.33a. By using the width of the Colorado River at the future USGS cableway for scale, bankfull width of the Paria River above the confluence with the right channel of the Colorado River (500 m below the width determination from the 1911 Kolb photograph) is estimated to be 25 m. The third photograph used in the average was taken by E.C. LaRue on September 1, 1915 (Figure 2.37c).[5] By using the same features used for scale in the 1911 Kolb photograph for a primary scale and by using the width between wagon wheel ruts crossing the Paria River channel (labeled **E** in Figure 2.37c) for a "backup" scale (the spacing between the wheel ruts is assumed to be 2 m), bankfull width in the right portion of this photograph (at the same location as the width determination from the 1911 Kolb photograph) is also estimated to be 25 m. The fourth photograph used in the 1911-1921 average was taken by E.C. LaRue on May 19, 1921 and appears above as Figure 2.33d. By using the wagon roads (wheel-rut spacing is again assumed to be 2 m) and the width of the Colorado River at the future USGS cableway for scale, bankfull width in the lower right portion of this photograph (400 m below the width determination from the 1911 Kolb and 1915 LaRue photographs and 100 m above the width determination from the 1915 Gregory photograph) is also estimated to be 25 m. The average bankfull depth in the four photographs is approximately 1-2 m. Positions of the average bankfull channel margins (26 m wide at 1.5 m above the bottom of the channel) appear in Figure 2.35a; the reach-averaged longitudinal bed slope associated with this time-averaged measurement is unknown.

The fourth and fifth measurements of cross-section channel geometry (Figure 2.35a) are from unpublished USGS discharge measurement field notes. The fourth measurement is the cross-section 458 m above the post-1925 gage surveyed on October 10, 1924 following the flood of September 10, 1924; the fifth measurement is the cross-section at the pre-1929 road ford (Figure 2.4) 183 m below the post-1925 gage surveyed on August 29, 1925 following the flood of August 27, 1925. Reach-averaged longitudinal bed slopes associated with these measurements are unknown.

The sixth measurement of cross-section channel geometry (Figure 2.35a) is also from unpublished USGS discharge measurement field notes. Following the 270m^3/s flood

---

[5]Note that the floodplain that appeared to be heavily vegetated in the 1911 Kolb photograph is now largely devoid of vegetation in September 1915.

of October 5, 1925, on November 4, 1925, USGS technicians surveyed an "average cross-section" located 180 m above the post-1925 gage that they felt was representative of the reach above the gage (distance is the 1925 distance). This cross-section appears in Figure 2.27 (Plate 1) and has been reversed in Figure 2.35a so that the higher bank is on the left, thus matching the asymmetry of other cross-sections in Figure 2.35a. As determined from data in Figures 2.28 and 2.29, the reach-averaged longitudinal bed slope associated with this measurement is approximately 0.004.

The seventh measurement of cross-section channel geometry (Figures 2.36a & 2.36b) results from reach-averaging the cross-sections surveyed on October 2, 1927 as part of the USGS slope-area survey following the September 13, 1927 flood. The technique used to calculate the reach-averaged cross-section geometry for this other USGS slope-area surveys is the same as was used to construct the 1993 reach-averaged cross-section as described in Section 2.5a-1. Cross-sections used in this reach average are the 10-2-27 cross-sections located 70, 200, and 250 m below the gage in Figure 2.27 (Plate 1). The reach-averaged longitudinal bed slope associated with this measurement is 0.0008.

The eighth measurement of cross-section channel geometry (Figures 2.36a & 2.36b) results from reach-averaging the cross-sections surveyed on September 10, 1929 as part of the USGS slope-area survey following the August 2, 1929 flood. Cross-sections used in this reach average are the 9-10-29 cross-sections located 2080, 1930, 1780, 1630, 1480, and 1330 m above the gage in Figure 2.27 (Plate 1).[6] The reach-averaged longitudinal bed slope associated with this measurement is 0.005.

The ninth measurement of cross-section channel geometry (Figures 2.36a & 2.36b) results from reach-averaging cross-sections surveyed in the reach above the gage on October 27, 1939 as part of the USGS slope-area survey following the September 13, 1939 flood. Cross-sections used in this reach average are the 10-27-39 cross-sections located 330, 240, 180, 100, and 50 m above the gage in Figure 2.27 (Plate 1).[7] The reach-averaged longitudinal bed slope associated with this measurement is 0.006.

The tenth measurement of cross-section channel geometry (Figures 2.35a & 2.35b) results from reach-averaging cross-sections surveyed on October 27, 1939 and September 14, 1940 in the reach below the gage as part of the USGS slope-area surveys following the September 13, 1939 and September 14, 1940 floods. Cross-sections used in this reach average are the 9-14-40 cross-section located 70 m below the gage and the 10-27-39 cross-

---

[6]Distances are the pre-channel-lengthening, 1929 distances.
[7]Distances are the pre-channel-lengthening, 1939 distances.

sections located 100, 140, 200, 250, and 290 m below the gage in Figure 2.27 (Plate 1). The reach-averaged longitudinal bed slope associated with this measurement is 0.003.

The eleventh measurement of cross-section channel geometry (Figures 2.35a & 2.35b) results from constructing a time average of the channel topography from the 65 discharge measurements made at the Cableway 2 from July 16, 1953 to June 23, 1972; the discharge measurements made after the first headcut passed the gage on August 14, 1972 are not included in this average. The reach-averaged longitudinal bed slopes at Cableway 2 ranged from about 0.004 to 0.003 during the period of 1953-1972.

The twelfth measurement of cross-section channel geometry (Figures 2.35a & 2.35b) results from reach-averaging cross-sections surveyed on September 18, 1963 and October 15, 1963 as part of the USGS slope area survey following the September 1, 1963 flood. Cross-sections used in this reach average are the 9-18-63 cross-sections located 300, 180, and 80 m above the gage and the 10-15-63 cross-sections located 240, 100, and 50 m above the gage in Figure 2.27 (Plate 1). The reach-averaged longitudinal bed slope associated with this measurement is 0.003.

The thirteenth measurement of cross-section channel geometry (Figures 2.35a & 2.35b) is the 1993 reach-averaged cross-section constructed in Section 2.5a-1; the reach-averaged longitudinal bed slope associated with this measurement is 0.003.

2.5b-4b: Statistical analysis of Paria River cross-section geometry

The second approach used to determine the long-term mean of, and to detect any systematic changes in, the reach-averaged cross-section geometry of the Paria River in the Lees Ferry study area was to compare statistically the geometry of the channel determined from the 2445 ice-free discharge measurements made in this reach of the river at discharges less than bankfull between November 22, 1923 and October 12, 1994.

Methodology

This analysis is a two-step process and determines whether or not data in separate bins are different at a chosen level of significance. First, the data are broken into separate bins and, if possible at the chosen level of significance, a regression line is fit to the data in each bin. Second, a test is conducted to determine whether or not variation in the system is minimized with one regression line fit to all of the data or by individual regression lines fit to the data in each bin. If, at the chosen level of significance, the variation in the system is minimized by individual regression fit to the data in each bin, the data in each bin are statistically different at the chosen level of significance.

In the first step of the analysis, data are first divided into separate bins and defined in terms of a dependent and an independent variable; for the analysis of cross-section channel geometry, the dependent variable is defined as the topwidth of flow in each discharge-measurement cross-section, and the independent variable is defined as the maximum depth of flow in each discharge-measurement cross-section. Second, for both the entire data set and for each data bin, the dependent variable is fit by a linear least-squares regression. Third, for both the entire data set and for each data bin, analysis of variance is used (as in the hydrologic-trend analyses in Section 2.4e) to test whether or not the variance of the residuals about the regression line is significantly different than the variance about the mean of the dependent variable. Three quantities are defined to describe the variation in the system: the total sum of squares, SS_t; the sum of squares due to regression, SS_r; and the residual sum of squares, SS_d. These quantities have n-1, 1, and n-2 degrees of freedom, respectively (where n is equal to the number of data points in the regression), and are related by $SS_r = SS_t - SS_d$. SS_r and SS_d are then respectively converted into the mean squares MS_r and MS_d. The variance ratio for the resulting F-test is:

$$F_1 = \frac{MS_r}{MS_d} = \frac{SS_r/1}{SS_d/(n-2)}. \tag{2.4}$$

If, at the chosen level of significance, the null hypothesis that the variance of the residuals about the regression line is no different than the variance of the residuals about the mean of the data cannot be rejected, the regression itself is rejected.

The second step of the analysis tests whether or not the variation in the system is minimized at a given level of significance by a common regression line through all of the data or by separate regression lines for each data bin. The analysis of variance methodology used is discussed on pages 453-455 of Griffiths (1967). In this section, j is defined to be equal to the total number of data points in the combined data bins, n is defined to be equal to the number of data points in each bin, and m is equal to the number of individual data bins. As in the first step of the analysis, three quantities are defined to describe the variation in the system: the residual sum of squares from the common regression line fit to the combined data bins, SS_{com} (with j-m-1 degrees of freedom); the sum of squares of the difference between the common regression line fit to the combined data bins and the individual regression lines fit to each bin, SS_{diff} (with m-1 degrees of freedom) and the residual sum of squares from individual regression lines fit to each bin, SS_{ind}. These quantities are related by $SS_{diff} = SS_{com} - SS_{ind}$. SS_{ind} is equal to the sum of SS_d for each bin. If data in a bin cannot be fit by a regression line at the chosen level of significance, SS_t (with one additional degree of freedom) instead of SS_d is used to

characterize the variation of data in that bin. DF_{ind}, i.e., the degrees of freedom associated with SS_{ind}, therefore, is the sum of the degrees of freedom associated with either SS_d or SS_t in each bin. SS_{diff} and SS_{ind} are then respectively converted into the mean squares MS_{diff} and MS_{ind}. The variance ratio for the resulting F-test is:

$$F_2 = \frac{MS_{diff}}{MS_{ind}} = \frac{SS_{diff}/(m-1)}{SS_{ind}/DF_{ind}}. \tag{2.5}$$

So, for a given level of significance, the test is whether the null hypothesis that a common regression line fits all of the data in the combined bins as well as individual regression lines in each bin can be rejected. If the null hypothesis is rejected, then the data bins of interest are, indeed, different at the given level of significance.

Application of the method to the analysis of Paria River cross-section geometry

Five tests were conducted with the data divided into two bins for each test; in none of the binning schemes used in this analysis did a linear regression fail the F-test in equation 2.4. Results from this analysis are presented in Table 2.5, with the type of channel change indicated when the change is significant at the 0.05 level of significance; the detailed statistics for this analysis are found in Appendix 1.

The first binning scheme divided the data at August 14-15, 1972 into two bins, one from November 22, 1923 through August 14, 1972 and one from August 14, 1972 through September 30, 1992 (Figure 2.38a). This binning scheme compares the cross-section channel geometry after the passage of the first headcut by the gage on August 14, 1972 with the cross-section channel geometry prior to passage of the headcut by the gage. The second binning scheme divided the data at August 14, 1972 and September 9, 1980 into two bins, one from November 22, 1923 through August 14, 1972 and one from September 9, 1980 through September 30, 1992 (Figure 2.38b). This binning scheme compares the channel geometry after the passage of the second headcut by the gage on September 9, 1980 with the channel geometry prior to the passage of the first headcut by the gage on August 14, 1972.

The third binning scheme was chosen to address the conclusion of Hereford (1986) that the cross-section geometry of the Paria River changed after 1939 with a decrease in the cross-section area of the channel corresponding to narrowing of the channel and development of new floodplains. This scheme divided the data at December 31, 1939 - January 1, 1940 into two bins, one from November 22, 1923 through December 31, 1939 and one from January 1, 1940 through August 14, 1972 (Figure 2.38c); the data after the passage of the first headcut were excluded from this and subsequent analyses.

Table 2.5: Summary of the statistical analysis of channel cross-section geometry.

TIME PERIODS COMPARED	LEVEL OF SIGNIFICANCE, p, AT WHICH THE NULL HYPOTHESIS THAT THE CHANNEL SHAPE IS UNCHANGED CAN BE REJECTED	TYPE OF CHANNEL SHAPE CHANGE
11-22-23 through 8-14-72 *compared with* 8-15-72 through 9-30-92	$p < 1.0e\text{-}16$	30% NARROWER AFTER PASSAGE OF 1st HEADCUT ON 8-15-72
11-22-23 through 8-14-72 *compared with* 9-9-80 through 9-30-92	$p = 1.4e\text{-}5$	30-40% NARROWER AFTER PASSAGE OF 2nd HEADCUT ON 9-9-80
11-22-23 through 12-31-39 *compared with* 1-1-40 through 8-14-72	$p = 0.58$	**NO CHANGE**
11-22-23 through 12-31-49 *compared with* 1-1-50 through 8-14-72	$p = 0.25$	**NO CHANGE**
11-22-23 through 12-31-59 *compared with* 1-1-60 through 8-14-72	$p = 0.0011$	SLIGHTLY WIDER AFTER 1-1-60

Figure 2.38: **(a)** Flow topwidth as a function of measured maximum depth with best-fit regression lines for the discharge measurements before and after the passage of the first headcut by the gage on August 14, 1972. **(b)** Flow topwidth as a function of measured maximum depth with best-fit regression lines for the discharge measurements before and the passage of the first headcut by the gage on August 14, 1972 and after the passage of the second headcut by the gage on September 9, 1980. **(c)** Flow topwidth as a function of measured maximum depth with best-fit regression lines for the discharge measurements made from 11-22-23 through 12-31-39 and 1-1-40 through 8-14-72. **(d)** Flow topwidth as a function of measured maximum depth with best-fit regression lines for the discharge measurements made from 11-22-23 through 12-31-49 and 1-1-50 through 8-14-72. **(e)** Flow topwidth as a function of measured maximum depth with best-fit regression lines for the discharge measurements made from 11-22-23 through 12-31-59 and 1-1-60 through 8-14-72.

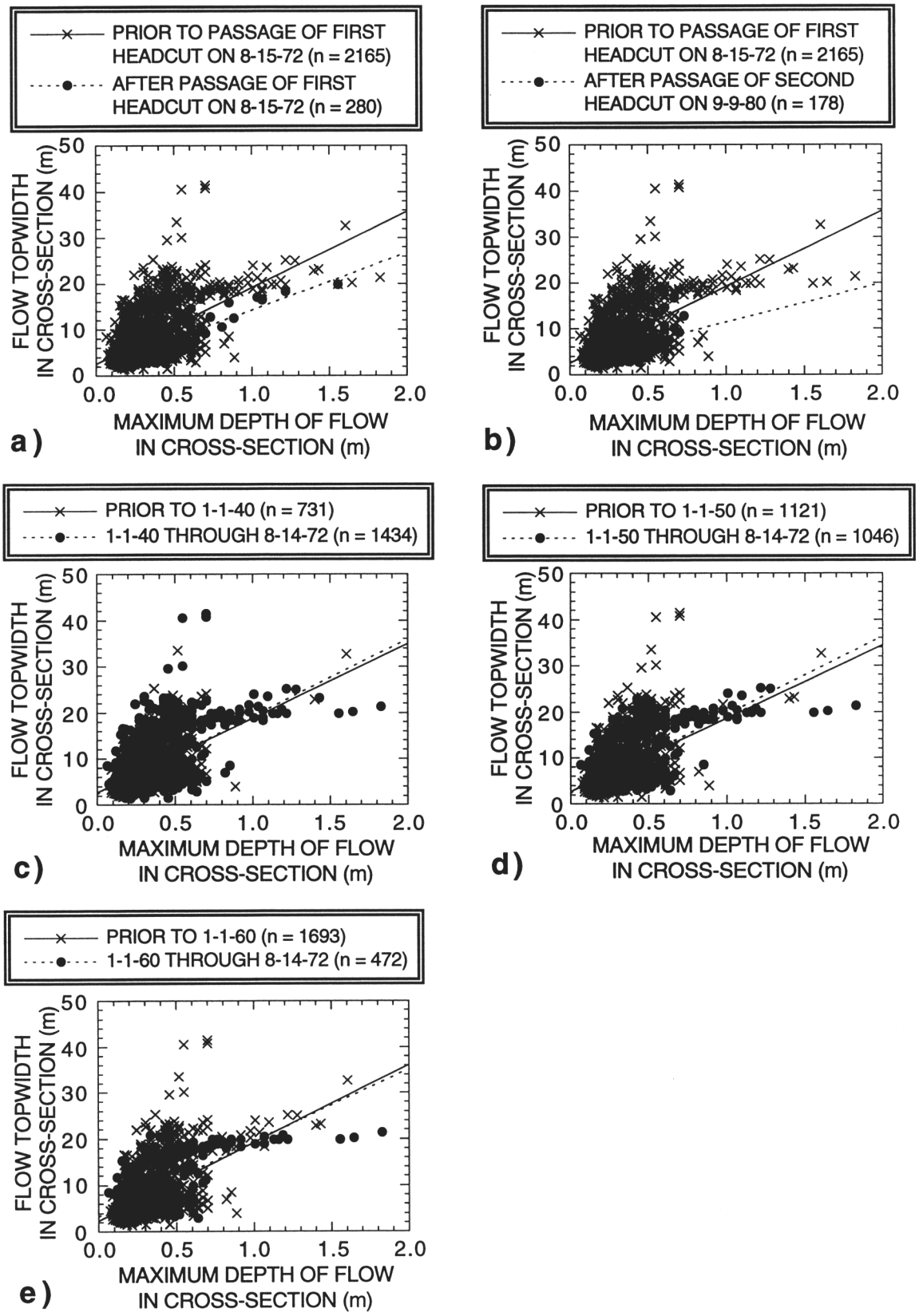
PRIOR TO PASSAGE OF FIRST HEADCUT ON 8-15-72 (n = 2165)
AFTER PASSAGE OF FIRST HEADCUT ON 8-15-72 (n = 280)
FLOW TOPWIDTH IN CROSS-SECTION (m)
MAXIMUM DEPTH OF FLOW IN CROSS-SECTION (m)
a)
PRIOR TO PASSAGE OF FIRST HEADCUT ON 8-15-72 (n = 2165)
AFTER PASSAGE OF SECOND HEADCUT ON 9-9-80 (n = 178)
FLOW TOPWIDTH IN CROSS-SECTION (m)
MAXIMUM DEPTH OF FLOW IN CROSS-SECTION (m)
b)
PRIOR TO 1-1-40 (n = 731)
1-1-40 THROUGH 8-14-72 (n = 1434)
FLOW TOPWIDTH IN CROSS-SECTION (m)
MAXIMUM DEPTH OF FLOW IN CROSS-SECTION (m)
c)
PRIOR TO 1-1-50 (n = 1121)
1-1-50 THROUGH 8-14-72 (n = 1046)
FLOW TOPWIDTH IN CROSS-SECTION (m)
MAXIMUM DEPTH OF FLOW IN CROSS-SECTION (m)
d)
PRIOR TO 1-1-60 (n = 1693)
1-1-60 THROUGH 8-14-72 (n = 472)
FLOW TOPWIDTH IN CROSS-SECTION (m)
MAXIMUM DEPTH OF FLOW IN CROSS-SECTION (m)
e)

The fourth binning scheme divided the data at December 31, 1949 - January 1, 1950 into two bins, one from November 22,1923 through December 31, 1949 and one from January 1, 1950 through August 14, 1972 (Figure 2.38d). The fifth binning scheme divided the data at December 31, 1959 - January 1, 1960 into two bins, one from November 22,1923 through December 31, 1959 and one from January 1, 1960 through August 14, 1972 (Figure 2.38e).

This statistical analysis of Paria River cross-section geometry yields four important results. First, the most significant change in cross-section channel geometry in the gage reach during the period 1923-1992 occurred with the passage of the first headcut by the gage on August 14, 1972. The post-incision (1972-1992) channel following the passage of this headcut channel was 30% narrower than the pre-incision (1923-1972) channel. Second, cross-section channel shape continued to change after the second headcut passed the gage on September 9, 1980; the 1980-1992 channel is 30-40% narrower than the pre-incision (1923-1972) channel. Third, cross-section channel geometry of the Paria River was constant during the period 1923-1959, challenging the conclusion of Hereford (1986) that the channel began to narrow in 1939. In fact, dividing the data at 1939-1940 and comparing cross-section channel geometry of the 1923-1939 channel to the 1940-1972 channel yields the statistically least significant difference over the entire period of record. Fourth, the channel began to widen slightly in the period 1960-1972; this result is also in contrast to the conclusions of Hereford (1986), W. Graf (1987), and J. Graf and others (1991) that the channel was narrowing with the formation of new floodplains during this time.

Comparison of topwidths of flow in the discharge measurement cross-sections with widths from the 1993 survey

One final comparison of cross-section geometric properties was conducted: comparison of the measured topwidths of flow used in the above statistical tests with measured channel widths in cross-sections from the 1993 survey (specifically widths from the 1993 average cross-section and three "end-member" cross-sections from the 1993 survey). This comparison indicates that the vast majority (over 90%) of the cross-section channel geometries that have existed in the gage reach between 1923 and 1972 fall within the bounds defined by the 1993 cross-section with the largest bankfull area and by the 1993 cross-section with the greatest bankfull depth (Figure 2.39). Thus, the current spatial average of channel geometries in the lower Paria River does indeed encompass the vast majority of historical channel geometries in the Paria River gage reach.

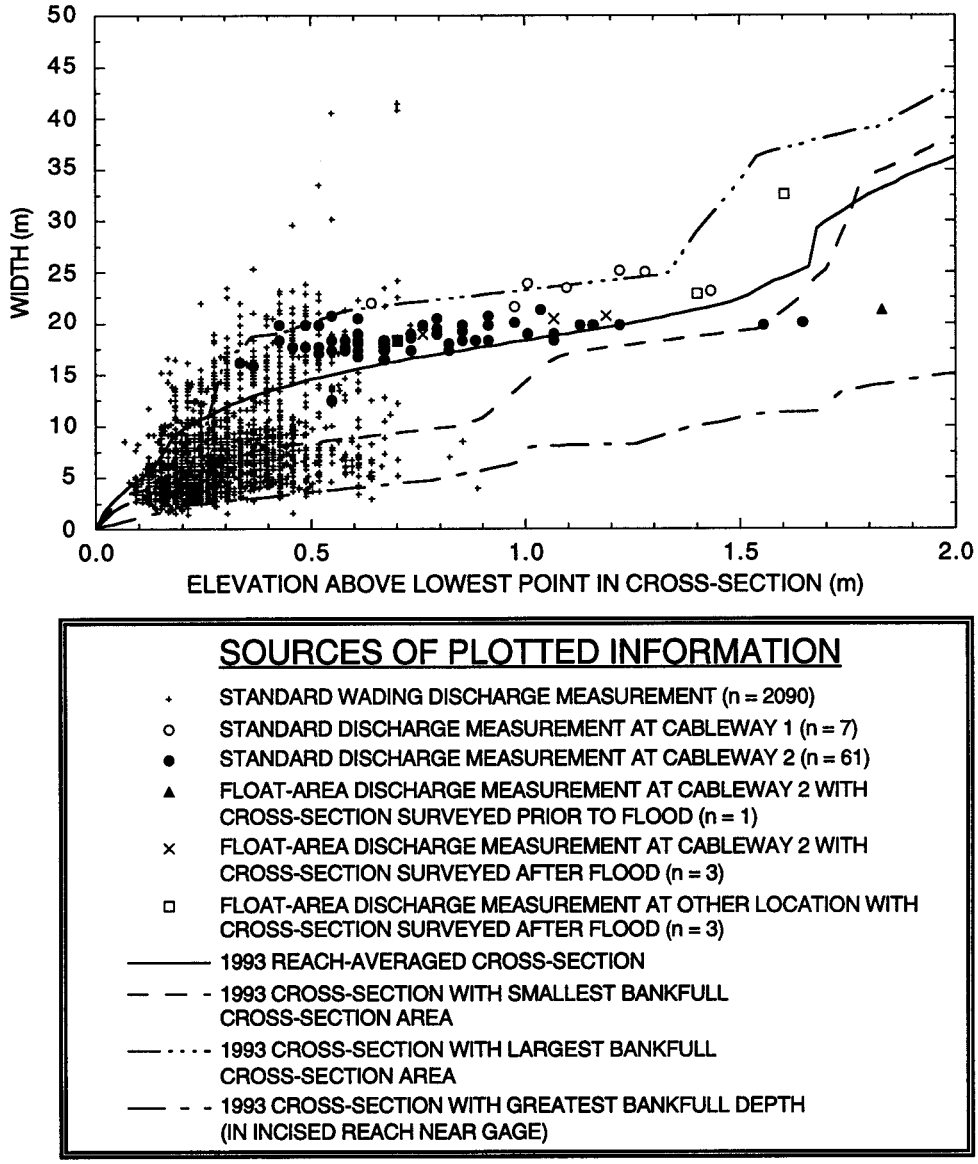

Figure 2.39: Comparison of widths as a function of elevation above the lowest point in a cross-section for: (1) six different types of USGS discharge measurements made between November 22, 1923 and August 14, 1972; and (2) four "types" of cross-sections from the 1993 survey: the 1993 reach-averaged cross-section; the 1993 cross-section with the smallest bankfull cross-section area that was within the 1993 3-reach composite; the 1993 cross-section with the largest bankfull cross-section area that was within the 1993 3-reach composite; and the 1993 cross-section with the greatest bankfull depth. Since some bed scour occurs in the channel cross-sections at higher stages, and because this figure compares width as a function of elevation measured at low flow (i.e., width as a function of elevation from the 1993 cross-sections and float-area measurements) against width as a function of elevation measured at high flow (i.e., width as a function of elevation from the standard discharge measurements) the elevations associated with widths for the higher flows in the both the 1993 cross-sections and the float-area measurements are probably low by about 10-20 cm.

2.5b-4c: Discussion of analyses of cross-section channel geometry and problems associated with stratigraphic analyses

The comparative and statistical analyses of cross-section channel geometry both show that the average cross-section channel geometry of the Lees Ferry reach of the Paria River did not change significantly during the period from 1872 to 1972, and that the modern reach-averaged cross-section channel geometry of the Paria River above the lower headcut in 1993 is still the same as the average cross-section channel geometry that existed near the gage from 1872 to 1972. These two analyses also highlight a problem with stratigraphy-based studies in rivers, in which floodplain stratigraphy is used, in part, to deduce channel changes over time, e.g., Hereford (1986) and W. Graf (1987). Stratigraphic analyses will only indicate where the river has deposited sediment; these analyses place no constraints on where or how much sediment the river has eroded. If the amount of deposition equals the amount of erosion in a reach over time, the reach-averaged cross-section area of the channel will remain unchanged, even though the channel locally may have moved substantially in both the lateral and vertical dimensions. Furthermore, by virtue of the lateral and vertical movement of the channel, new sections of floodplain sediment will always get locally preserved without any change in channel shape. Thus, stratigraphy alone can never do more than provide half the story in a fluvial environment and, in fact, can be misleading.

To illustrate a potential pitfall of stratigraphic analyses, the position of the floodplain surface through time determined by analysis of a stratigraphic section (Hereford, 1987, 1987a) is evaluated through the use of surveyed topographic data. A photograph of the stratigraphic section near the Paria River gage studied by Hereford (1986, 1987a) is shown in Figure 2.40a; in this photograph are three key stratigraphic horizons: the base of the post-1939 floodplain alluvium, the 1967 floodplain surface determined by Hereford (1986), and the October 15, 1963 floodplain surface determined from a USGS slope-area survey. Figure 2.40b shows the location of Hereford's floodplain stratigraphic section in relation to the cross-sections surveyed through the same location in 1939, 1963, and 1993. As shown in Figure 2.40b, at this location, the channel aggraded and moved to the right between 1939 and 1963 and degraded and moved back to the left between 1963 and 1993.

The base of Hereford's stratigraphic section, dated by him at 1939 based on photographic evidence, is in excellent agreement with the surveyed position of the sloping left margin of the channel on October 27, 1939 in Figure 2.40b. Unfortunately, little else in Hereford's stratigraphic section matches surveyed topographic data at this site. Hereford's dated 1967 horizon is 1 m below the surface of the floodplain as surveyed on

a)

Figure 2.40: **(a)** 1993 photograph of the stratigraphic section of Hereford (1986, 1987a); photograph by D.J. Topping, meter stick for scale. The letter **A** and black, dashed line indicate the position of stratigraphic horizon **A**, the angular contact between the post-1939 floodplain alluvium and the older, pre-1939 channel alluvium; the letter **B** indicates the position of stratigraphic horizon **B**, the 1967 floodplain surface dated by Hereford (1986) through the analysis of tamarisk tree rings; the letter **C** indicates the position of stratigraphic horizon **C**, the 1963 floodplain surface at this location determined from a cross-section from the USGS slope-area survey following the September 1, 1963 flood.

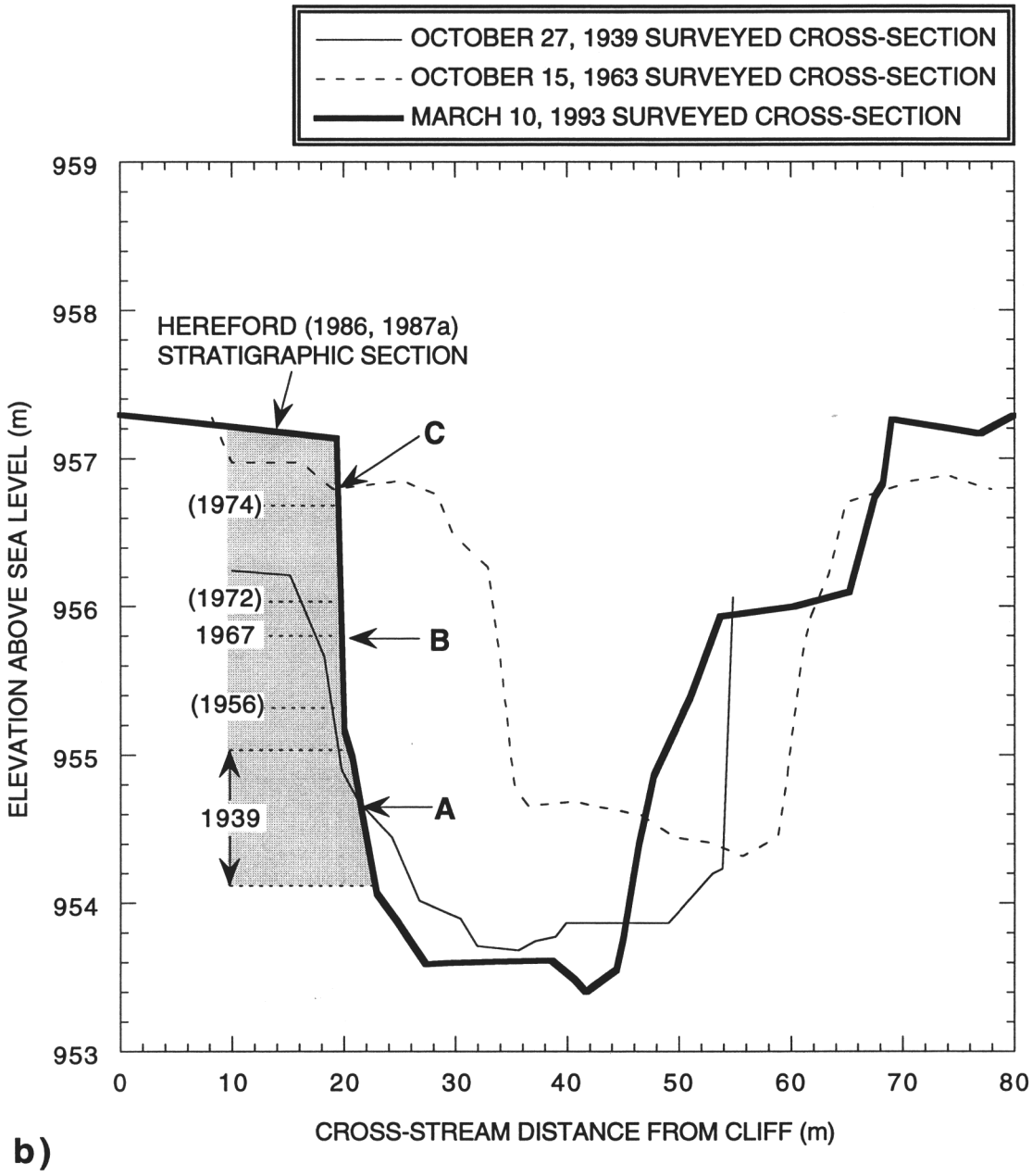

Figure 2.40 (continued): **(b)** Position of the stratigraphic section of Hereford (1986, 1987a) in relation to cross-sections surveyed in 1939, 1963, and 1993. Shaded region denotes the location of Hereford's stratigraphic section; dates in parentheses are the interpolated or extrapolated ages of Hereford (1986, 1987a). The letter **A** indicates the position of stratigraphic horizon **A** from Figure 2.40a, i.e., Hereford's 1939 surface based on photographic evidence; the letter **B** indicates the position of stratigraphic horizon **B** from Figure 2.40a, i.e., Hereford's 1967 floodplain surface based on tamarisk tree-rings; the letter **C** indicates the position of stratigraphic horizon **C** from Figure 2.40a, i.e., the actual surveyed 1963 floodplain surface.

October 15, 1963; thus, his interpolated ages 1956, 1972, and 1974 for key floodplain deposits that he correlates with similar flood deposits throughout the Paria River drainage basin are incorrect. The disagreement between the surveyed and stratigraphically determined positions of the channel and floodplain surfaces in Figure 2.40b clearly shows the lack of precision inherent in stratigraphic analyses; thus, stratigraphic analyses are of limited use in determining the amount of floodplain deposition over time in the Paria River basin.

2.5b-5: Has sediment been stored in the Lees Ferry reach since 1939?

The final question that needs to be addressed with regard to channel geometry is the question of sediment storage. That is, given the extensive lateral and vertical changes in the position of the channel and the local cross-section geometric changes that have been documented in the preceding sections of this chapter, has there been net storage of sediment in the Paria River since 1939 as suggested by Hereford (1986, 1987a, 1987b) and W. Graf (1987)? The answer provided to this question by analysis of surveyed cross-sections, spanning the time period from 1925-1929 to 1993, is that though sediment may have been stored in the Lees Ferry reach since 1939, the amount of post-1925 sediment storage is not significantly different than zero sediment storage.

Figure 2.41 shows the change in cross-section area of sediment stored in the channel bed, floodplains, and terraces in the Lees Ferry reach as a function of streamwise distance from the gage. This graph was constructed by determining change in cross-section sediment area in the cross-sections in Figure 2.27 (Plate 1) over five different time periods. As mentioned, these changes do not reflect mere channel narrowing or widening, but accompany major lateral and vertical changes in the position of the channel as well as major changes in the channel longitudinal slope.

Because no single survey prior to the 1993 survey covered a significant length of the channel, cross-sections surveyed over several years in different parts of the channel were first grouped and then compared to cross-sections surveyed in 1993. For example, for the time period from 1925-1929 to 1993, cross-sections that were surveyed from 1925 to 1929 were grouped and then compared to cross-sections surveyed in 1993, thus assuming that no significant change in sediment storage occurred between 1925 and 1929. Although this assumption may be false in certain cases (for example, in the reach below the gage, the cross-section surveyed on 8-29-25 was about twice as narrow as a cross-section surveyed near the same location on 10-2-27), this method of grouping data is still the best approach given the limited amount of data.

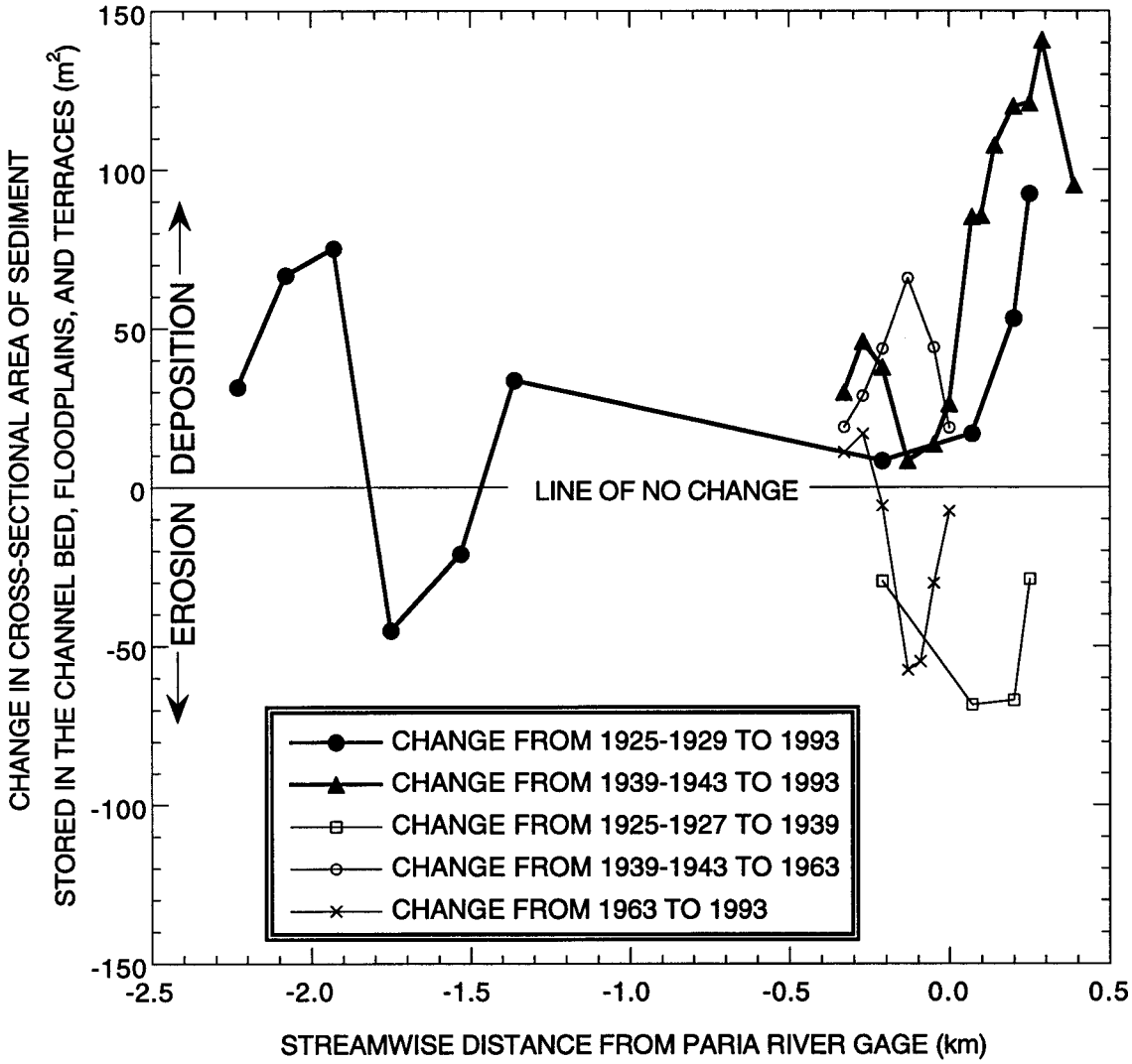

Figure 2.41: Change in the cross-section area of sediment stored in the Paria River system over 5 different time periods as a function of the streamwise distance from the post-1925 gage.

As shown in Figure 2.41, the absolute amount of change in sediment storage over time increases toward the Colorado River. In fact, the largest changes in sediment storage have occurred in the reach that was seasonally backwatered by the Colorado River prior to the construction of Glen Canyon Dam. In the reach within 1.8 km of the historic high-water confluence with the Colorado River that includes the gage, between 1925-1927 and 1939-1943, the measured mean±1σ change in cross-section area of sediment was -48.4±22.1 m^3 per cross-section; between 1939-1943 and 1963, the measured mean±1σ change in cross-section area of sediment was +36.6±18.2 m^3 per cross-section; and between 1963 and 1993, the measured mean±1σ change in cross-section area of sediment was -18.3±30.0 m^3 per cross-section. For the entire 2.6-km-long reach , the measured mean±1σ change in cross-section area of sediment between 1925-1929 and 1993 was +31.1±43.1 m^3 per cross-section; and, for the reach least directly influenced by the Colorado River, that is, the reach greater than 1 km above the gage, the measured mean±1σ change in cross-section area of sediment was +23.4±47.7 m^3 per cross-section. Though more cross-sections in Figure 2.41 have experienced net deposition than net erosion over the entire period of record, given the small number of surveyed cross-sections and the large standard deviations (i.e., the standard deviations are larger than the mean values), no significant difference exists between the calculated mean values and zero net sediment storage per cross-section for the period from 1925-1929 to 1993.

2.5b-6: Bed sediment

If the sediment transport of an alluvial river is not in spatial equilibrium over time (i.e., the sediment import into a reach does not equal the sediment export from the reach over time), both the channel geometry and the bed grain-size distribution of a reach will evolve in response to the change in the upstream sediment supply. Thus, to complete the investigation of potential temporal change in the Lees Ferry reach of the Paria River, the last item to be compared between past and present are the size-distributions of the sand, silt, and clay that compose the bed, the bar tops, and the banks (Figure 2.42). Between June 26, 1958 and May 27, 1971, the USGS collected 18 samples of the coarse material that typically covers the floor of the thalweg (defined as Type 1 sediment in Section 2.5a-1) and three samples of the fine material that typically covers the bar tops and banks (defined as Type 2 sediment in Section 2.5a-1). Comparisons of the mean and standard deviation of the amount in each size class at 1-ϕ intervals for the two types of bed sediment collected by the USGS from 1958 to 1971 with the samples collected in 1993 as part of this study are shown in Figure 2.42. These comparisons indicate that both the mean of the amount of

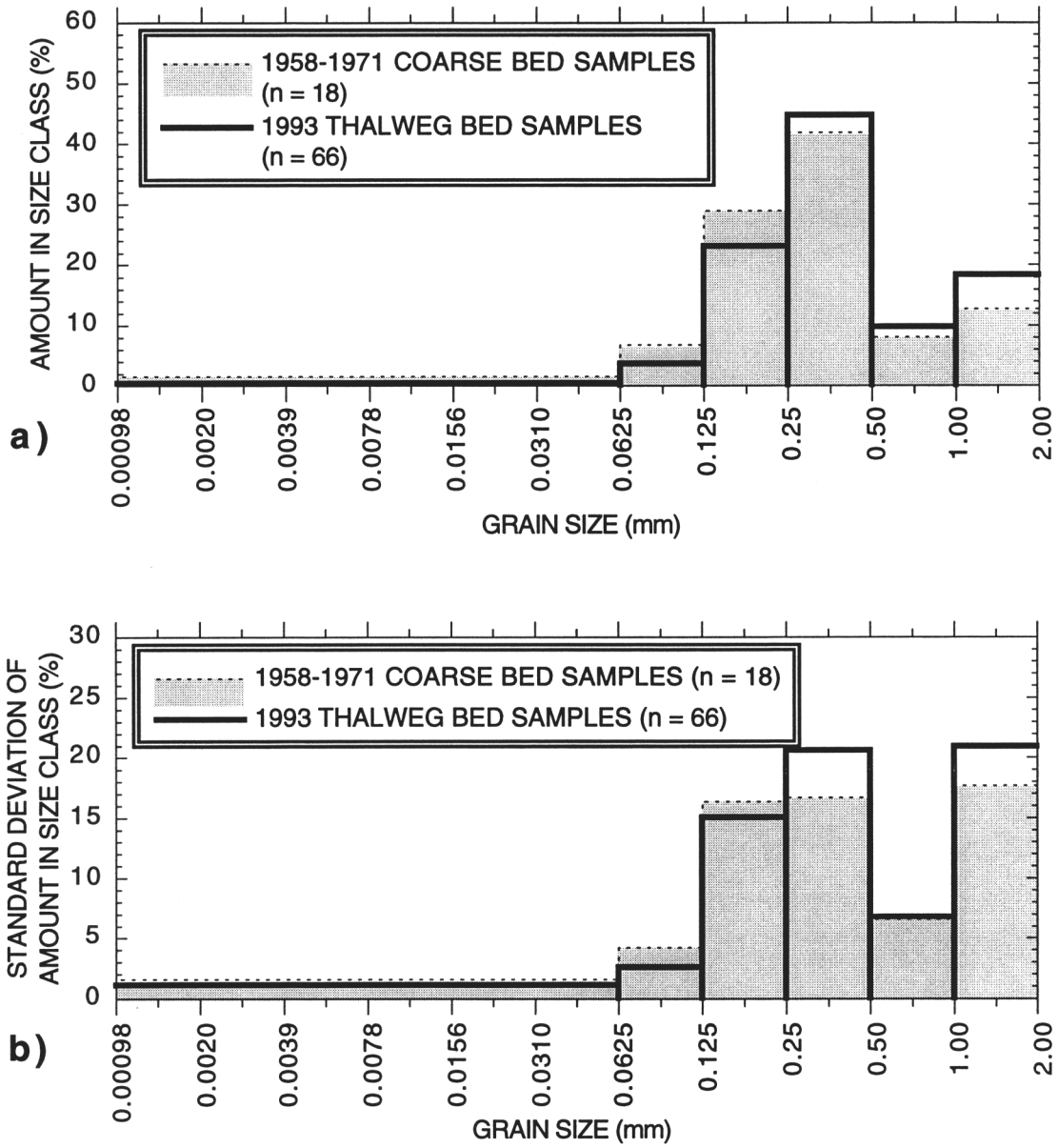

Figure 2.42: **(a)** The mean of the amount in each size class for the 1993 bed samples and the 1958-1971 USGS bed samples of coarse (Type 1) sediment. **(b)** The standard deviation among samples of the amount in each size class for the 1993 bed samples and the 1958-1971 USGS bed samples of coarse (Type 1) sediment.

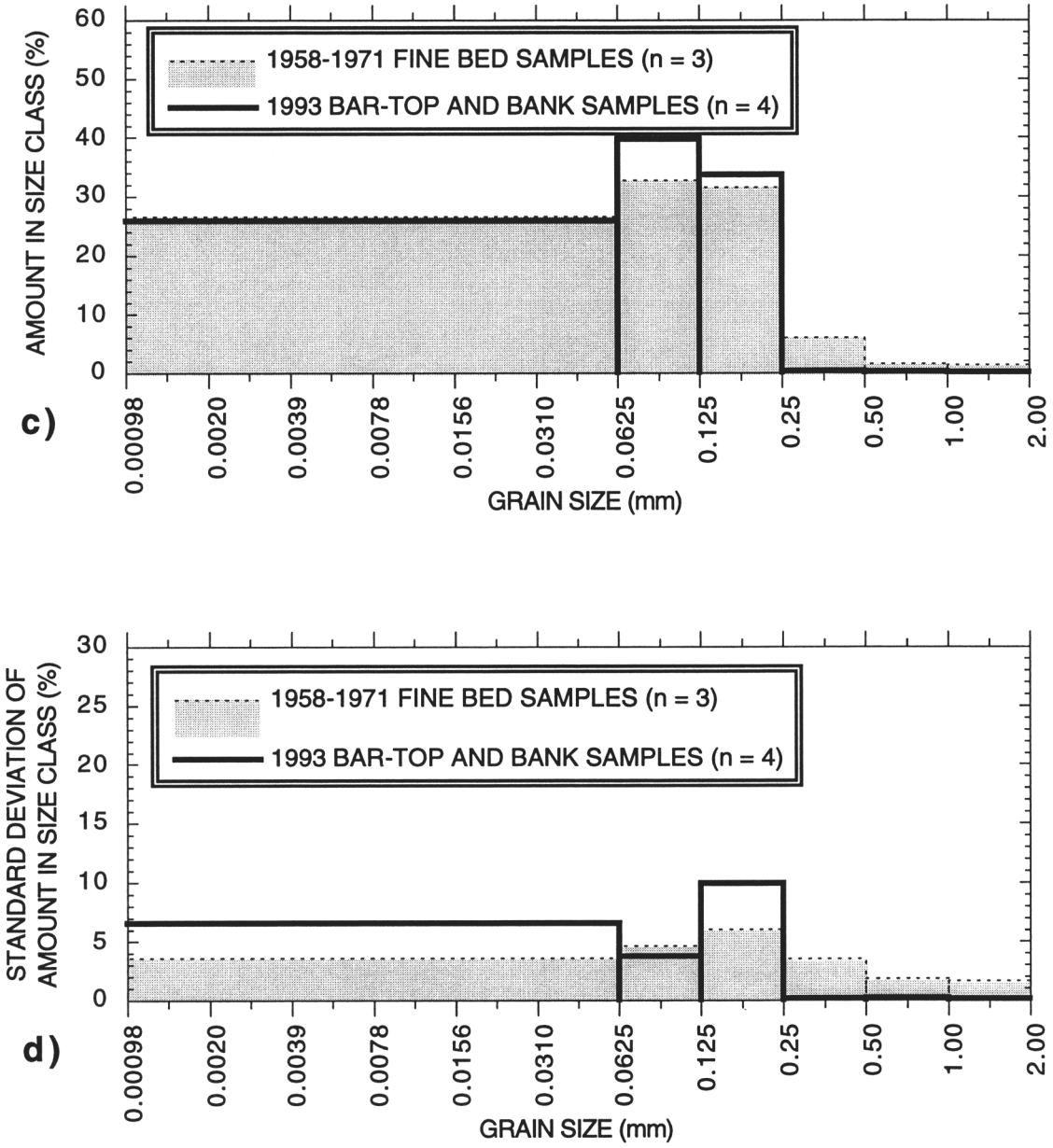

Figure 2.42 (continued): **(c)** The mean of the amount in each size class for the 1993 bed samples and the 1958-1971 USGS bed samples of fine (Type 2) sediment. **(d)** The standard deviation among samples of the amount in each size class for the 1993 bed samples and the 1958-1971 USGS bed samples of fine (Type 2) sediment.

each size class present in the bed and the standard deviation (among samples) of the amount of each size class present in the bed have been stable in the Lees Ferry reach of the Paria River over the last 40 years, and, therefore, can be reasonably extrapolated to be constant through time. Thus, when combined with the observed stability in the reach-averaged cross-section channel geometry for reaches of similar longitudinal slope, the stability of both the mean grain-size distribution and the spatial sorting of grain-size distributions in the reach (indicated by the similarity of the standard deviations among samples in the reach) provides further evidence of long-term stability of flow and sediment transport in the Paria River system.

2.5c: The Paria River below Cannonville, UT from 1951 to 1994

The 1994 field program

The goal of the 1994 field program at the study area below Cannonville, UT (see Figure 2.1) was a topographic and sedimentologic characterization of a portion of the modern upper Paria River system. During June 13-16, 1994, the longitudinal slope of the thalweg over 5.8 km of the channel in the vicinity of the USGS gaging station was surveyed with a Nikon automatic level. The upper end of this surveyed reach is 3.8 km above the USGS near Cannonville, UT gaging station and extends downstream to a position 2.0 km below the gage (Figure 2.43); the entire survey was tied in to the datum of the near Cannonville, UT gage. In addition to surveying the longitudinal profile of the thalweg, ten cross-sections were surveyed across the valley (*C-1* through *C-10* in Figures 2.1 and 2.43); these cross-sections were located at representative reaches that capture average channel and floodplain properties.

At each of the ten cross-sections, pebble counts were conducted using the method of Wolman (1954); these pebble counts were then composited into a single count to characterize the mean gravel grain-size distribution on the channel bed for the entire study area. The mean gravel grain-size distribution in the Cannonville study area has a D_{50} and D_{84} equal to 4 and 8 cm, respectively, and is nearly identical to the gravel grain-size distribution of Reach 3 in the Lees Ferry, AZ study area (these grain size distributions are compared in Figure 2.58 in Section 2.6c below). Furthermore, the mean 1994 gravel grain-size distribution in the Cannonville study area is equivalent to the gravel grain-size distribution measured by the USGS at the near Cannonville, UT gage on 7-14-58 (see Section 2.6c below). In addition to conducting pebble counts at each cross-section, the thickness of the sand, silt, and clay layer overlying the gravel was also measured, with the mean thickness of this layer being equal to about 2-4 cm in the Cannonville study area.

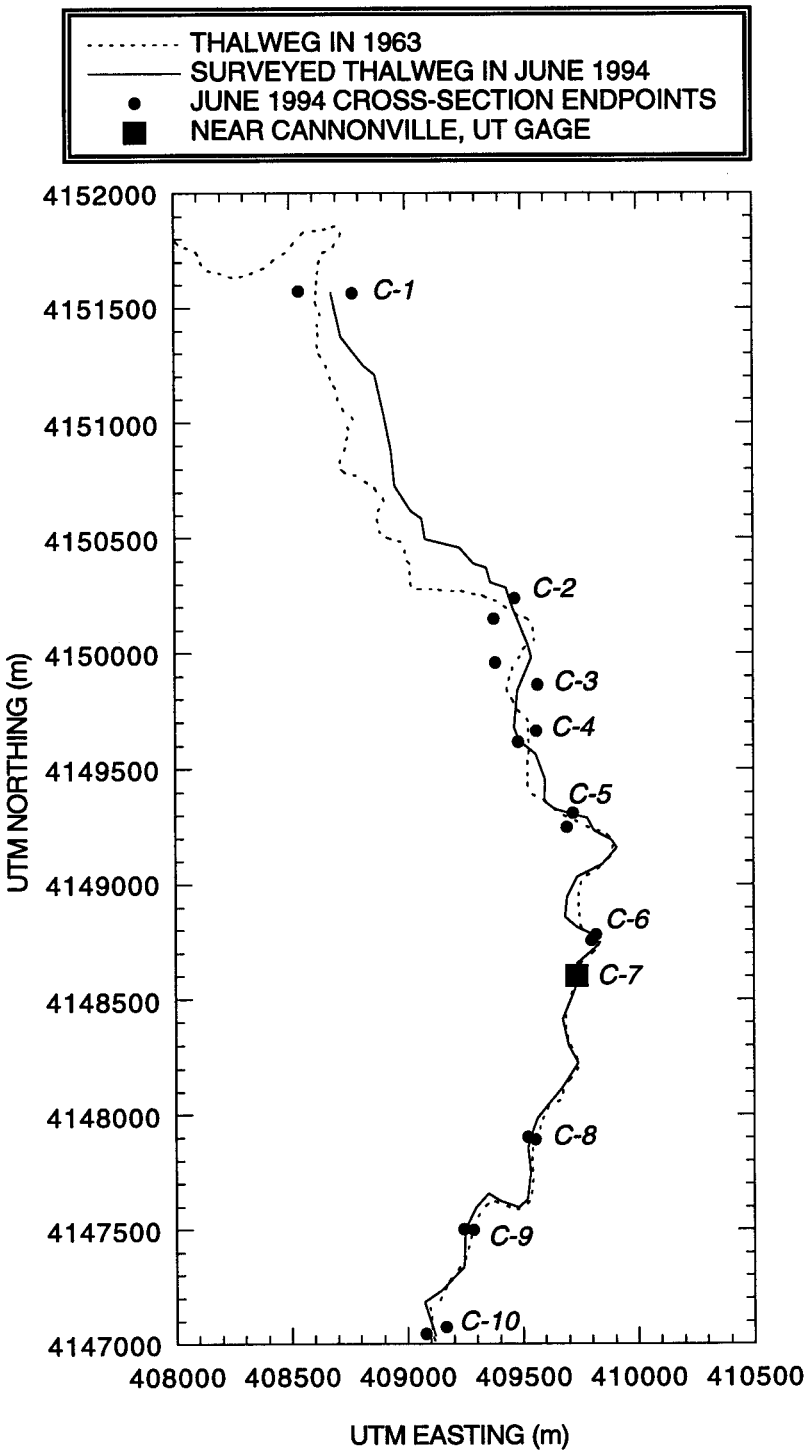

Figure 2.43: Map of the Cannonville study area showing the locations of the thalweg in 1993 and 1963, the locations of the endpoints of the 10 cross-sections surveyed in 1994, and the location of the near Cannonville, UT gage. The 1963 position of the thalweg was determined from USGS 7.5-minute topographic quadrangles.

Detailed description of the Cannonville study area in 1994

The Cannonville study area consists of 2.1 km of a channel in equilibrium with an active floodplain above 3.7 km of a deeply incised channel without floodplains and bordered by terraces. In the upper part of the study area, near cross-section *C-1*, the river has a longitudinal slope of 0.0086 and is approximately 70 m wide and 1 m deep at bankfull stage. It has a well-defined primary thalweg, a poorly defined secondary thalweg, and a mid-channel bar; the floodplain is approximately 100 m wide and terraces rise about 1 m above the floodplain. Between cross-sections *C-1* and *C-2*, the river becomes braided with numerous mid-channel bars and lightly vegetated islands; the full width of the channel including islands is over 250 m, however, the active width at bankfull stage is closer to 100 m (Figure 2.44a). The river collapses again into a single channel at cross-section *C-2*; and, from *C-2* to *C-3*, the bankfull width expands from 66 to 100 m while the maximum bankfull depth remains at about 1 m. Cross-section *C-3* is fairly representative of the shape of the upper equilibrium portion of the Cannonville study area and is shown in Figures 2.44b and 2.44c. Bankfull dimensions of cross-sections *C-1* through *C-3* are given in Table 2.7 in Section 2.6c below.

Halfway between cross-sections *C-3* and *C-4*, the river narrows and becomes incised in the terraces with no true floodplains existing adjacent to the channel (Figure 2.44d). This incision begins, unlike the head of the incised lowermost reach at Lees Ferry, AZ, with no break in longitudinal slope along the thalweg. At cross-section *C-5*, an abandoned meander is located on the terrace bordering the left margin of the active channel. The floor of this abandoned channel is 2 m above the floor of the active channel and 1 m below the top of the terrace; the abandoned channel has a longitudinal slope of 0.0079 (i.e., 89% of the slope of the active channel in the equilibrium reach upstream) and a cross-section geometry very similar to that found in cross-sections *C-1* through *C-3*. Given that this abandoned channel had a cross-section geometry and longitudinal slope roughly equal to the cross-section geometry and longitudinal slope of the modern equilibrium channel, and that this abandoned channel was the active channel sometime prior to the installation of the gage in 1951, this abandoned channel provides evidence that, as in the case of the Lees Ferry, AZ reach, the hydraulic geometry of the river in the Cannonville study area has been stable since at least the late 1940's.

Between cross-section *C-4* and the cross-section at the gage, *C-7*, the river continues to narrow and the longitudinal slope abruptly decreases from 0.0085 to 0.0069 (Figure 2.45a). From just above the gage to a point 600 m downstream, the river flows through a bedrock-walled channel that varies from 15 to 30 m in width (Figure 2.46). The

a)

Figure 2.44: **(a)** June 13, 1994 oblique cross-stream view from the left bank of the braided portion of the Paria River above cross-section *C-2*. Numerous islands are present in the left and center portions of the field of view; right bank of the river is in excess of 200 m from the camera. Two people, two backpacks, and a surveying transit in the left side of field of view for scale; photograph by D.J. Topping.

b)

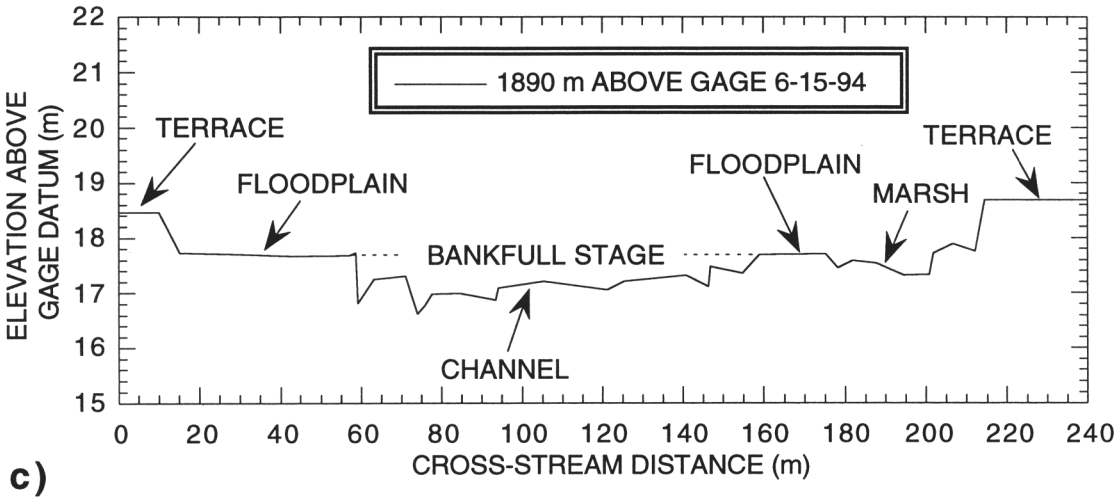

c)

Figure 2.44 (continued): **(b)** Downstream view of the Paria River from just above cross-section *C-3*; person holding stadia rod in background for scale. Photograph taken by D.J. Topping on June 13, 1994. **(c)** Cross-section *C-3* (surveyed on June 15, 1994) showing the bankfull stage and the location of the channel, floodplain, marsh, and terrace environments that typify the equilibrium channel portion of the Paria River in the Cannonville study area.

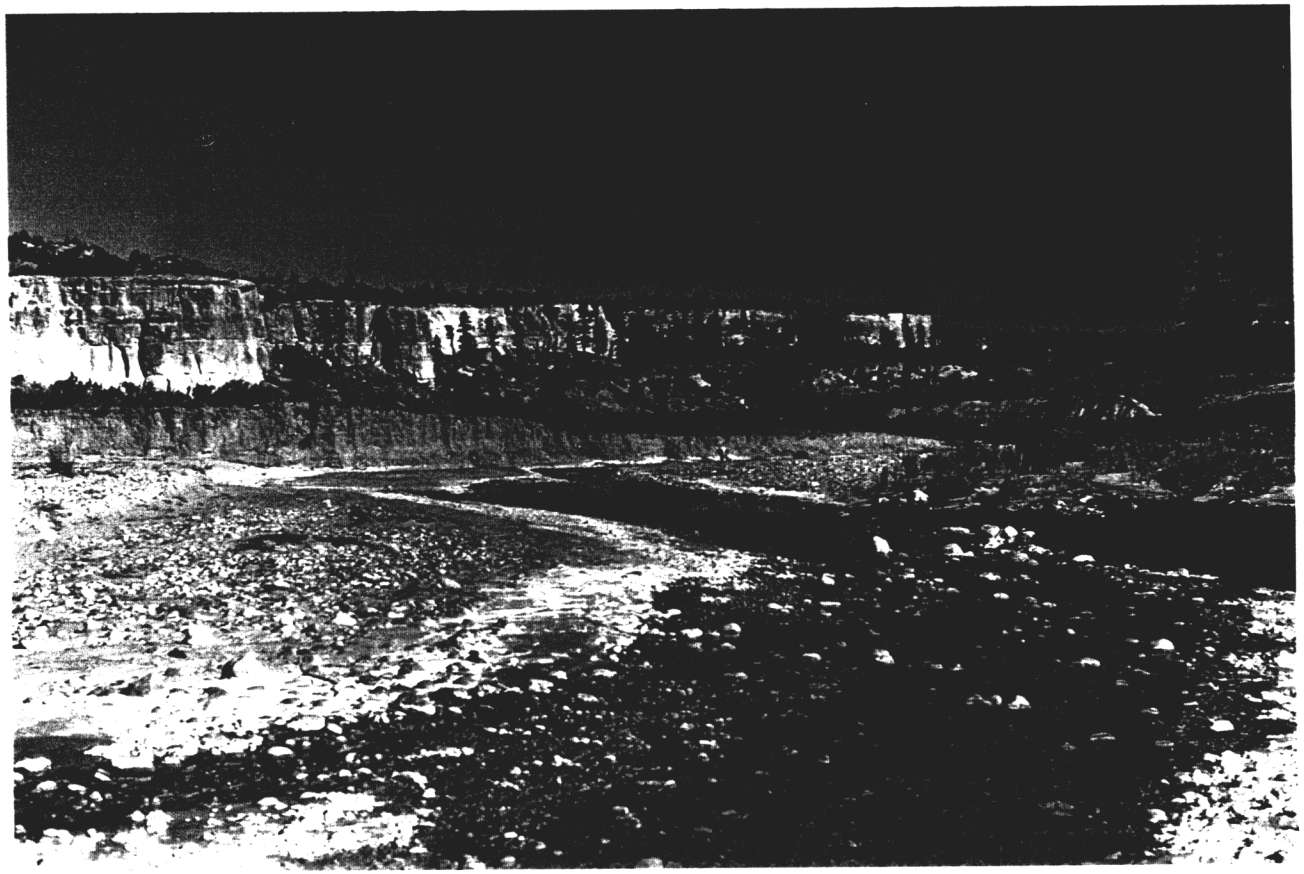

d)

Figure 2.44 (continued): (d) Downstream view of the upper portion of the incised reach of the Paria River below cross-section *C-4*; person and backpack in channel for scale. Photograph taken by D.J. Topping on June 13, 1994.

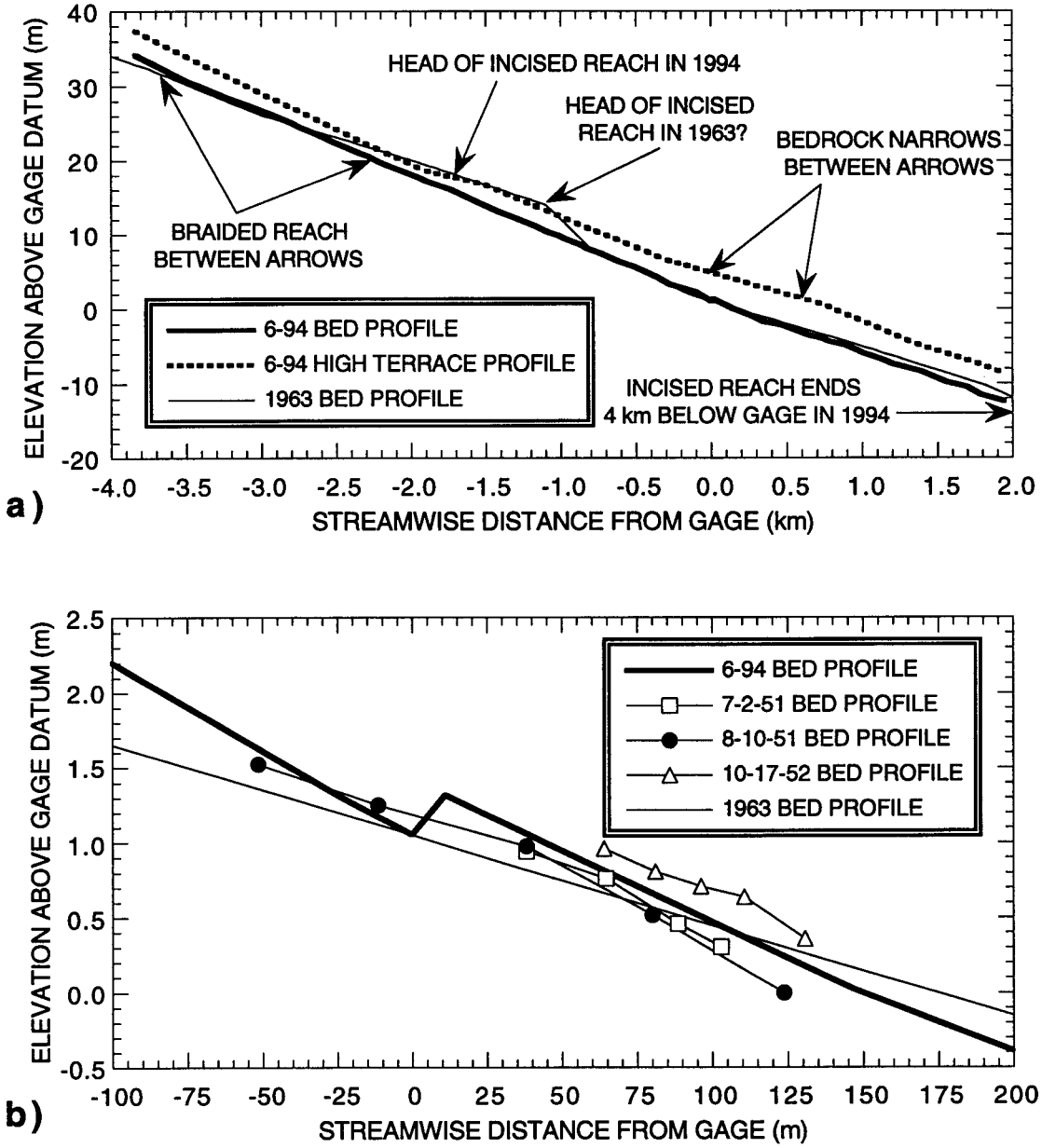

Figure 2.45: **(a)** Surveyed longitudinal profiles of the bed of the primary thalweg the high terrace in June 1994 in the Cannonville study area; also shown is the 1963 longitudinal bed profile determined from the USGS 7.5' topographic quadrangles. **(b)** Expanded view of the surveyed longitudinal profiles of the bed near the gage on July 2, 1951, August 10, 1951, October 17, 1952, and June 14, 1994; also shown is the 1963 longitudinal bed profile determined from the USGS 7.5' topographic quadrangles. The 7-2-51, 8-10-51, and 10-17-52 bed profiles are from USGS slope-area surveys.

a)

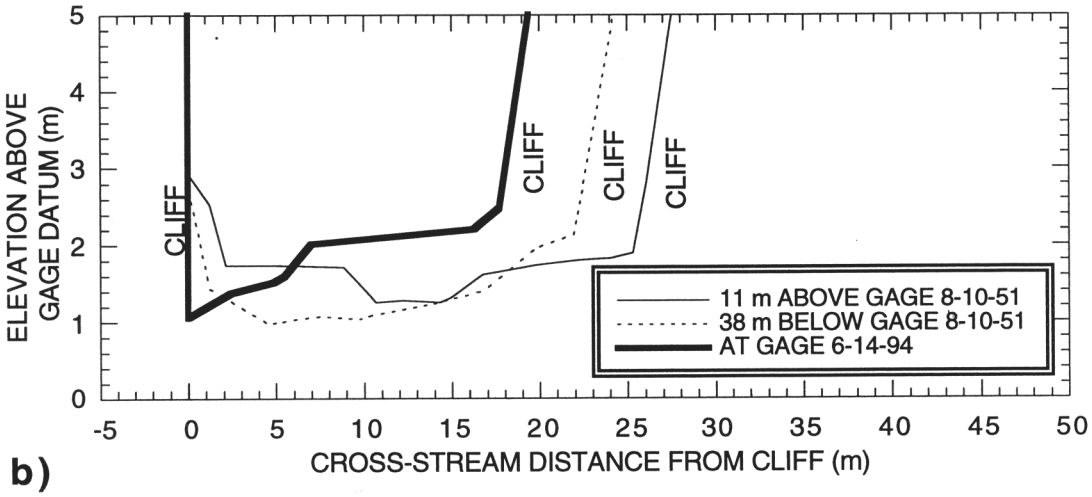

b)

Figure 2.46: **(a)** Downstream view of the largely bedrock-walled gage reach of the Paria River; person holding stadia rod for scale. Stilling well and shed of gage is visible on the left side of the channel behind the person with the stadia rod. Photograph taken by D.J. Topping on June 14, 1994. **(b)** Comparison of cross-section *C-7* (surveyed at the gage on June 14, 1994) with cross-sections surveyed 11 m above and 38 m below the gage on August 10, 1951 illustrating the stability of the minimum bed elevation at the gage.

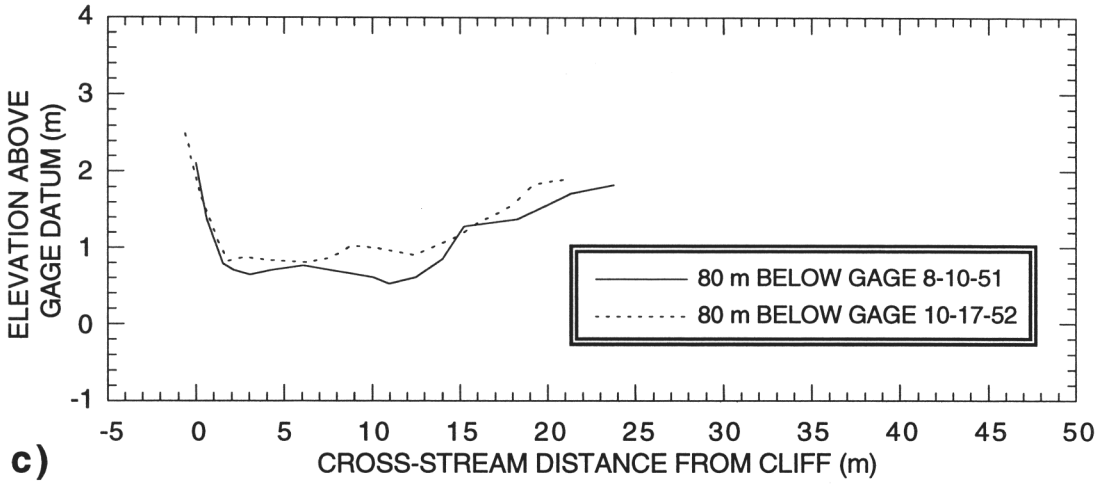

c)

d)

Figure 2.46 (continued): **(c)** Comparison of cross-sections surveyed 80 m below the gage on August 10, 1951 and October 17, 1952 illustrating that the annual variability in minimum bed elevation in the gage reach exceeds the long-term variability in minimum bed elevation at the gage from 1951 through 1994. **(d)** Downstream view of the bedrock-walled reach below the gage; person in distance for scale. Photograph taken by D.J. Topping on June 14, 1994.

floor of the channel remains a mixed gravel and sand bed, with no exposed bedrock. As illustrated in Figures 2.45b, 2.46b, and 2.46c, the minimum bed elevation near the gage has been essentially stable and has varied by no more than 30 cm since 1951. This small magnitude of bed elevation variation over 40 years is, in fact, equal to the magnitude of annual fluctuations in the elevation of the bed as shown by resurveys of the same cross-section 80 m below the gage on 8-10-51 and 8-17-52 (Figure 2.46c).

From a point 600 m below the gage through cross-section *C-10*, the river remains deeply incised in the terraces (Figures 2.47a and 2.47b), but widens slowly so that the channel is about 30 m wide at cross-section *C-10*. The incised reach abruptly ends 2 km below the downstream end of the 1994 survey at rockfall deposits located below the confluence with Rock Springs Creek. At this location, the terraces terminate on the upstream margins of rockfall deposits (Figures 2.47c and 2.47d); this relationship is most clearly preserved on the western margin of the canyon where the terrace onlaps the upstream margin of a rockfall deposit (Figure 2.47c). This geometry suggests that the incision of the 5 km-long reach extending from above the gage to the vicinity of the prominent rockfall debris below Rock Springs Creek was caused by the breach of an old rockfall/landslide dam that had temporarily elevated the upstream base level of the Paria River, causing deposition of the sediment comprising the modern terraces. For at least several kilometers below the rockfall deposits (Figure 2.48), the river consists of an equilibrium channel with active, wide floodplains and no terraces. In this portion of the river, mature stands of cottonwood, juniper, and Ponderosa pine are located both on the floodplains and very near the elevation of the floodplain surfaces (Figures 2.48c and 2.48d); thus, no indication of channel incision occurring over the last century exists below the rockfall debris below the confluence with Rock Springs Creek.

Constraints on the rate of headcut retreat and the possible age of the incised reach

Incision in the lower part of the Cannonville study area probably began around 1800 A.D. The stability of the bed at the gage places a significant constraint on the rate of headcut retreat at the upper end of the incised reach and allows the approximate age of incision to be estimated. Since the elevation of the bed at the gage has not changed since 1951, the head of the incised reach must have already retreated past the gage site by 1951. Therefore, if the position of the headcut 1000 m above the gage in the 1963 longitudinal profile in Figure 2.45a is correct, the head of the incised reach retreated 700 m from 1963 to its 1994 position above cross-section *C-4* at a rate of 23 m/yr; and, if the headcut were approximately 50 m above the gage in 1951 (i.e., the minimum distance required by the

a)

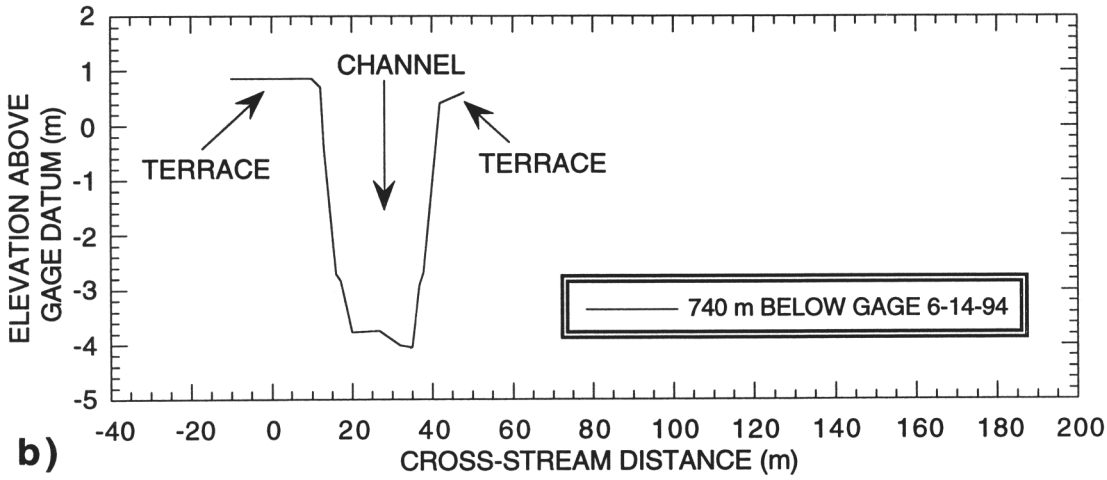

b)

Figure 2.47: **(a)** Downstream view of the Paria River from just above cross-section *C-8*; person standing at the location of cross-section *C-8* for scale. Photograph taken by D.J. Topping on June 14, 1994. **(b)** Cross-section *C-8* (surveyed on June 14, 1994) illustrating the typical features of the incised channel below the bedrock narrows; both terraces are composed of fluvial sediment.

c)

Figure 2.47 (continued): **(c)** Upstream view of the downstream end of the incised reach below the confluence with Rock Springs Creek. Portions of the rockfall debris interpreted to have temporarily elevated the base level of this portion of the Paria River can be seen on both sides of the river (upper-left and lower-right portions of the field of view). Terrace on the far side of the river rises 4-5 m above the present floor of the channel and onlaps the upstream margin of the rockfall deposit on the left side of the photograph. Photograph taken by D.J. Topping on April 11, 1997.

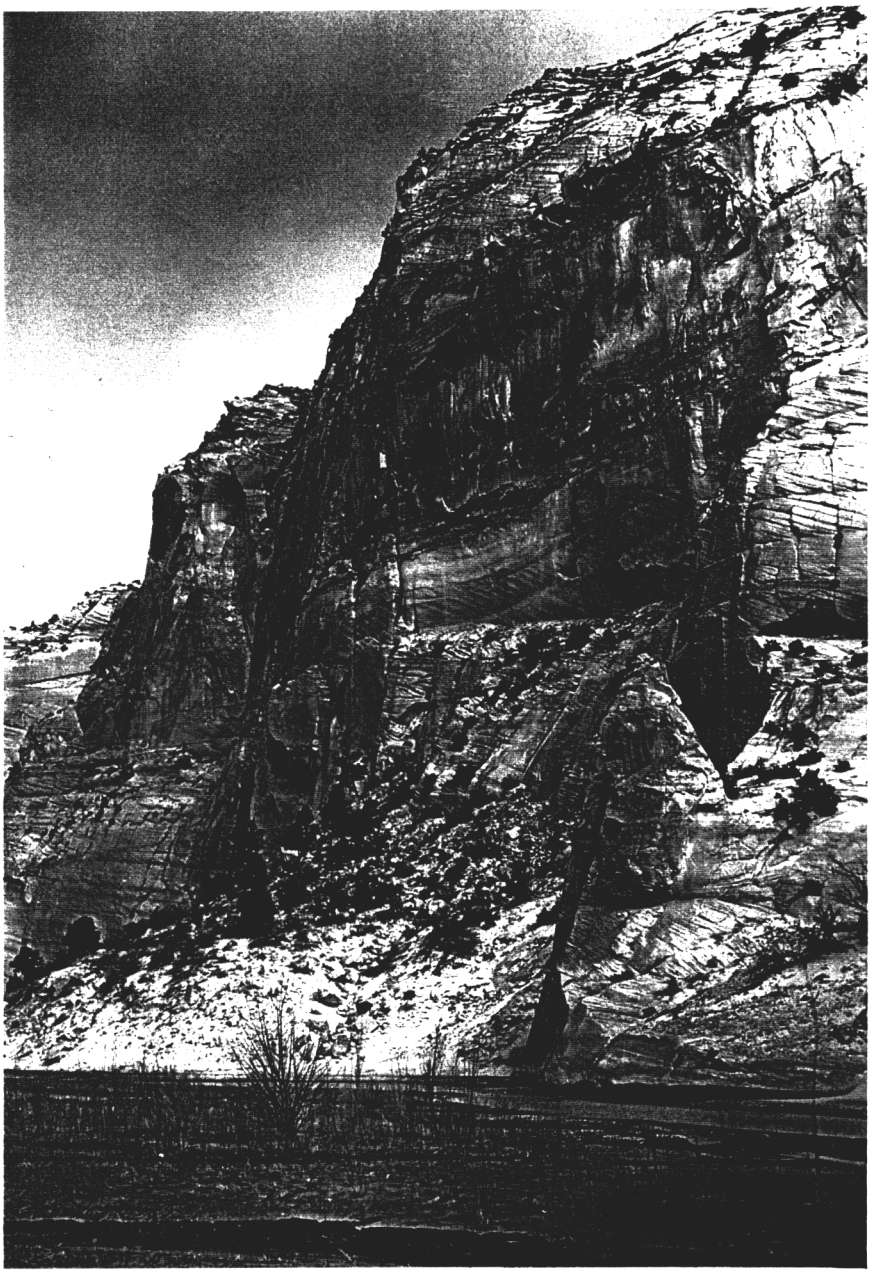

d)

Figure 2.47 (continued): (d) View of the rockfall scar and deposit on the left side of the Paria River below the confluence with Rock Springs Creek. The toe of this deposit appears in the lower-right portion of the field of view in Figure 2.47c; photograph in Figure 2.47c was taken from the "bedrock saddle" behind the prominent Navajo Sandstone pinnacle to the right of the rockfall deposit. Photograph taken by D.J. Topping on April 11, 1997.

Figure 2.48: **(a)** Downstream view of the equilibrium reach immediately downstream from the rockfall debris in Figures 2.47c and 2.47d; in this reach, no terraces are present, and floodplains extend from the channel to each canyon wall. Photograph taken by D.J. Topping on April 11, 1997. **(b)** Downstream view of the equilibrium reach 1 km below the camera position in Figure 2.48a. Photograph taken by D.J. Topping on June 14, 1994.

a)

b)

c)

Figure 2.48 (continued): **(c)** Mature junipers and cottonwoods growing on the floodplain of the Paria River immediately to the left of the view in Figure 2.48b; photograph taken by D.J. Topping on April 11, 1997.

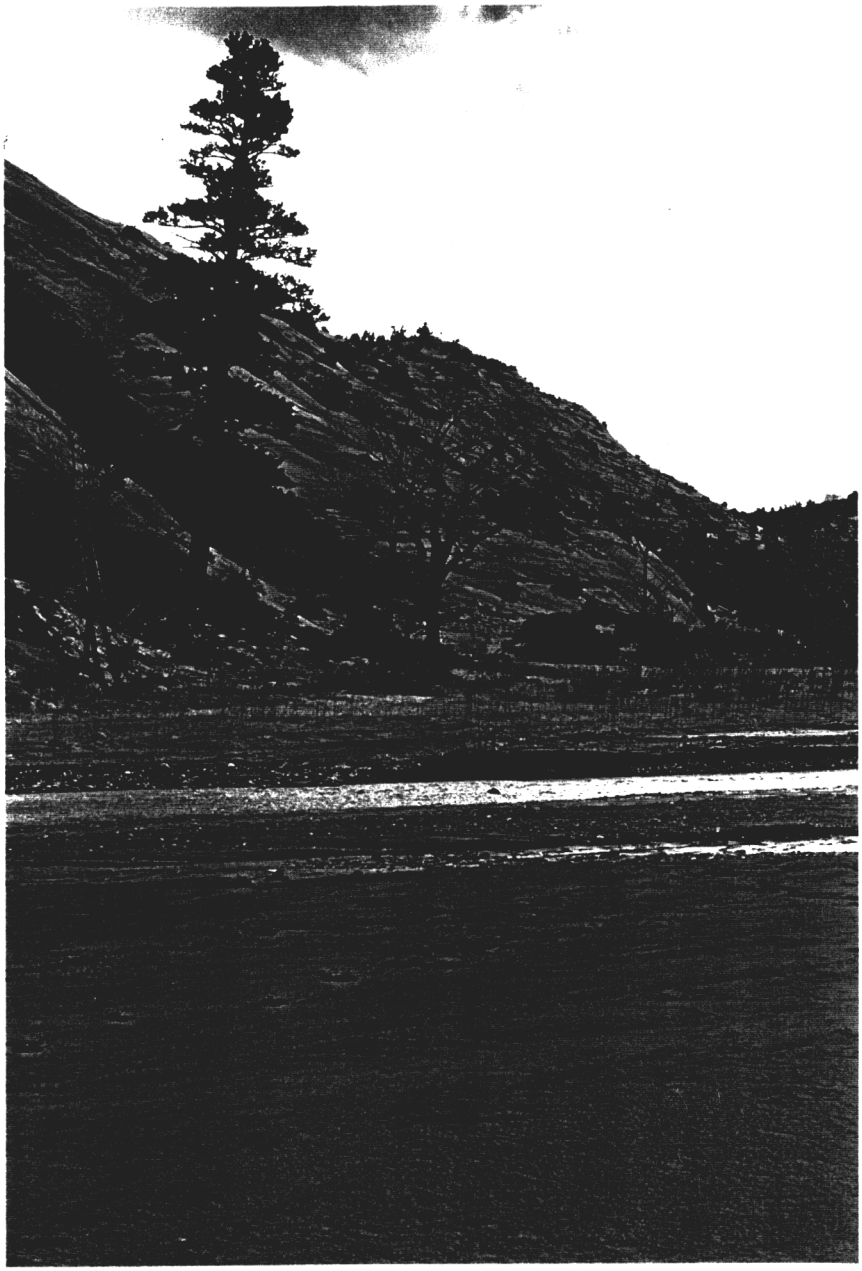

d)

Figure 2.48 (continued): (d) Cottonwoods growing on the floodplain and mature Ponderosa pine growing just above floodplain elevation 500 m downstream of the views in Figures 2.48b and 2.48c; photograph taken by D.J. Topping on April 11, 1997.

longitudinal bed profile from the 8-10-51 slope-area survey), the calculated retreat rate for the period from 1951 to 1994 would be 38 m/yr. Given a constant headcut migration rate of 30 m/yr, as justified by the conclusion that the hydrology of the Paria River has been effectively stationary over the last 1700 years (see Section 2.4), channel incision would have originated at the position of the rockfall debris, 4 km below the gage, sometime around 1800 A.D.

Summary of the Cannonville study area

In summary, the Cannonville study area of the Paria River consists of 2.1 km of channel in equilibrium with active floodplains followed by 3.7 km of channel without floodplains that has incised into terraces by as much as 3 m. Elevation of the bed at the gage has been stable since at least 1951, with incision originating 2 km below the end of the study area sometime around 1800 A.D. The equilibrium channel above the incised reach is, at the bankfull stage, about 1 m deep and ranges in active width from as little as 66 m to slightly more than 100 m; in braided portions of the channel, the full bankfull width may be in excess of 250 m. The channel is floored by gravel with a grain-size distribution that has been constant since at least 1958 and is equivalent to the 1993 grain-size distribution of gravel in equilibrium reaches in the Lees Ferry, AZ study area. Throughout the reach, the gravel is overlain on average by a mixture of sand, silt, and clay; in a cross-sectionally averaged sense, this layer ranges from 2-4 cm in thickness. In the upper part of the study area, from 1963 to 1994, the channel has laterally migrated several hundred meters across the valley and reworked significant quantities of floodplain sediment over the last 30 years (Figure 2.43). However, though the river has migrated extensively across the valley, evidence provided by the cross-section geometry and longitudinal slope of an abandoned channel adjacent to the upper portion of the incised reach suggests that the hydraulic geometry of the Cannonville reach has not changed since at least the late 1940's.

2.5d: The Paria River in the vicinity of Paria, Rock House, and Adairville, UT from 1877 to 1996

To characterize that portion of the Paria River that is transitional between the equilibrium channel types found below Cannonville, UT (i.e., broad and shallow at the bankfull stage with a steep longitudinal slope) and above Lees Ferry, AZ (i.e., relatively narrow and deep at the bankfull stage with a gentle longitudinal slope), field work was conducted on the Paria River in the vicinity of the townsites of Paria, Rock House, and Adairville, UT during June 1994 and April 1996. This portion of the river was the most

extensively developed reach in the late 1800's (note the grist and sorghum mills in Figure 2.49); moreover, it was also the reach with the most extensive channel changes occurring between 1884 and 1918 as documented by Gregory and Moore (1931) and Bailey (1935). It was chosen as a study area because the valley from above Paria to below Adairville was surveyed by the General Land Office in 1877 (Bailey and Burrill, 1877), with the portion below Paria being resurveyed in 1917 (Thoma and Rathbone, 1917); hence, maps of 34 and 8 km portions of the river are available from 1877 and 1917, respectively. Importantly, these maps were completed before and after the episodes of channel widening later documented by Gregory and Moore (1931) in this reach, making it possible to relate changes in channel width to changes in channel longitudinal slope. Also, this portion of the valley was desirable as a study area because it had been studied extensively by Gregory and Moore (1931), Bailey (1935), Hereford (1986, 1987a, 1987b), and W. Graf (1987).

Two portions of the cadastral survey of Bailey and Burrill (1877) are shown in Figure 2.49. As already noted (see Section 2.5b-1), channel widths from cadastral surveys cannot be used to reconstruct the cross-section morphology of the river channel [as done by Webb (1985) and Webb and others (1991)] because the widths reported by the surveyors refer to width of the low-flow water surface only, which for the Paria River is a fraction of the bankfull channel width. However, since the location of the river channel in the cadastral surveys is reasonably accurate, especially where the channel crosses section lines, cadastral surveys can be used to reconstruct changes in sinuosity over time and, therefore, changes in longitudinal channel slope over time. Positions of the Paria River channel in 1877, 1917, and 1976, and positions of the three major townsites in 1877, i.e. Paria, Rock House, and Adairville, with locations of their respective irrigation diversion dams, are shown in Figure 2.50.

<u>The 1994 and 1996 field programs and description of the river in 1994-1996</u>

To determine both the present cross-section channel geometry and the magnitude of the incision of the modern channel and floodplains into the 1877 floodplain surface, five cross-sections, *P-1* and *RH-1* through *RH-4*, were surveyed in the Paria-Adairville reach of the Paria River in June 1994 and April 1996 (Figure 2.50). In 1994-1996 and for the same hydrologic conditions, as the reach-average longitudinal channel slope decreased from 0.0084 to 0.004 through these five cross-sections, the equilibrium bankfull width decreased from 75 to 26 m and the equilibrium bankfull depth increased from 1 to 1.3 m. This observed relationship between the longitudinal slope and the cross-section geometry of the modern Paria River has major implications with regard to the interpretation of the hydrology of the system in the late 1800's. As will be shown in Section 2.6, the changes

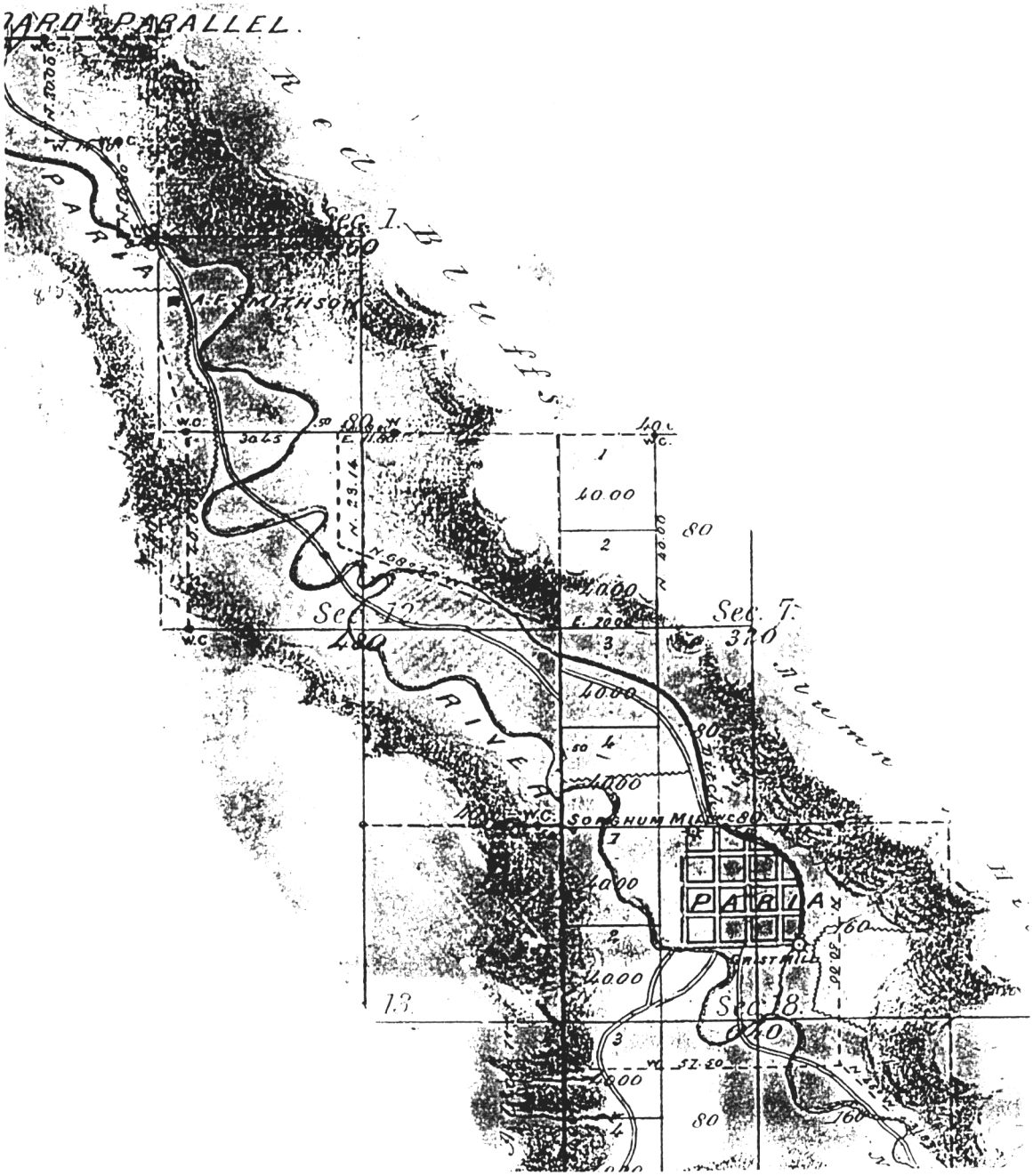

a)

Figure 2.49: **(a)** Portion of the map from the 1877 cadastral survey of Bailey and Burrill (1877) in the vicinity of Paria, UT. The 1877 location of the main Paria diversion dam is in the center of Section 12.

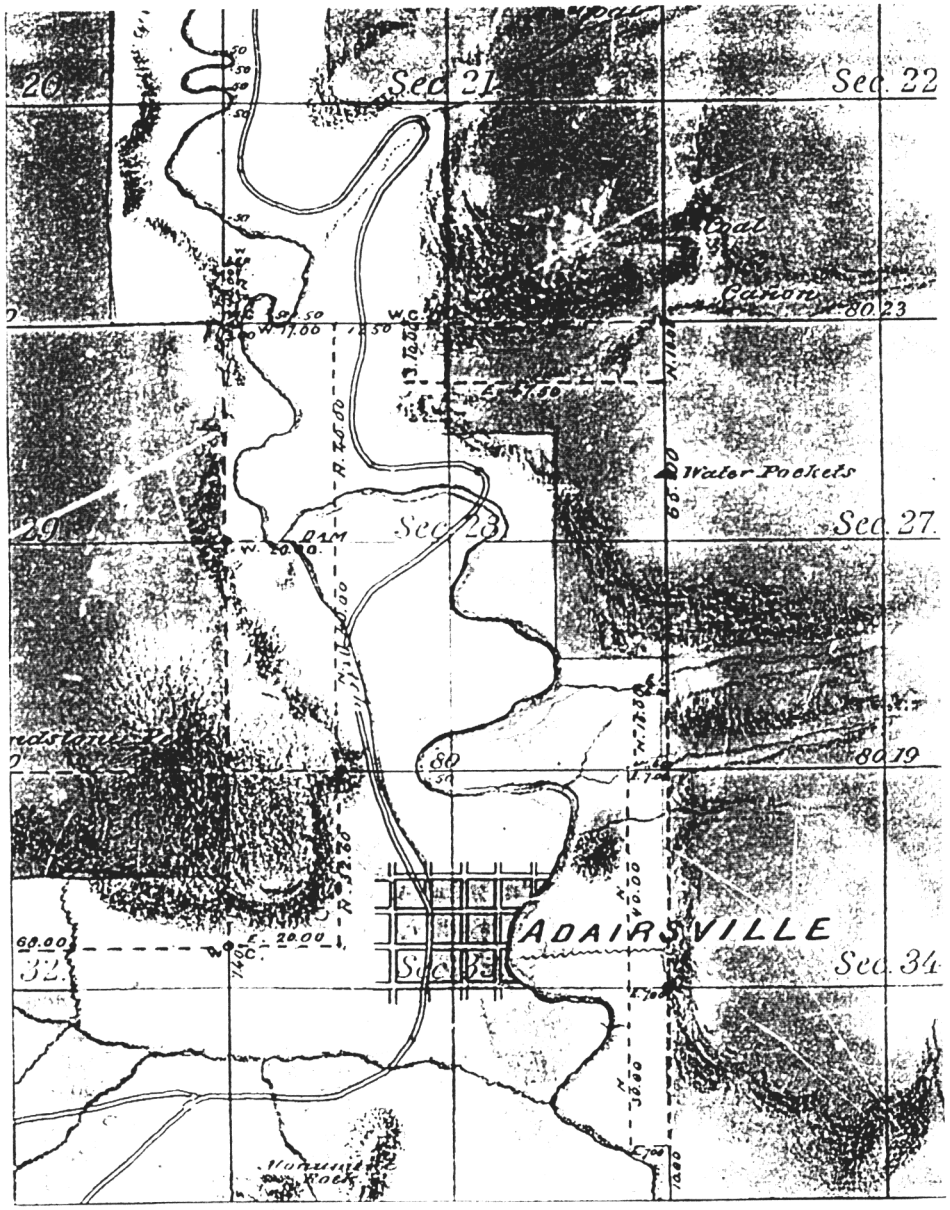

b)

Figure 2.49 (continued): **(b)** Portion of the map from the 1877 cadastral survey of Bailey and Burrill (1877) in the vicinity of Adairville, UT. The 1877 location of the main Adairville diversion dam is in the center of Section 28.

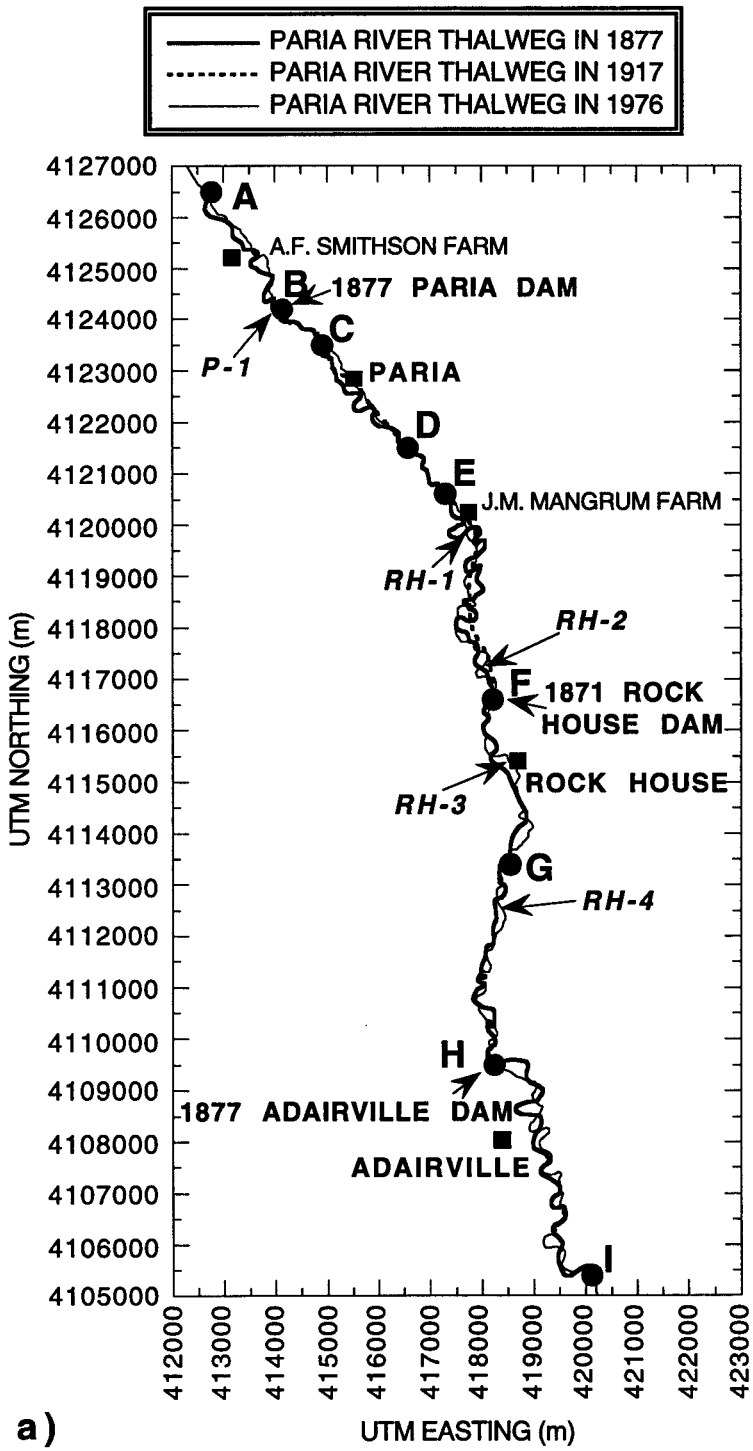

Figure 2.50: **(a)** Map of the Paria River thalweg in 1877, 1917, and 1976 in the Paria-Adairville, UT reach. Locations of division points between the 8 reaches for which slope determinations were made by both the contour-line and channel-length methods are labeled **A** through **I**; locations of five cross-sections, *P-1* and *RH-1* through *RH-4*, that were surveyed in 1994 and 1996 are also shown.

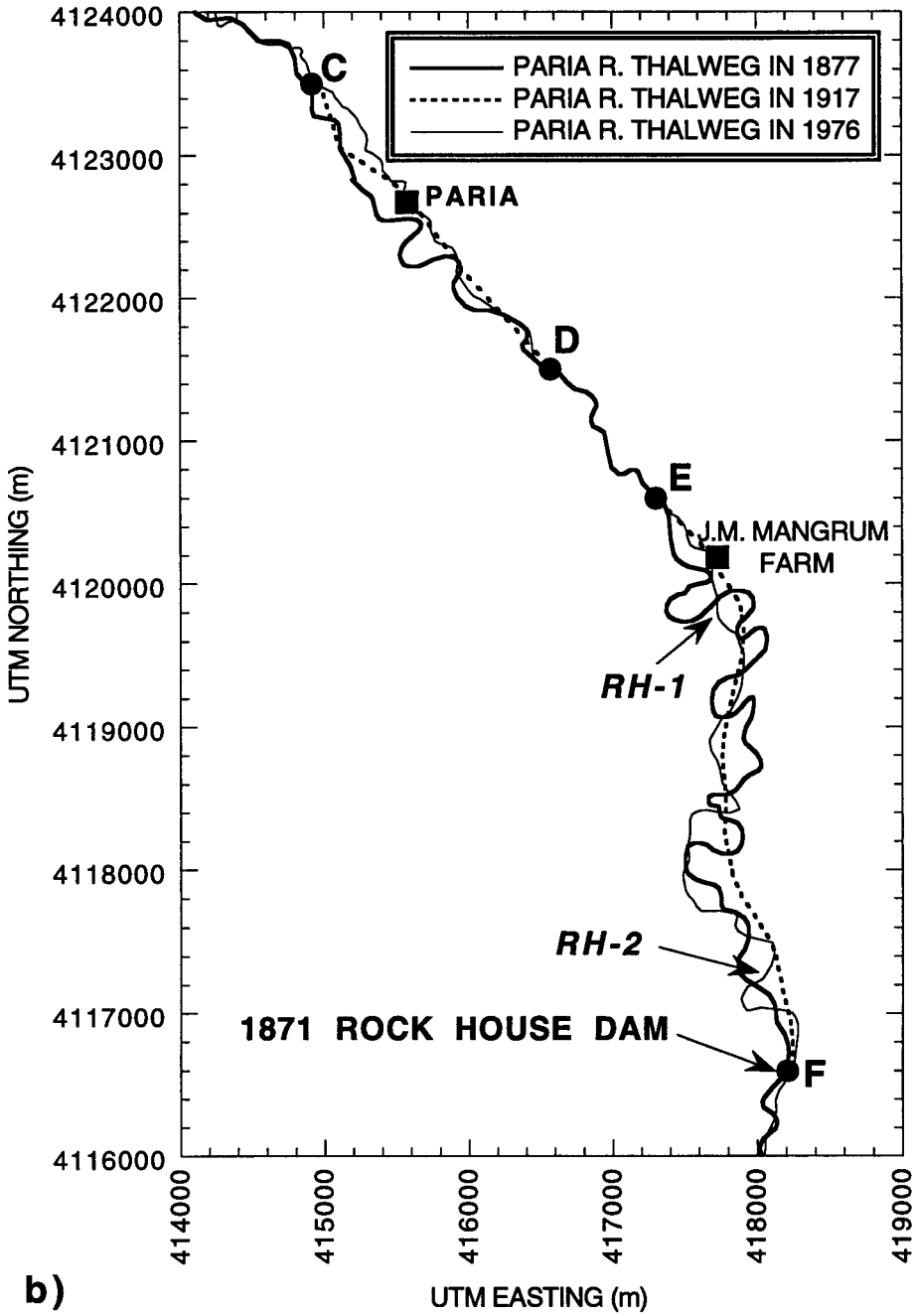

Figure 2.50 (continued): **(b)** Expanded view of Figure 2.50a for the reach of the Paria River from **C** to **F**. Locations of two cross-sections, *RH-1* and *RH-2*, that were surveyed in 1996 are shown.

in the Paria-Adairville reach of the Paria River that occurred between 1877 and 1917 (i.e., straightening and widening) and 1917 and 1973 (i.e., development of new meanders and narrowing) do not require a radical change in river hydrology, but are, in fact, fully compatible with a stable hydraulic geometry from 1877 through 1996.

On June 16, 1994, a cross-section was surveyed across a portion of the valley at the 1877 site of the irrigation dam (Figure 2.51) above the townsite of Paria (Figure 2.50a). This reach, like the equilibrium portion of the Cannonville study area, has a steep, i.e. 0.0084, longitudinal slope and is 1 m deep and 75 m wide at the bankfull stage. Because the 1994 floodplain slopes smoothly from the head of the 1877 irrigation ditch to the bankfull margin of the 1994 channel and the vertical distance from the head of the 1877 irrigation ditch to the floor of the 1994 channel is only 1.15 m (Figure 2.51), no evidence of significant post-1877 stream incision exists above the townsite of Paria. Below the cross-section at the 1877 irrigation dam, however, the river progressively incises into the 1877 floodplains until the maximum amount of incision, 4 m, is attained near location **E** (Figure 2.50). From location **E** to location **I**, the entire modern river channel and floodplain is deeply incised in the former 1877 floodplain, i.e., the Cottonwood Terrace of Hereford (1986), with the amount of incision slowly decreasing from 4 m at location **E** to less than 2 m at location **I**. The maximum of 4 m of post-1877 incision at location **E** is not surprising since the greatest amount of channel shortening in the Paria-Adairville reach, i.e., 42%, occurred in reach **E-F** between 1877 and 1917 (see Table 2.6 below).

To characterize the reach near the site of Rock House, UT, bankfull dimensions of four cross-sections were measured with a measuring tape on April 15, 1996 (Figure 2.52); these data are shown in Table 2.7 in Section 2.6c below. Longitudinal channel slopes were not measured at the locations of these cross-sections, but were determined from the 1976 USGS 7.5-minute topographic quadrangles. In 1996, bankfull depth and width in these four cross-sections varied as functions of the reach-averaged longitudinal slope; for example, for a longitudinal slope of 0.0053 at *RH-1*, the bankfull depth and width were 1 and 55 m, respectively and, for a slope of 0.0042 at *RH-2*, the bankfull depth and width were 1.3 and 26 m, respectively.

Reconstruction of changes in channel length, sinuosity, and slope from 1877 to 1976

To reconstruct changes in channel length over time, channel positions from the cadastral surveys were first drafted onto the 1976 USGS 7.5-minute topographic quadrangles and then digitized. Longitudinal slopes for the 1976 channel were determined by dividing the elevation drop between contour lines by the channel length between contour

a)

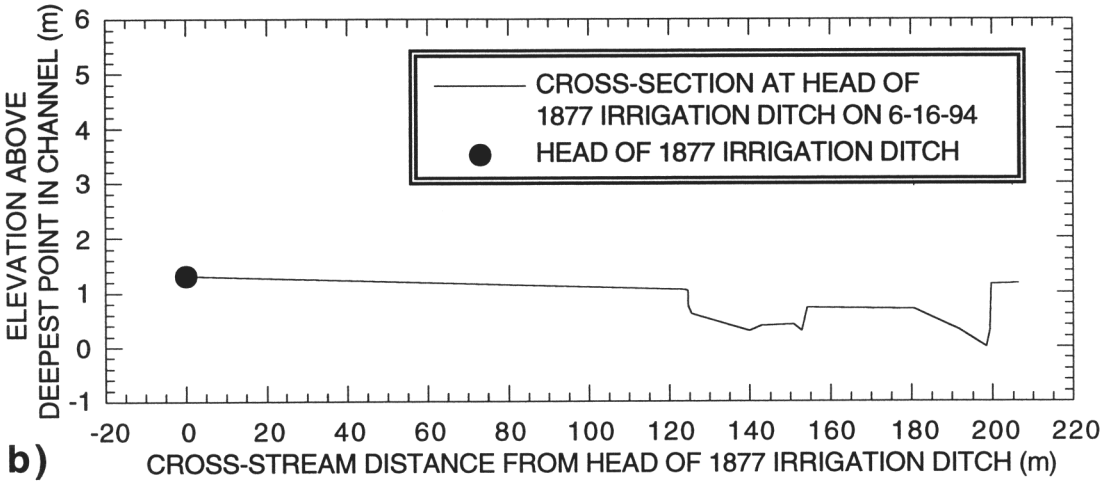

b)

Figure 2.51: **(a)** Cross-stream view, from the left bank to the right bank, of cross-section *P-1*; person with stadia rod for scale near tree on right bank. Photograph taken by D.J. Topping on June 16, 1994. **(b)** Cross-section *P-1* surveyed on June 16, 1994 at the location of the 1877 Paria, UT irrigation dam. Also shown is the surveyed position of the head of the 1877 irrigation ditch relative to the modern channel and floodplain.

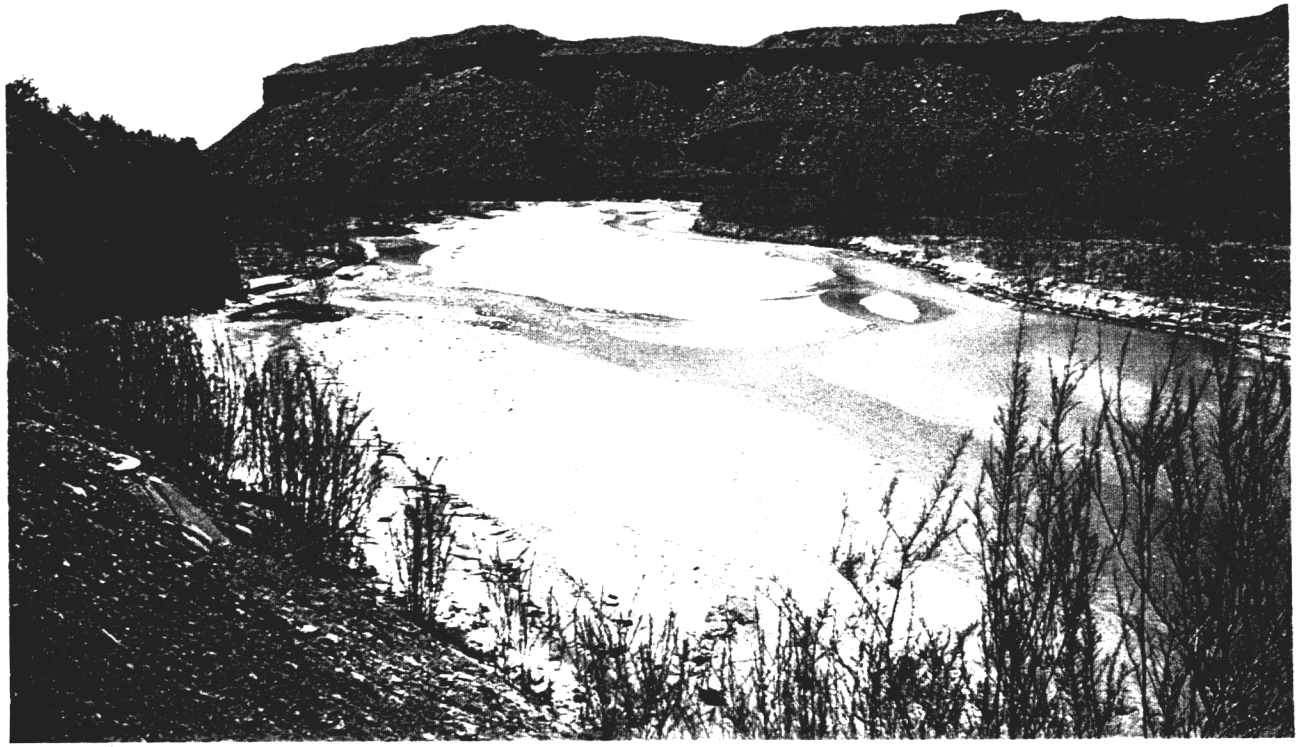

Figure 2.52: Downstream view of the reach in which the dimensions of cross-section *RH-3* were measured on April 15, 1996; reach is near the site of Rock House, UT ; mean bankfull dimensions of the channel are 35 m wide and 1.2 m deep. Photograph taken by D.J. Topping on April 15, 1996.

lines. Longitudinal slopes for the 1877 and 1917 channels were determined by two methods: the contour-line method, and the channel-length method. In the contour-line method, the longitudinal channel slopes for the 1877 and 1917 channels were determined by dividing the elevation drop between contour lines by the channel length; the 1976 contour lines were locally restored to their approximate 1877 positions by correcting for the effect of post-1877 channel incision. In the channel-length method, the channel was subdivided into eight reaches (Figure 2.50) and the mean longitudinal slope for each reach in 1877 and 1917 was determined by dividing the 1976 elevation drop along each reach by the channel length. Given that differences in the magnitude of channel incision may be as large as 4 m over several kilometers of channel length in certain reaches, greater error in slope may be accrued by this method than by the contour-line method. Changes in channel length and sinuosity, 1877 and 1917 longitudinal slopes determined by the contour-line and channel-length methods, and the 1976 longitudinal slope determined from the USGS 7.5-minute topographic quadrangles are shown in Table 2.6. Locations of the division points between the eight reaches appearing in Figure 2.50 and Table 2.6 were chosen at either: sites of the major irrigation diversion dams in the 1870's, endpoints of reaches covered by the 1877 and 1917 cadastral surveys (e.g., the 1917 survey only covered the reaches between **C** and **F**), or ends of bedrock-canyon reaches (e.g., the reach between **D** and **E** is located in the Middle Paria River Gorge that cuts through the Cockscomb).

The reaches that have undergone the most extensive changes in cross-section channel geometry in the Paria-Adairville reach between 1877 and 1976 have also undergone the most extensive changes in longitudinal channel slope. Reaches that were documented by Gregory and Moore (1931) to have undergone the most significant widening during the period from 1884 to 1918 [i.e., reaches **C-D** (Figure 2.53) and **E-F**] are those reaches that had the largest decreases in sinuosity and, therefore, the largest increases in longitudinal slope between 1877 and 1917 (Figure 2.50, Table 2.6). During the period from 1877 to 1917, virtually all of the meanders that existed in these reaches were cut off (Figure 2.50). Furthermore, reaches **C-D** and **E-F** are also the reaches that narrowed substantially from 1917 to 1996 (Hereford, 1986) as the longitudinal slope of the channel decreased in response to the development of new meanders.

The reconstructed 1877 longitudinal channel slopes in Table 2.6 also illustrate the probable early impact of irrigation development on the river in the Paria - Rock House - Adairville study area. Sinuosity of all but one reach, reach **F-G** below the Rock House Dam, decreased between 1877 and 1976 (Table 2.6). In 1877, the longitudinal channel slope of the river smoothly decreased from about 0.006 to 0.004 over the reaches from **A**

Table 2.6: Changes in channel length, sinuosity, and slope from 1877 to 1976 in the Paria-Adairville, UT reach.

REACH	1877 CHANNEL LENGTH (km)	1917 CHANNEL LENGTH (km)	1976 CHANNEL LENGTH (km)	1877-1976 CHANGE IN SINUOSITY	1877-1917 CHANGE IN SINUOSITY	1917-1976 CHANGE IN SINUOSITY	1877 SLOPE (contour-line method)	1877 SLOPE (channel-length method)	1917 SLOPE (contour-line method)	1917 SLOPE (channel-length method)	1976 SLOPE
A-B	3.98	—	3.05	-23%	—	—	0.0068	0.0057	—	—	0.0074
B-C	1.34	—	1.31	-2%	—	—	0.0044	0.0052	—	—	0.0051
C-D	3.44	2.62	2.85	-17%	-24%	+8%	0.0053	0.0058	0.0088	0.0076	0.0070
D-E*	1.34	1.34	1.34	0%	0%	0%	0.0037	0.0062	0.0071	0.0062	0.0062
E-F	7.37	4.28	5.54	-25%	-42%	+29%	0.0042	0.0035	0.0073	0.0061	0.0047
F-G	3.90	—	4.27	+9%	—	—	0.0062	0.0064	—	—	0.0058
G-H	5.46	—	5.01	-8%	—	—	0.0037	0.0036	—	—	0.0039
H-I	7.73	—	7.37	-5%	—	—	0.0039	0.0040	—	—	0.0042

Notes:
* This is the narrow Middle Paria River Gorge reach through the Cockscomb; because the magnitude of incision increases dramatically through this reach and no change in channel-length in this reach is possible, the 1877 slope of 0.0037 determined by the contour-line method is probably more accurate than the 0.0062 slope determined by the channel-length method.

Figure 2.53: June 1918 upstream view of the Paria River immediately upstream of Paria, UT. Note the extensive vegetated floodplain bordering the channel below the terrace in the distance; the upper surface of this floodplain is about 1 m above the floor of the active channel and 2-3 m below the top of the terrace. Photograph taken by H.E. Gregory.

to **F**, abruptly increased to in excess of 0.006 in reach **F-G**, then abruptly decreased again to 0.004 from location **G** to **I**; thus, this pattern suggests that a headcut was already present in this part of the valley in 1877. Furthermore, because this headcut was located below the first irrigation dam ever built on the Paria River, the 1877 existence of this nickpoint in the longitudinal profile of the river suggests strongly that the irrigation development in the 1870's initiated the destabilization of this portion of the Paria River.

Bankfull width of the channel and existence of floodplains near Paria in 1918

As in the case of the Lees Ferry study area, reaches of the upper Paria River with similar longitudinal slopes have had stable cross-section geometries over the period from 1918 to 1994. Full (including the widths of islands) and active (including only the widths of channels) bankfull widths of the 1918 channel (with a longitudinal slope equal to 0.0088) near Paria are similar to the full and active bankfull widths of the 1994 equilibrium channel (with a longitudinal slope equal to 0.0086) in the Cannonville study area. The full width of the Paria River 300 m above the townsite of Paria in 1918-1922 was equal to about 100-200 m and the active width was equal to about 100-150 m. Approximate 1918-1922 channel widths of the Paria River near the townsite of Paria were determined by matching photographed features both in Figure 2.53 and another H.E. Gregory photograph taken in 1922 (H.E. Gregory photograph no. 391, U.S. Geological Survey Photographic Library, Denver, CO) to features in the USGS 7.5-minute topographic and orthophotoquad quadrangles.

Not only has the cross-section geometry of the upper portion of the Paria River been stable for reaches of similar longitudinal slope since at least 1918, but the cross-section geometry of the upper portion of the river has also included active floodplains since at least 1918. In contrast to the conclusion of Hereford (1986, 1987a) that the channel of the Paria River lacked floodplains prior to 1940 and just as in the Lees Ferry study area, floodplains have existed in the reach near Paria since at least 1918 (Figure 2.53). Existence of the 1918 floodplain indicates that the important assumption used by Hereford (1987b) and W. Graf (1987) in calculating post-1940 sediment storage in the Paria River basin (i.e., that all floodplain sediment between the terraces was deposited after the early 1940's) is questionable. Furthermore, as in both the Cannonville and Lees Ferry study areas, the river has laterally migrated across the valley in the Paria-Adairville reach since 1877 and reworked large quantities of floodplain sediment (Figure 2.50), thus indicating that the conclusion of Hereford (1986, 1987a) that post-1940 sediment accumulation in the Paria

River valley was chiefly by vertical accretion without significant lateral migration of the channel is also misleading.

2.5e: The Paria River below the near Kanab, UT gage from 1971 to 1995

To characterize the portion of the river from the gage near Kanab, UT through the Lower Gorge to Lees Ferry, AZ, bankfull dimensions of seven cross-sections (*LG-1* through *LG-7* in Figure 2.1) were measured with a measuring tape in April 1995 from the post-1966 near Kanab, UT gage to Lees Ferry, AZ; dimensions of the 7 cross-sections are shown in Table 2.7 in Section 2.6 below. This survey revealed that the minimum bed elevation of the channel at the near Kanab, UT gage has been stable over time. Less than 5 cm of bed elevation change has occurred at this site since 1971, with only 1.5 cm of bed elevation change occurring since 1974 (Figure 2.54).

To characterize the mean gravel grain-size distribution in the Lower Paria River Gorge, two pebble counts were conducted by the method of Wolman (1954) at cross-sections *LG-3* and *LG-4* (Figure 2.55) and were composited; this grain-size distribution is shown in Figure 2.58 in Section 2.6c below. This grain-size distribution has a D_{50} and D_{84} equal to 5 and 10 cm, respectively, and is similar to both the mean gravel grain-size distribution from the Cannonville study area and the gravel grain-size distribution from Reach 3 in the Lees Ferry study area. Measurements of the thickness of the sand, silt, and clay layer over the gravel at cross-section *LG-4* indicate that the amount of sand, silt, and clay on the bed is also similar to the amount on the bed at Lees Ferry, AZ and is 11±22 cm.

2.5f: Summary of Paria River channel properties

Modern

For equilibrium reaches of the modern Paria River, i.e., reaches with active floodplains, the reach-averaged maximum bankfull depth is inversely proportional to the reach-averaged longitudinal channel slope, and the reach-averaged bankfull width is directly proportional to the reach-averaged longitudinal channel slope. The floor of the channel is composed of gravel overlain by a layer of sand, silt, and clay; and the banks are composed of a mixture of sand, silt, clay. For at least the lower 83% of the 157-km-long river, the grain-size distribution of the gravel that composes the floor of the channel is constant; and, as indicated by measurement of the gravel grain-size distribution at the near Cannonville, UT gage in 1958, the grain-size distribution of the gravel has not changed with respect to time.

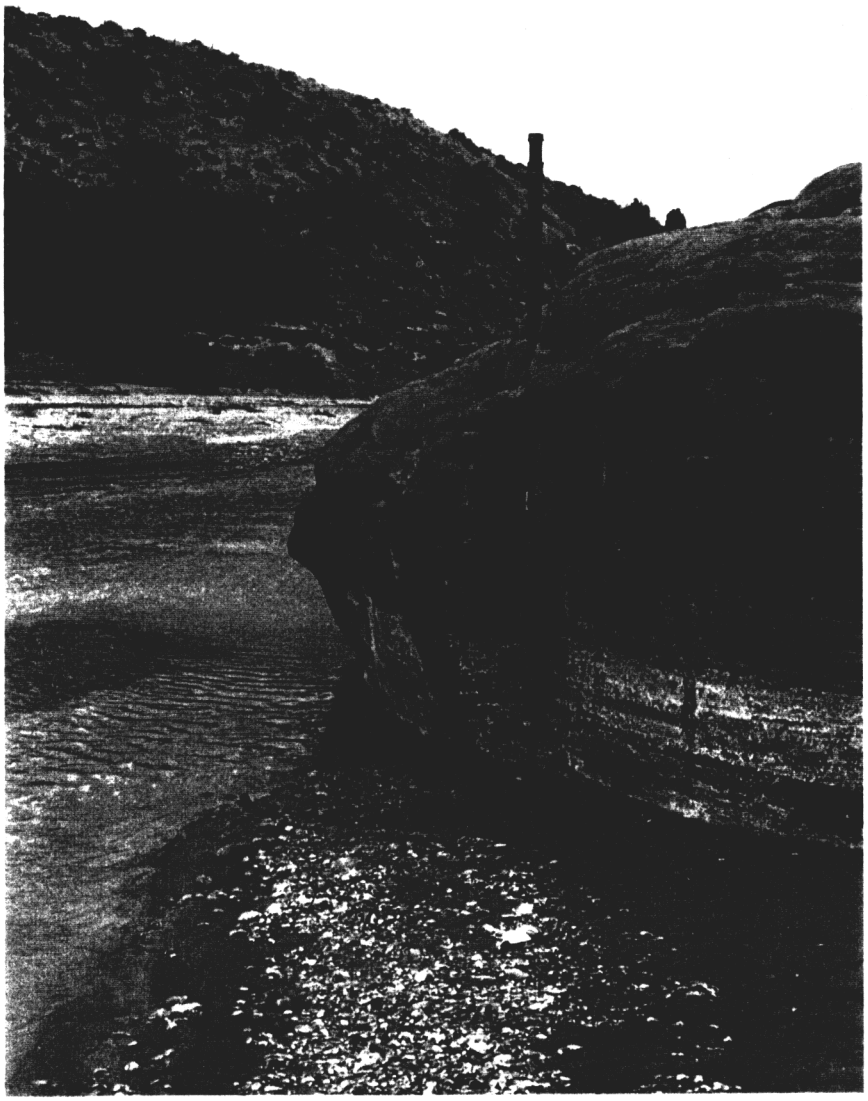

Figure 2.54: April 10, 1995 photograph of the near Kanab, UT annual-crest gage on the left bank of the Paria River; photograph taken by D.J. Topping.

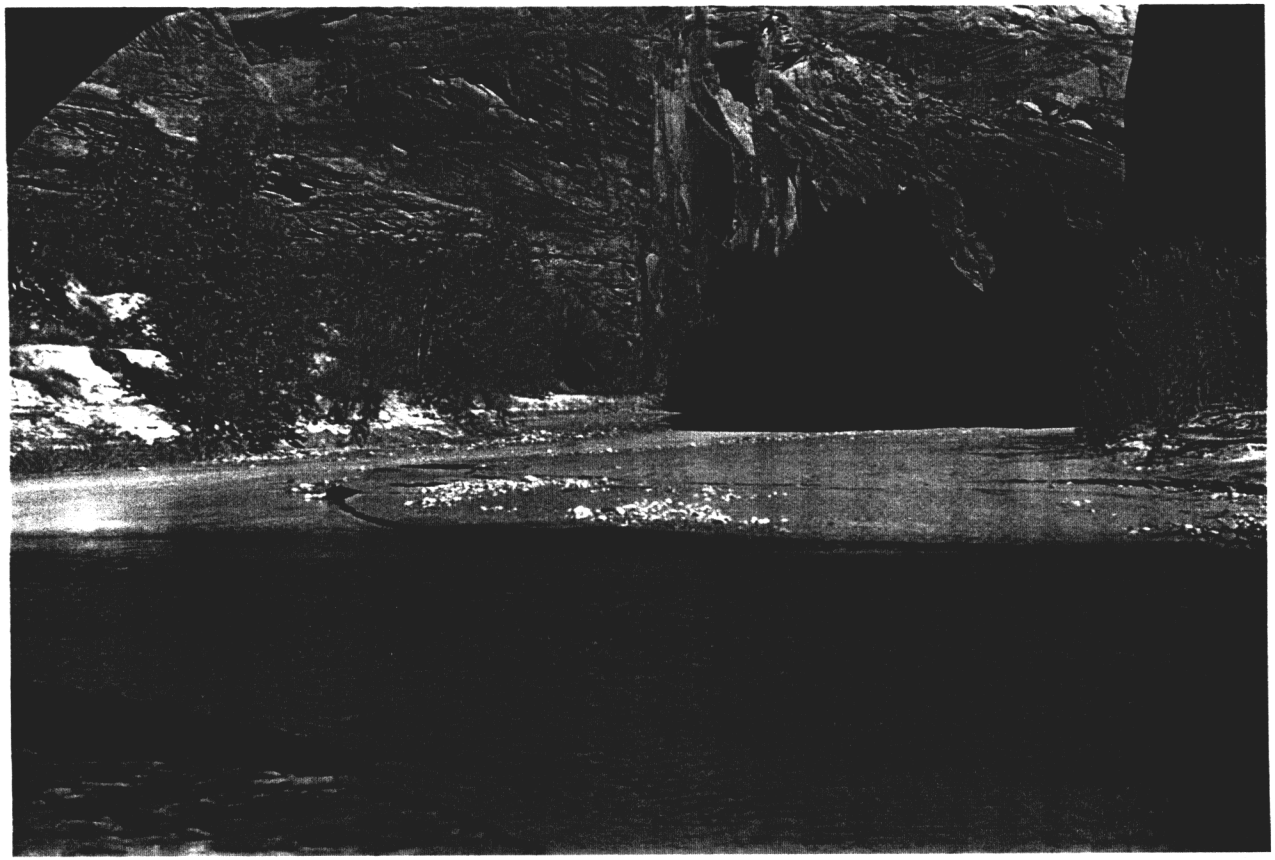

Figure 2.55: April 12, 1995 upstream view of the Paria River at cross-section *LG-4*. Camera position in UTM coordinates is approximately 4093180 m north and 423900 m east; photograph taken by D.J. Topping.

Approximately four grain-size distributions of the mixture of sand, silt, and clay are present in the system. The coarsest grain-size distribution of sand, silt, and clay overlies the gravel on the floor of the thalweg and the finest grain-size distribution in the system comprises the bar tops and banks. Measurements in equilibrium portions of the Cannonville study area, the Lower Paria River Gorge, and the Lees Ferry study area indicate that similar amounts of sand, silt, and clay overlie the gravel in these three reaches. In the Cannonville study area, 2.5 m^3 of sand, silt, and clay overlie the gravel on the floor of the channel per meter of channel length; at cross-section *LG-4* in the Lower Paria River Gorge, 2.2 m^3 of sand, silt, and clay overlie the gravel on the floor of the channel per meter of channel length; and, in the Lees Ferry study area, 2.3 m^3 of sand, silt, and clay overlie the gravel on the floor of the channel per meter of channel length. Thus, the amount of sand, silt, and clay in the Lees Ferry study area is fairly representative of the amount of sand, silt, and clay in the system.

Past changes

The primary sources of information used in this study to reconstruct past channel geometries were direct measurements of channel geometry from surveys, rather than the indirect methods used by previous workers, for the following reasons. The method utilized by Webb (1985) and Webb and others (1991) of using widths measured in the cadastral surveys to reconstruct bankfull channel geometries can grossly underestimate bankfull widths. The method utilized by numerous workers of using repeat photography without independent measurements of either surveyed topography or measured distances in the field of view can be misleading in the reconstruction of topographic changes. The stratigraphic methods of Hereford (1986, 1987a) using tamarisk tree-ring age control do not agree with topographic surveys of channel and floodplain surfaces.

In the studied lower 83% of the Paria River system, the only changes in equilibrium cross-section geometry of alluvial reaches that have occurred since the 1870's have been coupled to changes in the reach-averaged longitudinal slope of the channel. In other words, for a fixed longitudinal slope, the river cross-section channel geometry has been constant since the 1870's. Aggradation and incision in the river has been local in nature and largely driven by local base-level changes, e.g., 1909-1996 aggradation and incision in the lowermost portion of the Lees Ferry study area driven by base level fluctuations at the confluence with the Colorado River, 1877-1917 incision in the Paria-Adairville reach associated with meander cutoffs, and aggradation and incision in the Lower Gorge associated with the km^3-scale Chinle landslides. Furthermore, the incised reaches that

occur in the system are all discontinuous in the streamwise direction, e.g., the incision near Cannonville that began circa-1800 does not extend all of the way to Paria downstream. No evidence for isochronous aggradation and degradation in the Paria River basin, as suggested by Hereford (1986, 1987a) and W. Graf (1987), exists.

Floodplain sediments have been reworked over time as the channel has laterally migrated across the valley floor. In contrast to the conclusions of Hereford (1986, 1987a, 1987b) and W. Graf (1987), floodplains existed prior to 1940; photographs from 1873, 1911, 1915, 1918, 1921, and 1939 from the lower and upper portions of the river all document the existence of floodplains. The single largest change that has occurred in the Paria River system over the last century has not been geomorphic, but, rather, botanical. Floodplains of the river have been densely colonized by two non-native species that first arrived in the region in the late 1930's, tamarisk and Russian olive; photographs taken prior to the mid-1960's show that the floodplains were only lightly to moderately vegetated. Thus, the current floodplain surfaces of the Paria River may be more stable than the floodplain surfaces that existed along the channel prior to the mid-1960's.

Section 2.6: HYDRAULIC GEOMETRY OF THE PARIA RIVER

2.6a: Introduction and working hypothesis

As defined by Leopold and Maddock (1953), the water discharge, sediment load, and cross-section channel geometry of an alluvial river are coupled and together compose the hydraulic geometry of a river channel. The original hydraulic geometry framework of Leopold and Maddock (1953) has been modified herein to include effects of longitudinal channel slope and bed roughness. These two factors were originally recognized by Leopold and Maddock (1953) as important but were excluded from their empirically based analyses because of data limitations.

Since quantity of data is not a limitation in this study, all of the physical variables of river channel geometry first identified by Mackin (1948), Leopold and Maddock (1953), and Leopold and Miller (1956) have been included in analyses presented below of the modern and historical hydraulic geometry of the Paria River. The physical variables that describe the hydraulic geometry of a self-formed alluvial river channel are typically divided in two categories, independent and dependent. In this study, the chosen independent variables are: (1) water discharge, (2) sediment load, and (3) grain-size distribution of bed sediment; and, the chosen dependent variables are: (1) reach-averaged longitudinal slope, (2) reach-averaged maximum depth, (3) reach-averaged mean depth, (4) reach-averaged width, and (5) reach-averaged mean velocity. The independent variables are controlled by

local geology and climate, while the dependent variables all vary interdependently to conserve the conveyed mass of water and sediment through the channel. Interdependence of these variables leads to the important concept of equivalent hydraulic geometries that can be stated in the following manner: "For a fixed channel elevation drop over a given valley length, there exists a continuum of local channel geometries, ranging from meandering to braided, that have equivalent hydraulic geometries and transport the same amount of water and sediment". Thus, a change in the reach-averaged cross-section geometry of a channel may be balanced by a change in the reach-averaged longitudinal slope, and dies not necessarily reflect a change in hydrology, i.e., climate.

Although the above empirical framework of hydraulic geometry is useful in making geomorphic interpretations, it can be somewhat confusing. Thus, to avoid any possible confusion, the entire concept of hydraulic geometry has been recast in a physically based framework that can be stated as a working hypothesis combined with a truism. The working hypothesis is that "the reach-averaged maximum depth is determined by the length scale on the bed responsible for setting the spatially averaged bed roughness". The truism is that "for all sediment transporting flows, the mass of water and sediment must be conserved for the geometry of a river channel to be stable." In other words, this truism states that for all discharges that transport sediment, the mass of sediment being transported into a chosen reach must equal the mass of sediment being transported out of that reach or the channel geometry will change.

To determine the mean hydraulic geometry of a river, one must calculate the stable shape of the river channel for all flows in the instantaneous discharge time series. Since this exercise is an overly daunting task, the approach taken in this study has been the standard approach used by previous workers to relate the stable hydraulic geometry of a reach to a characteristic channel-forming discharge, specifically, the bankfull flow. In the case of the Paria River, as will be shown in Chapter 4, the bankfull flow does not transport the most sediment over time, hence it does not equal the "effective discharge" defined by Wolman and Miller (1960) and used Andrews (1980). Rather, it is the channel-forming flow only in the sense that it occurs frequently enough, i.e., every 2.2 years on average, to prevent the successful colonization of the higher floor of the channel by vegetation.

A physically based formulation of hydraulic geometry

Calculation of the stable hydraulic geometry, for straight reaches, that satisfies conservation of the mass of water and sediment for the bankfull flow is a 2-step process. Step 1 relates the maximum bankfull depth to the length scale on the bed responsible for

setting the spatially averaged bed roughness. Step 2 conserves the mass of water and sediment in a reach. Solution of these two steps requires that seven physical assumptions be made: (1) unsteadiness of flow is unimportant to the geomorphology; (2) to remove the effects of the local convective accelerations in the flow and sediment-transport fields responsible for the development of local variation in channel geometry within a reach, all quantities below are reach-averaged and, thus, derived for the reach-averaged equilibrium cross-section; (3) since the reaches of interest are straight, the reach-averaged cross-stream velocities are zero, and the flow is approximated as uniform; (4) since, at bankfull stage, the form drag due to bars in a gravel-bedded river is on the order of 10% of τ_b (Parker and Peterson, 1980) and the banks are relatively smooth, all of the reach-averaged roughness in the system is treated as bed roughness with the effects of bar and bank form drag neglected; (5) the bed grain-size distribution is approximated as invariant with cross-stream position; (6) for most situations the longitudinal slope of the channel will adjust much more slowly than the other "dependent" variables, thus, it may be treated as relatively "independent" and the last of the "dependent" variables to adjust to a change in either the water discharge, sediment load, or grain-size distribution of the bed sediment; and, (7) the angle of the side slopes of banks and bars is fixed at 15°. The side slopes of bars and banks is held constant at 15° for two reasons: 15° is the empirically observed mean bank angle in the Paria River system; and 15° is the approximate mean bank angle required by the inclusion of both the streamwise boundary shear stress and the pseudo-gravitational shear stress components in the calculation of the stable angle of submerged side slopes in a river as derived by Ikeda (1982) and Nelson and Smith (1989).

(STEP 1) In gravel-bedded rivers, the maximum bankfull depth, h_{BF}, is hypothesized to be set by a combination of the longitudinal slope of the channel and the critical shear stress for the grain-size on the bed that dominates the spatially averaged bed roughness. For steady, uniform flow, the balance that relates the reach-averaged maximum bankfull depth to the longitudinal slope of the channel and the critical shear stress for D_{84} is a rearrangement of the physical balance between the critical shear stress for D_{84} and the depth-slope product:

$$h_{BF} = \tau_{cr(D_{84})} / \rho g S, \tag{2.6}$$

where $\tau_{cr(D_{84})}$ is the critical shear stress for D_{84} set by the method of Wiberg and Smith (1987a) for a value of D/k_s of 1 (D is the nominal grain diameter and k_s is the bed roughness length), ρ is the density of water, g is the gravitational acceleration, and S is the reach-averaged longitudinal slope of the channel. Since the angle of the side slopes of

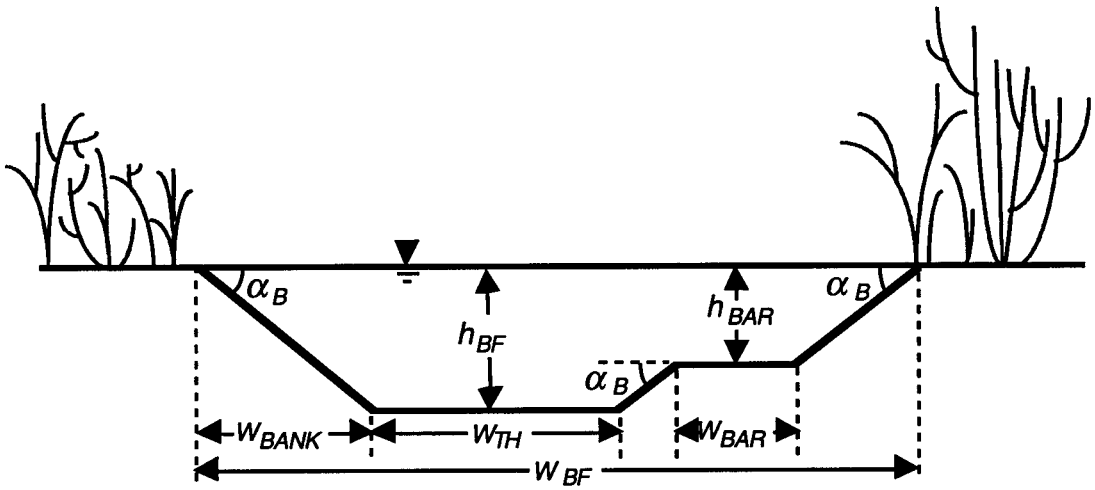

Figure 2.56: Definition sketch showing features in the reach-averaged equilibrium cross-section used in hydraulic geometry calculations. Previously undefined terms are: W_{TH}, the width of the thalweg, W_{BAR}, the width of the bar region, and W_{BF}, the bankfull width of the channel.

banks and bars, α_B, is fixed, the width of one of the bank regions is set by the magnitude of h_{BF} as:

$$W_{BANK} = \frac{h_{BF}}{\tan \alpha_B}. \tag{2.7}$$

(STEP 2) Step 2 calculates the bankfull cross-section geometry by conserving the mass of water and sediment in a reach. This is accomplished by equating the bankfull water discharge, Q_{BF}, and the bankfull sediment load, Q_{sBF}, between reaches with no intervening tributary or spring inflow. The cross-section is first assumed to trapezoidal with the depth of the thalweg, i.e., the central, flat-bottomed portion, equal to h_{BF}. If for the cross-section area that conserves the mass of water, this shape produces a calculated sediment load in excess of Q_{sBF}, the shape of the cross-section is modified to include shallower bar regions whose width is varied until the mass of both water and sediment is conserved (Figure 2.56). Since sediment transport is required for bars to grow, the depth of the flow over a bar will decrease until τ_b equals $\tau_{cr(D_{50})}$, therefore, the depth over the modeled bar regions is set as:

$$h_{BAR} = \tau_{cr(D_{50})}/\rho g S. \tag{2.8}$$

The equation by which the bankfull unit discharge at each cross-stream position in the cross-section is calculated is simply:

$$q_{BF} = h\frac{u_*}{k}\ln\left(\frac{0.48h}{0.1D_{84}}\right), \tag{2.9}$$

where $u_* = \sqrt{\tau_b/\rho}$ is the shear velocity at each cross-stream position and h is the local depth of the bankfull flow at each cross-stream position; and, since the flow is steady and uniform, the boundary shear stress at each cross-stream position is set equal to the depth-slope product, such that

$$\tau_b = \rho g h S. \tag{2.10}$$

To conserve the mass of water from reach to reach,

$$Q_{BF} = \int_0^{W_{BF}} q_{BF} dy = \text{constant}. \tag{2.11}$$

The expanded version of equation 2.11, for the channel shape in Figure 2.56 is:

$$Q_{BF} = 2\left[\frac{2}{5}\left(\frac{h_{BF}^{\frac{5}{2}}\sqrt{gS}}{k\tan\alpha_B}\right)\ln\left(\frac{0.48h_{BF}}{0.1D_{84}}\right) - \frac{4}{25}\left(\frac{h_{BF}}{\tan\alpha_B}\right)^{\frac{5}{2}}\right] +$$
$$W_{TH}\left[\frac{h_{BF}^{\frac{3}{2}}\sqrt{gS}}{k}\ln\left(\frac{0.48h_{BF}}{0.1D_{84}}\right)\right] + W_{BAR}\left[\frac{h_{BAR}^{\frac{3}{2}}\sqrt{gS}}{k}\ln\left(\frac{0.48h_{BAR}}{0.1D_{84}}\right)\right]. \tag{2.12}$$

Many equations for calculating bedload transport exist in the literature. Most treat the bedload-transport rate as a nonlinear function of the nondimensional shear stress and

differ mainly in detail. These differences are due to the fact that each of these engineering equations was designed to predict the absolute magnitude of the bedload-transport rate for a specific application through the adjustment of free coefficients. Since only the relative magnitude of Q_{sBF} between reaches is of interest in this application, however, and not the absolute magnitude of Q_{sBF}, the bedload transport relationship of Fernandez Luque and van Beek (1976) was chosen to calculate the value of the unit sediment flux at each cross-stream position in the cross-section because: it is simple with only one adjustable coefficient; and it is designed to work for low transport stages. Thus, the equation by which the bankfull unit sediment flux is calculated at each cross-stream position is:

$$q_{sBF} = \left[\left(\frac{\rho_s - \rho}{\rho}\right) g\left(\mathrm{D}_{50}\right)^3\right]^{\frac{1}{2}} 5.7\left(\tau_* - \left(\tau_*\right)_{cr}\right)^{\frac{3}{2}} \qquad \text{where } \tau_b > \tau_{cr(\mathrm{D}_{50})}, \quad (2.13a)$$

or

$$q_{sBF} = 0 \qquad \text{where } \tau_b \le \tau_{cr(\mathrm{D}_{50})}. \quad (2.13b)$$

In equation 2.13a, the nondimensional stress is:

$$\tau_* = \frac{\tau_b}{(\rho_s - \rho) g \mathrm{D}_{50}}. \quad (2.14)$$

To conserve the mass of sediment from reach to reach,

$$Q_{sBF} = \int_0^{W_{BF}} q_{sBF} dy = \text{constant}. \quad (2.15)$$

The expanded version of equation 2.15, for the channel shape in Figure 2.56 is:

$$Q_{sBF} = \left[\left(\frac{\rho_s - \rho}{\rho}\right) g\left(\mathrm{D}_{50}\right)^3\right]^{\frac{1}{2}}$$
$$5.7\left\{2\left[\frac{\left(\frac{\rho h_{BF} S}{(\rho_s - \rho)\mathrm{D}_{50}} - \left(\tau_*\right)_{cr}\right)^{\frac{5}{2}}}{\frac{5}{2}\tan\alpha_B\left(\frac{\rho S}{(\rho_s - \rho)\mathrm{D}_{50}}\right)}\right] + W_{TH}\left[\frac{\rho h_{BF} S}{(\rho_s - \rho)\mathrm{D}_{50}} - \left(\tau_*\right)_{cr}\right]^{\frac{3}{2}}\right\}. \quad (2.16)$$

The width of the thalweg can be determined by rearranging equation 2.16 and solving for the value of W_{TH} for a known Q_{sBF}; and, the width of the bar region can determined by combining equations 2.12 and 2.16, rearranging, and solving for W_{BAR} in terms of the known Q_{BF} and Q_{sBF}. The equation that determines the bankfull width is, thus:

$$W_{BF} = 2W_{BANK} + W_{TH} + W_{BAR} = 2\frac{h_{BF}}{\tan\alpha_B} + W_{TH} + W_{BAR}. \quad (2.17)$$

This model does not specify whether a channel is single or multiple threaded; and, the three widths that together sum to equal the bankfull width are cumulative quantities, e.g., W_{TH}, W_{BAR}, and W_{BANK} indicate the cumulative width of all, bars, and bank and bar side-slopes in the channel, respectively. Thus, in a situation where the width of the bar region is much larger than the width of the thalweg, the river may braid because of channel-scale lateral instabilities in the flow and sediment transport.

In summary, the hydraulic geometry theory outlined above is applied to a river as follows: (1) Q_{BF}, Q_{sBF}, the grain-size distribution of bed sediment, and S are imposed; (2) h_{BF} is determined from equation 2.6; (3) α_B, the bank and bar side-slope angle, is fixed at 15°, thus W_{BANK} is set by h_{BF}, (4) the value of W_{TH} is determined by equation 2.16, and (5) and W_{BAR} is determined by equation 2.12.

2.6b: Reach-averaged maximum bankfull depth

Most previous attempts to model bankfull depth of self-formed gravel channels have been transport based rather than roughness based (e.g., Parker, 1978a; Parker; 1979; Ikeda and others, 1988; Ikeda and Izumi, 1990; Paola and Mohrig, 1996). These studies have assumed that for a gravel channel to be stable, the shear stress at the toe of the bank must be at critical for initiation of sediment transport. Parker (1978a) originally defined the "stable channel paradox" that states that gravel channels cannot both be stable and be actively transporting sediment. He resolved this paradox by incorporating the effects of the lateral diffusion of downstream momentum to redistribute the cross-stream boundary shear stress such that it would be at critical at the toe of the bank and about 20% higher in the center. Based on Parker's approach, Parker (1979), Ikeda and Izumi (1990), and Paola and Mohrig (1996) used values of about 1.2 to 1.23 times the critical shear stress of D_{50}, and values of the nondimensional Shields stress from 0.03 to 0.05, to relate the maximum bankfull depth to the longitudinal slope. Ikeda and others (1988) found that using the critical shear stress for D_{50} underpredicted bankfull depths in laboratory and natural mixed grain-size channels and thus incorporated sorting, based on the work of Egiazaroff (1965), in the relationship for determining bankfull depth. Transport-based approaches, however, tend to underpredict the maximum bankfull depth of most gravel-bedded rivers (Figure 2.57). Indeed, Andrews (1984) found empirically that, in a significant number of the gravel rivers he studied in Colorado, the boundary shear stress was high enough to entrain particles as large as D_{90} at bankfull discharges.

This study differs markedly from those listed above by hypothesizing that the reach-averaged maximum bankfull depth is set not by a transport-based criterion, but rather

by a criterion based on the spatially averaged roughness. Specifically, it is hypothesized that the reach-averaged maximum bankfull depth of self-formed gravel rivers with erodible gravel or sandy banks scales with the critical shear stress of the particle size on the bed that dominates the spatially averaged bed roughness. Numerous studies (e.g., Dietrich and Whiting, 1989; Wiberg and Smith, 1991; Nelson and Smith, 1991;Pitlick, 1992) have shown that the spatially averaged bed roughness scales with D_{84}. Furthermore, Pitlick (1992) showed that, at higher transport stages, i.e., approximately twice that for initiation of sediment transport, the bed roughness still scales with D_{84}, but increases fivefold over the value at lower transport stages.

Pitlick (1992) interpreted this increase in roughness as due to the breakup of the stable gravel pavement and the corresponding growth of gravel bedforms. Since the sorting of the bed in many gravel-bedded rivers is such that D_{84} is about twice the diameter of D_{50} (e.g., Church and Rood, 1983), the critical shear stress for D_{84} is about twice that of D_{50} and thus corresponds to a transport stage of 2. Up to a transport stage of about 2, although bed material is already in transport, D_{84} is relatively stable and dominates the spatially averaged bed roughness; and, when the critical shear stress for D_{84} is attained at a transport stage near 2, dunes begin to grow and the spatially averaged bed roughness increases dramatically. Thus, the depth associated with the critical shear stress for D_{84} is the greatest depth at which the bed roughness is still relatively low. For this reason alone, since the bed roughness would be much higher at greater bankfull depths, potentially resulting in greater extraction of momentum from the flow than would occur from bank erosion, the channel should widen rather than deepen with an increase in the magnitude of the bankfull discharge.

To test the above hypothesis that the reach-averaged maximum bankfull depth for a given reach-averaged longitudinal slope is set by the critical shear stress for D_{84}, the maximum bankfull depth predicted by equation 2.6 was tested against data from: (1) 160 alluvial gravel-bedded rivers with gravel or sand banks compiled by Church and Rood (1983); (2) the 13 alluvial gravel-bedded rivers of Hey and Thorne (1987) that fell into their Vegetation Category 1 (i.e., channels with grassy banks); (3) the 42 laboratory experiments of Wolman and Brush (1961); (4) the 34 laboratory experiments of Ikeda (1981); and (5) the 20 laboratory experiments of Ikeda and others (1988). In using the data from the Church and Rood (1983) compilation, no data from degrading or aggrading channels were used in the test of the hypothesis; and, if the bankfull channel geometry was not available for a site, the geometry of the channel during the 2-year flood was used as a surrogate for the bankfull channel geometry. Data from the 173 rivers in the Church and Rood (1983)

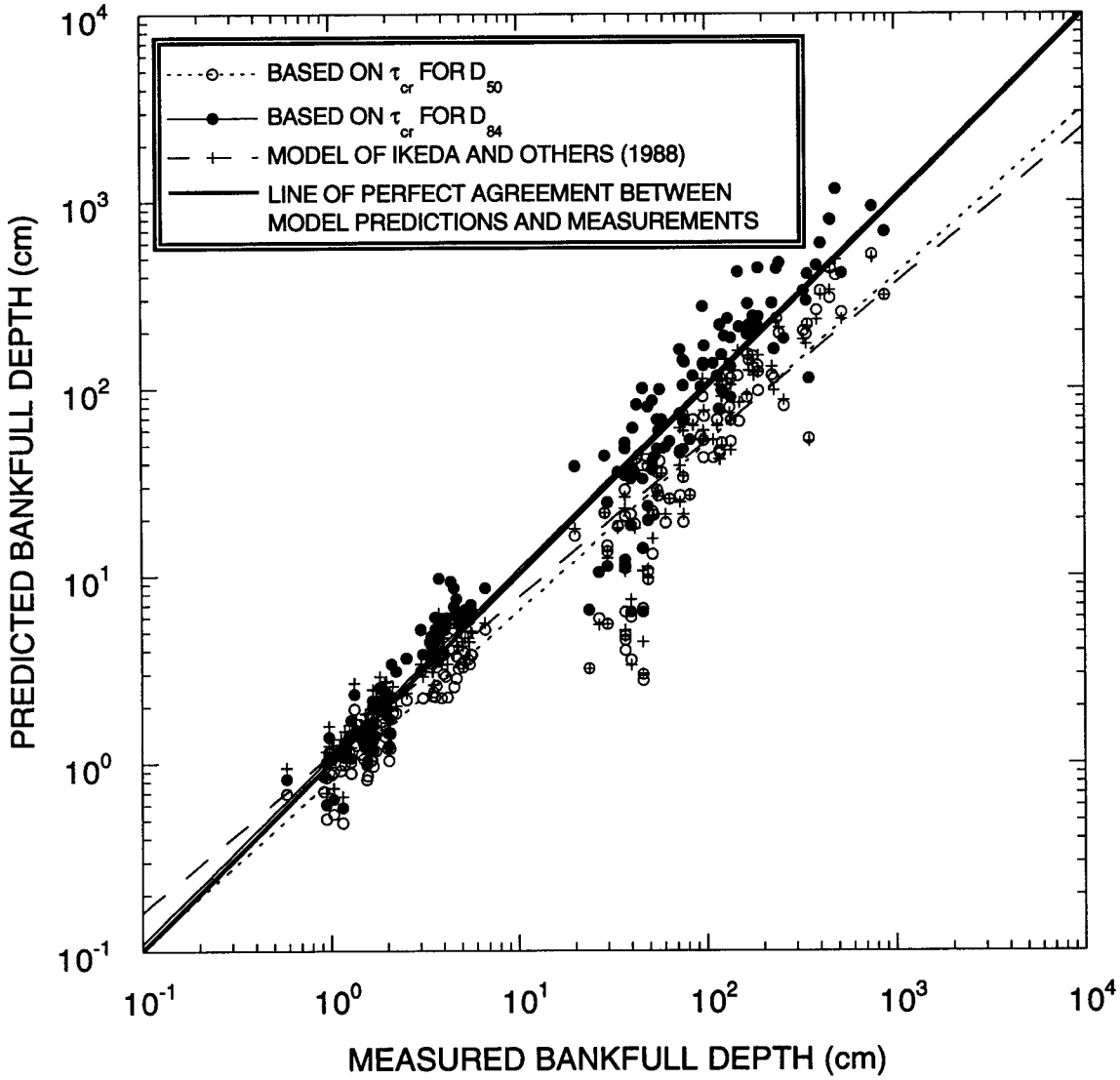

Figure 2.57: Predicted (by three different methods) vs. measured bankfull depth for the 96 laboratory and 95 gravel-bedded river cases; the laboratory cases are those with measured bankfull depths less than 10 cm. Also shown are the log-linear regressions associated with the predictions made by each method. For the methods based on $\tau_{cr(D_{50})}$ and $\tau_{cr(D_{84})}$, the critical shear stress of either D_{50} or D_{84} was determined by the method of Wiberg and Smith (1987a) for a D/k_s of 1.0.

and Hey and Thorne (1987) data sets were first filtered to insure that only data from self-formed channels were retained; this filter excluded all channels in which the critical shear stress for D_{50} on the bed [determined by the method of Wiberg and Smith (1987a) for a D/k_s of 1.0] was not equaled or exceeded at bankfull stage. This was done so that only those rivers would be included in the test that could actively transport material composing the bed, i.e., self-formed channels, and not the rivers with channels that were developed on pre-existing gravel lags. After this filter was applied, only 85 of the 160 rivers of Church and Rood (1983) and 10 of the 13 rivers of Hey and Thorne (1987) were retained in the analysis.

As indicated by the trends of the three log-linear regressions relative to the trend of the line of perfect agreement between model predictions and measurements in Figure 2.57, the method of predicting the maximum bankfull depth based on $\tau_{cr(D_{84})}$ works the best for both the laboratory and the natural gravel-bedded river cases. Indeed, the log-linear regression fit to the predictions of the maximum bankfull depth based on this method falls virtually on top of the line of perfect agreement. In contrast, the two methods based on $\tau_{cr(D_{50})}$ adequately predict only the bankfull depth of the laboratory coarse-sand channels and significantly underpredict the bankfull depth of the natural gravel-bedded rivers. Though the near-perfect agreement between the model predictions of the maximum bankfull depth based on $\tau_{cr(D_{84})}$ and the measurements of bankfull depth does lend support to the hypothesis that bankfull depth in gravel-bedded rivers is physically set by a roughness rather than a transport criterion, it does not preclude the possibility, however, that the bankfull depth in gravel-bedded rivers is actually set by $\tau_{cr(D_{50})}$ and that form drag from channel-scale features in natural gravel-bedded rivers is large enough to make $\tau_{cr(D_{84})}$ appear to be the better predictor of bankfull depth in Figure 2.57.

2.6c: Application of the hydraulic geometry model to the modern Paria River system

In this section, the hydrology of the Paria River presented in Section 2.4 and the channel morphology of the modern Paria River presented in Section 2.5 are placed in the context of the hydraulic geometry model developed in Sections 2.6a and 2.6b. Assumptions necessary to apply this model are: first, the thin layer of sand, silt, and clay that covers the gravel bed of the Paria River at low flows is completely in suspension at bankfull flows such that the majority of the bed surface at bankfull discharge is gravel; and second, the roughness of the sandy banks at bankfull discharge is comparable to the roughness of the gravel bed such that the perimeter of the entire channel can be treated as

though it were completely composed of the same gravel grain-size distribution. Work presented in Chapter 4 shows that these assumptions are reasonable.

The Paria River is an ideal site to apply and test the model. The bankfull discharge is constant at about 90 m^3/s over at least the lower 81% of the 157 km-long river; and the grain-size distribution of the gravel that comprises the bed of the channel is constant over the lower 83% of the 157 km-long river (Figure 2.58). Moreover, because the bankfull water discharge and bed sediment grain-size distribution are constant over the lower 81% of the river, the bankfull sediment load should also be constant over the lower 81% of the river. Therefore, changes in the longitudinal slope of the channel should be completely balanced by changes in the maximum bankfull depth, cross-section area, and bankfull width.

Over the studied lower 130 km of the Paria River channel, the maximum bankfull depth set by $\tau_{cr(D_{84})}$ is in excellent agreement with measurements of maximum bankfull depth from the 15 equilibrium reaches, i.e., reaches with active floodplains, studied between Cannonville and Lees Ferry and from Reaches 1, 2, and 3 in the Lees Ferry study area (Figure 2.60). As shown in Figure 2.59, and for the reasons stated in Section 2.6b, both the $\tau_{cr(D_{50})}$-based approach of Parker (1979) and the $\tau_{cr(D_{50})}$ with sorting-based approach of Ikeda and others (1988) underpredict the maximum bankfull depth of the Paria River.

Because the bankfull sediment load should be constant from the near Cannonville, UT gage to Lees Ferry, the reach-averaged cross-section geometries were calculated in an upstream direction from Lees Ferry to Cannonville using the bankfull sediment load calculated for the Lees Ferry reach as input. The following were used as input into the calculation of the reach-averaged cross-section geometry of the Lees Ferry reach: (1) the reach-averaged longitudinal slope from the 1993 3-reach composite of 0.004; (2) a D_{84} of 8.8 cm and a D_{50} of 4 cm; and (3) a bankfull water discharge of 90 m^3/s. The value of Q_{sBF} was determined for the Lees Ferry reach of the river by setting W_{BAR} equal to zero and calculating the value of W_{TH} in equation 2.12, and then substituting this value into equation 2.16 resulting in a calculated value of $Q_{sBF} = 3.8 \times 10^4$ cm^3/s. Success of this approach to modeling hydraulic geometry is illustrated in Figure 2.60 and Table 2.7. The mean and standard deviation of the model-predicted to measured ratios for the dependent hydraulic geometry variables in Table 2.7 illustrate that, on average, the model predictions are indistinguishable from the measurements at one standard deviation. Furthermore, Figures 2.60a and 2.60b illustrate how a narrow, single-threaded river with a gentle

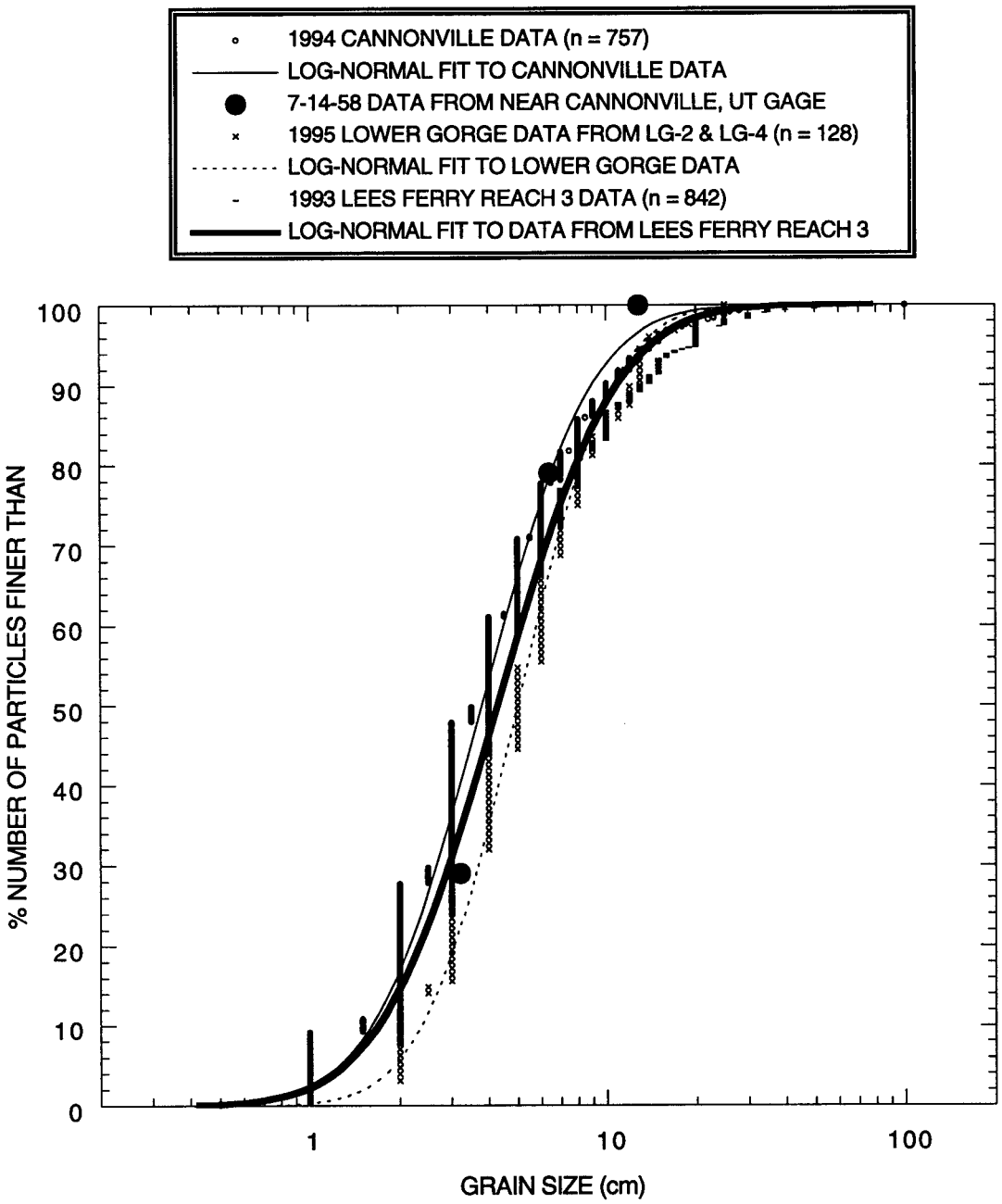

Figure 2.58: Comparison of the cumulative grain-size distributions of gravel comprising the bed of the Paria River channel: (1) in the Cannonville study area in June 1994, (2) at the near Cannonville, UT gage on July 14, 1958, (3) at cross-sections *LG-2* and *LG-4* in the Lower Paria River Gorge in April 1995, and (4) in Reach 3 of the 1993 3-reach composite in the Lees Ferry study area in March 1993.

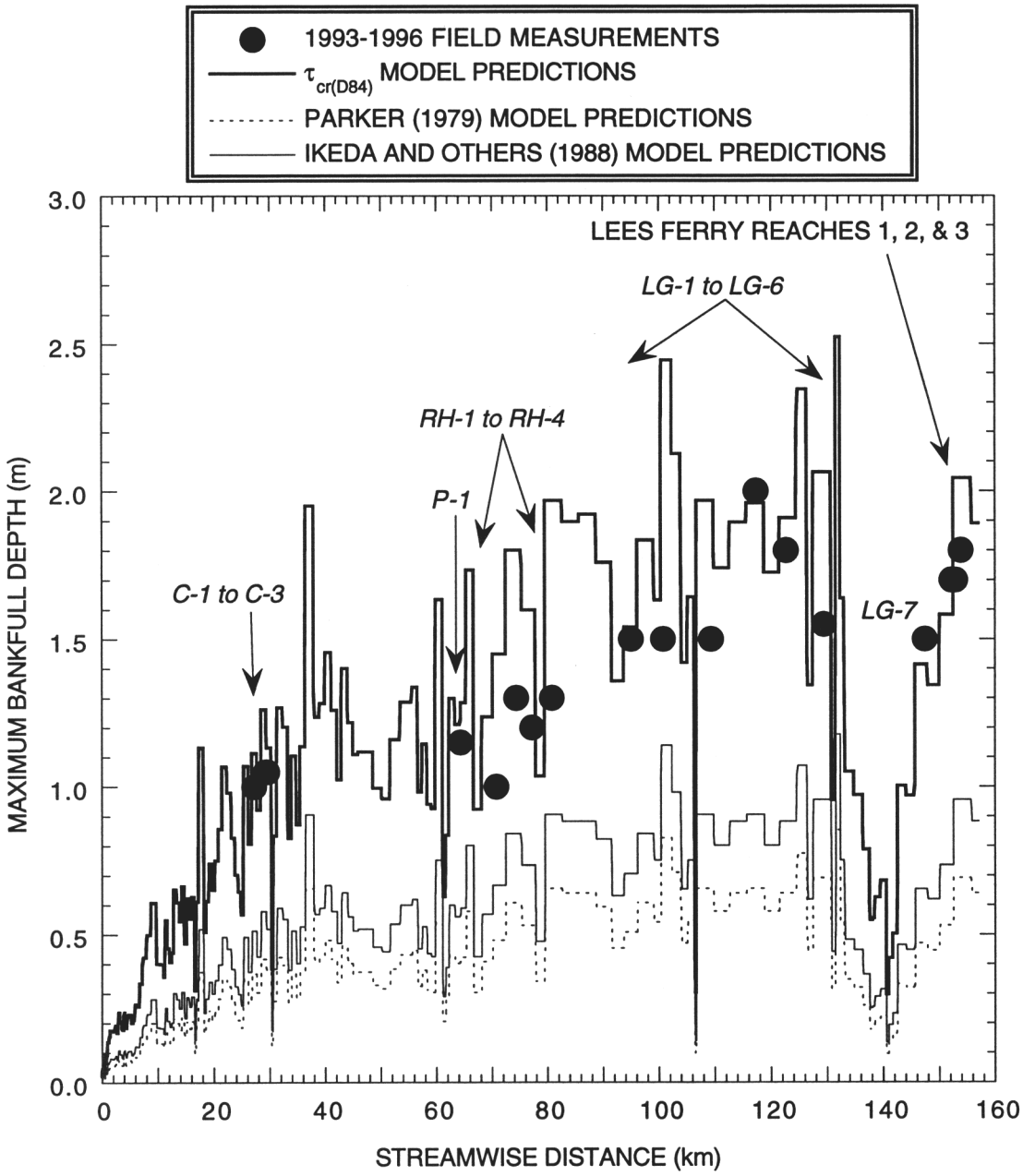

Figure 2.59: Comparison of the predictions of the model based on $\tau_{cr(D_{84})}$, the model of Parker (1979), and the model of Ikeda and others (1988) with measurements of the maximum bankfull depth in 18 different equilibrium reaches from Cannonville to Lees Ferry; for these calculations, D_{84} = 8.8 cm and D_{50} = 4 cm. Longitudinal slopes used to calculate the maximum bankfull depth were determined for channel segments between contour lines on the USGS 7.5' topographic quadrangles by dividing the drop between contour lines by the intervening channel length, hence the blockiness in the maximum bankfull depth predictions merely reflects locations of contour lines.

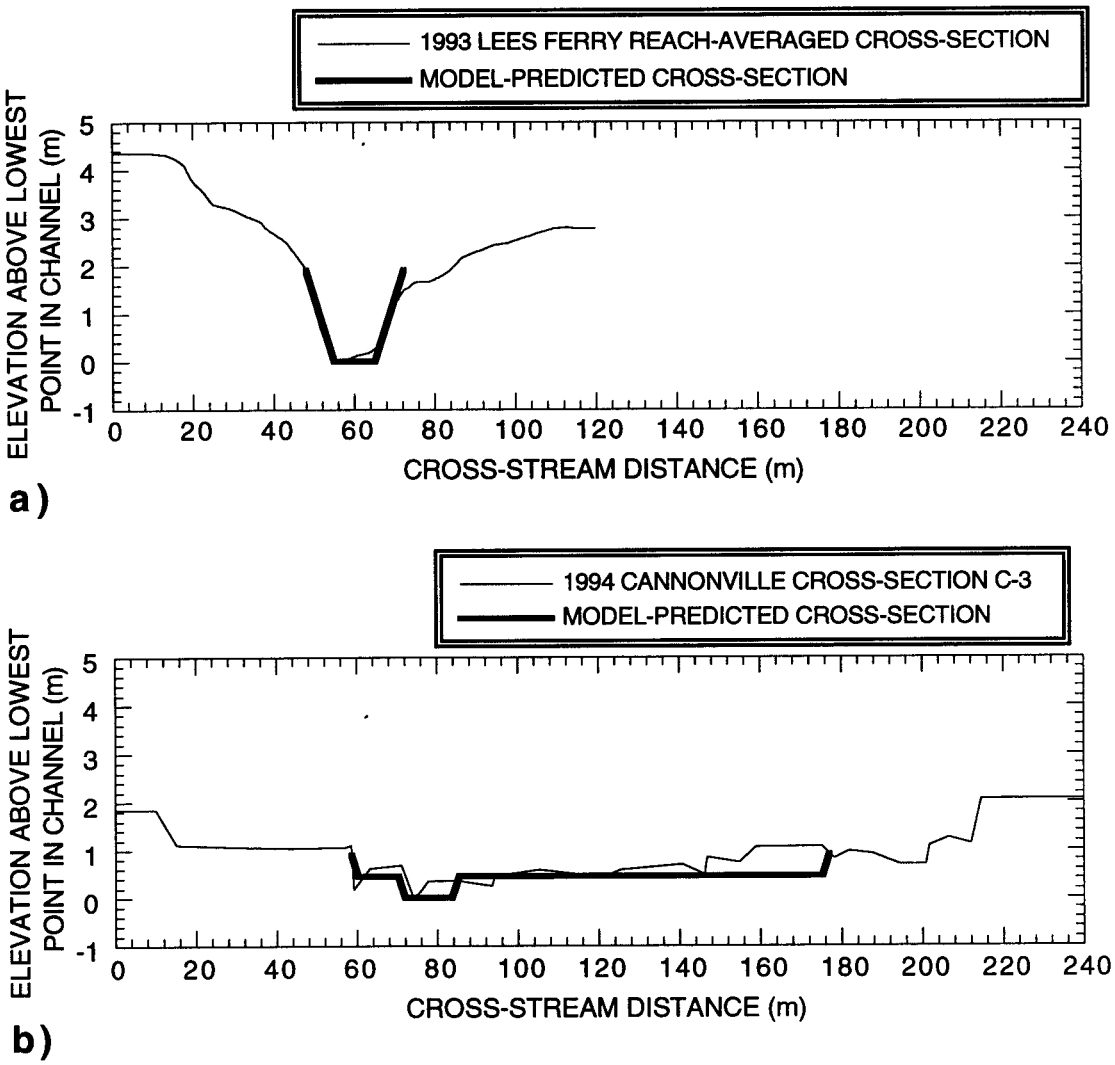

Figure 2.60: **(a)** Comparison of the reach-averaged cross-section predicted by the hydraulic geometry model with the 1993 Lees Ferry reach-averaged cross-section; input into hydraulic geometry model: D_{84} = 8.8 cm, D_{50} = 4 cm, S = 0.004, Q_{BF} = 90 m^3/s. Calculated Q_{sBF} = 3.8 x10^4 cm^3/s. **(b)** Comparison of the reach-averaged cross-section predicted by the hydraulic geometry model with the 1994 Cannonville cross-section C-3; input into hydraulic geometry model: D_{84} = 8.8 cm, D_{50} = 4 cm, S = 0.0086, Q_{BF} = 90 m^3/s, Q_{sBF} = 3.8 x10^4 cm^3/s. Since the model does not specify the location of the thalweg, it was positioned to match the location of the surveyed thalweg.

Table 2.7: Predicted and measured hydraulic geometry properties for the Paria River in 1993-1996.

LOCATION	S	PRED. h_{BF} (m)	MEAS. h_{BF} (m)	(PRED. h_{BF})/ (MEAS. h_{BF})	PRED. MEAN BANK-FULL DEPTH (m)	MEAS. MEAN BANK-FULL DEPTH (m)	(PREDICTED MEAN BANK-FULL DEPTH / MEASURED MEAN BANK-FULL DEPTH)	PRED. W_{BF} (m)	MEAS. W_{BF} (m)	(PRED. W_{BF}/ (MEAS. W_{BF})	INPUT Q_{sBF} (cm^3/s)	CALCU-LATED Q_{sBF} (cm^3/s)	(INPUT Q_{sBF})/ (CALCU-LATED Q_{sBF})
C-1	0.0086	0.88	1.05	0.84	0.46	0.62	0.74	118	70	1.69	3.8×10^4	6.8×10^4	0.56
C-1	0.0069*	1.11	1.05	1.06	0.60	0.62	0.97	80	70	1.14	3.8×10^4	2.7×10^4	1.41
C-2	0.0086	0.88	1.00	0.88	0.46	0.52	0.88	118	66	1.79	3.8×10^4	4.2×10^4	0.90
C-2	0.0061*	1.25	1.00	1.25	0.70	0.52	1.35	64	66	0.97	3.8×10^4	7.9×10^3	4.81
C-3	0.0086	0.88	1.00	0.88	0.46	0.51	0.90	118	100	1.18	3.8×10^4	3.5×10^4	1.09
C-3	0.0068*	1.12	1.00	1.12	0.61	0.51	1.20	78	100	0.78	3.8×10^4	1.0×10^4	3.80
P-1	0.0084	0.91	1.05	0.87	0.47	0.54	0.87	114	75	1.52	3.8×10^4	4.5×10^4	0.84
P-1	0.0060*	1.27	1.05	1.21	0.72	0.54	1.33	61	75	0.81	3.8×10^4	7.3×10^3	5.21
RH-1	0.0053*	1.44	1.0	1.44	0.85	—	—	48	55 † (45+10)	0.87	3.8×10^4	—	—
RH-2	0.0042*	1.82	1.3	1.40	1.23	—	—	28	26	1.08	3.8×10^4	—	—
RH-3	0.0048*	1.59	1.2	1.33	0.99	—	—	38	35	1.09	3.8×10^4	—	—
RH-4	0.0039*	1.96	1.3	1.51	1.37	—	—	24	45 † (38+7)	0.53	3.7×10^4 §	—	—
LG-1	0.0050*	1.53	1.5	1.02	0.92	—	—	42	25	1.68	3.8×10^4	—	—
LG-2	0.0031*	2.46	1.5	1.64	1.49	—	—	23	19	1.21	2.5×10^4 §	—	—
LG-3	0.0039*	1.96	1.5	1.31	1.37	—	—	24	30	0.80	3.7×10^4 §	—	—
LG-4	0.0039*	1.96	2.0	0.98	1.37	—	—	24	28	0.86	3.7×10^4 §	—	—
LG-5	0.0040*	1.91	1.8	1.06	1.35	—	—	24	20	1.20	3.8×10^4	—	—
LG-6	0.0037*	2.06	1.6	1.29	1.40	—	—	24	25	0.96	3.4×10^4 §	—	—
LG-7	0.0054*	1.41	1.5	0.94	0.83	—	—	50	21	2.38	3.8×10^4	—	—
LEES FERRY	0.0040	1.91	1.80	1.06	1.35	1.40	0.96	24	23	1.04	3.8×10^4	2.4×10^4	1.58
LEES FERRY	0.0041*	1.86	1.80	1.03	1.29	1.40	0.92	26	23	1.13	3.8×10^4	2.6×10^4	1.46
MEAN±1σ		---	---	**1.15±0.26**	---	---	**0.87±0.08**	---	---	**1.24±0.46**	---	---	**0.99±0.38**

Notes:
Since h_{BF} and W_{BF} were measured with a measuring tape at cross-sections *RH-1* through *LG-7*, the mean bankfull depth and the calculated Q_{sBF} could not be determined.
* Indicates that S was determined from the USGS 7.5' topographic quadrangles. Shaded rows are redundant analyses using map-determined slopes for cross-sections with surveyed slopes and are not included in the determination of the means and standard deviations in the last row.
† Channel widths in parentheses are main thalweg and back-bar channel widths and sum to equal W.
§ Since S was less than 0.004 in these reaches, no cross-section could be constructed by the model for the input $Q_{sBF} = 3.8 \times 10^4$ cm/s determined by the model for the Lees Ferry cross-section predicted for $Q_{BF} = 90$ m^3/s.

longitudinal slope may, in fact, have a hydraulic geometry equivalent to that of a wide, quasi-braided river with a steep longitudinal slope.

Application of the hydraulic geometry theory to the modern Paria River illustrates how the transformation of a narrow single-threaded stream to a wide braided stream may occur without any change in the bankfull water discharge or sediment load and can result from only a steepening of the longitudinal slope. For example, if the longitudinal slope of the reach for the Lees Ferry cross-section depicted in Figure 2.60a could be steepened to equal that of the reach for the Cannonville cross-section depicted in Figure 2.60b by cutting off meanders, the Lees Ferry reach would, by conservation of water and sediment mass, shallow, widen, and eventually take on the appearance of the quasi-braided Cannonville reach.

Model-based speculation on changes in hydraulic geometry with climate

Application of the hydraulic geometry model to various hypothetical changes in climate suggests that the most effective way to change a narrow meandering single-threaded stream to a wide braided river, as occurred during the late 1800's in many alluvial rivers in the southwestern United States, in addition to the Paria-Adairville reach of the Paria River, is not to change the climate at all, but to keep the same water discharge and sediment load and increase the longitudinal slope by cutting off meanders either naturally or by artificial means. Since the hydraulic geometry model has been found to work well in characterizing the modern geometries of portions of the modern Paria River channel in equilibrium with active floodplains, it has been used to speculate systematically on how two very different cross-section geometries, with identical hydraulic geometries (i.e., the model-predicted 1990's hydraulic geometries at Lees Ferry and Cannonville) should respond to changes in climate given all possible combinations of changes in the bankfull water discharge and bankfull sediment load that might occur with such a change. Table 2.8 illustrates the various predicted changes in the various dependent hydraulic geometry variables for these two different cross-section geometries. For predictions in Table 2.8 based on changes in both bankfull water discharge and sediment load, water discharge and sediment load were varied at the same rate, regardless of whether these two quantities changed in the same or opposing directions. Furthermore, for all predictions in Table 2.8, grain-size distribution of the bed was held constant, and longitudinal slope was varied only when no change in any of the other dependent variables could predict a bankfull channel geometry that could transport the amounts of water and sediment required by the imposed changes in Q_{BF} and Q_{sBF}.

Table 2.8: Modeled 1990's initial magnitudes of and model-predicted changes in dependent hydraulic geometry variables for the reach-averaged equilibrium cross-sections in the Lees Ferry and Cannonville study areas.

LEES FERRY	**INITIAL MAGNITUDE OF:**						
	h_{BF}	MEAN BANKFULL DEPTH	W_{BF}	W_{TH}	$2W_{BANK}$	W_{BAR}	S
	1.91 m	1.35 m	24.4 m	10.2 m	14.2 m	0 m	0.004
IMPOSED CHANGE	**PREDICTED CHANGE IN:**						
	h_{BF}	MEAN BANKFULL DEPTH	W_{BF}	W_{TH}	$2W_{BANK}$	W_{BAR}	S
Q_{BF} DECREASES, Q_{sBF} DECREASES	-	-	-	-	-	0	+
Q_{BF} DECREASES, Q_{sBF} CONSTANT	-	-	-	+	-	0	+
Q_{BF} DECREASES, Q_{sBF} INCREASES	-	-	+	+	-	0	+
Q_{BF} CONSTANT, Q_{sBF} DECREASES	0	+	+	-	0	+	0
Q_{BF} CONSTANT, Q_{sBF} CONSTANT	0	0	0	0	0	0	0
Q_{BF} CONSTANT, Q_{sBF} INCREASES	-	+	+	+	-	0	+
Q_{BF} INCREASES, Q_{sBF} DECREASES	0	+	+	-	0	+	0
Q_{BF} INCREASES, Q_{sBF} CONSTANT	0	+	+	-	0	+	0
Q_{BF} INCREASES, Q_{sBF} INCREASES	0	+	+	+	0	+	0
CANNONVILLE	**INITIAL MAGNITUDE OF:**						
	h_{BF}	MEAN BANKFULL DEPTH	W_{BF}	W_{TH}	$2W_{BANK}$	W_{BAR}	S
	0.89 m	0.46 m	118.4 m	11.8 m	6.6 m	99.9 m	0.0086
IMPOSED CHANGE	**PREDICTED CHANGE IN:**						
	h_{BF}	MEAN BANKFULL DEPTH	W_{BF}	W_{TH}	$2W_{BANK}$	W_{BAR}	S
Q_{BF} DECREASES, Q_{sBF} DECREASES	0	-	-	-	0	-	0
Q_{BF} DECREASES, Q_{sBF} CONSTANT	0	-	-	-	0	-	0
Q_{BF} DECREASES, Q_{sBF} INCREASES	-	-	-	+	-	-	+
Q_{BF} CONSTANT, Q_{sBF} DECREASES	0	+	+	-	0	+	0
Q_{BF} CONSTANT, Q_{sBF} CONSTANT	0	0	0	0	0	0	0
Q_{BF} CONSTANT, Q_{sBF} INCREASES	0	-	-	+	0	-	0
Q_{BF} INCREASES, Q_{sBF} DECREASES	0	+	+	-	0	+	0
Q_{BF} INCREASES, Q_{sBF} CONSTANT	0	+	+	-	0	+	0
Q_{BF} INCREASES, Q_{sBF} INCREASES	0	+	+	+	0	+	0

Notes:
0 indicates no change, **+** indicates increase, **-** indicates decrease. Shaded boxes indicate dependent hydraulic geometry variables that behave differently depending on whether the modeled initial equilibrium cross-section included bar areas; see text for explanation.

Given identical changes in Q_{BF} and Q_{sBF}, a single thread channel, like the channel at Lees Ferry, will not necessarily behave in the same way as a quasi-braided channel, like the channel near Cannonville. Simply stated, when a change requiring a narrowing of the bar region is predicted for a channel without bars initially, other dependent hydraulic geometry variables must adjust such that mass of water and sediment is conserved. For example, for all cases where Q_{sBF} decreases and the case where Q_{BF} is constant and Q_{sBF} increases, a narrowing of the bar region is predicted in the Cannonville reach, while the Lees Ferry reach changes differently because, as a relatively narrow single-threaded stream, it has no bar region to narrow (Table 2.8).

Because Q_{BF} and Q_{sBF} are coupled and not likely to change either independently or in opposing manners during a change in climate, only those changes in the dependent hydraulic geometry variables, given a decrease or increase in both Q_{BF} and Q_{sBF}, are considered. For both initial types of channels, narrow single-threaded (Lees Ferry) and wide quasi-braided (Cannonville), a change in climate from dry to wet should increase both Q_{BF} and Q_{sBF} and cause an increase in both the mean bankfull depth and bankfull width, thus causing an increase in the bankfull cross-section area of the channel. These changes in mean bankfull depth and bankfull width would occur through major increases in both the width of the thalweg and the bar region. For the opposite change in climate, a change from wet to dry that causes a decrease in Q_{BF} and Q_{sBF}, both types of channels are predicted to change in the same fashion, with a major decrease in both the mean bankfull depth and bankfull width, but with one important difference. In the quasi-braided channel, the bar region is predicted to narrow; but, since the single-threaded stream has no "bar region" and the bed grain-size distribution is not allowed to change, the maximum bankfull depth must decrease and the longitudinal slope of the channel must increase in order to accommodate the same decrease in Q_{BF} and Q_{sBF}.

In summary, for a river with a relatively stable longitudinal slope, a climate change in either direction should affect the mean bankfull depth and bankfull width through major changes in only the widths of the thalweg and bar region. A change from a dry to a wet climate should not necessarily result in the transformation from a meandering single-threaded stream to a wide braided stream, but, rather, it should result in the transformation from a meandering single-threaded stream to a meandering single-threaded stream with both a wider thalweg and a wider bar region.

2.6d: Application of the hydraulic geometry model to historical channel geometric changes in the Lees Ferry, AZ and Paria-Adairville, UT reaches with hydrologic and sediment-transport implications

Since historical changes in cross-section geometry in both the Lees Ferry, AZ and the Paria-Adairville, UT reaches have accompanied significant changes in longitudinal slope, the hydraulic geometry model was used to determine if the changes in the longitudinal slope could account for most, if not all, of the observed changes in cross-section geometry in these two reaches.

Lees Ferry, AZ reach

In the context of the hydraulic geometry model, all changes in the cross-section geometry of equilibrium reaches in the Lees Ferry study area for the period from 1872 to 1993 can be accounted for to within 10% through changes only in the longitudinal slope, with no significant change in hydrology or sediment transport (Figure 2.61). In Figure 2.61, the values of the bankfull water discharge, bankfull sediment load, and bed grain-size distribution are held constant to investigate only the effect of changing the longitudinal slope on the cross-sectional geometry. As shown in Figure 2.61a, the model-predicted cross-section geometry calculated for a longitudinal slope of 0.004 is in agreement with both the cross-section geometries of the November 1925 to March 1993 reaches with known longitudinal slopes within 15% of 0.0035 and the June 1872 to August 1925 reaches with unknown longitudinal slopes. As shown in Figure 2.61b, the model-predicted cross-section geometry calculated for a longitudinal slope of 0.005 is slightly narrower and deeper than the reach-averaged cross-section geometry of the September 1929 reach with a measured longitudinal slope of 0.005; however, only either a 10% increase in the model-input longitudinal slope or a 10% decrease in D_{84} would substantially improve the agreement between model prediction and measurement. As shown in Figure 2.61c, the model-predicted cross-section geometry calculated for a longitudinal slope of 0.006 is slightly wider than the reach-averaged cross-section geometry of the October 1939 reach with a longitudinal slope of 0.006; however, only either a 10% reduction in the model-input longitudinal slope or a 10% increase in D_{84} would substantially improve the agreement between model prediction and measurement. The model successfully predicts the observation (see Figures 2.25, 2.27 and 2.36) that the equilibrium channel should extend from terrace margin to terrace margin and have no floodplains in the steep 1939 reach above the gage (Figure 2.61c). Likewise, it also successfully predicts the observation (see Figures 2.25, 2.27, and 2.35) that the equilibrium channel should have floodplains in the more gently sloping 1939 reach below the gage (Figure 2.61a).

Figure 2.61: **(a)** Comparison of the model-predicted cross-sectional geometry for inputs of Q_{BF} = 90 m^3/s, Q_{sBF} = 3.8x10^4 cm^3/s, D_{84} = 8.8 cm, D_{50} = 4 cm, and S = 0.004 with all of the "Category 1" cross-sectional geometry data in Figure 2.35, i.e., all data from the channels with active floodplains with channel longitudinal slopes within 15% of 0.0035 from 1925 to 1993 or with unknown longitudinal slopes from 1872 to 1925. **(b)** Comparison of the model-predicted cross-sectional geometry for inputs of Q_{BF} = 90 m^3/s, Q_{sBF} = 3.8x10^4 cm^3/s, D_{84} = 8.8 cm, D_{50} = 4 cm, and S = 0.005 with the reach-averaged cross-section from the September 1929 reach with a longitudinal slope of 0.005; the model-predicted cross-section for Q_{BF} = 90 m^3/s, Q_{sBF} = 3.8x10^4 cm^3/s, D_{84} = 8.8 cm, D_{50} = 4 cm, and S = 0.0055 is also shown to illustrate that the model-predicted and measured cross-section geometry agree to within 10%. **(c)** Comparison of the model-predicted cross-sectional geometry for inputs of Q_{BF} = 90 m^3/s, Q_{sBF} = 3.8x10^4 cm^3/s, D_{84} = 8.8 cm, D_{50} = 4 cm, and S = 0.006 with the reach-averaged cross-section from the October 1939 reach above the gage with a longitudinal slope of 0.006; the model-predicted cross-section for Q_{BF} = 90 m^3/s, Q_{sBF} = 3.8x10^4 cm^3/s, D_{84} = 8.8 cm, D_{50} = 4 cm, and S = 0.0054 is also shown to illustrate that the difference between the model-predicted and measured cross-section geometry agree to within 10%.

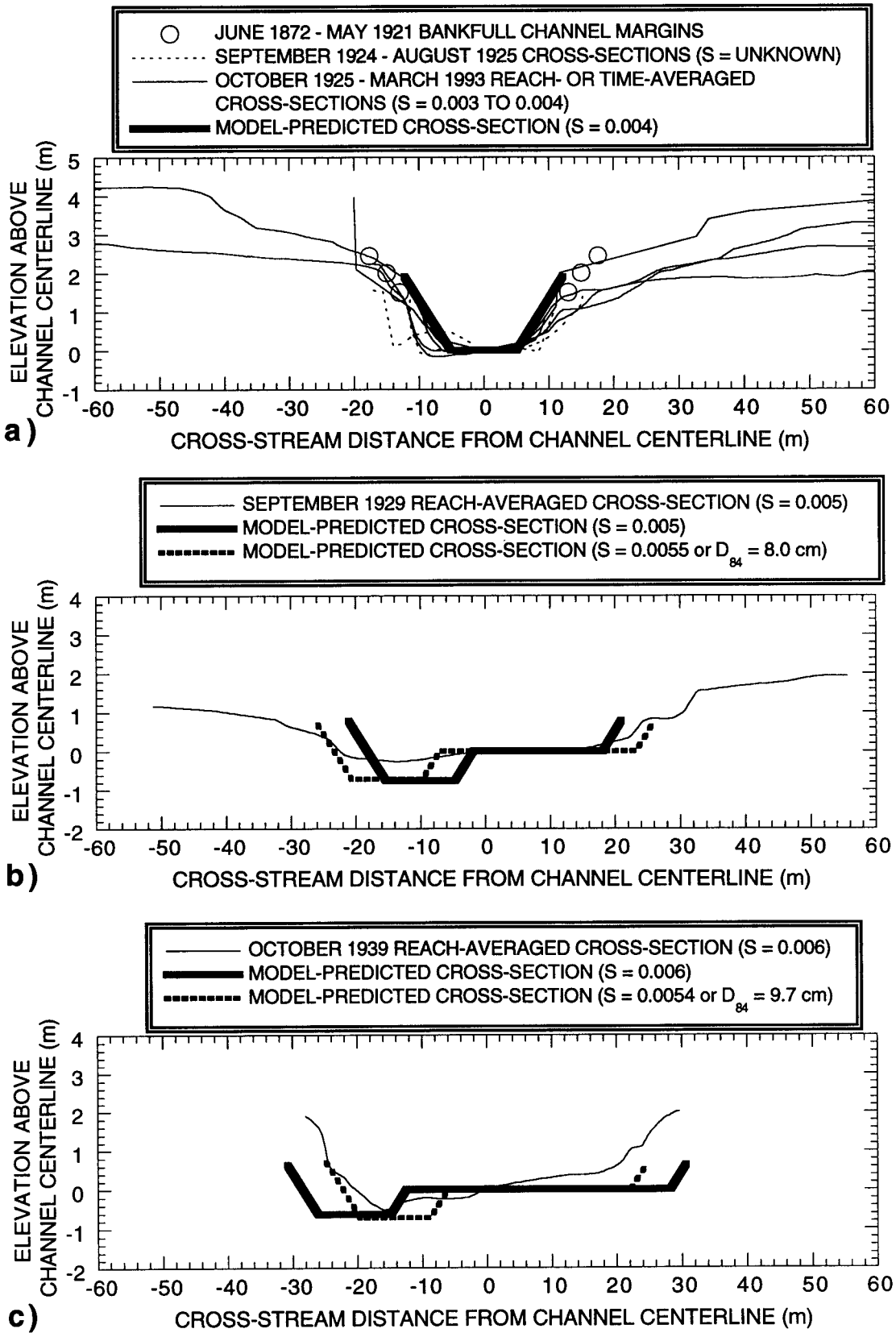
JUNE 1872 - MAY 1921 BANKFULL CHANNEL MARGINS
SEPTEMBER 1924 - AUGUST 1925 CROSS-SECTIONS (S = UNKNOWN)
OCTOBER 1925 - MARCH 1993 REACH- OR TIME-AVERAGED CROSS-SECTIONS (S = 0.003 TO 0.004)
MODEL-PREDICTED CROSS-SECTION (S = 0.004)
ELEVATION ABOVE CHANNEL CENTERLINE (m)
CROSS-STREAM DISTANCE FROM CHANNEL CENTERLINE (m)
a)
SEPTEMBER 1929 REACH-AVERAGED CROSS-SECTION (S = 0.005)
MODEL-PREDICTED CROSS-SECTION (S = 0.005)
MODEL-PREDICTED CROSS-SECTION (S = 0.0055 or D84 = 8.0 cm)
ELEVATION ABOVE CHANNEL CENTERLINE (m)
CROSS-STREAM DISTANCE FROM CHANNEL CENTERLINE (m)
b)
OCTOBER 1939 REACH-AVERAGED CROSS-SECTION (S = 0.006)
MODEL-PREDICTED CROSS-SECTION (S = 0.006)
MODEL-PREDICTED CROSS-SECTION (S = 0.0054 or D84 = 9.7 cm)
ELEVATION ABOVE CHANNEL CENTERLINE (m)
CROSS-STREAM DISTANCE FROM CHANNEL CENTERLINE (m)
c)

Paria-Adairville, UT reach

In the context of the hydraulic geometry theory, and similar to the findings in the Lees Ferry study area, all changes in cross-section geometry in the Paria-Adairville reach for the period from 1877 to 1917 and 1917 to 1976 can be reasonably accounted for through changes only in the longitudinal slope, with no significant change in hydrology or sediment transport (Table 2.9). As shown in Section 2.5d, the Paria River in the Paria-Adairville reach has undergone significant changes in sinuosity, longitudinal slope, and channel cross-section geometry over the past 120 years, especially in reaches **C-D** and **E-F** (see Section 2.4d). As reach **C-D** straightened and steepened between 1884 and 1917 from a longitudinal slope of 0.0053-0.0058 to a longitudinal slope of 0.0076-0.0088 (Table 2.6), the bankfull width increased to be about 100-150 m by June 1918 (Figure 2.53). In contrast, the width of the low-flow water surface, i.e., the width of the thalweg, in reaches **C-D** and **E-F** remained relatively constant as the river widened. As indicated by the cadastral surveys of Bailey and Burrill (1877) and Thoma and Rathbone (1917), the width of the thalweg these 2 reaches in March 1877 was 11.3±2.0 m and in March 1917 was 13.1±9.3 m.

To evaluate the extent to which the changes in channel cross-section geometry from 1877 to 1976 were due only to changes in longitudinal slope, the changes in reaches C-D and E-F were placed in the context of the hydraulic geometry model. Table 2.9 shows the model-predicted changes, in terms of both the magnitude and percent, in the reach-averaged cross-section geometry in reaches **C-D** and **E-F** from 1877 to 1917 and from 1917 to 1976 using as input the longitudinal slope of these reaches in 1877, 1917, and 1976 determined from both the contour-line and channel-length methods that were developed in Section 2.4d. In addition to the usual dependent hydraulic geometry variables and the bankfull sediment load, a new quantity, the cumulative volume of the bankfull channel in each reach, V_{BF}, is shown in Table 2.9. V_{BF} of each reach at each time is calculated by multiplying the predicted reach-averaged bankfull cross-section area, i.e., the mean bankfull depth multiplied by the bankfull width, by the length of the reach in Table 2.7. Since a negative change in V_{BF} indicates net positive change in sediment storage, this quantity allows the model-predicted change in the volume of sediment stored in floodplains and bars in each reach to be evaluated.

As shown in Table 2.9, model predictions of the channel geometric changes that arise from only a change in the longitudinal slope are fully compatible with the data. Because more data exist as to the nature of channel changes in reach **C-D** than reach **E-F**, reach **C-D** is the focus of the following discussion; and, because longitudinal slopes

Table 2.9: Predicted reach-scale channel-geometric changes near Paria, UT from 1877 to 1976 keeping reach-averaged hydraulic geometry constant.

	1877	CHANGE FROM 1877 TO 1917		1917	CHANGE FROM 1917 TO 1976		1976	1877	CHANGE FROM 1877 TO 1917		1917	CHANGE FROM 1917 TO 1976		1976
	REACH C-D							**REACH E-F**						
	CONTOUR-LINE METHOD							CONTOUR-LINE METHOD						
S	0.0053		+66%	0.0088		-20%	0.0070	0.0042		+74%	0.0073		-36%	0.0047
h_{BF} (m)	1.44	-0.57 m	-40%	0.87	+0.22 m	+25%	1.09	1.82	-0.77 m	-42%	1.05	+0.57 m	+54%	1.62
Q_{BF} (m^3/s)	90	0	0%	90	0	0%	90	90	0	0%	90	0	0%	90
Q_{sBF} (cm^3/s)	3.8×10^4	0	0%	3.8×10^4	0	0%	3.8×10^4	3.8×10^4	0	0%	3.8×10^4	0	0%	3.8×10^4
MEAN BANKFULL DEPTH (m)	0.85	-0.41 m	-48%	0.44	+0.15 m	+34%	0.59	1.23	-0.67 m	-54%	0.56	+0.46 m	+82%	1.02
W_{BF} (m)	47.8	+75.3 m	+158%	123.1	-40.8 m	-33%	82.3	27.9	+60.9 m	+218%	88.8	-52.2 m	-59%	36.6
W_{TH} (m)	10.9	+0.9 m	+8%	11.8	-0.3 m	-3%	11.5	10.3	+1.2 m	+12%	11.5	-0.9 m	-8%	10.6
W_{BAR} (m)	26.1	+78.7 m	+302%	104.8	-42.1 m	-40%	62.7	4.0	+65.5 m	+1638%	69.5	-55.6 m	-80%	13.9
$2W_{BANK}$ (m)	10.8	-4.3 m	-40%	6.5	+1.6 m	+25%	8.1	13.6	-5.8 m	-43%	7.8	+4.3 m	+55%	12.1
V_{BF}(m^3)	1.40×10^5	+2000 m^3	+1%	1.42×10^5	-4000 m^3	-3%	1.38×10^5	2.53×10^5	-40000 m^3	-16%	2.13×10^5	-6000m^3	-3%	2.07×10^5
	CHANNEL-LENGTH METHOD							CHANNEL-LENGTH METHOD						
S	0.0058		+31%	0.0076		-8%	0.0070	0.0035		+74%	0.0061		-23%	0.0047
h_{BF} (m)	1.32	-0.32 m	-24%	1.00	+0.09 m	+9%	1.09	2.18	-0.93 m	-43%	1.25	+0.37 m	+30%	1.62
Q_{BF} (m^3/s)	90	0	0%	90	0	0%	90	90	0	0%	90	0	0%	90
Q_{sBF} (cm^3/s)	3.8×10^4	0	0%	3.8×10^4	0	0%	3.8×10^4	3.1×10^4	+7000 cm^3/s	+23%	3.8×10^4	0	0%	3.8×10^4
MEAN BANKFULL DEPTH (m)	0.75	-0.22 m	-29%	0.53	+0.06 m	+11%	0.59	1.43	-0.73 m	-51%	0.70	+0.32 m	+46%	1.02
W_{BF} (m)	57.5	+34.6 m	+66%	95.4	-13.1 m	- 14%	82.3	23.5	+40 m	+170%	63.5	-26.9 m	-42%	36.6
W_{TH} (m)	11.1	+0.5 m	+5%	11.6	-0.1 m	-1%	11.5	7.2	+4.0 m	+56%	11.2	-0.6 m	-5%	10.6
W_{BAR} (m)	36.6	+39.8 m	+109%	76.4	-13.7 m	-18%	62.7	0.0	+43.0 m	$+\infty$%	43.0	-29.1 m	-68%	13.9
$2W_{BANK}$ (m)	9.8	- 2.4 m	- 24%	7.4	+0.7 m	+9 %	8.1	16.3	-7 m	-43%	9.3	+2.8 m	+30%	12.1
V_{BF}(m^3)	1.48×10^5	-16000 m^3	-11%	1.32×10^5	+6000 m^3	+5%	1.38×10^5	2.48×10^5	-58000 m^3	- 23%	1.90×10^5	+17000 m^3	+9%	2.07×10^5

determined by the contour-line method are probably more accurate than those determined by the channel-length method (see Section 2.5d), the channel changes discussed below are based on longitudinal slopes determined by the contour line method. The model predicts that from 1877 to 1917, the bankfull width should increase from 48 to 123 m and the thalweg width should increase slightly from 10.9 m to 11.8 m as the longitudinal slope increases from 0.0053 to 0.0088. In other words, the model predicts that the increase in bankfull width of reach **C-D** is manifested by a major increase in only the width of the bar region. These values are in agreement with the reconstructed June 1918 bankfull width of 100-150 m and with the measured negligible change in the width of the thalweg of reaches **C-D** and **E-F** from 11.3±2.0 m in 1877 to 13.1±9.3 m in 1917. Also, the model predicts that from 1917 to 1976, the bankfull width should decrease from 123 to 82 m and the thalweg width should decrease slightly from 11.8 to 11.5 m as the longitudinal slope decreases from 0.0088 to 0.0070. Again, this prediction is compatible with the June 1994 surveyed cross-section geometry of the river at the site of the 1877 Paria irrigation dam, where the bankfull and thalweg widths were 75 m and 10 m, respectively (Figure 2.51).

Agreement between the predictions of the hydraulic geometry model with observations from reach **C-D** indicates that the 1877-1976 changes in cross-section channel geometry of the Paria River in the Paria-Adairville reach can be explained as a function of a change in only the longitudinal slope of the channel, with no required change in hydrology or sediment transport. Furthermore, and in opposition to the predictions of the types of channel changes expected in a climate change, in which the bankfull water discharge and sediment load should both either increase or decrease, the model predicts that if only the slope of a river changes, the width of the thalweg should not change significantly. That this model prediction is in close agreement with measurements that show that the width of the low-flow water surface has not changed significantly since 1877 lends further support to the changes in cross-section geometry in the Paria-Adairville reach being driven only by changes in longitudinal slope. Thus, although local channel cross-section geometry changed substantially, the hydraulic geometry remained relatively constant in the Paria-Adairville reach from 1877 to 1976, indicating that, despite the transformation from meandering to braiding from 1877 to 1917 and the slow transformation back to meandering from 1917 to 1976, the river has been in reasonable equilibrium with the same hydrology, the same sediment load, and, therefore, the same climate from 1877 to the present.

Three possibilities exist for the cause of the increase in longitudinal slope that triggered the channel widening and transformation from meandering to braiding in the late

1800's and early 1900's in the Paria-Adairville reach of the Paria River. These possibilities are: (1) the occurrence of a single catastrophic flood, e.g., a 1000-year flood, that caused the cutoff of all of the meanders; (2) the human impact on the river channel and floodplain being great enough such that a relatively common flood, e.g., a 20-year flood, could cause the straightening of the channel; and (3) artificial straightening of the channel by the settlers. Though the peak discharges of the floods in the late 1800's can never be known, the first possible trigger mechanism, i.e., that a single catastrophic flood caused the change in slope, can probably be excluded as the cause because the channel changes were reported to have begun during a flood in 1883 (Gregory and Moore, 1931) and, as shown in Section 2.4d, the largest post-1880 flood occurred in September 1909 and was only about 25% larger than the largest flood during the period of Lees Ferry gage record. The second possible trigger mechanism, i.e., human impact changing the behavior of the river during normal flooding, is the most likely cause of the increase in slope given the number of irrigation diversion dams, the stripping of native vegetation on the floodplains for agricultural development[8], and the installation of straight roads cutting across meanders in this reach. Indeed, comparison of Figures 2.50b and 2.49a shows that much of the 1917 channel of the Paria River followed the 1877 course of a road. The third possible trigger mechanism, i.e., that the farmers might have locally straightened the channel to add to the amount of land under cultivation, however, cannot be disregarded. Since the irrigation ditch was on the east side of the valley and the river meandered across the center of the valley, it would have been advantageous to straighten the channel so that irrigation water could flow across larger fields located on the east side of the river. No records indicate that this actually occurred at Paria, but examples of the artificial straightening of channels are not uncommon in the literature. For example, in Johnson Canyon, 40 km west of the Paria River valley, Hyrum S. Shumway straightened a channel in his field in the 1880's to improve drainage and inadvertently began the process of arroyo formation (Webb and others, 1991).

2.6e: Hydraulic geometry summary with implications for the prediction of long-term sediment transport rates in the Paria River basin

In summary, a physically based model has been developed for predicting the reach-averaged equilibrium hydraulic geometry of a gravel-bedded river with erodible gravel or sand banks. The hydraulic geometry model is based on a working hypothesis that states: the reach-averaged maximum bankfull depth scales with the critical shear stress of particle

---

[8]Gregory and Moore (1931) indicate that 12.2 km^2 were under irrigated cultivation at Paria.

size on the bed that dominates the spatially averaged bed roughness, i.e. D_{84}, and a truism that states: the stable reach-averaged bankfull cross-section geometry is that which conserves the mass of water and sediment moving through the reach. The important ramification of this combined hypothesis and truism is that there is a wide range of cross-section geometries and longitudinal slopes that combine to form the equivalent hydraulic geometry; for example, a steep, wide, braided channel may have the same hydraulic geometry as a gently sloping, narrow, single-threaded channel.

Application of the hydraulic geometry model to the modern Paria River indicates that the reach-averaged equilibrium cross-section geometries over the lower 81% of the Paria River are different only as a function of longitudinal slope and compose one equivalent hydraulic geometry. Application of the hydraulic geometry model to observed historical changes in cross-section geometry in the Lees Ferry, AZ study area and Paria-Adairville, UT reach suggests that all historical change in cross-section geometry of the Paria River can be predicted (to within about 10%) as a function of measured change in longitudinal slope, with no required change in either bankfull water discharge or bankfull sediment load. No major climate change is required to explain the arroyo-type channel changes in the late 1800's and early 1900's. The most likely cause of the initiation of the late 1800's channel changes is that a normal-sized flood occurred in a river system heavily perturbed by the Mormon pioneers (i.e., irrigation dams, no floodplain vegetation, and roads cutting directly across meanders), and initiated the straightening and steeping of the channel that ultimately led to the widening that destroyed the community of Paria, UT.

Channel planform changes from braiding to meandering within an equivalent hydraulic geometry do not store or erode large quantities of sediment in the system and only local channel incision or aggradation caused by local changes in base level (e.g., near the confluence with the Colorado River, above the landslide dam below the Cannonville study area, and in the reach with major meander cutoffs between Paria and Rock House) is responsible for the majority of change in sediment storage in the Paria River system. Therefore, a detailed flow and sediment-transport model based on an equilibrium hydraulic geometry and a given supply of sand, silt, and clay should adequately predict the long-term sediment yield from the Paria River; this model is developed in Chapter 3 and tested and applied in Chapter 4. Furthermore, since the reach-averaged equilibrium hydraulic geometry of the Paria River has been constant from the 1870's to the present, and because no noticeable impact on the Paria River is evident from the largest statistically significant climate change suggested by tree-ring data during the last 1700 years, long-term sediment-transport rates should be predictable over periods of at least several hundred years.